DOKUZ EYLÜL UNIVERSITY
GRADUATE SCHOOL OF NATURAL AND APPLIED SCIENCES

EXPERIMENTAL INVESTIGATION OF VELOCITY AND TEMPERATURE DISTRIBUTION INSIDE A SPLIT AIR CONDITIONERS INDOOR UNIT

by

Özgün ÖZER

November, 2011

İZMİR

EXPERIMENTAL INVESTIGATION OF VELOCITY AND TEMPERATURE DISTRIBUTION INSIDE A SPLIT AIR CONDITIONERS INDOOR UNIT

A Thesis Submitted to the
Graduate School of Natural and Applied Sciences of Dokuz Eylül University
In Partial Fulfillment of the Requirements for the Degree of Master of Science
in
Mechanical Engineering, Energy Program.

by

Özgün ÖZER

November, 2011

İZMİR

M.Sc THESIS EXAMINATION RESULT FORM

We have read the thesis entitled **"EXPERIMENTAL INVESTIGATION OF VELOCITY AND TEMPERATURE DISTRIBUTION INSIDE A SPLIT AIR CONDITIONERS INDOOR UNIT"** completed by **ÖZGÜN ÖZER** under supervision of **ASSOC. PROF. DR. DİLEK KUMLUTAŞ** and we certify that in our opinion it is fully adequate, in scope and in quality, as a thesis for the degree of Master of Science.

Assoc. Prof. Dr. Dilek KUMLUTAŞ

Supervisor

Prof. Dr. İsmail H. TAVMAN

(Jury Member)

Assist. Prof. Dr. M. Turhan GOBAN

(Jury Member)

Prof.Dr. Mustafa SABUNCU

Director

Graduate School of Natural and Applied Sciences

ACKNOWLEDGEMENTS

First of all, I would like to thank the project executive and my supervisor Assoc. Prof. Dr. Dilek KUMLUTAŞ for providing every need and beyond for this thesis and our other studies. Without her determination, her hard work about this project and her guidance, this thesis cannot be accomplished.

I would like to specially thank to M. Sc. Ziya Haktan KARADENİZ for his advises, mental and scientific support and his help in experiments. I feel lucky and proud for working with him as a colleague and a student.

This study is supported by the Ministry of Science, Industry and Technology, with the 00343.STZ.2008-2 encoded SANTEZ project and Vestel Air-Conditioner Product Company. I would like to express my gratitude about being in this project.

I would also like to thank Assist Prof Dr. Alpaslan TURGUT, Assist Prof Dr. Levent ÇETİN and Dr. Özgün BAŞER for their contributions to my academic and scientific understanding and view of life.

Thanks our study group, mainly my project partners Funda KURU, Değer AKIN, Mete ÖZŞEN and Hasan AVCI, for their acompany and brain storming which created a creative study media.

I would like to present my sincere gratitude to my associate Çağlar EBEPERİ and my dear old friend Gün ÖZBEN, for their graphical assist and support to my life.

As final, I'm really grateful for having such wonderful parents Suna and Cengiz ÖZER. I'm happly admit that their patience, teachings and support; made me who I am and without that this thesis could not be finished.

Özgün ÖZER

EXPERIMENTAL INVESTIGATION OF VELOCITY AND TEMPERATURE DISTRIBUTION INSIDE A SPLIT AIR CONDITIONERS INDOOR UNIT

ABSTRACT

In this thesis, experimental methods that can determine the velocity profile inside the split air conditioner and measure the temperature distribution are investigated. Therefore the study separated into two main issue; flow field investigation and temperature distribution investigation. In both issues the measurement methods are examined and an optimum method chosen.

In flow field investigation section Particle Image Velocimetry (PIV) Method came forward as the most practical and effective method. Therefore PIV, stereo PIV, Panoramic PIV and endoscopic PIV methods applied to split air conditioner indoor unit for determining air flow characteristics for different areas of the system. In temperature distribution investigation section existing method didn't fulfill the expectations of this study, therefore a novel method, "Meshed Infrared Thermography" is designed and introduced.

After the determination of the methods, experimental set ups has been designed and prepared for the current Split Air Conditioner models. As the following step of the study various of experiments carried out and the experimental data compared with conventional methods.

As a result of this study; temperature distribution outside and inside of the SAC indoor unit body has been visualized, systems thermal design investigated. The flow structure in side of the split air conditioner and the temperature distribution of the air at the exit of the SAC indoor unit has been determined.

Keywords: particle image velocimetry, meshed infrared thermography, split air conditioner

SPLİT KLİMA İÇ ÜNİTESİNİN İÇİNDEKİ HIZ VE SICAKLIK DAĞILIMLARININ DENEYSEL OLARAK İNCELENMESİ

ÖZ

Bu çalışmada, split klima iç ünitesinin içindeki hız profilini ve sıcaklık dağılımını belirleyebilecek deneysel yöntemleri incelenmiştir. Bu nedenle çalışma iki ana konudan oluşmaktadır; akış alanı incelemesi ve sıcaklık dağılımı incelenmesi. İki konuda da ölçüm metotları incelenmiş ve en uygun yöntem seçilmiştir.

Akış alanı inceleme bölümünde Parçacık Görüntülemeli Hız Ölçümü (PGHÖ) yöntemi, en pratik ve etkili yöntem olarak öne çıkmıştır. Bu nedenle PGHÖ, stereo PGHÖ, panoramik PGHÖ ve endoskopik PGHÖ yöntemleri, split klimanın farklı bölümlerindeki akış yapılarının incelenmesinde kullanılmıştır. Sıcaklık dağılımının incelenmesi bölümünde ise mevcut yöntemlerin beklentileri karşılayamaması nedeni ile "Ağ Yapılı Kızılötesi Sıcaklık Ölçümü" (AYKSÖ) yöntemi geliştirilerek sunulmuştur.

Yöntemlerin kararlaştırılmasının ardından mevcut split klima modelleri için deney düzenekleri tasarlanmış ve hazırlanmıştır. Çalışmanın takip eden adımı olarak çeşitli deneyler gerçekleştirilmiş ve bu deneylerden elde edilen deney verileri konvansiyonel yöntemlerle elde edilen veriler ile karşılaştırılmıştır.

Bu çalışmanın sonucu olarak; split klima iç ünitesi gövdesinin içinde ve dışındaki sıcaklık dağılımları görselleştirilmiştir. Ayrıca split klima iç ünitesi içindeki akış yapısı ve çıkışındaki havanın sıcak dağılımı belirlenmiştir.

Anahtar sözcükler: parçacık görüntülemeli hız ölçümü, ağ yapılı kızılötesi sıcaklık ölçümü, split klima

CONTENTS

Page

CHAPTER ONE
INTRODUCTION OF SPLIT AIR CONDITIONERS

Split air conditioners (SAC) are specially designed heat pumps which consist of two separate units. One of these units places at outdoor and the other is to the indoor and each has heat exchanger therefore using of the refrigeration cycle they can transfer heat between indoor air and atmosphere. So SACs can both heat and cool and at the cooling process also do dehumidification. These advantages makes SAC's a very suitable choice for single volume Heating Ventilating and Air Conditioning (HVAC) applications. The only flaw of the SACs is ventilating which user can solve this problem by simply opening the window for a time if the outer atmosphere is convenient. Therefore split air conditioner system used especially tropical and subtropical parts of the world.

In spite of the widely use of air conditioners in the whole world, during the literature search, a small number of studies found that is directly about SACs and these are mostly numerical studies. The pioneer of these studies is the paper written by Shih, Hou & Chiang (2008). In their study, SAC indoor unit is two dimensionally analyzed by computational fluid dynamics (CFD) method and different cross fans have been compared.

Although there is a small number of studies directly investigates the SAC's, there is so many studies about its components. One of these studies is performed by Yan & Sheen (2000). They have studied the fin-and-tube heat exchangers with palates. The first part of study investigates the relations between friction factor-f, dimensionless heat transfer coefficient (Colburn j-factor) and Reynolds number. The second part investigates relation between the dimensional heat transfer coefficient, the pressure drop and the frontal air velocity. As the final result they offer an evaluation method for comparing different kinds of heat exchangers.

Tuztas & Egrican (2002) also studied the performance of heat exchangers experimentally in a wind tunnel. As the result of study they determined the heat transfer coefficients and frictions factors of the studied finned-tube heat exchangers.

A more recent study about heat exchangers is made by Gemici, Eğrican & Koca (2010). Six different type of finned tube heat exchangers' heat transfer coefficient has been investigated under the under dehumidifying and dry conditions both theoretically and experimentally. The effects of design parameters such as finning factor (ratio between fins and tubes outside area to tubes outside area), on Colburn j-factor are also investigated.

Another important component of the SAC is Cross-Flow Fan (CFF) which is subject of many scientific studies but it is still not completely system because of its complex and transiently changing flow characteristic. Eck (1973)'s study on CFF, firstly showed the driving effect of the eccentric vortex on CFF flow structure. The eccentric vortex forms between the vortex wall and CFF as the CFF start to turn. This vortex's centeroids randomly change position and also its wideness chage as the CFF works but generally never disappears. The low pressure created by the fan sucks the air and creates a flow field.

Yamafuji studied this vortex experimentally and analytically (Yamafuji, 1975a, 1975b). By his experimental set up he succeed to visualize the eccentric vortex and transient structure of it and the flow it created.

Susumu Murata is one of the most important scientists experimentally investigating CFF and he has many papers published in this topic between 1976 and 1995 with his colleagues. The flow inside the CFF is also studied by Murata et al. by using pitot tube (Murata, Ogawa, Shimizu, Nishihara & Kinoshita, 1978).

The casing also has an important effect on CFF's flow performance. Murata and Nishihara firstly studied this effect and found out that the geometrical design of the casing has an influence on stability of the flow (Murata, Nishihara, 1976a, 1976b).

After this study, Tanaka & Murata (1994) studied Reynolds Number and fan size effect on flow structure and performance. The study aimed to find an affinity law for CFF and its casing but the study wasn't fully accomplished. However the result of the study showed the size of the fan, the gap between rotor and the vortex wall, surface roughness, the thickness of the blade and flow condition of the suction section have effect on CFF performance. These parameters can be used to find a general law that can explain flow field and performance of CFF.

Uskaner and Göksel are also studied rotor parameters with a similar experimental setup as Murata et. al. The study point out as the number of airfoils and the cord length increases also the performance increases. They also show the airfoil angle has an important effect on the flow.

Other then these studies, there are some numerical study on CFF. Numerical studies have both advantages and disadvantages on this subject. Numerical analysis always has the ability investigate many cases more economically and relatively fast. But while studying on a complex system which hasn't been solved entirely, then the method need to be checked with an experimental data.

Gabi and Klemm are the ones who answers this situation firstly by making a study which inspects the CFF both numerically and experimentally. Particle Image Velocimetry (PIV) is used as the experimental method and it is extremely advantages for comparing with computational fluid dynamics (CFD). This study has an importance that it show the reliability of the numerical methods. So after that there is a large number of studies that investigate the CFF and SAC numerically.

As an example of these studies, Seo et. al.'s study on effect of blade angle on the flow characteristics in the vicinity of the diffuser blades of a SAC indoor unit can be considered (Seo, Kim & Kim, 2009). They showed the diffuser blades has an effect on SAC's flow characteristic with a numerical study. Karadeniz et. al. investigated this effect experimentally by using PIV method (Karadeniz, Kumlutaş & Özer, 2011). This study will also be mentioned in the following chapters of this thesis.

Therefore it can be generalized as all the previous studies found in the literature experimentally investigate a component of the SAC separately which necessarily neglects the effects of the other components or investigate the system numerically (some parts or the whole system) which some ideal boundary condition must be made.

The aim of this study is to investigate methods that can determine the velocity profile inside the split air conditioner and measure the temperature distribution within a surrounding that is as similar as possible to the working conditions. At this point the study can be separated into two main issue; velocity measurement and temperature measurement. In both issues the measurement methods have been examined, an optimum method has been chosen and these methods are used for investigating the spilt air conditioner indoor unit.

1.1 History of Air Conditioners Development

In 1758, Benjamin Franklin and John Hadley, professor of chemistry at Cambridge University, conducted an experiment to explore the principle of evaporation as a means to rapidly cool an object. Franklin and Hadley confirmed that evaporation of highly volatile liquids such as alcohol and ether could be used to drive down the temperature of an object past the freezing point of water. They conducted their experiment with the bulb of a mercury thermometer as their object and with a bellows used to "quicken" the evaporation; they lowered the temperature of the thermometer bulb to -14 °C while the ambient temperature was 18 °C. Franklin noted that soon after they passed the freezing point of water (0 °C) a thin film of ice formed on the surface of the thermometer's bulb and that the ice mass was about a quarter inch thick when they stopped the experiment upon reaching -14 °C. In 1820, British scientist and inventor Michael Faraday discovered that compressing and liquefying ammonia could chill air when the liquefied ammonia was allowed to evaporate. In 1842, Florida physician John Gorrie used compressor technology to create ice, which he used to cool air for his patients in his hospital in Apalachicola, Florida. He hoped

eventually to use his ice-making machine to regulate the temperature of buildings. He even envisioned centralized air conditioning that could cool entire cities. Though his prototype leaked and performed irregularly, Gorrie was granted a patent in 1851 for his ice-making machine. His hopes for its success vanished soon afterward when his chief financial backer died; Gorrie did not get the money he needed to develop the machine. According to his biographer Vivian M. Sherlock, he blamed the "Ice King", Frederic Tudor, for his failure, suspecting that Tudor had launched a smear campaign against his invention. Dr. Gorrie died impoverished in 1855 and the idea of air conditioning faded away for 50 years.
(http://en.wikipedia.org/wiki/Air_conditioner)

Early commercial applications of air conditioning were manufactured to cool air for industrial processing rather than personal comfort. In 1902 the first modern electrical air conditioning was invented by Willis Haviland Carrier in Syracuse, New York. Designed to improve manufacturing process control in a printing plant, his invention controlled not only temperature but also humidity. The low heat and humidity were to help maintain consistent paper dimensions and ink alignment. Later Carrier's technology was applied to increase productivity in the workplace, and The Carrier Air Conditioning Company of America was formed to meet rising demand. Over time air conditioning came to be used to improve comfort in homes and automobiles. Residential sales expanded dramatically in the 1950s. In 1906, Stuart W. Cramer of Charlotte, North Carolina, was exploring ways to add moisture to the air in his textile mill. Cramer coined the term "air conditioning", using it in a patent claim he filed that year as an analogue to "water conditioning", then a well-known process for making textiles easier to process. He combined moisture with ventilation to "condition" and change the air in the factories, controlling the humidity so necessary in textile plants. Willis Carrier adopted the term and incorporated it into the name of his company. This evaporation of water in air, to provide a cooling effect, is now known as evaporative cooling.

The first air conditioners and refrigerators employed toxic or flammable gases like ammonia, methyl chloride, and propane, which could result in fatal accidents when

they leaked. Thomas Midgley, Jr. created the first chlorofluorocarbon gas, Freon, in 1928. The refrigerant was much safer for humans but was later found to be harmful to the atmosphere's ozone layer. Freon is a trademark name of DuPont for any chlorofluorocarbon (CFC), hydrogenated CFC (HCFC), or hydro fluorocarbon (HFC) refrigerant, the name of each including a number indicating molecular composition (R-11, R-12, R-22, R-134A). The blend most used in direct-expansion home and building comfort cooling is an HCFC known as R-22. It is to be phased out for use in new equipment by 2010 and completely discontinued by 2020. R-12 was the most common blend used in automobiles in the United States until 1994 when most changed to R-134A. R-11 and R-12 are no longer manufactured in the United.

States, the only source for purchase being the cleaned and purified gas recovered from other air conditioner systems. Several non-ozone depleting refrigerants have been developed as alternatives, including R-410A, known by the brand name Puron. The most common ozone-depleting refrigerants are R-22, R-11, and R-123. Innovation in air conditioning technologies continues, with much recent emphasis placed on energy efficiency and improving indoor air quality. As an alternative to conventional refrigerants, natural alternatives like CO2 (R-744) have been proposed.

1.2 Split Air Conditioners Components and Working Principles

1.2.1 General Working Principles

A heat pump is a machine or device that moves heat from one location (the 'source') at a lower temperature to another location (the 'sink' or 'heat sink') at a higher temperature using mechanical work or a high-temperature heat source (ASHRAE, 2004). Thus a heat pump may be thought of a "heater" if the objective is to warm the heat sink (as when warming the inside of a home on a cold day), or a "refrigerator" if the objective is to cool the heat source (as in the normal operation of a freezer) (Çengel & Boles, 1986). In either case, the operating principles are identical. Heat is moved from a cold place to a warm place.

A split air conditioners are heat pumps and work by a refrigeration circle which can change the working direction. In summer heat is pumped from cooler inside to hotter surrounding so the heat exchangers in the indoor unit works as evaporators and the heat exchangers in outdoor unit works as condensers. In winter the cross valve change position so the system works oppositely therefore the indoor heat exchangers works as condensers and outdoor heat exchangers works as evaporators so heat is pumped to cooler surrounding to warmer inside.

Transferring heat from a cooler place to warmer place is seem to be a violation of the rule of diffusion which tells “the heat always moves a warmer source to cooler one” but in refrigeration circle the heat doesn’t transported by diffusion of the sensible heat. In refrigeration cycle, latent heat is transported by the mass transfer of the refrigerants.

Refrigerants are the working fluids in refrigeration, air- conditioning, and heat-pumping systems. They absorb heat from one area, such as an air-conditioned space, and reject it into another, such as outdoors, usually through evaporation and condensation. These phase changes occur both in absorption and mechanical vapor compression systems, but not in systems operating on a gas cycle using a fluid such as air. The design of the refrigeration equipment depends strongly on the properties of the selected refrigerant (ASHRAE, 2005).

The refrigerants cycle the system involves four main components. These are the compressor, the condenser, the expansion valve and the evaporator. The refrigerant enters the compressor as a vapor and is compressed to the condenser pressure. It leaves the compressor at a relatively high temperature and cools down and condenses as it flows through the coils of the condenser by rejecting heat to the surrounding medium. It then enters a capillary tube where its pressure and temperature drop drastically due to the throttling effect. The low-temperature refrigerant then enters the evaporator, where it evaporates by absorbing heat from the refrigerated space.

The cycle is completed as the refrigerant leaves the evaporator and the reenters the compressor (Çengel & Boles, 2006).

This system is schematically shown on Figure 1.1. The blue lines shows the cycle while the SAC working in the cooling mode and the red lines shows the cycle while the SAC working in the heating mode.

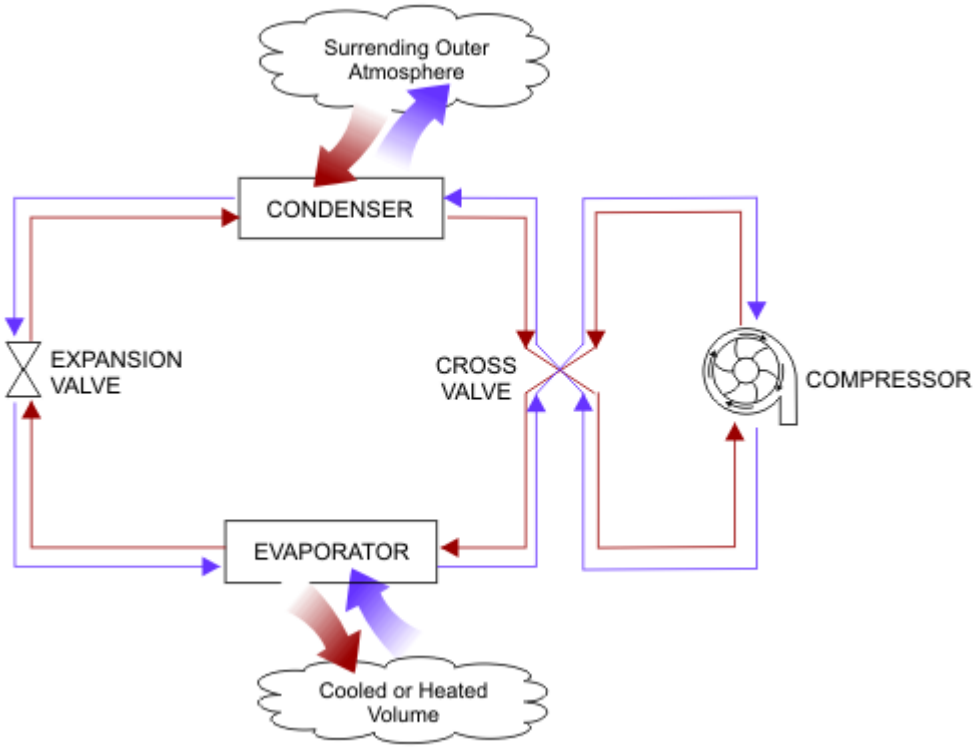

Figure 1.1 Schematic of the SAC.

Figure 1.2 shows the T-s diagram for the ideal vapor-compression refrigeration cycle. There is four thermodynamic process emerge in this cycle: Between point 1-2 Isentropic compression in a compressor, 2-3 Constant-pressure heat rejection in a condenser, 3-4 Throttling in an expansion device, 4-1 Constant-pressure heat absorption in an evaporator.

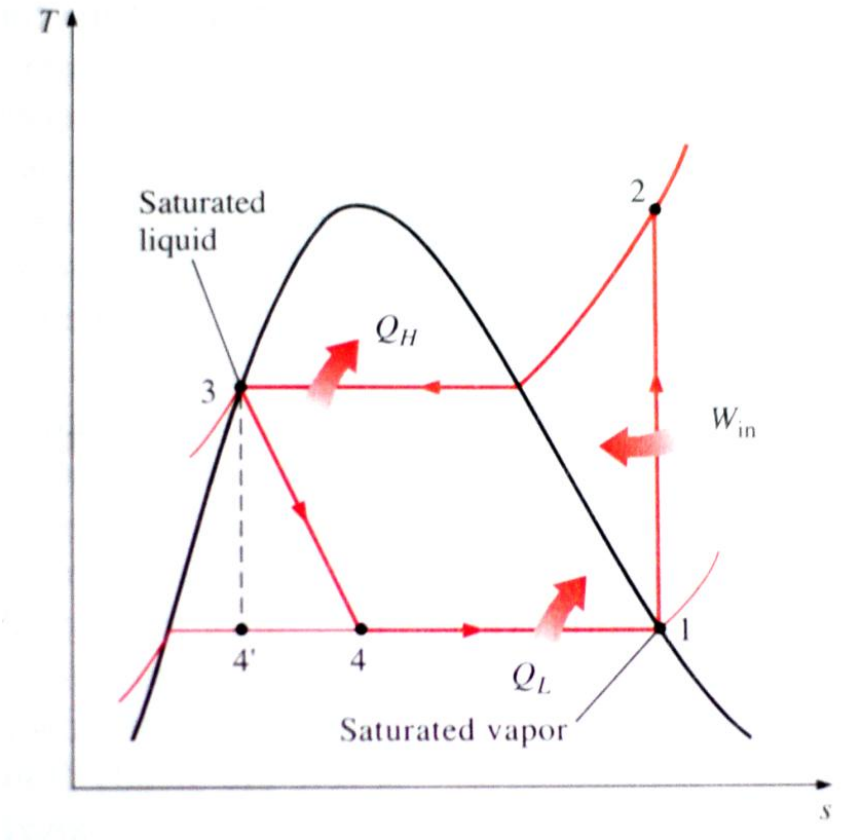

Figure 1.2 T-s diagram for the ideal vapor-compression refrigeration cycle.

The saturated liquid refrigerant at point 3 is throttled to the evaporator pressure by passing it through an expansion valve or capillary tube. The temperature of the refrigerant drops below the temperature of the refrigerated space during this process. The refrigerant enters the evaporator at state 4 as a low-quality saturated mixture, and it completely evaporates by absorbing heat from the refrigerated space. The refrigerant leaves the evaporator as saturated vapor and reenters the compressor, completing the cycle (Çengel & Boles, 2006).

Although the ideal cycle is important for understanding the system, in reality the actual cycle is different than the ideal one (Figure 1.3). In actual cycle the heat transfer to the surrounding medium and pressure drops by the fluid friction causes the irreversibilities so the performance of the system drops.

In the ideal cycle, it is assumed that the refrigerant leaves the evaporator and enters the compressor as saturated vapor but in reality generally it does not happens because of the difficulty to control the state of a substance that absolutely. Therefore system design that refrigerant slightly superheat at the compressor. This guaranties no liquid would enter the compressor. There are also heat gains and pressure drops along the pipes which increase the specific volume, this affects the compressor performance negatively because steady-flow work is proportional to the specific volume.

The compression process in the ideal cycle is internally reversible and adiabatic, and thus isentropic. The actual compression process, however, involves frictional effects, which increase the entropy, and heat transfer, which may increase or decrease the entropy, depending on the direction. Therefore, the entropy of the refrigerant may increase (process t-2) or decrease (process 1-2') during an actual compression process, depending on which effects dominate. The compression process 1-2' may be even more desirable than the isentropic compression process since the specific volume of the refrigerant and thus the work input requirement are smaller in this case. Therefore, the refrigerant should be cooled during the compression process whenever it is practical and economical to do so (Çengel & Boles, 2006).

In ideal cycle, it is also assumed that the satured liquid leave the condenser at the compressor exit pressure however in practice there will be some pressure drops in the condenser. So this time, the system will be design to overcool to prevent liquid at the throttling valve. However this situation is not critical as the others because if the refrigerant enters the evaporator with a lower enthalpy and thus can absorb more heat from the cooled medium. The pressure drop is also nearly negligible because the throttling valve and the evaporator are usually located very close to each other.

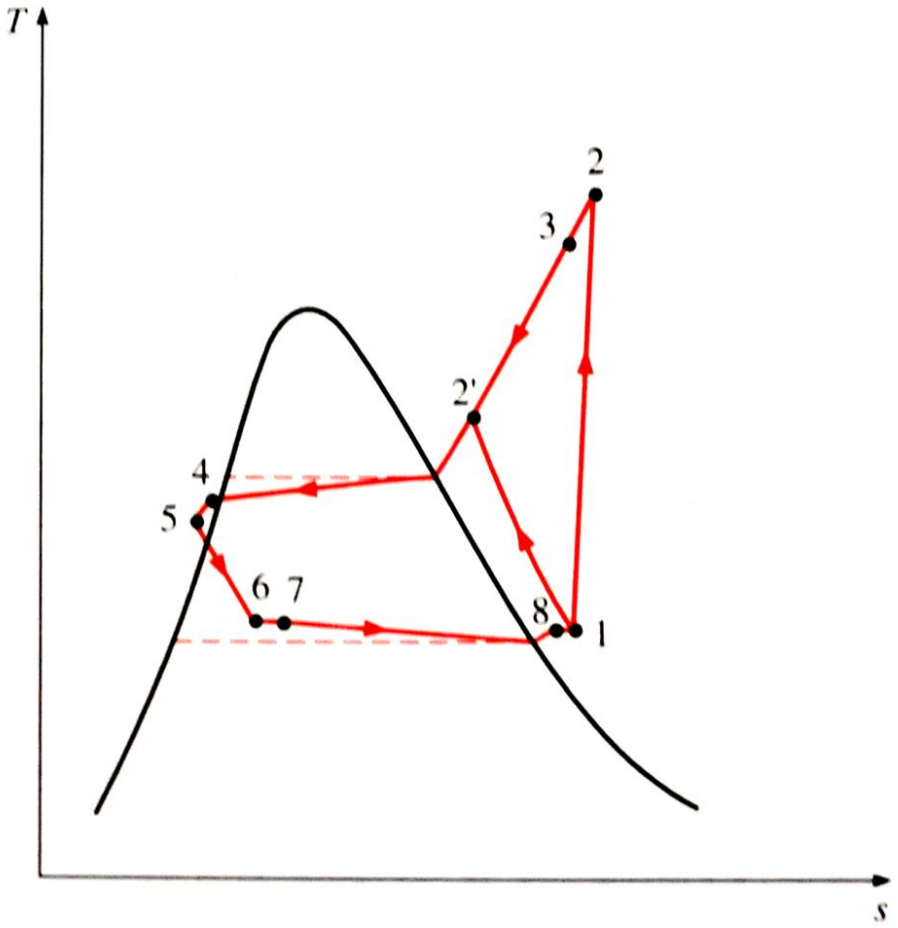

Figure 1.3 T-s diagram for the actual vapor-compression refrigeration cycle.

1.2.2 Working Principles of Split Air Conditioner Indoor Unit

The basic concept of the SAC's indoor unit same as the outdoor unit which is the refrigerant fluid came and change phase inside of the heat exchanger while the air is driven by a mechanical fan on the heat exchanger so heat transfer take place between the surface of the heat exchanger and air more efficiently then the air leaves the unit. Although this is also the same principle of as the outdoor unit, they cannot be designed as the same because they have totally different constraints.

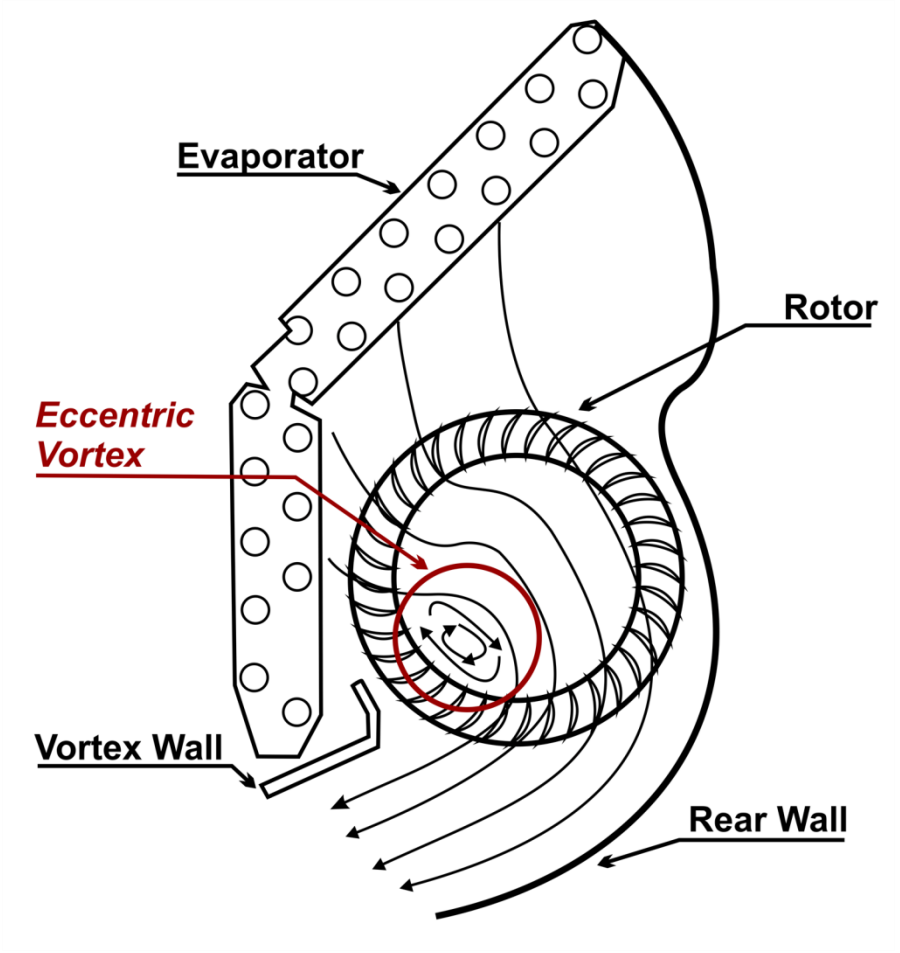

Figure 1.4 Inside structure and components of a SAC indoor unit.

The indoor unit design must be reasonably small for esthetical needs because will be placed in the household and also the air velocity at the exit of the unit must satisfy the comfort conditions. In this situation CFF is a more suitable choice because more compact systems can be design.

The CFF drives the air by the eccentric vortex. As the rotor blades passes near the vortex wall the flow passes an extremely narrow section between the blade and the vortex wall. This causes a huge increment on the flow velocity and decrement on the static pressure as Daniel Bernoulli suggested (White, 1999).

So a low pressure area occurs on the around the vortex wall and the rotor blades near it which changes position (seem) randomly as the blades pass by near the vortex wall. The air is sucked to this low pressure area this creates the eccentric vortex

(Figure 1.4) and also creates the air flow that is driven by the fan. The flow pattern is effected by the rotor parameters (such as number of blades, angle of blades, the diameter of the rotor…etc.), rear wall geometry and the vortex wall geometry. In Figure 1.5 stream lines of a CFF is shown which is introduced by Eck (1973).

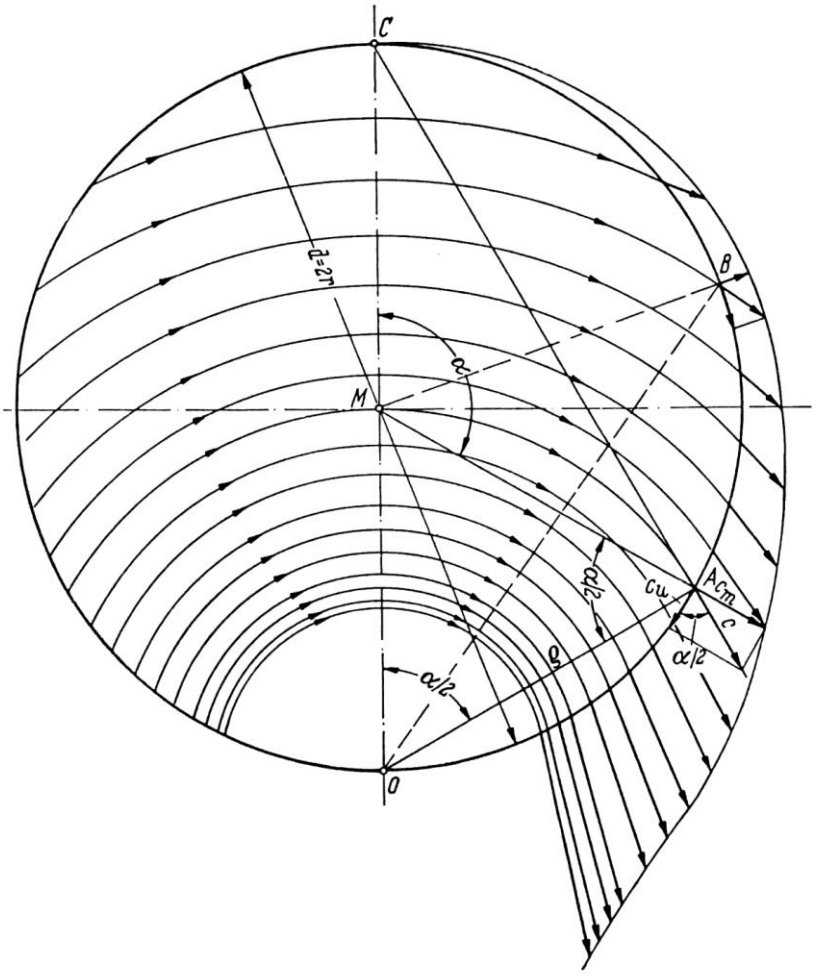

Figure 1.5 Stream lines inside of a CFF (Eck, 1973)

Therefore it can be said the location and the geometry of the CFF, rear wall and vortex wall is very critical for a stable and efficient flow. Another important design parameter is location of the heat exchangers. The heat exchangers must be placed according to the flow profile created by the CFF. If the flow does not pass the heat exchanger properly the heat transfer and the efficiency of the heat exchanger will drop dramatically. In some situation in this study, non-flow interacted coils are removed because they had no effect on the heat transfers.

1.3 Economical Conditions of Split Air Conditioner Market of Turkey

Because of these advantages of the system, as the new companies join the air conditioning sector every year, split air conditioner production also grow in the number, is shown in Figure 1.5. In 2006 there was 61 company that producing air conditioner in Turkey. There is a great leap in the number in 2007, the number of the companies became 70 with an increase of 16.7%. In 2008 only two new companies entered the sector while the economic crisis has shown its signs. Inspite of the crisis hit the world economy and the sector in 2009, only 4 companies left the sector in 2009 and 2010.

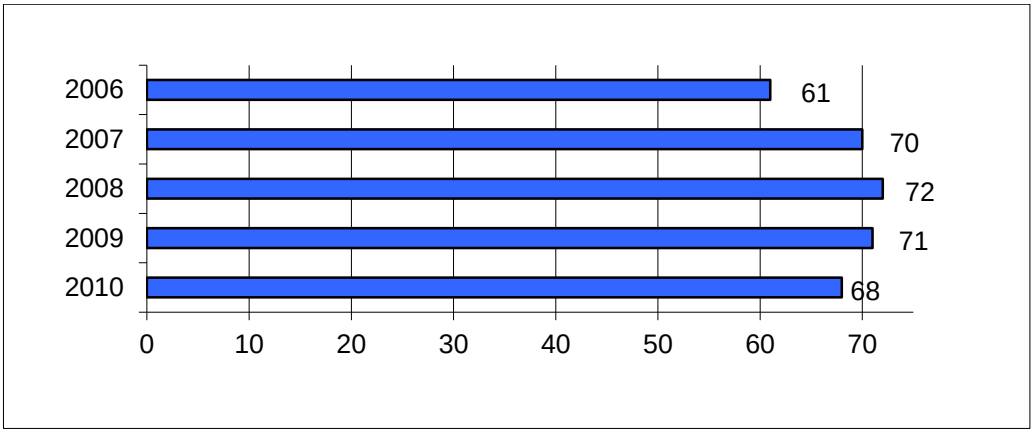

Figure 1.6 Numbers of companies in air conditioner sector between 2006 and 2010

It can be seen in Figure 1.6, 1.7, and 1.8 that till 2008 the sales increased rapidly. In 2006 the total sales were 1,616,449 and 78.51 % of it was local sales and 1,025,966 of this number were produced in Turkey. The following years 2007 and 2008 the production rise 28.83 % and 26.02 % therefore the production became 1,665,665 with an increment 61.59 %. In these three years while the split air conditioner indoor unit imports lessen to 461,112 from 647,705 with a decrement of 28.80 %, the exports advanced dramatically from 347,232 to 981,588 with an increment of 282.69 %. Thus it can be said that split air conditioner sector grow strong and has a positive effect on income of Turkey until the economic crisis in 2009.

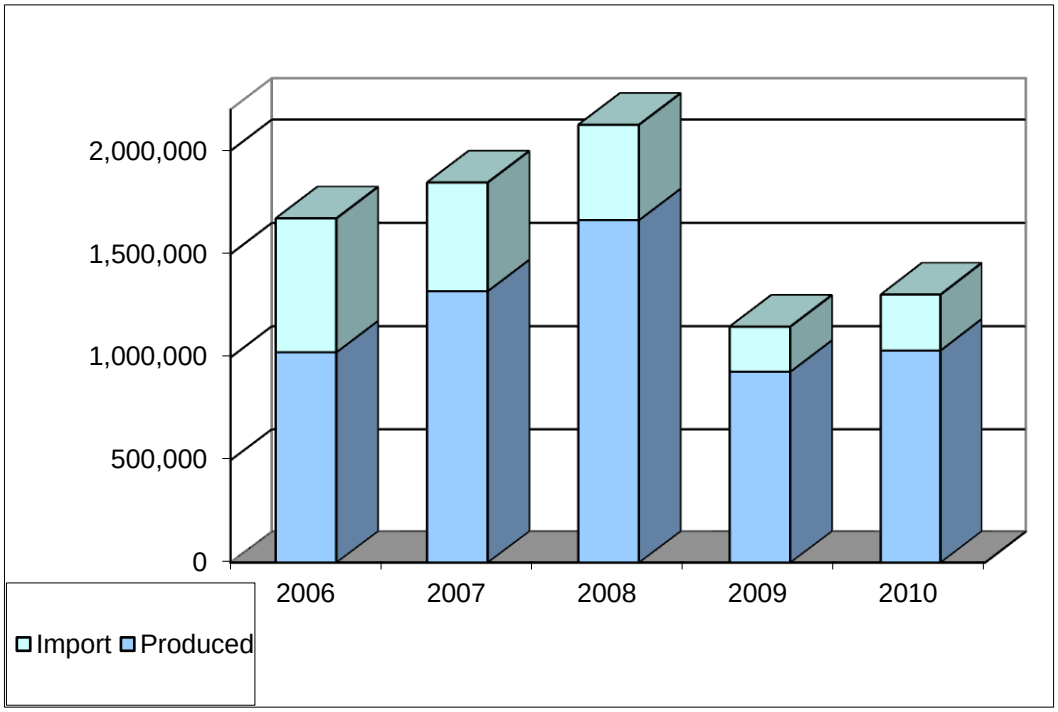

Figure 1.7 Numbers of imported and produced SAC indoor unit by Turkey.

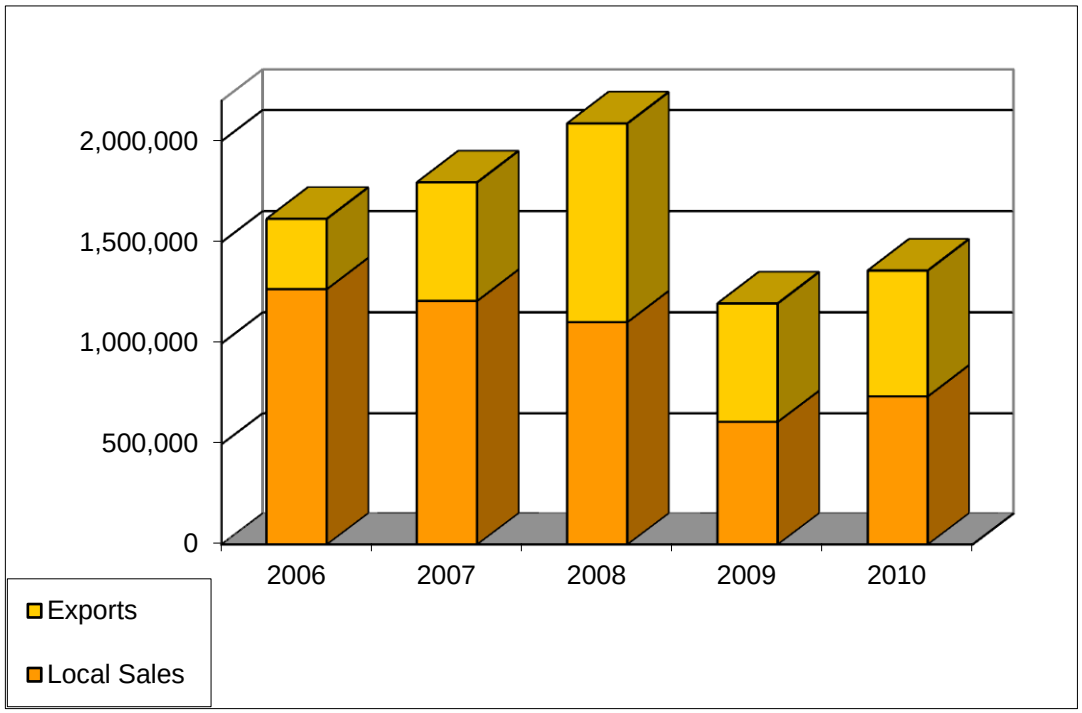

Figure 1.8 Numbers of exports and local sales SAC indoor unit by Turkey.

In 2009, the total sales dropped to 1,149,858 from 2,126,777; exports decreased 40.28 % and local sales decreased 44.66 %. This huge fall slightly covered in 2010 with an increment in exports 6.5 % and in local sales 20.71% but compared to 2008 the sales is still 38.64 % down in 2010.(Table 1.1 and Figure 1.6)

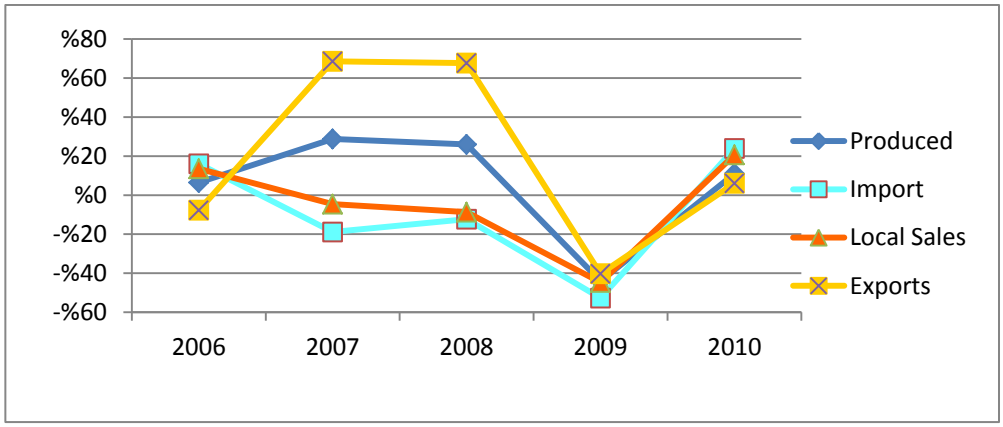

Figure 1.9 Relative Change in Sales of SAC Indoor Unit.

Although the economical crisis crushed the split air conditioner market, split air conditioners still used widely in the world, especially in the tropic, sub-tropic and Mediterranean climate areas where in summer cooling is important and in winter there isn't a strong heat loss occurred.

Table 1.1 Numbers of SAC that sold by Turkey.

		Produced	Import	Local Sales	Exports
Split Air Conditioners (indoor units)	**2006**	1.025.966	647.705	1.269.217	347.232
	2007	1.321.779	525.638	1.211.230	585.323
	2008	1.665.665	461.112	1.106.357	981.588
	2009	931.804	218.053	612.220	586.247
	2010	1.034.608	270.357	739.001	621.693

….Especially capitals and urbanized areas in hot parts of the world where most of the population lives in small high-rise flats mostly uses Japanese-made domestic air conditioners are usually window or split types, the latter being

more modern and expensive. In Israel, virtually all residential systems are split types. In Europe, home air conditioning is generally less common. Southern European countries such as Greece have seen a wide proliferation of home air-conditioning units in recent years. In another southern European country, Malta, it is estimated that around 55 % of households have an air conditioner installed. (http://en.wikipedia.org/wiki/Air_conditioner).

Therefore as the world economy recovers, Turkey has to reclaim the market that was lost at the time of crisis and even there is an opportunity to enlarge the market share. Producing more efficient and economical split air conditioners are definitely increase the probability of fulfilling this opportunity.

1.4 Motivation

This thesis is supported by SAN-TEZ project which has the aim of solving a company's research and development problem by the aid of university. In this project our goal was to enhance the performance of split air conditioners and its development methods.

For achieving "the enhancing the performance of a split air conditioner", using a better refregerent, increasing efficiency of the compressor or the other thermodynamic devices is always a trivial solution. This approach could not be used in current situation because of the company does not produce the thermodynamic components like expansion valve or compressor. So this kind of approach would mean just buying more expensive components and this would increase the production costs which will also affect the selling price of the products. On the other hand the company produces its own indoor unit body and heat exchangers. The enhancements on these components will not increase the costs dramatically but can affect the performance strongly, even may upgrade the energy class.

So directing the R&D sources on developing aerodynamics of the body, is a more affordable and more advantageous decision. To completing this task, the velocity and the temperature distribution is needed to be known. By having access to such a knowledge the problems in the system can be identified more quickly and also these data can be used as inputs or control data for CFD studies.

CHAPTER TWO
MEASUREMENT METHODS

In this chapter velocity and temperature measurement methods that can be used in SAC indoor unit will be investigated. In first part the alternative methods will be compared the optimum method will be determined. In the following parts of this chapter, the determined experimental methods and the experimental setups that are used in this study will be introduced in details.

2.1 A General View on Velocity Measurement Methods

In the preliminary study stage of a study, one of the most important subjects is choosing the right experimental method that can be used practically and satisfied the project's requirements. For making the right decision the needed specs of the system is determined then the importance of that spec defined for final decision.

One of the most important spec is interrogation area, the measured dimension in space. The conventional measurement method like using probe generally measures a location can be called a point where there are more advanced measurement methods that can measure velocity from a whole area and even a volume. For investigating such system which every component effect the other the widest area that is inspected at once is better. Otherwise a scanning process will be need which would mean only average data will be obtain and no instantaneous data can be used. For investigating a flow field at least an area will be more advantages then point-measurement methods.

Another important spec is accessibility inside of the system. SAC indoor unit geometry is nearly a closed box, so the measurement method needs to have the ability to acquire data in that medium.

The other criteria is having a practical usage because the project that supported this thesis also aims to improve the company's research and development process so the experimental setup that is build will used by the company after the project is

over. At this situation experiment system must not be dependent to the users experience and it would be better if the system is easy to use.

The final criteria is naturally economical value because although the project has a pretty large funding according to Turkey's economical conditions it has its limits.

For propose of answering all of these needs, recently available velocity measurement methods are inspected.

2.1.1 Constant Temperature Anemometry and Other Probe Used Methods

These method measure the velocity on a local position where a measurement extension device called probe is placed. Probe is connected to a data logger or a computer with an ability to record input data. The probe generally sends input data as electricity currency. Some experimental setup includes software which interprets the electricity data to velocity.

Figure 2.1 Air velocity probe (www.olmega.com)

There are two types of velocity measurement probe in general. One type has a fan which turns as the air passes through inside. These ones are very easy to use and do not need extra calibration about air temperature. In Figure 2.1 an air velocity

measurement probe with a fan and its data acquisition device is shown. The disadvantages of this system are they can only measure velocity in one direction and the result changes as the user changes the position of the probe. So the results are highly dependent to the user and sometimes even the same user may measure different values from the same setup because of the misuse.

The other type is known as constant temperature anemometry or hot-wires anemometry and it is a more advanced measurement system.

2.1.1.1 Constant Temperature Anemometry Working Principles

CTA measures velocity or temperature on spot. Working principle is based on convectional heat transfer which can be explained as cooling effect of a flow on a heated body (Figure 2.2). Convective heat transfer Q from a wire is a function of the velocity U, the temperature difference between the fluid and the wire T_∞-T_0 and the physical properties of the fluid. Therefore in the experiment the fluid's physical properties must be known and the system must be calibrated according to this data. The heat loss is measured by a Wheatstone bridge.

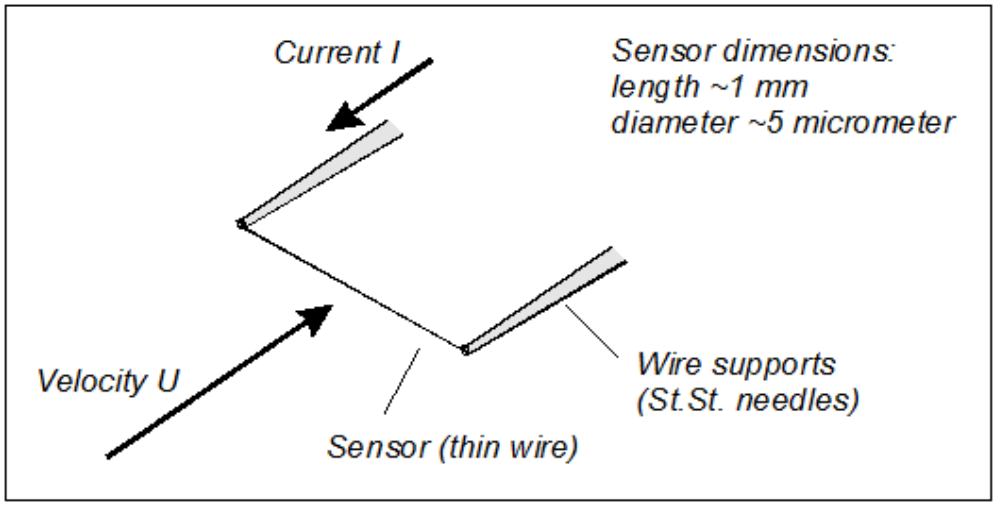

Figure 2.2 One dimensional CTA probe (http://www.dantecdynamics.com/)

The wire R_w is connected to one arm of the Wheatstone bridge and heated by a current. A servo amplifier keeps the bridge in balance by controlling the current to

the sensor so that the resistance – and hence the temperature- is kept constant, independent of the cooling imposed by the fluid. The bridge voltage, E, represents the heat transfer and is thus a direct measure of the velocity. A probe which has three wire can also measure three dimensional velocity (Figure 2.3).

The combination of the sensors low thermal inertia and the high gain of the servo loop amplifier give a very fast response to fluctuations in the flow.Therefore if the system has a strong data acquisition system then a very high temporal resolution data can be obtained.

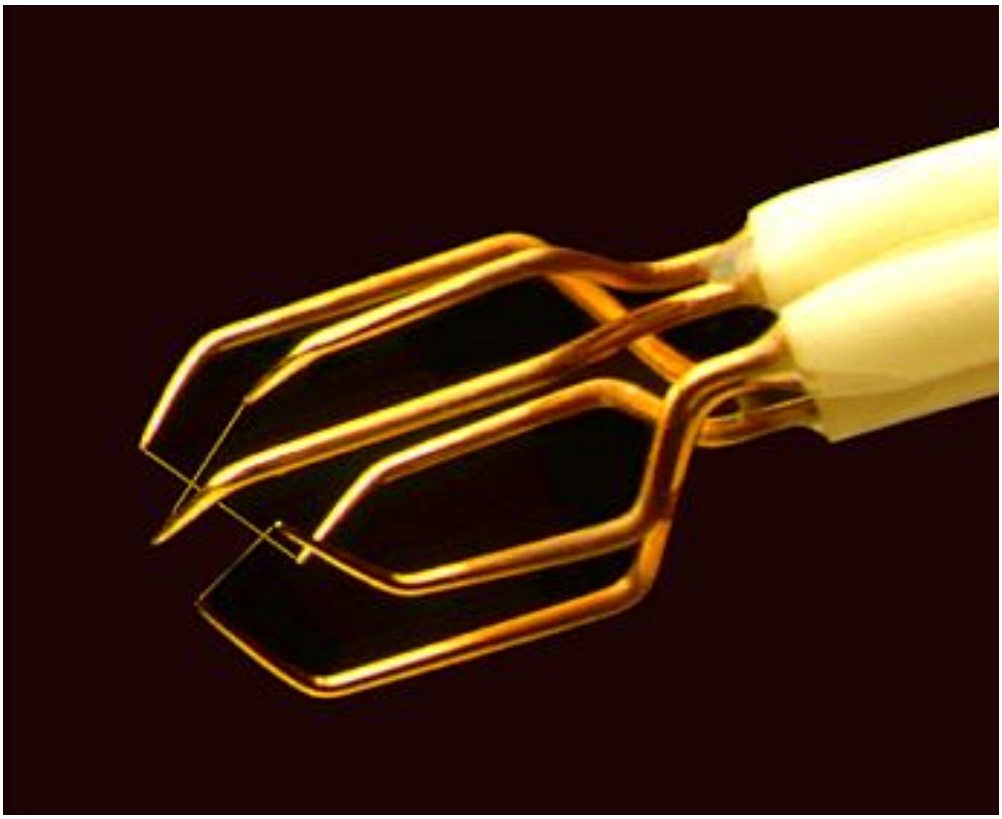

Figure 2.3 Three dimensional CTA probe (http://www.dantecdynamics.com/)

2.1.1.1.1 The Wheatstone bridge. The Wheatstone bridge (Figure 2.4) illustrates the concept of a difference measurement, which can be extremely accurate. Variations on the Wheatstone bridge can be used to measure capacitance, inductance, impedance and other quantities, such as the amount of combustible gases in a sample, with an explosimeter. The Kelvin Bridge was specially adapted from the

Wheatstone bridge for measuring very low resistances. In many cases, the significance of measuring the unknown resistance is related to measuring the impact of some physical phenomenon - such as force, temperature, pressure, etc. - which thereby allows the use of Wheatstone bridge in measuring those elements indirectly. The concept was extended to alternating current measurements by James Clerk Maxwell in 1865 and further improved by Alan Blumlein in about 1926.

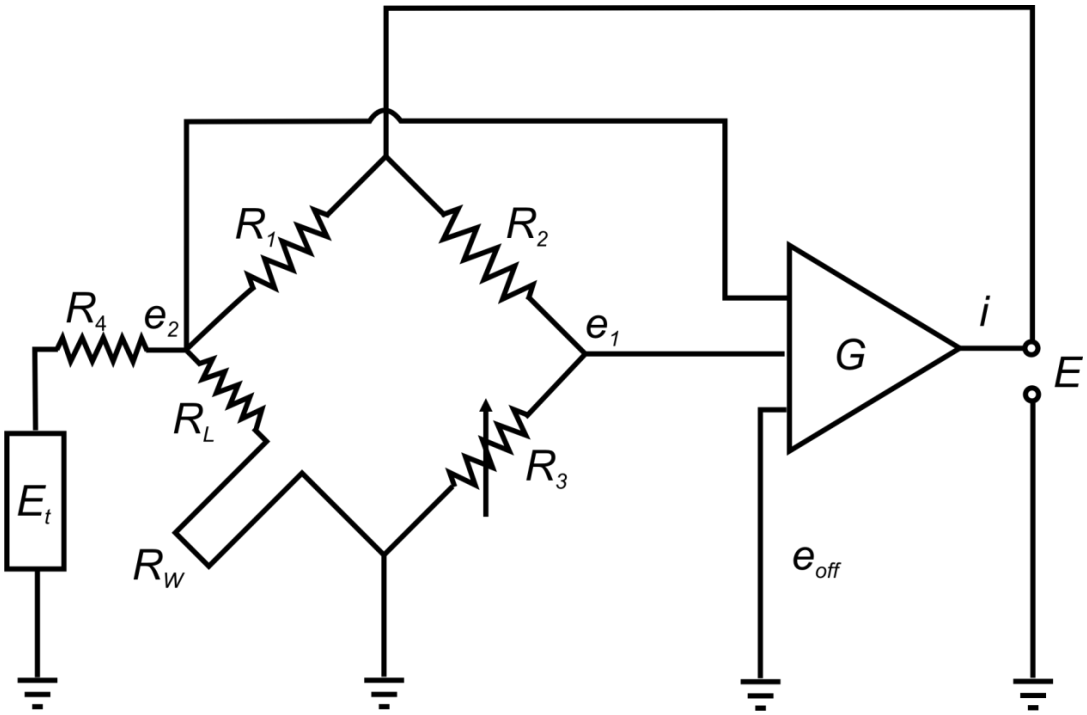

Figure 2.4 The Wheatstone bridge schematics.

2.1.1.2 Final Evaluation of CTA and the Other Probe Using Methods

These methods are least satisfying the needs of this study. The main of this study is to obtain a velocity profile. For this purpose a scanning process is need which will be done by a computer controlled traverse or a user. The user method is not suitable for obtaining a flow field because any move of the user hand will affect the results. The other alternative, computer controlled traverse is nearly as expensive as state of art optical methods which are seem to have more advantage.

Another way to obtain a velocity profile is placing more than one probe in the interrogation area so the scanning won't be needed. But these methods are intrusive so there is a possibility that the prior placed probes will change the flow pattern and mislead the other probes data at the high flow speeds.

However these methods still have the advantage of being easy to use and also these are the classical methods that their reliability is proved in so many studies. Therefore these methods didn't used as the main measurement methods, these conventional methods used for fast inspection of the SAC.

2.1.2 Laser Doppler Anemometry (LDA)

LDA is an optical measurement method based on Doppler Effect and like all optical measurement method LDA is non-intrusive method which means no probe or other equipment used inside the measurement area.

For LDA measurement, first of all the flow must be seeded with tracer particles. Therefore it can be said that LDA is an indirect measurement method which means it does not measure the velocity of the fluid directly but it measures the tracer particles velocity. So the tracer particles must be chosen carefully to be fully coherent with the flow.

LDA systems include a special laser probe which sends laser beams to the point where the velocity measurement planed (Figure 2.5). These beams carefully calibrated and focused to that interrogation point. While the tracer particles pass through this interrogation point they reflect the laser beams back with the Doppler Effect and these beams collected with photoreceptors. The data obtained from photoreceptors instantaneously processed in a computer and velocity measurement can be seen instantly.

LDA system also has the ability to measure three dimensional velocity data but for this purpose more laser beam must be calibrated to the interrogation point and

more than one laser output device needed. In LDA process fiber optic cables used to transfer laser beams to laser output device so one laser can provide the beams needed.

There are three main downsides of this system. First of all the measurement take place only if the tracer particle passes through the interrogation point so there is no fixed temporal resolution.

The second disadvantage of this system is same as the CTA or other probe used method. The system only measures velocity on a point so to obtain a velocity profile this method also need a scanning process.

Figure 2.5 LDA laser (http://www.dantecdynamics.com/)

The last downside of this system is the calibration process needs experience and it makes the system hard to use. Although lately new LDA systems designed which do not need calibration, at the time of beginning of this study these solutions were not available.

2.1.2.1 Doppler Effect

The Doppler effect (or Doppler shift), named after Austrian physicist Christian Doppler who proposed it in 1842 in Prague, is the change in frequency of a wave for an observer moving relative to the source of the wave. It is commonly heard when a vehicle sounding a siren or horn approaches, passes, and recedes from an observer. The received frequency is higher (compared to the emitted frequency) during the approach, it is identical at the instant of passing by, and it is lower during the recession. (http://en.wikipedia.org/wiki/Doppler_effect)

The relative changes in frequency can be explained as follows. When the source of the waves is moving toward the observer, each successive wave crest is emitted from a position closer to the observer than the previous wave. Therefore each wave takes slightly less time to reach the observer than the previous wave. Therefore the time between the arrivals of successive wave crests at the observer is reduced, causing an increase in the frequency. While they are traveling, the distance between successive wave fronts is reduced; so the waves "bunch together". Conversely, if the source of waves is moving away from the observer, each wave is emitted from a position farther from the observer than the previous wave, so the arrival time between successive waves is increased, reducing the frequency. The distance between successive wave fronts is increased, so the waves "spread out" (Figure 2.6).

For waves that propagate in a medium, such as sound waves, the velocity of the observer and of the source is relative to the medium in which the waves are transmitted. The total Doppler Effect may therefore result from motion of the source, motion of the observer, or motion of the medium. Each of these effects is analyzed separately. For waves which do not require a medium, such as light or gravity in general relativity, only the relative difference in velocity between the observer and the source needs to be considered.

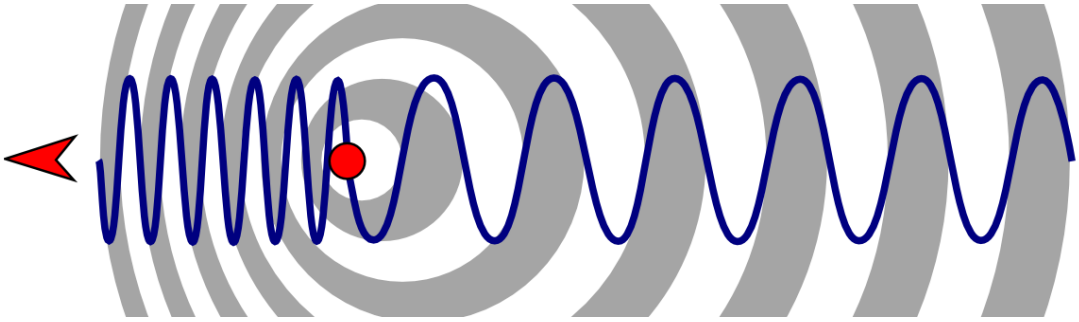

Figure 2.6 Schematic presentation of the Doppler Effect (http://en.wikipedia.org/wiki/Doppler_effect)

2.1.2.2 Final Evaluation of LDA

LDA method's success in aerodynamics is well-known especially detecting aerodynamic error. However the need of sending multiple laser beams to the interrogation point makes very hard to investigate a closed volume. Therefore the system is not suitable for fully investigating the SAC indoor unit. Beside that as a point measurement method a scanning process would be needed and no instantaneous velocity profile can be obtained with this system.

From these aspects the LDA method could not fulfill the needs for investigating the velocity profile of SAC indoor unit.

2.1.3 Particle Image Velocimetry (PIV) and Particle Tracking Velocimetry (PTV)

PIV is a flow visualization method however it has the ability to make both qualitative and quantitative unlike other flow visualization methods like dye injection which can only gives qualitative results. As all visualization methods and LDA, PIV is also a non-intrusive method. This allows the use of PIV in high-speed flows with shocks or in boundary layers close to the wall, where the flow may be disturbed by the presence of the probes.

In PIV application the flow is also seeded with the tracer particles like the LDA method and it can be also said that PIV is also an indirect measurement method which means it does not measure the velocity of the fluid directly but it measures the

tracer particles velocity. So the tracer particles must be chosen carefully to be fully coherent with the flow.

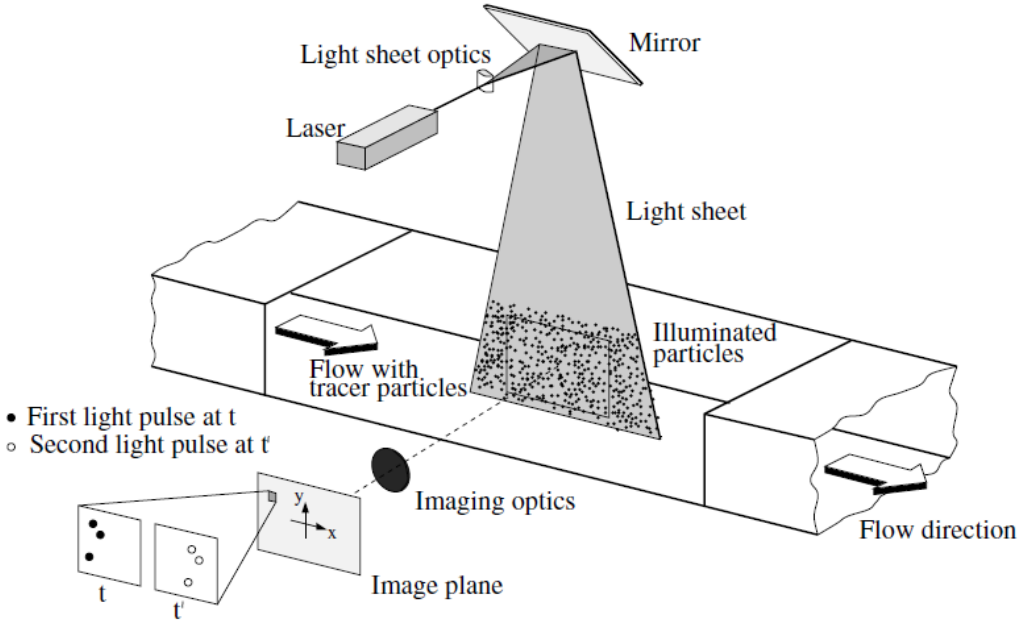

Figure 2.7 An experimental arrangement of PIV in a wind tunnel (Raffel, Willert, Wereley, Kompenhans, 2007).

While these particles passing through the interrogation area their two (or more) images are captured consecutively by high speed camera. A short time passes between the two images and at that time the tracer particles moves (Figure 2.7). Therefore the tracer particle has different location in these two images. When the displacement between these two measured and it is divided to the time between two images shot, the velocity of the tracer particle has been found out. PIV and PTV methods uses the same equipments and they have only slight differences in application. In PIV tracer particles location determined in groups in PTV every tracer particle followed alone. So PIV gives more information about the whole flow field because a denser seeding can be used which will cover the entire flow field.

This is the most important advantage of PIV. In one measurement the whole interrogation area is inspected so instantaneous flow structures also can be studied.

Beyond that there is a technique called endoscopic PIV which grants the ability to study in closed system. Although some opening will be need to send the light sheet

to the interrogation area, one opening will be enough unlike the other measurement methods.

As a final evaluation, PIV has the advantage of being a non-intrusive and whole field measurement method with an ability to investigate closed systems, therefore the PIV method has been the most suitable method among the resent velocity measurement methods for the investigation of the SAC indoor unit.

2.2 Particle Image Velocimetry (PIV)

2.2.1 History of PIV

Fluids' chaotic motion is always an interest subject to watch for human beings. It is hard to resist watching the lissome movements of a smoke of a fire or roaring rough movements of a sea. Leonardo da Vinci (lived between 1452-1519) who was the Italian Renaissance painter, sculptor, architect, engineer, scientist and mathematician, was the first one tried to visualize the structures of this phenomena. At first he drew several sketches of the flowing water and he captured the flow pattern very sharply (Figure 2.8). Later he even studied cardiovascular system and perfectly drew the aortic valve vortices (Figure 2.9).

> In this respect, Leonardo believed in flow visualization as an important tool for discovery and exploration, and he masterfully followed this principle in his studies of heart valves. We believe there is strong evidence to suggest that Leonardo used his simple glass model to simulate flow dynamics inside the aortic root, he conducted the first scientific flow visualization in the history of science about 400 years ahead of Osborn Reynolds' celebrated pipe flow visualization studies. (Gharib, Kremers , Koochesfahani & Kemp, 2002)

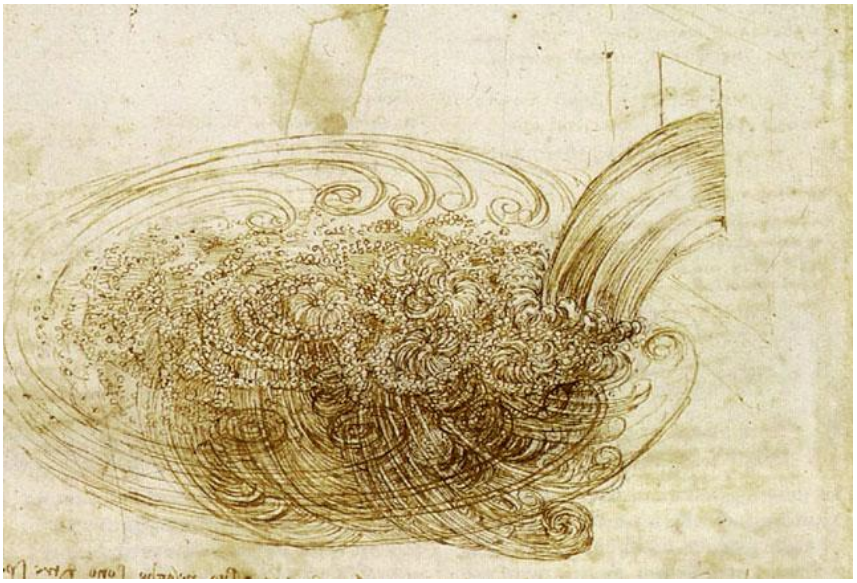

Figure 2.8 Leonardo da Vinci's "a free water jet issuing from a square hole into a pool" (Gad-el-Hak, 2000)

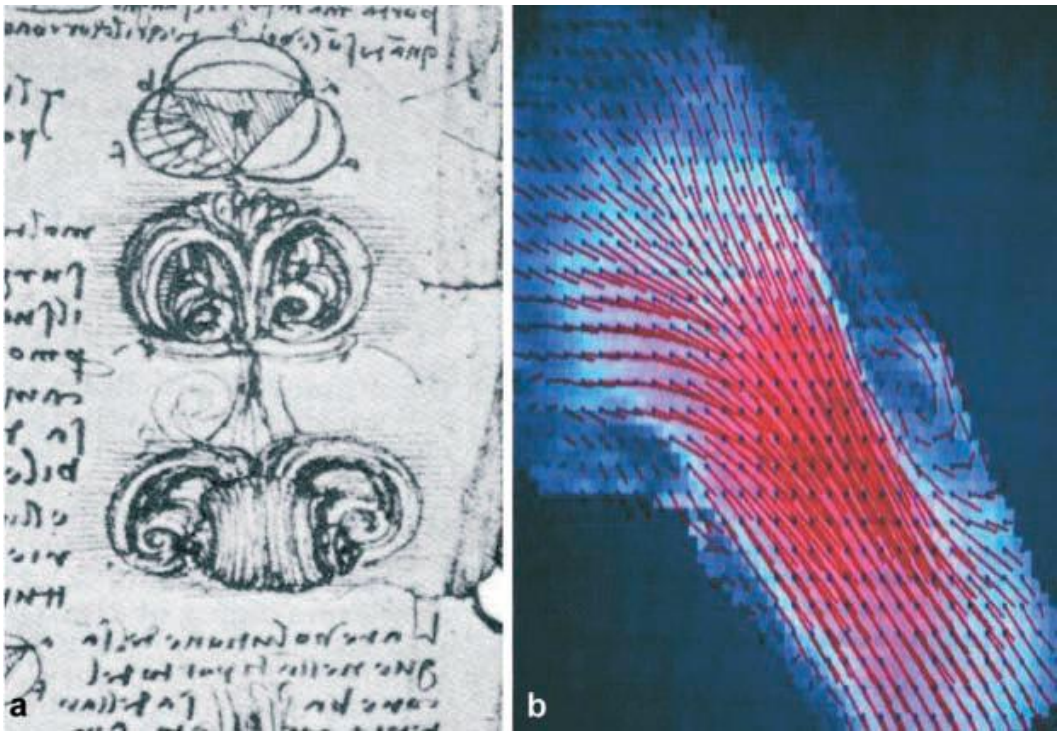

Figure 2.9 Leonardo da Vinci's the aortic valve vortices drawing compared with an MRI data (Gharib, Kremers , Koochesfahani & Kemp, 2002)

Decades after the studies of Leonardo da Vinci, in 20th century Ludwig Prandtl (Figure 2.10) used the method of adding particles or objects to a fluid in order to

observe its flow in a more systematic manner and made very important studies on flow characterization.

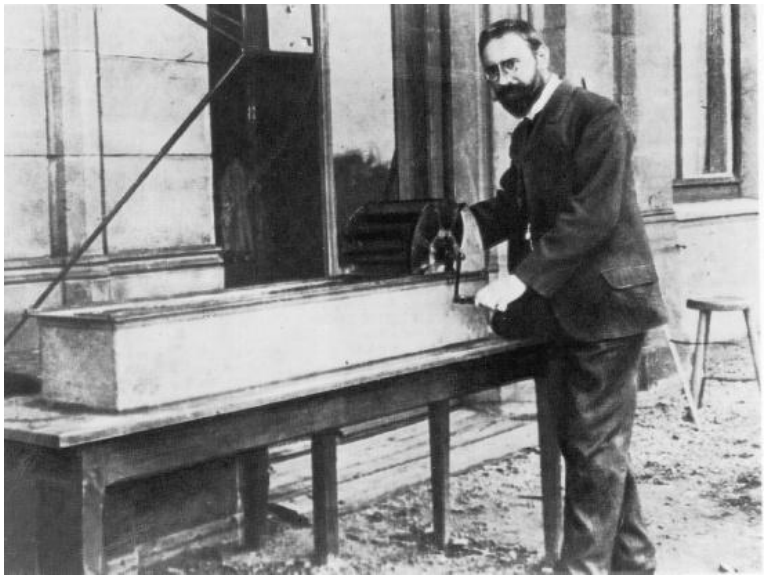

Figure 2.10 Ludwig Prandtl is standing in front of his water tunnel for flow visualization in 1904 (Raffel, Willert, Wereley, Kompenhans, 2007).

Prandtl built a water tunnel for studying steady and unsteady flows by adding mica particles to visualize the flow (Figure 2.11). He investigated two dimensional models like square, circles…etc. and gathered important knowledge about their flow structures.

Although the studies of da Vinci is far beyond his era and Prandtl has made very important studies on aerodynamics, there is a flaw which is their works only gives qualitative information about the flow structure so in some circumstances it will not be enough for a system design.

As the need of quantitative measurement raised, LDA came forward as the first laser used low measurement system. It was able to obtain all of a fluid's velocity measurements at a specific point; it can be considered the 2-dimensional PIV's immediate predecessor.

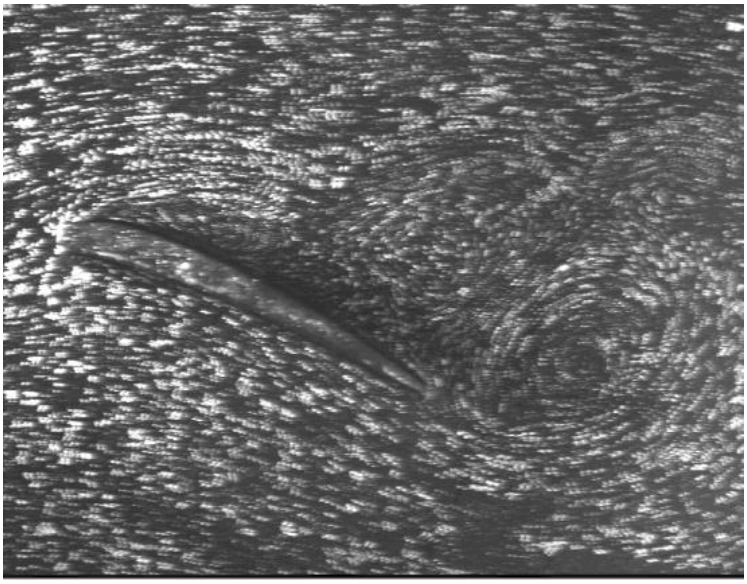

Figure 2.11 Separated flow behind wing, visualized with modern equipment in a replica of Ludwig Prandtl's tunnel. (Raffel, Willert, Wereley, Kompenhans, 2007).

The most rudimentary form of PIV could probably be traced far back in history to the first time a person possessing the concept of velocity watched small debris moving on the surface of a flowing stream. For example, Figure 2.12 shows algae floating on the waters of a moat in the backs of Trinity College, Cambridge, UK. It is almost inconceivable that a great intellect like Isaac Newton would not have observed the moving patterns and seen the potential for visualizing and even measuring the surface velocity from the displacements of the particles of algae. From this viewpoint, particle velocimetry is old and very simple. However, in its modern form, PIV means the accurate, quantitative measurement of fluid velocity vectors at a very large number of points simultaneously, and we now understand that this is, indeed, a very challenging, complicated, and relatively recent achievement (Adrian, 2005).

PIV itself found its roots in Laser speckle velocimetry, a technique that several groups began experimenting with in the late 1970s. In the early 1980s it was found that it was advantageous to decrease the particle concentration down to levels where individual particles could be observed. At these particle densities it was further noticed that it was easier to study the flows if they were split into many very small

'interrogation' areas, that could be analyzed individually to generate one velocity for each area. The images were usually recorded using analog cameras and needed immense amount of computing power to be analyzed.

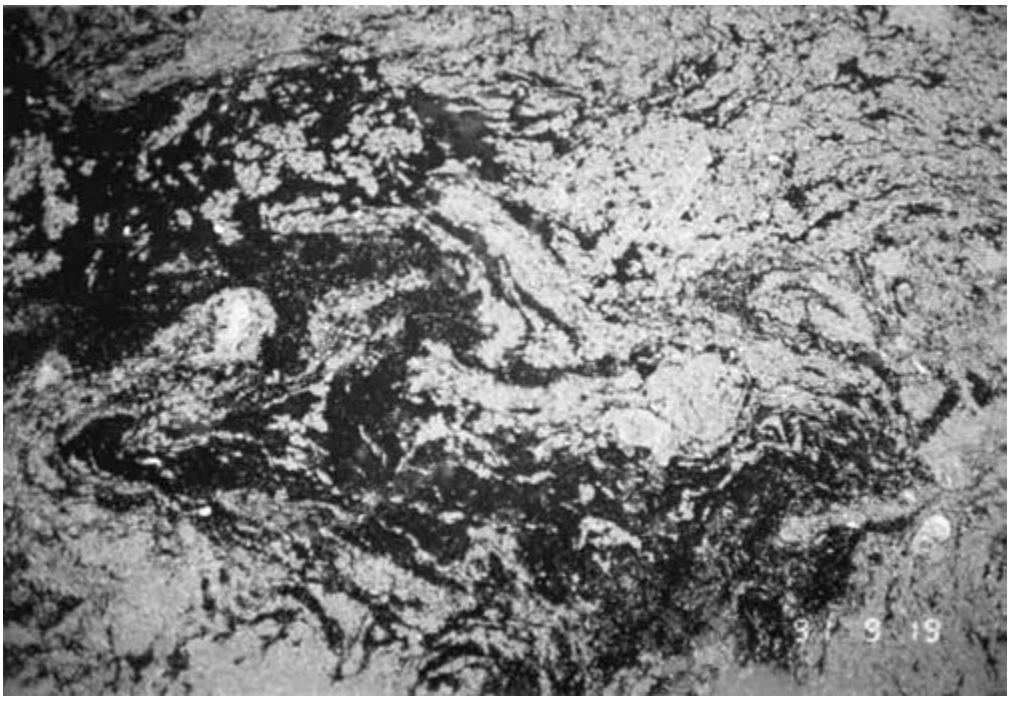

Figure 2.12 Algae floating on the surface of water serve as flow markers for elementary particle image velocimetry. (Adrean, 2005)

With the increasing power of computers and widespread use of CCD cameras it became tempting to do everything digitally. The implication of doing so was analyzed during 1990s and over time digital PIV became increasingly common, to the point that it today totally dominates.

Today PIV is a very reliable experiment system which advances rapidly. Figure 2.13 shows the PIV experiment of Prandlt's experiment shown in Figure 2.11. Although this experiment is a great improvement compared to the original experiment, it shows little about PIV's resent capabilities. Today even volumetric PIV measurement techniques come forward.

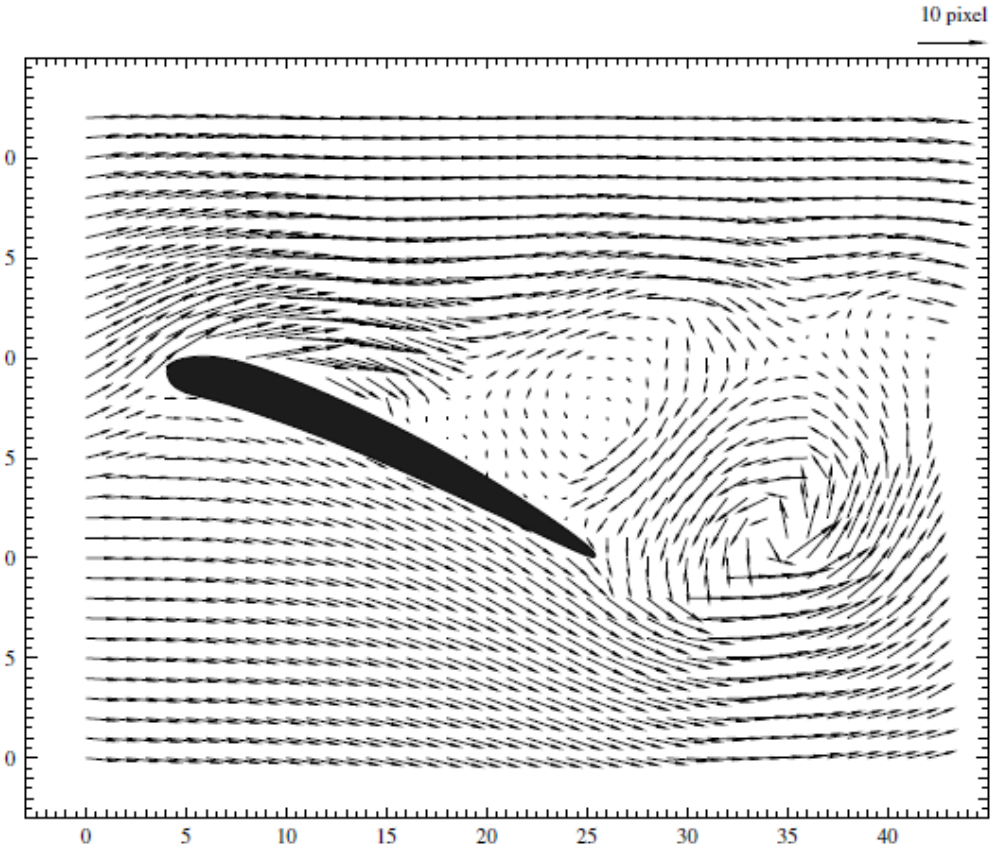

Figure 2.13 Vector map of instantaneous velocity field corresponding to 2.11 (Raffel, Willert, Wereley, Kompenhans, 2007).

2.2.2 Methodology of PIV

PIV is a special flow visualization method which can be used both qualitative and quantitative measurement. For succeeding this purpose, flow is seeded with tracer particles that can move by coherently with the flow and can reflect light.

While these particles pass the area of interest, they are illuminated with a high power light source (generally a laser) by creating a light sheet for imaging with PIV cameras. Although recently some high power Light-emitting diode (LED) is used for this illumination, lasers are still commonly used for this purpose because creating a light sheet is more practical with them.

Light sheet is need because cameras create two dimensional projection of three dimensional spaces. Therefore convensional PIV measurement must be done on a plane (which is created by light sheet) otherwise the particles position cannot be determined. This can be also explained mathematically that a camera creates two dimensional data, so three dimensional data cannot be measured with one camera. For measuring third component of the velocity, an extra camera can be placed with an angle to gain two more inputs so three dimensional data can be obtain.

Also the clearness and the sharpness of these images is important therefore high shutter speed used for capturing these images. The high shutter speed means the light sensitive media will be exposed to light for a short amount of time. This time is around 1/6250000 of second which means really small amount of light will be captured. This is also the main reason of high power light source is needed.

Image couples taken rapidly and potion of the particles compared with a computer program in the repeating images. The displacement of the particles in two images divided to the time between the two images capture time gives the velocity. In PIV applications a denser particle density used, so the first image separated to interrogation areas and these areas are searched in the second image with a cross correlation process.

2.2.3 Equipment and Apparatus of PIV

As it is also mentioned in the previous parts of this study conversional PIV setup consists of five components. These components are the laser (light source), camera and lens setup (imaging equipment), synchronizer, fog generator (seeding device) and analysis computer. Although these components exist in every PIV setup, they can have different specs according to the system that is needed to investigate. Table 2.1 shows the components of the present PIV setup that is used in this study and Figure 2.14

Table 2.1 Specifications of the PIV system components.

Component	*Specifications*
1) Laser	135mJ, 15Fps double pulse ND:Yag Laser
2) Camera & Lens	Flow Sence Mark II, 4 MPx, square sensor camera. 60mm f 2 Zeiss Planar Macro Lens
3) Synchronizer	Dantec Dynamics Synchronizer Box
4) Fog Generator	Safex fog generator, with extra clean fog fluid
5) Computer	Dell T7500 work station, 12 GB ram, Raid 0

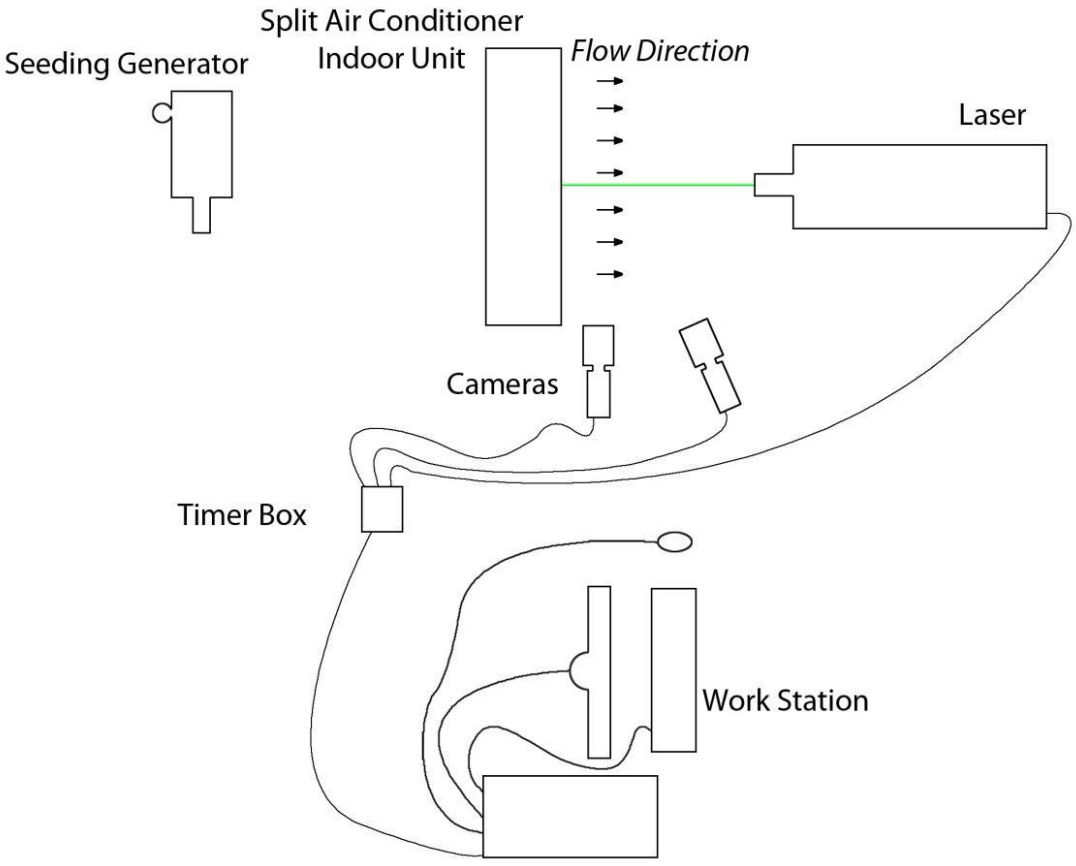

Figure 2.14 The components of the PIV setup that is used in this study.

2.2.3.1 Seeding particles

The seeding particles are an inherently critical component of the PIV system. Depending on the fluid under investigation, the particles must be able to match the fluid properties reasonably well. Otherwise they will not follow the flow satisfactorily enough for the PIV analysis to be considered accurate. While the actual particle choice is dependent on the nature of the fluid, generally for macro PIV investigations they are glass beads, polystyrene, aluminum flakes or oil droplets (if the fluid under investigation is a gas). Refractive index for the seeding particles should be different from the fluid which they are seeding, so that the laser sheet incident on the fluid flow will reflect off of the particles and be scattered towards the camera.

The particles are typically of a diameter on the order of 10 to 100 micrometers. As for sizing, the particles should be small enough so that response time of the particles to the motion of the fluid is reasonably short to accurately follow the flow, yet large enough to scatter a significant quantity of the incident laser light. Due to the small size of the particles, the particles motion is dominated by stokes drag and settling or rising affects. Approximating the particles as spherical particles of very low Reynolds number, then the ability of the particles to follow the fluid's flow is directly proportional to the difference in density between the particles and the fluid and directly proportional to the square of the particles' diameters. The scattered light from the particles is dominated by Mie scattering and so is also proportional to the square of the particles' diameters. Thus the particle size needs to be balanced to scatter enough light to accurately visualize all particles within the laser sheet plane but small enough to accurately follow the flow.

The particle distribution density is also important for the final analysis of a PIV process. In PIV a mid-density is needed for using cross correlation to measure the displacement. In Figure 2.15 different particle densities is shown. The image (b) is suitable for PIV applications. A looser particle distribution like image (a) in Figure

2.15 will not support the velocity information from whole image but it can be used for PTV. A denser particle distribution like image (b) in Figure 2.15 also cannot be used for cross correlation because the particle structure cannot be recognized in image pairs however this image can be used an elder method Particle Speckle Velocimetry which gives a general information about the flow structure. The seeding mechanism needs to also be designed for not to disturbing the flow.

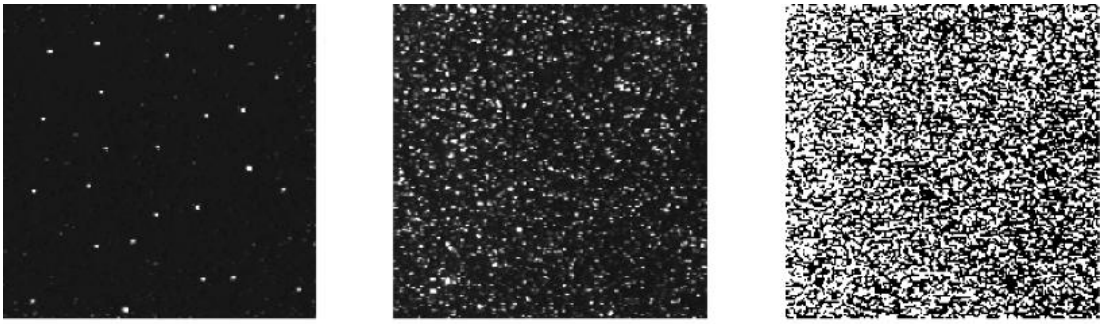

Figure 2.15 Different particle distribution densities (Raffel, Willert, Wereley, Kompenhans, 2007).

2.2.3.2 Cameras and lenses

To perform PIV analysis on the flow, two exposures of laser light are required upon the camera from the flow. Originally, with the inability of cameras to capture multiple frames at high speeds, both exposures were captured on the same frame and this single frame was used to determine the flow. A process called autocorrelation was used for this analysis. However, as a result of autocorrelation the direction of the flow becomes unclear, as it is not clear which particle spots are from the first pulse and which are from the second pulse. Faster digital cameras using CCD chips were developed since then that can capture two frames at high speed with a few hundred ns difference between the frames. This has allowed each exposure to be isolated on its own frame for more accurate cross-correlation analysis. The limitation of typical cameras is that this fast speed is limited to a pair of shots. This is because each pair of shots must be transferred to the computer before another pair of shots can be

taken. Typical cameras can only take a pair of shots at a much slower speed. High speed CCD cameras are available but are much more expensive.

The correct lens for the camera should also be selected to properly focus on and visualize the particles within the investigation area. Lens is an optic component that consists of one or more pieces of glass which are aligned in a common axis. Some lenses may have single piece of glass or element that axial thickness is small compared with its diameter. These are called simple lenses. There are also thick lenses which have more components to correct aberrations or for other purposes. These extra components may have air volumes between or can be cemented together.

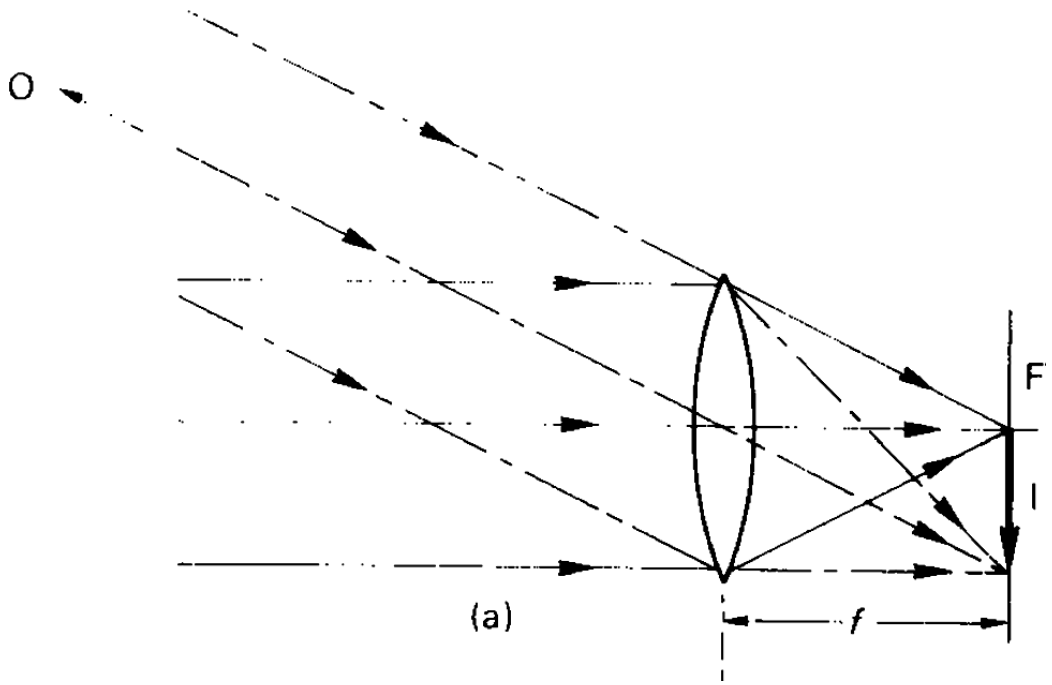

Figure 2.16 The schematic of lens and its focal plane (Jacob, Ray, Attridge & Axford, 2000).

The lenses direct all the light to a point. The rays that reach the lens from any point on the object are effectively parallel. As before the image is formed close to the lens, inverted, laterally reversed and real. The image plane in which this image is formed is termed the principal focal plane (F). For a flat distant object and an ‘ideal’ lens, every image point lies in this plane. The point of intersection of the focal plane and the optical axis is termed the rear principal focus (or simply the focus) of the

lens, and the distance from this point to the lens is termed the focal length (f) of the lens (Jacob, Ray, Attridge & Axford, 2000). The schematic of this system can be seen in Figure 2.16.

Focal length also has a relation with the angle of view (AOV) because the image is created on focal plane. As the focal length shortens the AOV gets larger. The size of the image area is also important between the relation of AOV and the focal length Figure 2.17 shows the relation between focal length and AOV.

Lenses have three different definitions depending on the focal length and the image area which are normal lenses, telephoto lenses and wide angle lenses. A normal lens has a focal length which is equal to the diagonal of the light sensitive device (CCD, CMOS or film) therefore creates an image near the perspective that a human eye sees. In this study, Flowsence Mark II is used and it has a 15x15 mm2 sensor area therefore the normal lens focal length is 21.42 mm. In this study, a 50mm lens is used, which works as a telephoto lens with our camera. The telephoto lenses have a greater focal length than a normal lenses and it magnify the objects in the image so the objects are seen bigger and closer while the wide angle lenses do the opposite. Wide angle lenses have a larger AOV and they have advantage while photographing large areas in a close range but it has some perspective distortions which make them hard to use in scientific applications.

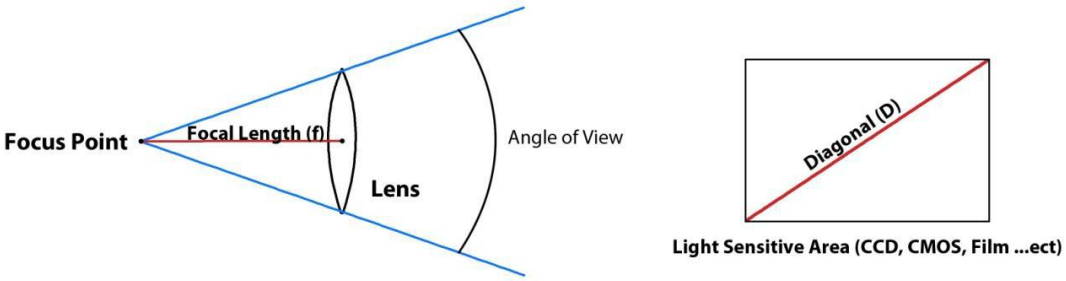

Figure 2.17 The focal length and diagonal of the light sensitive area.

2.2.3.3 Laser and optics

For macro PIV setups, lasers are predominant due to their ability to produce high-power light beams with short pulse durations. This yields short exposure times for each frame. Nd:YAG lasers, commonly used in PIV setups, emit primarily at 1064 nm wavelength and its harmonics (532, 266, etc.) For safety reasons, the laser emission is typically bandpass filtered to isolate the 532 nm harmonics (this is green light, the only harmonic able to be seen by the naked eye). A fiber optic cable or liquid light guide might be used to direct the laser light to the experimental setup.

The optics consists of a spherical lens and cylindrical lens combination. The cylindrical lens expands the laser into a plane while the spherical lens compresses the plane into a thin sheet. This is critical as the PIV technique cannot generally measure motion normal to the laser sheet and so ideally this is eliminated by maintaining an entirely 2-dimensional laser sheet. It should be noted though that the spherical lens cannot compress the laser sheet into an actual 2-dimensional plane. The minimum thickness is on the order of the wavelength of the laser light and occurs at a finite distance from the optics setup (the focal point of the spherical lens). This is the ideal location to place the analysis area of the experiment.

2.2.3.4 Synchronizer

The synchronizer acts as an external trigger for both the camera(s) and the laser. While analogue systems in the form of a photo sensor, rotating aperture and a light source have been used in the past, most systems in use today are digital. Controlled by a computer, the synchronizer can dictate the timing of each frame of the CCD camera's sequence in conjunction with the firing of the laser to within 1 ns precision. Thus the time between each pulse of the laser and the placement of the laser shot in reference to the camera's timing can be accurately controlled. Knowledge of this timing is critical as it is needed to determine the velocity of the fluid in the PIV analysis. Stand-alone electronic synchronizers, called digital delay generators, offer variable resolution timing from as low as 250 ps to as high as several ms. With up to

eight channels of synchronized timing, they offer the means to control several flash lamps and Q-switches as well as provide for multiple camera exposures.

2.2.3.5 Analysis

The frames are split into a large number of interrogation areas, or windows. It is then possible to calculate a displacement vector for each window with help of signal processing and autocorrelation or cross-correlation techniques. This is converted to a velocity using the time between laser shots and the physical size of each pixel on the camera. The size of the interrogation window should be chosen to have at least 6 particles per window on average. A visual example of PIV Analysis can be seen here.

The synchronizer controls the timing between image exposures and also permits image pairs to be acquired at various times along the flow. For accurate PIV analysis, it is ideal that the region of the flow that is of interest should display an average particle displacement of about 8 pixels. This is a compromise between a longer time spacing which would allow the particles to travel further between frames, making it harder to identify which interrogation window traveled to which point, and a shorter time spacing, which could make it overly difficult to identify any displacement within the flow.

The scattered light from each particle should be in the region of 2 to 4 pixels across on the image. If too large an area is recorded, particle image size drops and peak locking might occur with loss of sub pixel precision. There are methods to overcome the peak-locking effect, but they require some additional work.

PIV analysis of a stalled flat plate, shear rate superimposed

If there is in house PIV expertise and time to develop a system, even though it is not trivial, it is possible to build a custom PIV system. Research grade PIV systems do, however, have high power lasers and high end camera specifications for being able to take measurements with the broadest spectrum of experiments required in

research. If, for example, you want to spend less money, of course you get less resolution and lower frame rates. There are also PIV analysis software available in the open source community. The results can have similar or even better quality compared to the expensive commercial PIV systems. Commercial timing electronics come in varying resolutions. A typical example is Berkeley Nucleonics. Some of the major commercial PIV companies include TSI, LaVision and Dantec.

2.2.4 Advanced PIV Setups

As it is mentioned in the previous parts of this study, PIV setups can alter for the needs of the study. In this part phenomenal PIV setups are presented. Stereoscopic PIV, panoramic PIV and endoscopic PIV methods are also used in present study.

2.2.4.1 Stereoscopic PIV (SPIV)

SPIV utilizes two cameras with separate viewing angles to extract the z-axis displacement. Both cameras must be focused on the same spot in the flow and must be properly focused to have the same point in focus. Figure 2.18 shows schematic of the SPIV system and Figure 2.19 is a photograph of the present SPIV system.

As it mentioned before in basic PIV, two dimensional velocity measurement of an investigation plane can be done. The SPIV measurement gives the third velocity component on the same plane. So it can be said that by SPIV we can gather three dimensional velocity data of a plane. This also has the advantage of correcting the geometric distortion caused by the lens which will be explained in the part 2.2.5.4.

In Figure 2.19 the image taken before an experiment so the seeding were not distributed to flow homogeneously but the image shows that two cameras pointed at the same view. It is also important to find out that the camera on the right (which looks the system with an angle) see the SAC indoor unit as back ground. This can cause some reflection problem. This is one of the main problems of the SPIV.

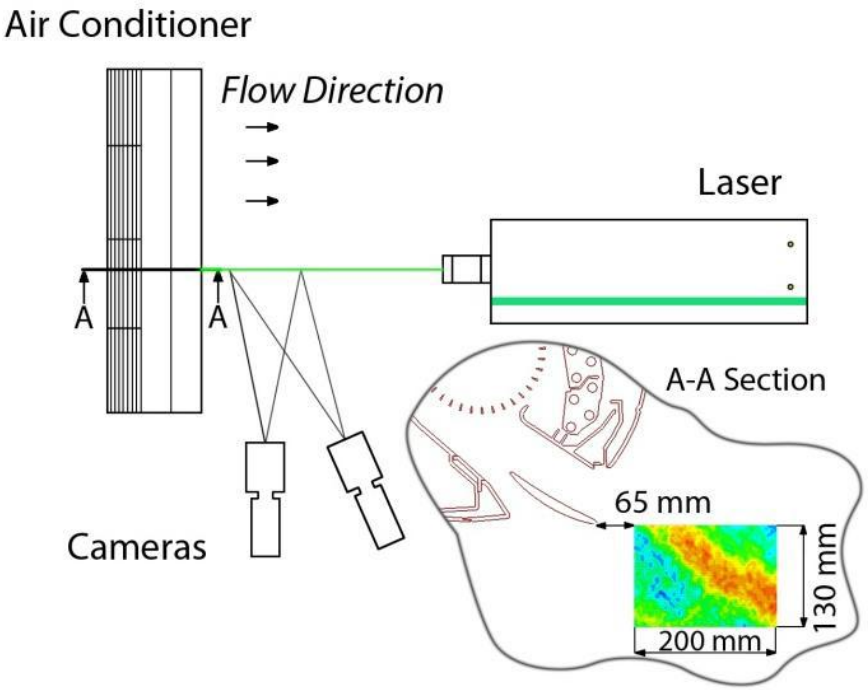

Figure 2.18 SPIV setup of the present study.

Another need of SPIV is an open space is needed for both cameras to see the area of interest. SPIV's usage in close system is extremely a hard problem to solve.

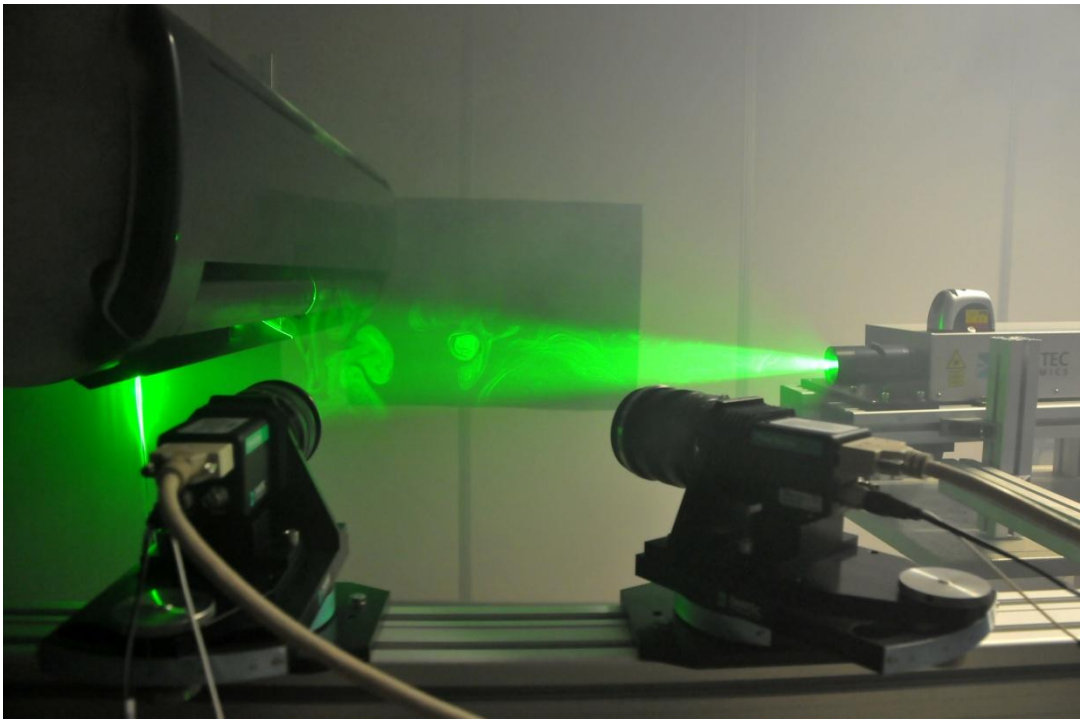

Figure 2.19 Photography of the SPIV setup.

One of the most critical process of the SPIV process is calibrating the two cameras image. In Figure 2.20 shows the positions of the calibration target, the cameras, and the images captured by each camera. As it is shown the camera in the right look the calibration target with an angle and sees the target with a perspective effect. The calibration target is used for to show the analysis program which point in image on the left corresponds to the point in the image on the right.

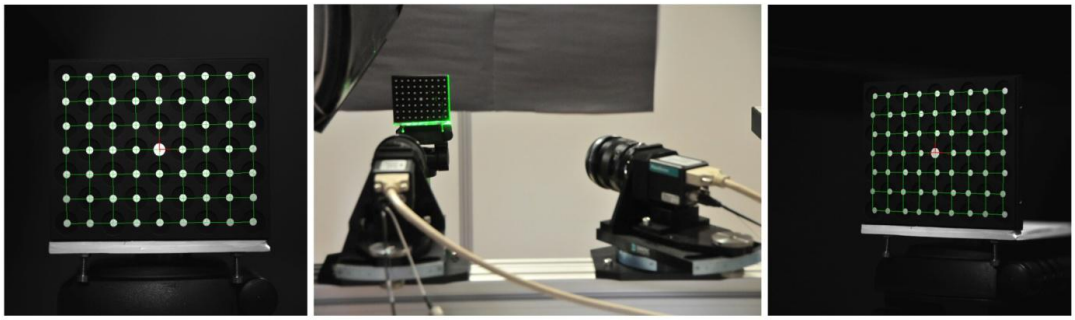

Figure 2.20 Images of the calibration target with both cameras.

2.2.4.2 Dual plane stereoscopic PIV

This is an expansion of stereoscopic PIV by adding a second plane of investigation directly offset from the first one. Four cameras are required for this analysis. The two planes of laser light are created by splitting the laser emission with a beam splitter into two beams. Each beam is then polarized orthogonally with respect to one another. Next, they are transmitted through a set of optics and used to illuminate one of the two planes simultaneously.

The four cameras are paired into groups of two. Each pair focuses on one of the laser sheets in the same manner as single-plane SPIV. Each of the four cameras has a polarizing filter designed to only let pass the polarized scattered light from the respective planes of interest. This essentially creates a system by which two separate stereoscopic PIV analysis setups are run simultaneously with only a minimal separation distance between the planes of interest. This technique allows measure the

third dimension velocity gradient. It can be said that this techniques is one step closer to the volumetric PIV.

2.2.4.3 Panoramic PIV

This technique can be used for widening the interrogation plane. In a PIV application the camera's distance to the light sheet is important because it affects the field of view and depth of view. Also the particles in the image must be equal or wider than 1 pixel otherwise a sub-pixel measurement error may occur because the image will not represent the particle position correctly.

The panoramic PIV is a solution to this matter if the system consist two cameras. These two cameras placed parallel and some of their field of view is collide with each other for merging process. The setup can be seen in Figure 2.21. The cameras work simultaneously during the experiment.

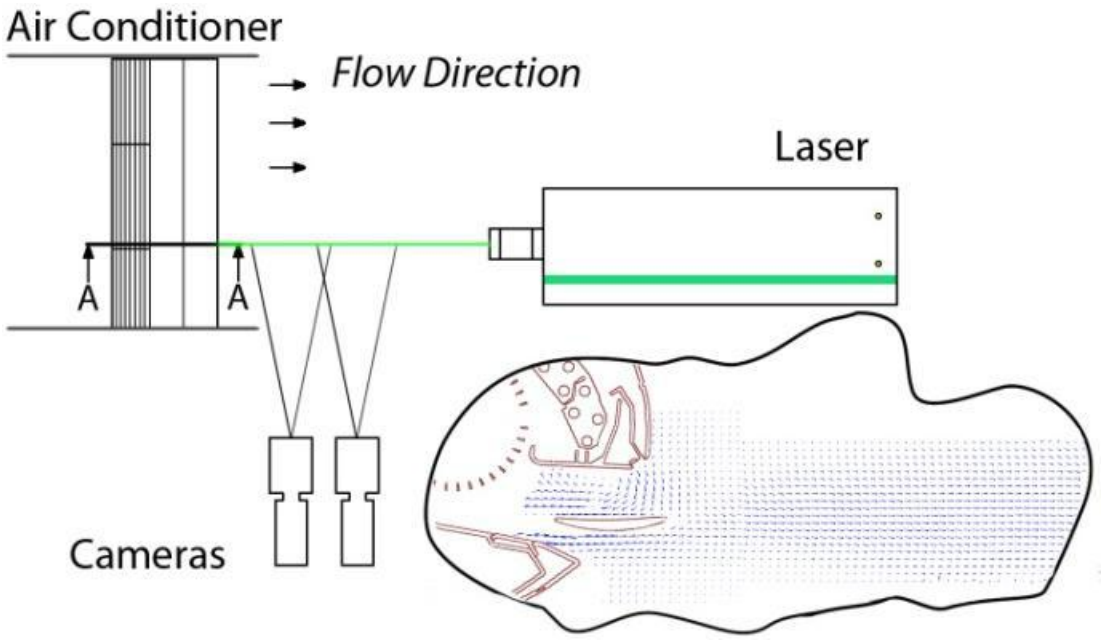

Figure 2.21 The panoramic PIV setup of the current study.

The only down side of this method is the images that are captured by the camera nearer to the light source is more bright than the other cameras. But this problem can be solved by image processing.

2.2.4.4 Endoscopic PIV (EPIV)

The Endoscopic PIV (EPIV) has the same components as the conventional PIV but one difference. An endoscope is added in front of the laser which transfers the laser as a beam to the area of interest and then it creates the light sheet. Figure 2.22 show the endoscope that is connected to the laser and it carries the light beam to the area of interests which is inside of the SAC.

Transferring the light sheet is not enough for a PIV experiment also optical access is need for imaging the light sheet. For this purpose a cut of SAC model was prepared (Figure 2.23, 2.24, 2.25). Also the holes were prepared for endoscope to enter the system. These holes can be closed while they are not used for preventing to harm the flow field.

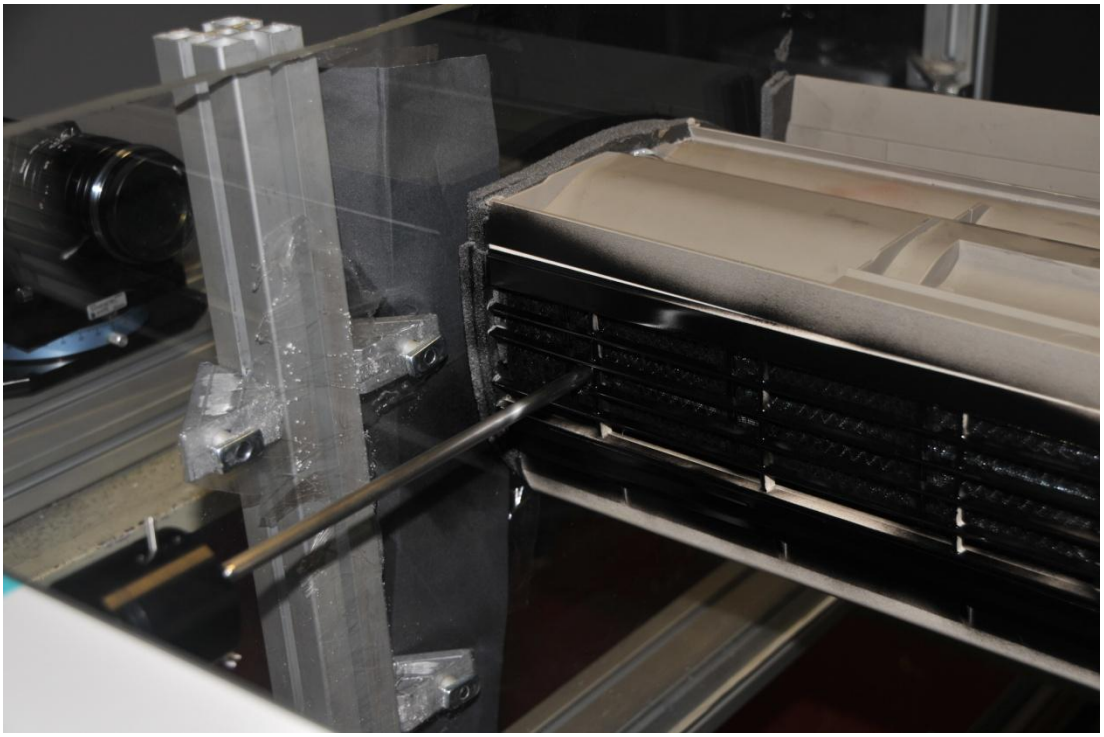

Figure 2.22 Endoscope that came out from laser and enters the SAC.

The only problem can occur in this application is sometimes the light sheets wideness cannot be enough to illuminate the whole are of interest. In Figure 2.23

shows two images from different EPIV experiments. The image on the left shows a light sheet that is not fills the area of interest. The image on the right shows the light sheet that fills the area interest.

Figure 2.23 Two images of light sheets that are taken from different EPIV experiments.

If the endoscope is not enough for investigating the area of interest then there are two possible solutions. The first one is to use another endoscope with a enough light sheet angle. The alternative is to send the laser beam naked and then to open to a light sheet. Figure 2.24 shows the schematic of such a system and Figure 2.25 shows the image of its application.

In application of this technique some cylindrical glasses were used as a cylindrical lens. The cylinders with different diameters examined for deciding which one created the suitable light sheet for the area of interest and the most suitable one was chosen. It can be seen in Figure 2.25 that the light sheet isn't as smooth as the endoscope because of the surface errors of the cylinder which wasn't produced as a lens. This problem is solved in the image processing step of the experiment with average filtering.

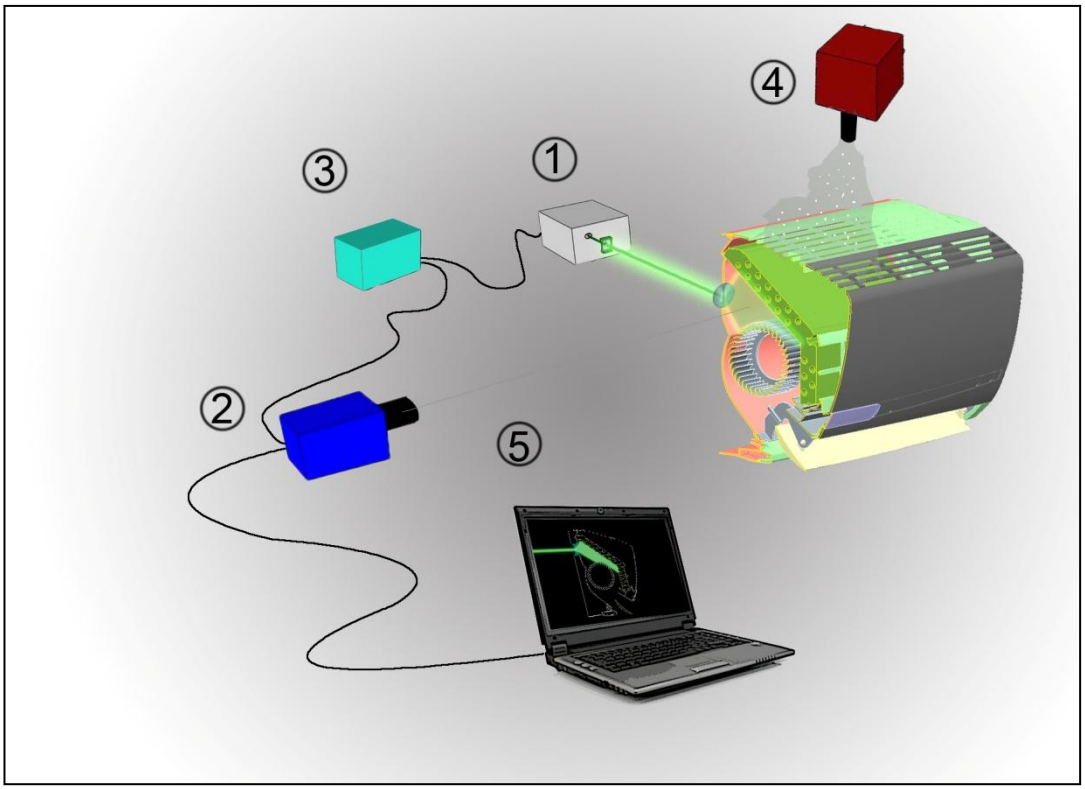

Figure 2.24 Schematic of a EPIV setup that the laser beam sent on a cylindrical lens for creating the light sheet.

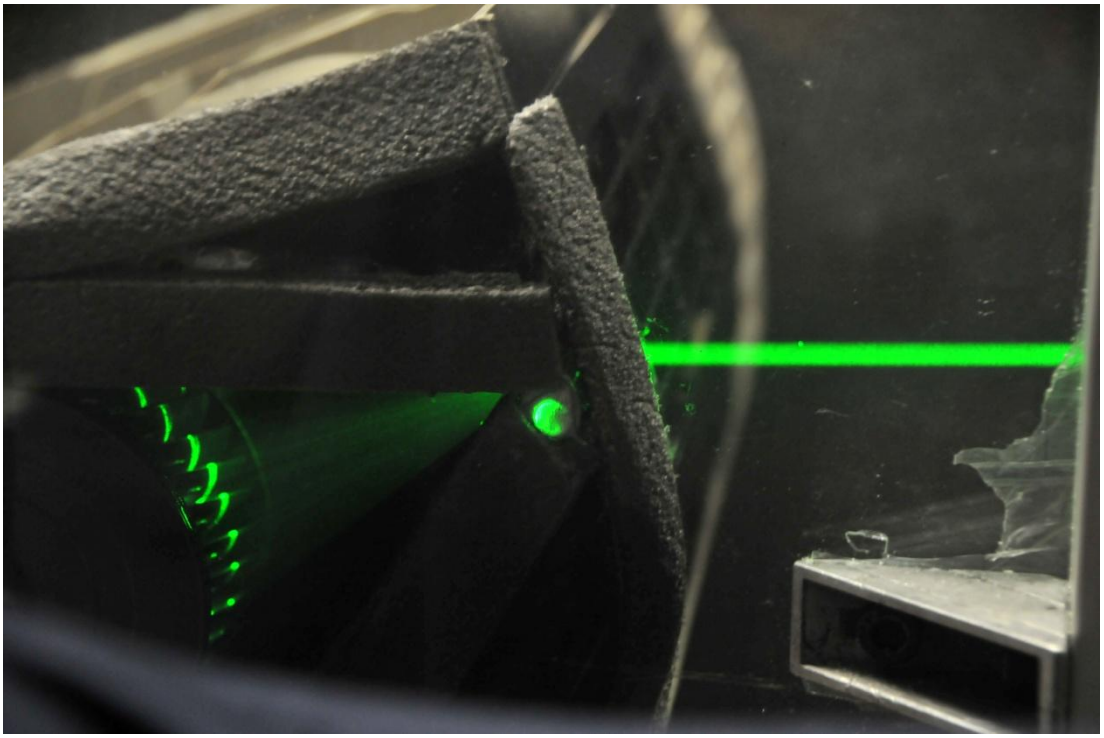

Figure 2.25 Image of the laser beam and cylindrical lens that creates the light sheet.

2.2.4.5 Micro PIV

With the use of an epifluorescent microscope, microscopic flows can be analyzed. Micro PIV makes use of fluorescing particles that excite at a specific wavelength and emit at another wavelength. Laser light is reflected through a dichroic mirror, travels through an objective lens that focuses on the point of interest, and illuminates a regional volume. The emission from the particles, along with reflected laser light, shines back through the objective, the dichroic mirror and through an emission filter that blocks the laser light. Where PIV draws its 2-dimensional analysis properties from the planar nature of the laser sheet, micro PIV utilizes the ability of the objective lens to focus on only one plane at a time, thus creating a 2-dimensional plane of viewable particles.

MicroPIV particles are on the order of several hundred nm in diameter, meaning they are extremely susceptible to Brownian motion. Thus, a special ensemble averaging analysis technique must be utilized for this technique. The cross-correlation of a series of basic PIV analysis are averaged together to determine the actual velocity field. Thus, only steady flows can be investigated. Special preprocessing techniques must also be utilized since the images tend to have a zero-displacement bias from background noise and low signal-noise ratios. Usually, high numerical aperture objectives are also used to capture the maximum emission light possible. Optic choice is also critical for the same reasons.

2.2.4.6 Holographic PIV

Holographic PIV (HPIV) encompasses a variety of experimental techniques which use the interference of coherent light scattered by a particle and a reference beam to encode information of the amplitude and phase of the scattered light incident on a sensor plane. This encoded information, known as a hologram, can then be used to reconstruct the original intensity field by illuminating the hologram with the original reference beam via optical methods or digital approximations. The intensity field is interrogated using 3-D cross-correlation techniques to yield a velocity field.

Off-axis HPIV uses separate beams to provide the object and reference waves. This setup is used to avoid speckle noise form being generated from interference of the two waves within the scattering medium, which would occur if they were both propagated through the medium.

In-line holography is another approach that provides some unique advantages for particle imaging. Perhaps the largest of these is the use of forward scattered light, which are orders of magnitude brighter than scattering oriented normal to the beam direction. Additionally, the optical setup of such systems is much simpler because the residual light does not need to be separated and recombined at a different location. The in-line configuration also provides a relatively easy extension to apply CCD sensors, creating a separate class of experiments known as digital in-line holography. The complexity of such setups shifts from the optical setup to image post-processing, which involves the use of simulated reference beams.

A variety of issues degrade the quality of HPIV results. The first class of issues involves the reconstruction itself. In holography, the object wave of a particle is typically assumed to be spherical; however, due to Mie scattering theory, this wave is a complex shape which can distort the reconstructed particle. Another issue is the presence of substantial speckle noise which lowers the overall signal-to-noise ratio of particle images. This effect is of greater concern for in-line holographic systems because the reference beam is propagated through the volume along with the scattered object beam. Noise can also be introduced through impurities in the scattering medium, such as temperature variations and window blemishes. Because holography requires coherent imaging, these effects are much more severe than traditional imaging conditions. The combination of these factors increases the complexity of the correlation process. In particular, the speckle noise in an HPIV recording often prevents traditional image-based correlation methods from being used. Instead, single particle identification and correlation are implemented, which set limits on particle number density.

2.2.4.7 Scanning PIV

By using a rotating mirror, a high-speed camera and correcting for geometric changes, PIV can be performed nearly instantly on a set of planes throughout the flow field. Fluid properties between the planes can then be interpolated. Thus, a quasi-volumetric analysis can be performed on a target volume. Scanning PIV can be performed in conjunction with the other 2-dimensional PIV methods described to approximate a 3-dimensional volumetric analysis.

2.2.4.8 Tomographic PIV

Tomographic PIV is based on the illumination, recording, and reconstruction of tracer particles within a 3-D measurement volume. The technique uses several cameras to record simultaneous views of the illuminated volume, which is then reconstructed to yield a discretized 3-D intensity field. A pair of intensity fields are analyzed using 3-D cross-correlation algorithms to calculate the 3-D, 3-C velocity field within the volume. The Tomo-PIV setup can be seen in Figure 2.26.

The reconstruction procedure is a complex under-determined inverse problem. The primary complication is that a single set of views can result from a large number of 3-D volumes. Procedures to properly determine the unique volume from a set of views are the foundation for the field of tomography. In most Tomo-PIV experiments, the multiplicative algebraic reconstruction technique (MART) is used. The advantage of this pixel-by-pixel reconstruction technique is that it avoids the need to identify individual particles.

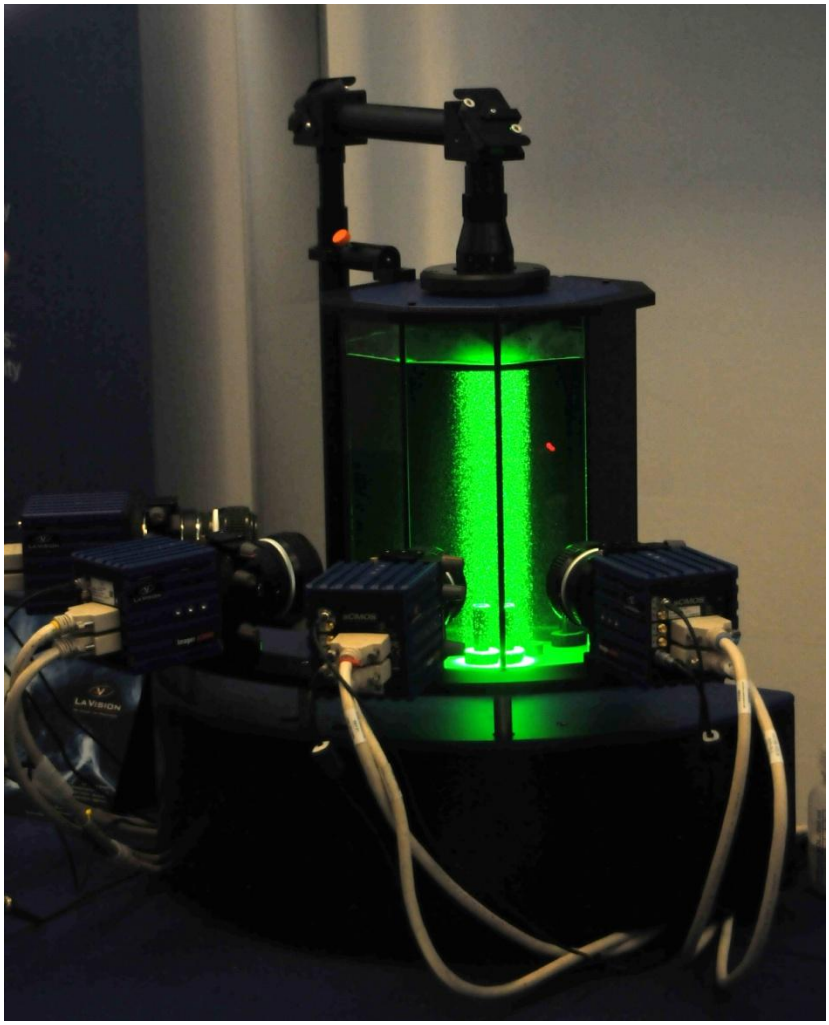

Figure 2.26 Image of a tomo-PIV setup that is presented in PIV 2011 Kobe, Japan

2.2.5 Method Improvement Studies for PIV

Method improvement studies are parametric studies that are made for finding the most efficient way to use the PIV setup. Therefore further studies can be done faster and with less computational and storage resources.

For this purpose various experiments made in front of the SAC's exit. This area chosen for this study because of it is easier to apply PIV in this area. Several investigation planes decided on the SAC for experiments. These planes positions on the SAC are shown in Figure 2.27.

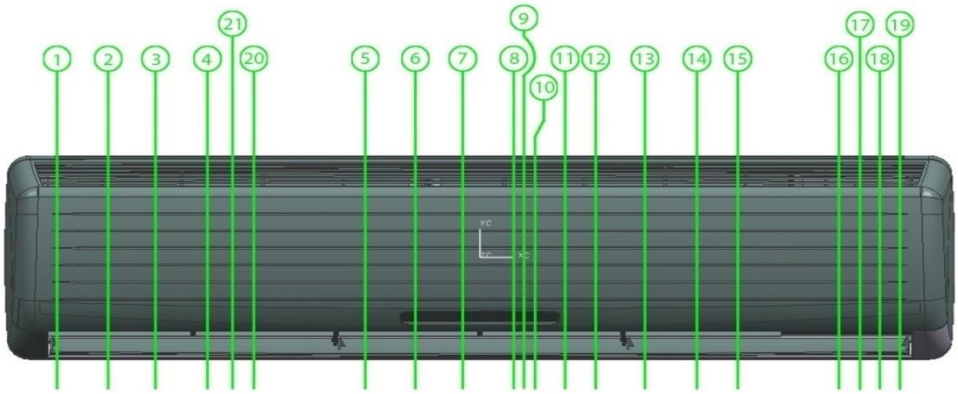

Figure 2.27 Investigated planes for method improvement on the SAC.

2.2.5.1 Effects of the surrounding walls

Three different positions in the test room were studied to find out the effects of the surrounding walls on the outflow of the device (Figure 2.28). These kind of obstacles may be found in the real operating conditions of the device, but for correctly determining the performance exterior effects should be minimized.

The first position shown in Figure 2.28 (gray), represents the layout when the system was first set up. It is expected that the wall against the indoor unit would affect the outflow of the device. However, this position was studied for easily distinguishing the effects of the wall that may be seen in the further studies. Second position (red) has a similar condition with the first one. Therefore the measurements of this position were made just for a couple of points for comparison. Third position (blue) is the most appropriate one compared with the others. The gap between the device and the rear wall is left to simulate the conditions in the test chambers used for the standardization studies of the indoor unit.

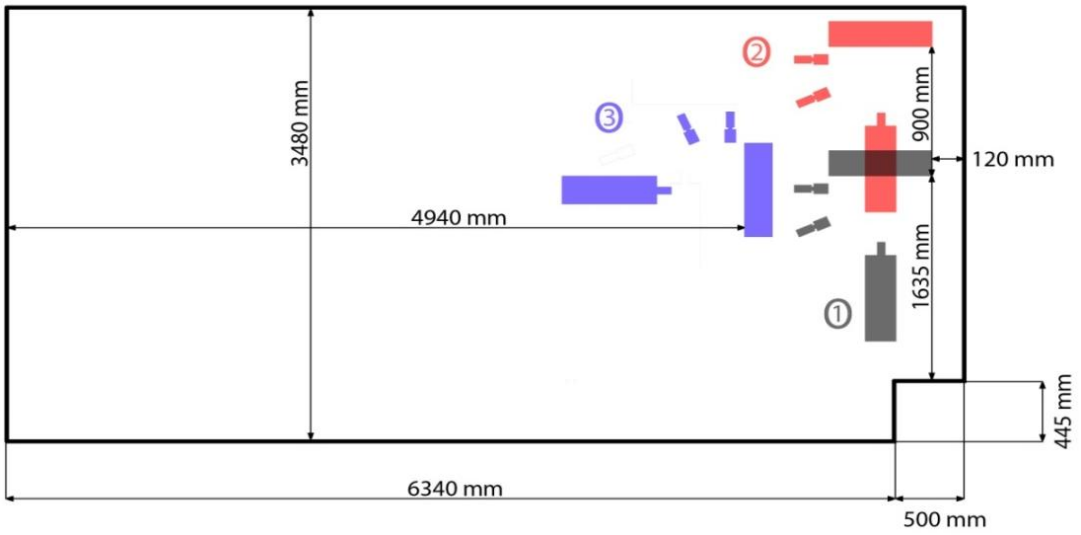

Figure 2.28 Test room and there different test positions.

Results of the measurements on the planes 1, 2 and 21 are given in the Figures 2.29, 2.30 and 2.31 respectively. Planes 1 and 2 are situated in one side of the device where the outflow is relatively slower, while plane 21 is at the middle part where outflow is faster. All the PIV results in this report are given as the average of the two hundred vector fields obtained from four hundred image pairs taken by two PIV cameras. By taking the average of the vector fields, instantaneous fluctuations in the flow are eliminated and distinguishing the flows under different ambient conditions became possible.

Vectors given in the Figures represent the two dimensional flow in the light sheet, while the colors represent the flow through the third dimension in the light sheet. Red tones are for the flow coming out of the paper plane, blue tones are for the flow inside the paper plane and green tones are for still part in the third dimension.

As the vector fields are examined, for the first position of the setup, flow is upward in the first plane where the velocities are smaller (Figure 2.29 a), as the velocities increase flow turns downward (Figure 2.30 result-a) where for the Plane 21 flow is directed along the diagonal of the interested area as expected (Figure 2.31 result-a). For the third position, flow is cached at the lower left triangular part of the interested area directed along the diagonal for all the considered cases (Figure 2.29

result-b, Figure 2.30 result-b, Figure 2.31 result-b), but blowing area gets wider in the middle parts of the device (Figure 2.31 result-b).

As the in-plane third dimension of the flow is examined, for the first position there is a calm part (indicated with the green tones) on the diagonal of the interested area for planes 1 and 21 (Figure 2.29 result-a and Figure 2.31 result-a) but it is unclear for the Plane 2 as seen in Figure 2.30 result-a. Besides, as the upper right corner and lower left corner has opposite color tones (blue and red respectively) in Figure 2.29 result-a, we can say that flow is twisted in the counter clock wise (CCW) direction while it's blown along the diagonal. In Figure 2.30 result-a this event is not seen clearly, but a small blue toned part on the upper right corner and the red parts look like as if same twisting movement continues in Plane 2. As we get closer to the middle part of the device (Figure 2.31 result-a) twisting movement is again seen but in the clock wise (CW) direction. There may be a breaking point between Plane 2 and 21 where twisting motion becomes invisible and turns just the opposite but this event hasn't been investigated yet.

For the third position there is not any big difference between the planes as in the first position. In Plane 1 (Figure 2.29 result-b), flow starts to twist CCW direction as in Plane 2 (Figure 2.30 result-b) this twisting motion is more active than Plane 1. In Plane 21 (Figure 2.31 result-b) twisting diameter became smaller but again turns CCW direction. The direction of twisting doesn't change for the third position; therefore we may say that effect of the surrounding walls is dominant for the first position. This phenomenon may be investigated deeper during further studies.

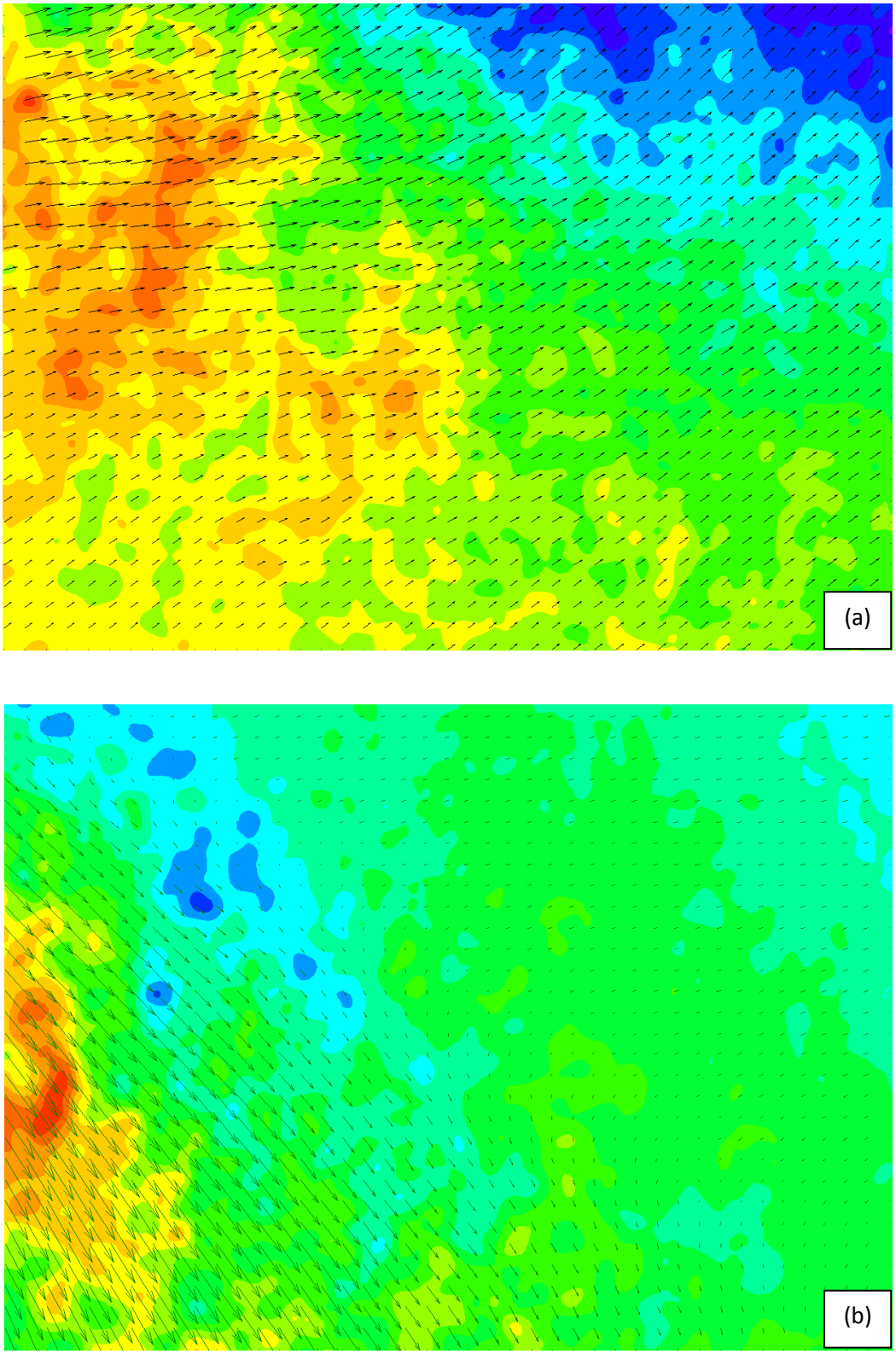

Figure 2.29 Flow in the 1. plane; a- first position, b- third position

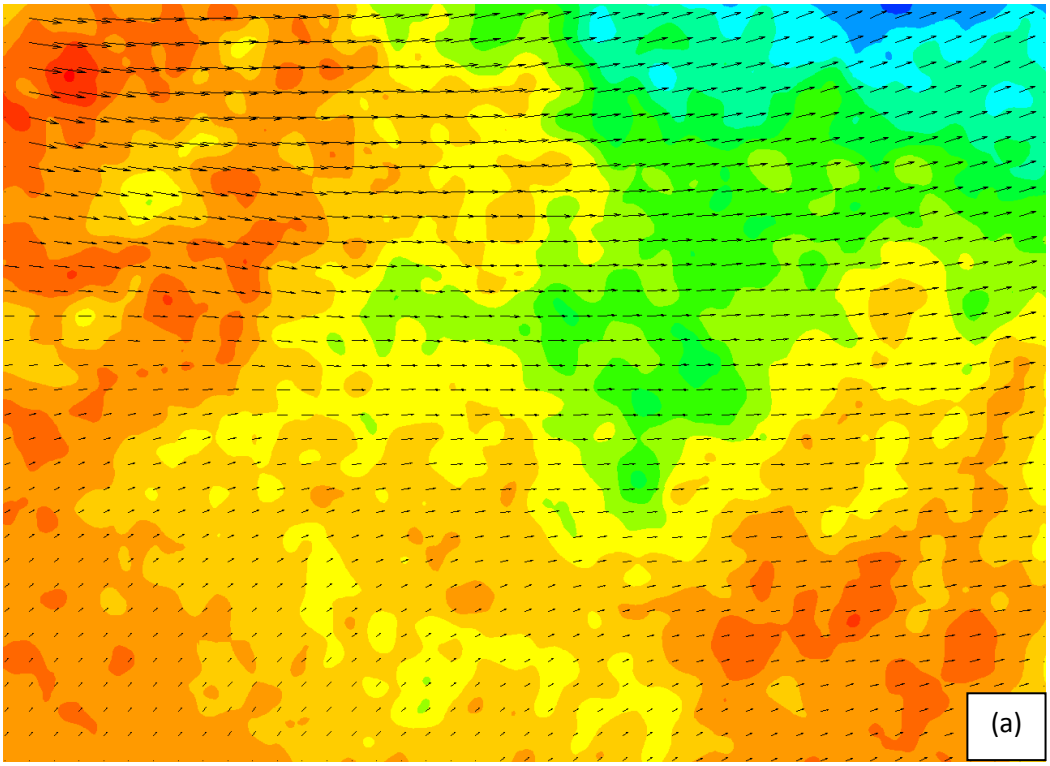

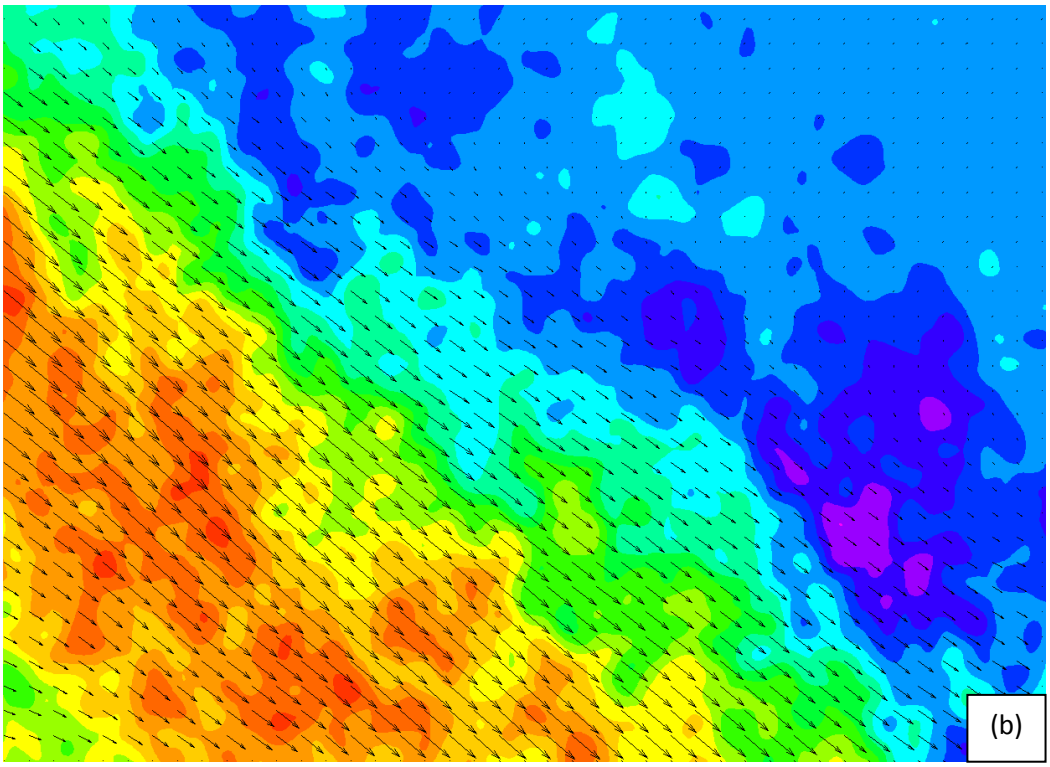

Figure 2.30 Flow in the 2. plane; a- first position, b- third position

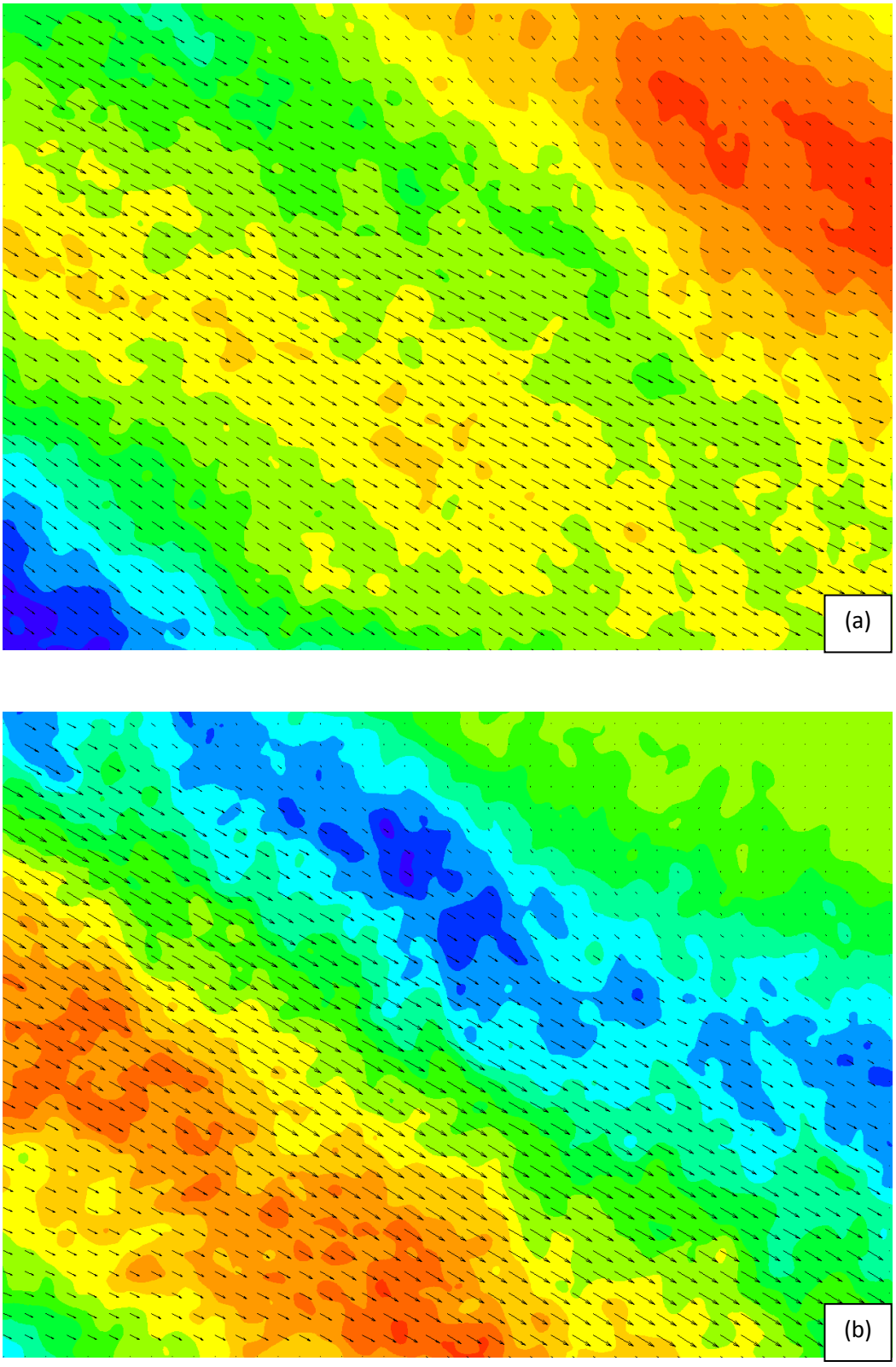

Figure 2.31 Flow in the 21. plane; a- first position, b- third position

2.2.5.2 Effects of the number of image pairs

Another study made for method improvement was on number of image pairs. This is important for total measurement time. But a more important point is that as the number of image pairs increase, amount of data for analyzing and storage also increase. Besides time for analyzing was taken on interested plane for determining optimum number of image pairs becomes longer. As the number of image pairs decrease, measurements may not be adequate for defining the general flow characteristics. Therefore optimum number of image pairs should be decided for optimizing PIV measurements. 10, 20, 50, 100, 200 image pairs

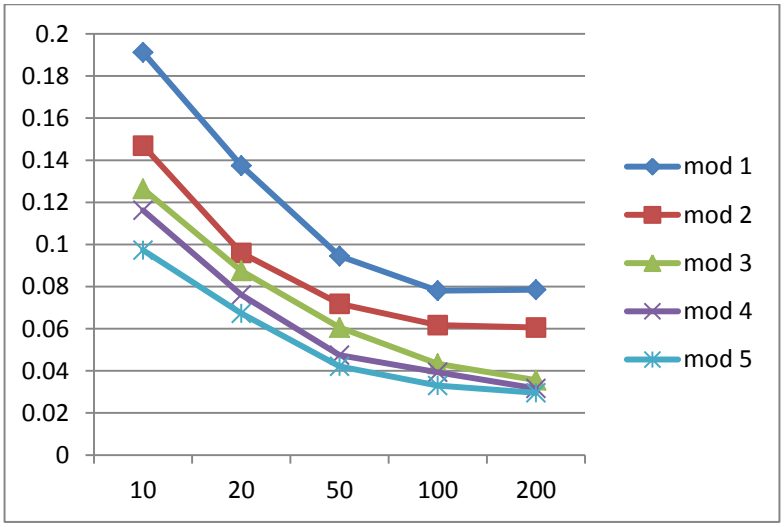

Figure 2.32 Change of first five POD modes versus number of image pairs.

Figure 2.32 shows the change of number of image pairs with respect to POD (Proper Orthogonal Decomposition) modes which describes the dominant components of the flow having different energy levels. The POD mode with the highest amount of energy is Mode 1. As seen in Figure 2.32, the energy indicated by Mode 1 decreases as the number of image pairs increase to a level of 100 image pairs. The reason is that, the number of modes is equal to number of image pairs as a result of the method. But the change of energy between consecutive number of image pairs decreases as the number of image pairs increases. This leads to result between 100 and 200 image pairs as there is almost no change of energy level

between these two points. This fact occurs for other POD modes, but the change of energy between consecutive numbers of image pairs is getting smaller as the POD mode number increase. As a result 100 image pairs are enough for modes 1 and 2 but for modes 3, 4 and 5 more image pairs are needed for obtaining better results.

2.2.5.3 The effect of time between laser pulses

The last study for method improvement was about the effect of time between laser pulses on PIV measurements. Time between pulses should be properly selected depending on the velocity of the fluid at the interested area. Otherwise it is not possible to obtain correct vector fields from the particle images. If the velocity is not known before the measurements, accuracy of the results may be checked by analyzing the cross correlation map. If the velocity is known, it is better to calculate how much the particles would displace between consecutive images and select the time between pulses referring this calculation. Time between pulses was calculated as 40 µs before the experiments but for being certain 80 µs and 120 µs were also used for measurements.

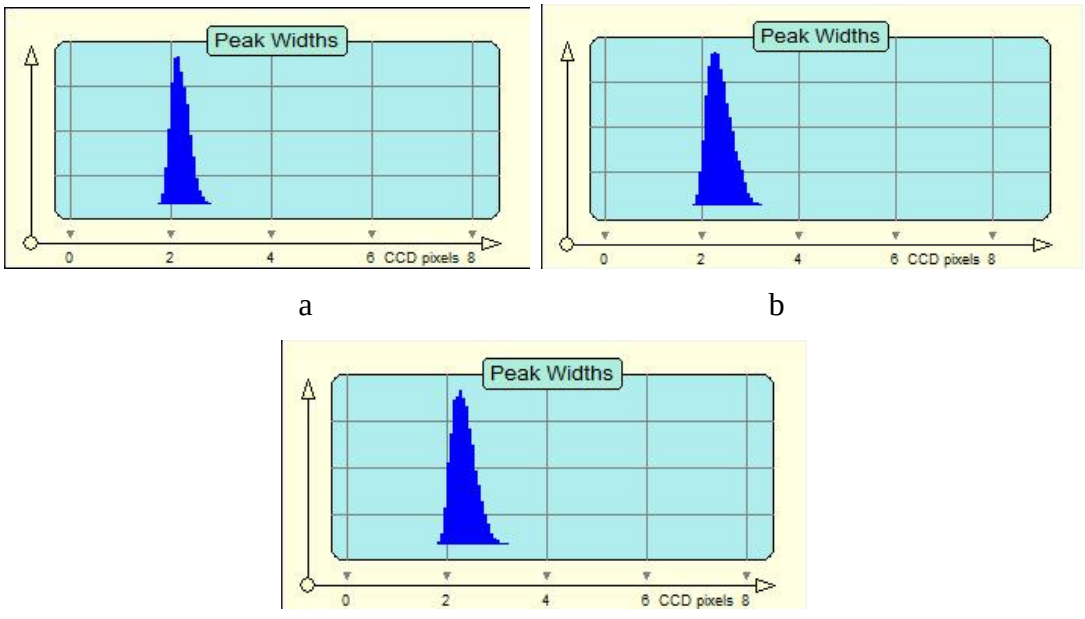

Figure 2.33 Histogram of cross correlation peak widths for different time between laser pulses, a - 40µs, b - 80 µs, c -120 µs.

Histograms of cross correlation peak widths for different time between pulses values were given in Figure 2.33. The histogram curve is close to left side (peak widths are smaller) and thinner than the others (peaks have similar forms for more points) for 40 µs. Therefore results for 40 µs of time between laser pulses are better than 80 µs and 120 µs.

2.2.5.4 Perspective Errors in PIV Applications

PIV is a highly dependents on optics devices. Optics both used in front of laser as light sheet optics and in front of the camera as lens so it can be said the design and the composition of these components are crucial for the success of a PIV experiment. Even the chosen components are state of art technology; there can be major measurement errors due to wrong usage. In this part of the study, the perspective error sources and solutions will be reviewed and an experimental example will be investigated.

Although there is a widespread thought that is “photography is a tool that perfectly reflects reality”, artists and exactly scientists are well aware of this is not true. Photography is just a method that records an image which is focused on to a light-sensitive material, chemically or digitally by using optic components and camera. The recorded image is called a representation of the object which means the image itself is not the object but it’s merely a two dimensional copy of it. As the equipment and usage change, image could be a very alike of the real object or can be transformation of it. When photography is used in scientific applications these deformation of the reality is undesired. Such study is made by A.K. Prasad (2000) and showed perspective error can be significantly contaminating in-plane measurements when the relative out-of-plane component is large. An angle of 5 degree can cause an error of %10 in the in-plane measurement when the out-of-plane displacement is similar to the in-plane. Prasad suggested that using the SPIV method will reduce this effect.

This study emphasizes theoretically the lens choice can reduce this effect and also SPIV effect will be investigated experimentally on an example.

2.2.5.4.1 Geometric Perspective Distortion of the Lens'. A photographic image creates a two dimensional projection of a three dimensional space. Therefore in the process of the transformation of the three dimensional data to the two dimensional data, perspective distortion can be occurred especially when a wide angle lens is used. In Figure 2.34, the points which have the same distance to the camera is marked with black that created an arc. Red lines show the relation between the AOV and the viewed area by a wide angle lens; the blue lines show the same relation for a telephoto lens. It can be seen as the AOV of the lens decreases the difference between the arc and the object plane also decreases which also means that as the focal length of the lens grew bigger the perspective distortion will also be decreased due to decrement of the angle of view therefore the 2D projection also converges to the real vision. On the other hand, with the wide angle lens there is a much bigger difference between the visualized area and the projection. This situation will create a perspective difference between the middle area and the outer areas. This effect can be seen in Figure 2.34.

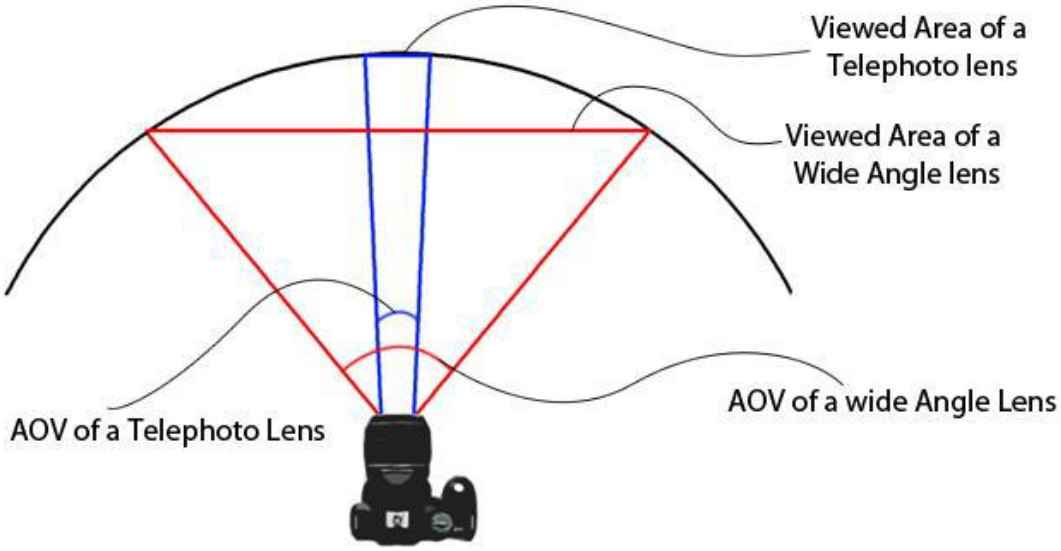

Figure 2.34 The relation between different AOV's.

The geometric distortion caused by the usage of wide angle lens is shown on an example circle in Figure 2.35. On the middle of the object plane there is no deformation effect tough as the circle goes to the sides and Θ angle increases the circle is seen larger in horizontal and it became deformed to an ellipse.

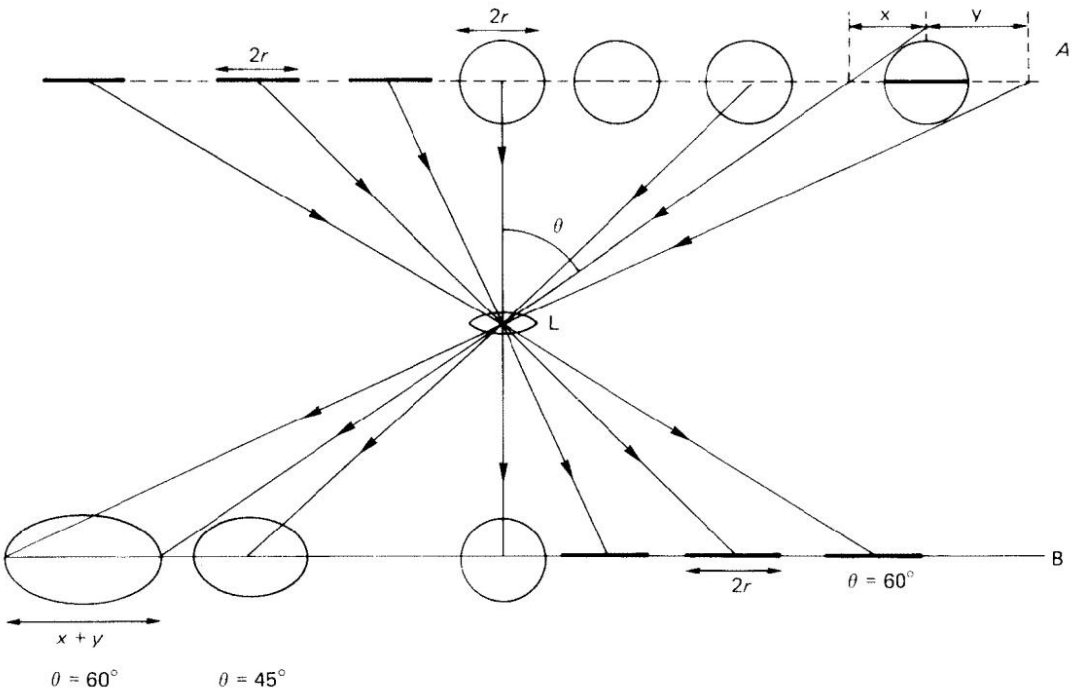

Figure 2.35 Geometric distortion due to use of wide angle (Jacob, Ray, Attridge & Axford, 2000).

The clear solution of geometrical distortion is the usage of a lens which has 75 or a larger angle of view. These lenses are preliminarily defined as normal focal length or telephoto lens. This effect can be seen in Figure 2.36 by investigating two threshold photograph of a checker board calibration target. The photograph (a) in the Figure 2.36 is taken by a telephoto lens and the perspective deformation has been solved while in Figure 2.36 the photograph (b) is taken by a wide angle lens, in which the middle area of the image has a larger scale then the corner sides. Therefore the vertical lines became curved and this is called the barreling effect.

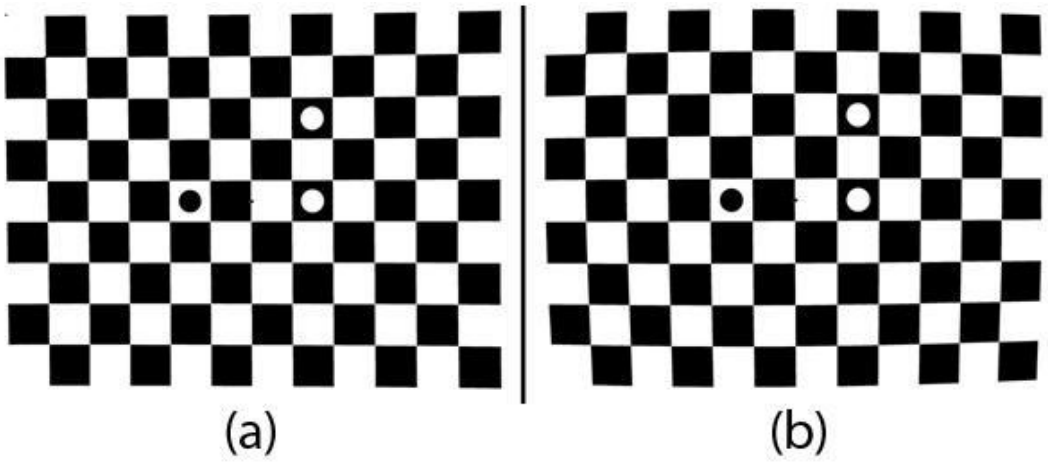

Figure 2.36 Checker Board Calibration target shot with a Telephoto Lens (a) and shot with a wide angle lens (b).

To see the same area with lenses which has different focal lengths, the shooting distance must be changed. As the telephoto lens has a small angle of view, the image is taken from a further distance then the wide angle lens.

The geometrical distortion can also be solved with computer algorithms, if the interrogation area can be assumed as two-dimensional. In PIV applications, out of plane components must be considered before this assumption to be done.

Prasad declared that the perspective error can significantly contaminate in-plane measurements when the relative out-of-plane component is large as well as when the angle subtended by the particle to the camera-axis is large (Prasad, 2000).

If flow can be assumed two dimensional, a standard single camera PIV process can be applied to the system for the measurement, otherwise preferring SPIV would be a solution for preventing measurement errors.

As a validation of previous part, an experimental study was made by using the SPIV at the outside of a split air conditioner indoor unit which is known as theoretically creating two dimensional flows. The laser and the split air conditioner indoor unit are placed as looking each other so the light sheet is created parallel to the flow direction. Camera one is positioned on the left side of the indoor unit and seeing the light sheet vertically. Camera two is placed at the same vertical distance to the light sheet but it sees the interrogation area with an angle of 55 degrees so that the out of plane displacement can be captured in the images. Cameras are calibrated by using a 2 layered calibration target with the size of 95x75 mm and the seeding was done by filling all the test room with smoke which has an average particle size of 1 μm.

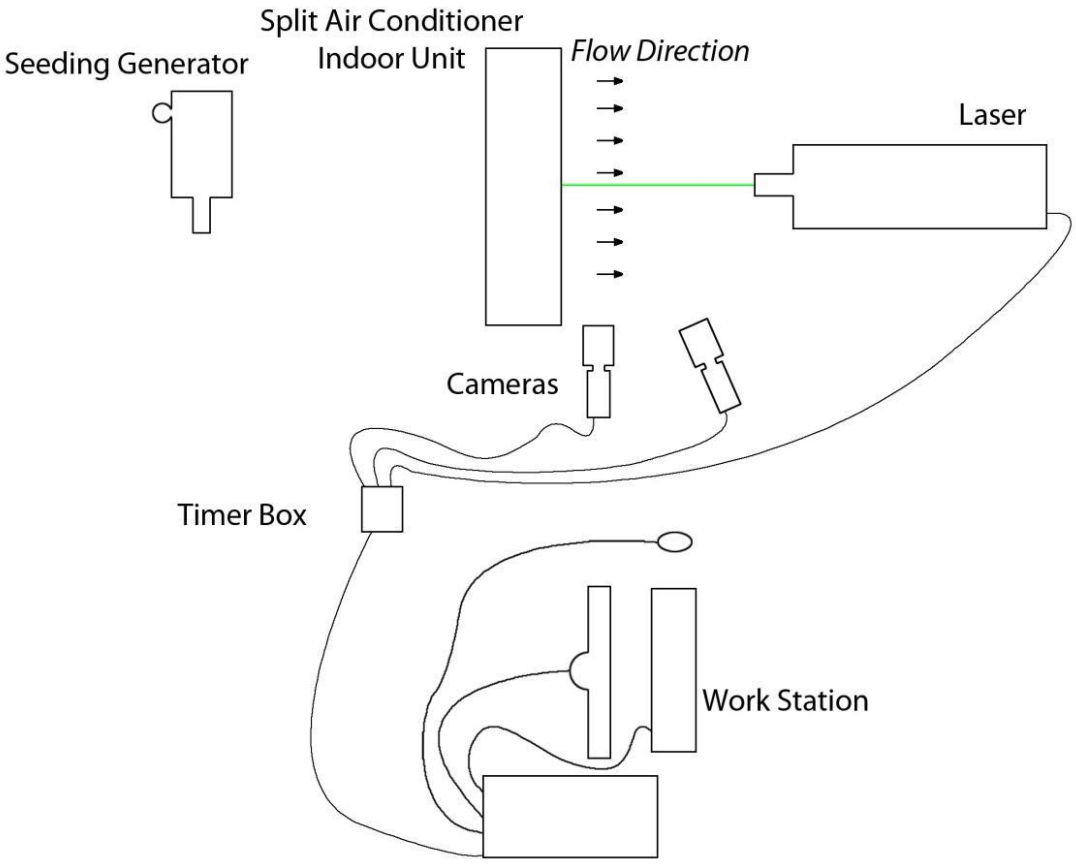

Figure 2.37 The experimental setup that is used for this study.

After the data acquisition from two cameras was completed, two different post processing were done to compare PIV and SPIV. In process one, only the vertical

looking camera's images are analyzed as PIV results and in process two the images from both two cameras are used in SPIV method which creates a three dimensional vectors on planar domains. Dynamic Studio and Matlab are used for data processing and comparison.

The purpose of the experiment was to see the effect of the out of plane component of the flow in PIV and SPIV methods so two different planes are selected for experiments and these planes can be seen in Figure 2.38. The Plane 1 is close to the left edge of the air conditioner where both the in plane and the out of plane are small in scale and also in plane components are much dominant. On the other side Plane 2 is near to the middle area of the air conditioner where the average velocity value is near to the maximum value among the total system. Because of this, the vertical directing airfoils has a strong baffle effect on the flow and creates third dimensional flow components at this area. Also the expansion of the jet flow creates out of plane velocity components.

Average vector maps acquired by PIV and SPIV methods can be seen in Figure 2.39, 2.40, 2.41. and 2.42. Figure 2.39 and 2.40 are data were taken from Plane 1 and Figure 2.41-2.42 were taken in Plane 2, on the middle area. Although the main flow characteristics do not significantly change, the vectors in the territories where the out of plane components and in plane components are in the same order of magnitude differ dramatically.

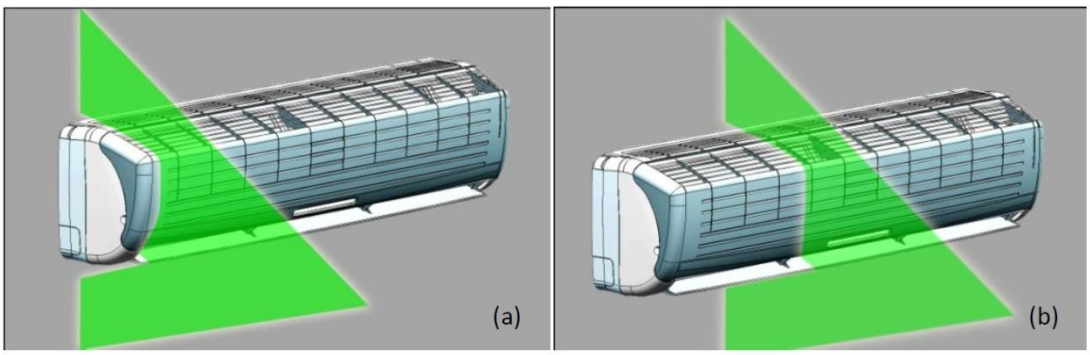

Figure 2.38 investigation planes used for this study. (a) Plane 1, (b) Plane 2.

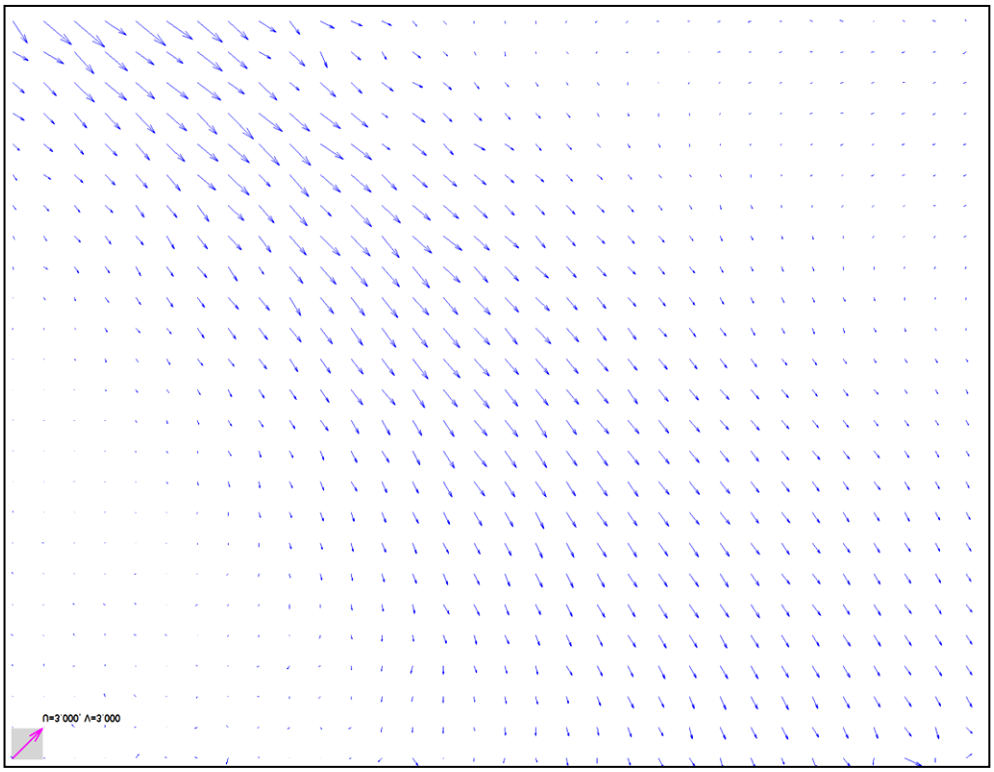

Figure 2.39 Plane 1 PIV mean vector map.

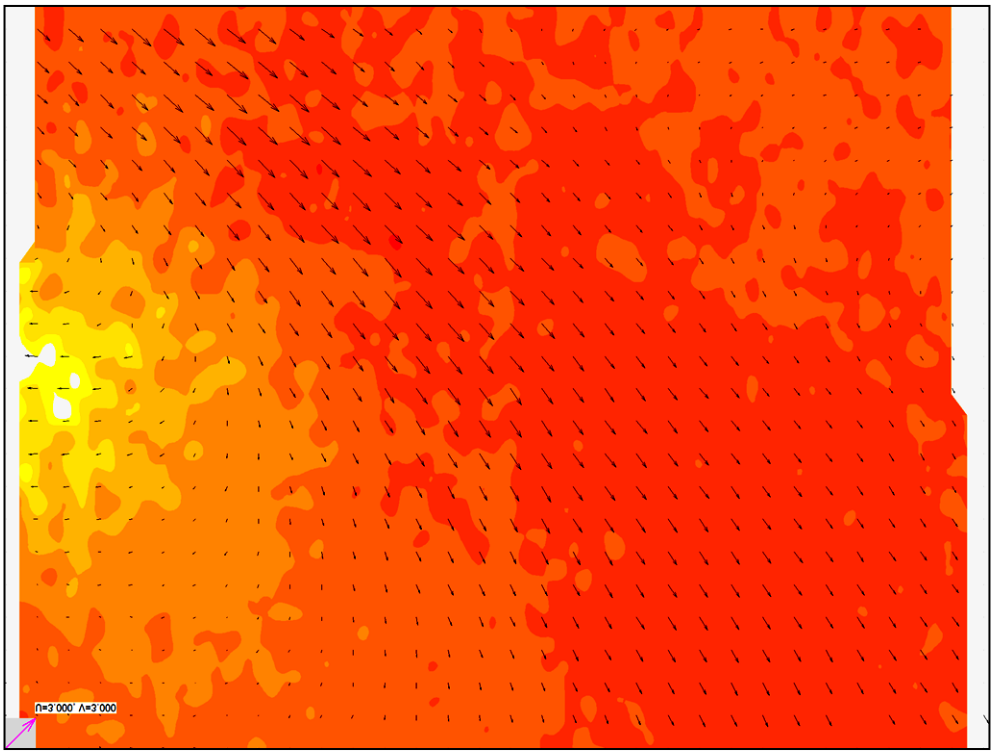

Figure 2.40 Plane 1 SPIV mean vector map.

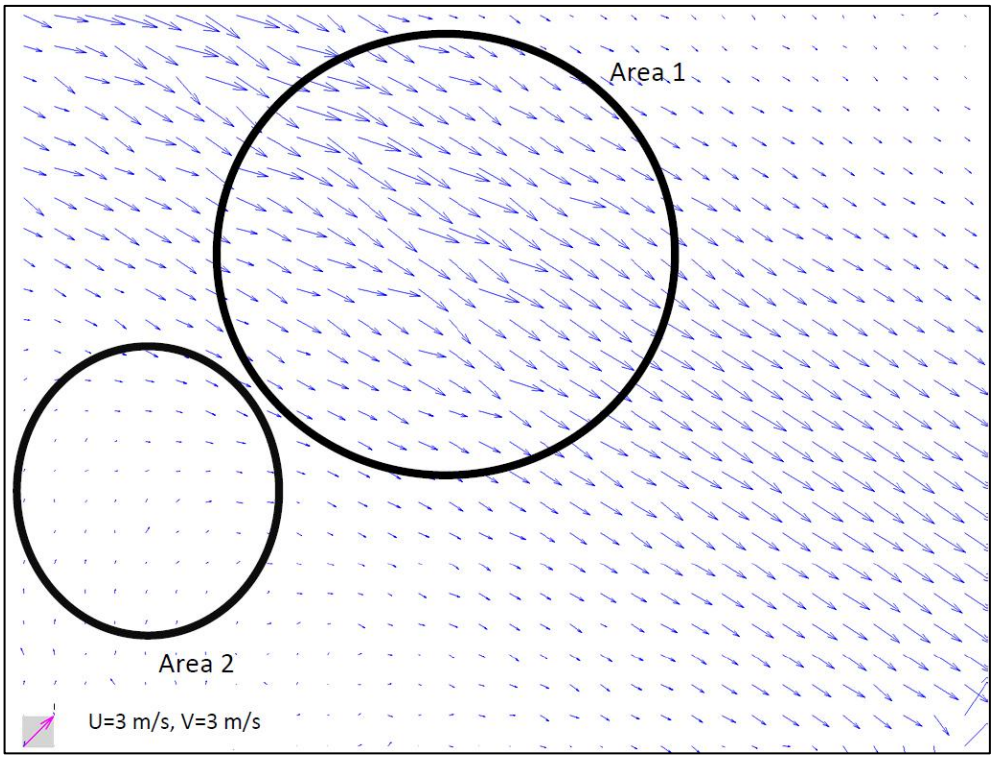

Figure 2.41 Plane 2 PIV mean vector map.

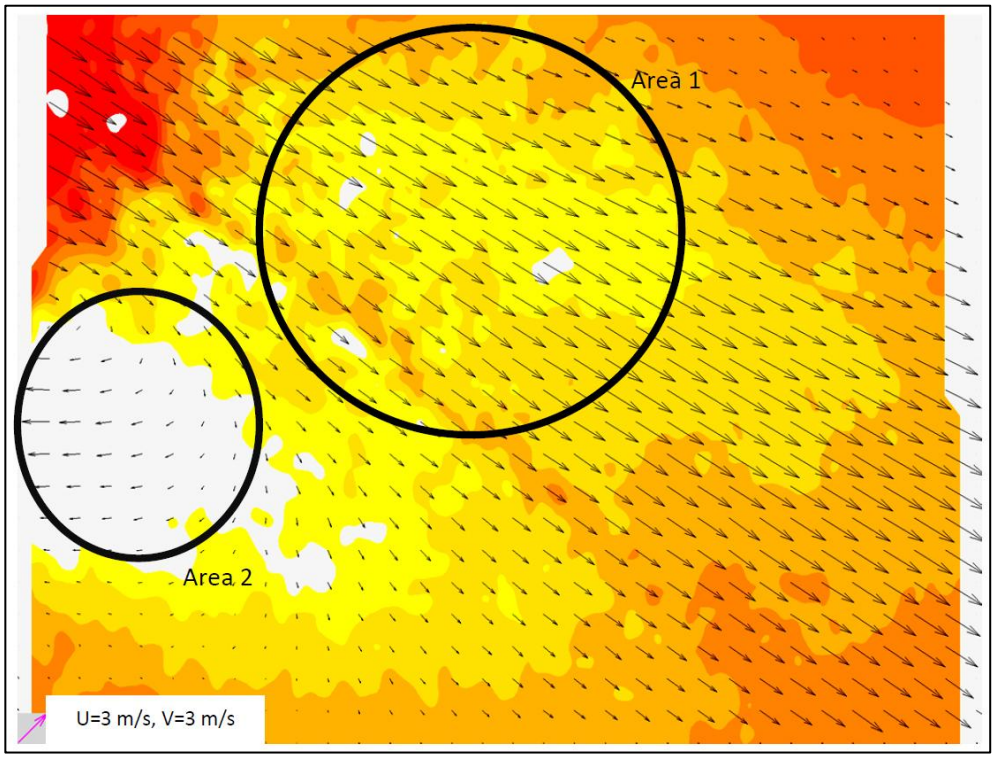

Figure 2.42 Plane 2 SPIV mean vector map.

In data acquired at Plane 1 the in-plane components are very dominant and there is a slight difference between PIV and SPIV measurement. But in experiment at Plane 2 has more incoherent areas between PIV and SPIV measurement (Figure 2.41-2.42). The area 1 in PIV measurement there are inconsistent vectors some follows the direction of the flow and others are pointing a bit upwards. This is caused by perspective distortion of the out of plane component and can be carefully filtered by a coherence filter or median filtering though in some areas the deformed vectors are majority therefore there is a probability in filtering process, that the right vectors can also be filtered instead of the deformed ones.

The errors in area two is much significant. In PIV measurement a back flow area is totally missed and this situation, the PIV measurement does not show the flow structure correctly.

This shows, although PIV is an advanced flow visualization and measurement tool, the misusage of the system cause magnificent error which miss lead the researcher. Therefore a process of careful error analyses and validation experiments must be done. The correct visualization data only can be obtained at a carefully designed system and controlled circumstances.

2.3 A General View on Temperature Measurement Methods

As it is mentioned before in the preliminary study stage of the study, one of the most important subjects is choosing the right experimental method that can be used practically and satisfied the study's requirements.

For making the right decision the needed specs of the system is determined then the importance of that spec defined for final decision. However in temperature measurement there are two different type of study. Measuring the solid body temperatures like heat exchangers and measuring the air temperature that passes the system. So every measure method will be investigated for both purposes.

2.3.1 CTA and Thermocouples

CTA method is investigated at the velocity measurement part of this chapter in details. The temperature measurement process is pretty much the same as the velocity measurement. However in temperature measurement CTA has alternative tools, thermocouples.

A thermocouple is a device consisting of two different conductors (usually metal alloys) that produce a voltage proportional to a temperature difference between either end of the pair of conductors. Thermocouples are a widely used type of temperature sensor for measurement and control and can also be used to convert a heat gradient into electricity. They are inexpensive, interchangeable, are supplied with standard connectors, and can measure a wide range of temperatures. In contrast to most other methods of temperature measurement, thermocouples are self powered and require no external form of excitation. The main limitation with thermocouples is accuracy and system errors of less than one degree Celsius (C) can be difficult to achieve.

Any junction of dissimilar metals will produce an electric potential related to temperature. Thermocouples for practical measurement of temperature are junctions of specific alloys which have a predictable and repeatable relationship between temperature and voltage. Different alloys are used for different temperature ranges. Properties such as resistance to corrosion may also be important when choosing a type of thermocouple. Where the measurement point is far from the measuring instrument, the intermediate connection can be made by extension wires which are less costly than the materials used to make the sensor. Thermocouples are usually standardized against a reference temperature of 0 degrees Celsius; practical instruments use electronic methods of cold-junction compensation to adjust for varying temperature at the instrument terminals. Electronic instruments can also compensate for the varying characteristics of the thermocouple, and so improve the precision and accuracy of measurements.

2.3.1.1 Working Principles of Thermocouples

In 1821, the German–Estonian physicist Thomas Johann Seebeck discovered that when any conductor is subjected to a thermal gradient, it will generate a voltage. This is now known as the thermoelectric effect or Seebeck effect. Any attempt to measure this voltage necessarily involves connecting another conductor to the "hot" end. This additional conductor will then also experience the temperature gradient, and develop a voltage of its own which will oppose the original. Fortunately, the magnitude of the effect depends on the metal in use. Using a dissimilar metal to complete the circuit creates a circuit in which the two legs generate different voltages, leaving a small difference in voltage available for measurement. That difference increases with temperature, and is between 1 and 70 microvolts per degree Celsius (μV/°C) for standard metal combinations.

The voltage is not generated at the junction of the two metals of the thermocouple but rather along that portion of the length of the two dissimilar metals that is subjected to a temperature gradient. Because both lengths of dissimilar metals experience the same temperature gradient, the end result is a measurement of the temperature at the thermocouple junction.

Thermocouples measure the temperature difference between two points, not absolute temperature. To measure a single temperature one of the junctions—normally the cold junction—is maintained at a known reference temperature, and the other junction is at the temperature to be sensed.

Having a junction of known temperature, while useful for laboratory calibration, is not convenient for most measurement and control applications. Instead, they incorporate an artificial cold junction using a thermally sensitive device such as a thermistor or diode to measure the temperature of the input connections at the instrument, with special care being taken to minimize any temperature gradient between terminals. Hence, the voltage from a known cold junction can be simulated, and the appropriate correction applied. This is known as cold junction compensation.

Some integrated circuits such as the LT1025 are designed to output a compensated voltage based on thermocouple type and cold junction temperature.

There are also different types of thermocouples according to the material. Table 2.2 shows the properties of different thermocouples.

Table 2.2 Properties of different thermocouples

Type	Temperature Range (C) (continues)	Temperature Range (C) (Short Term)	Tolerance (C)
K	0 to 1100	-180 to 1300	±1.5 between −40 °C and 375 °C ±0.004×T between 375 °C and 1000 °C
J	0 to 750	-180 to 800	±1.5 between −40 °C and 375 °C ±0.004×T between 375 °C and 750 °C
N	0 to 1100	-270 to 1300	±1.5 between −40 °C and 375 °C ±0.004×T between 375 °C and 1000 °C
R	0 to 1600	-50 to 1700	±1.0 between 0 °C and 1100 °C ±[1 + 0.003×(T − 1100)] between 1100 °C and 1600 °C
S	0 to 1600	-50 to 1750	±1.0 between 0 °C and 1100 °C ±[1 + 0.003×(T − 1100)] between 1100 °C and 1600 °C
B	200 to 1700	0 to 1820	-
T	-185 to 300	-250 to 400	±0.5 between −40 °C and 125 °C ±0.004×T between 125 °C and 350 °C
E	0 to 800	-40 to 900	±1.5 between −40 °C and 375 °C ±0.004×T between 375 °C and 800 °C
Crome/AuFe	-272 to 300	N/A	Reproducibility 0.2% of the voltage; each sensor needs individual calibration.

2.3.1.2 Final Evaluation of CTA and Thermocouples

Although CTA is precise method that can measure the temperature of the flow, it needs calibration as the flow speed varies. This situation makes the scanning process more difficult, especially while working with the SACs which blow very dynamic flow structure. So it was not suitable for being the main research tool. However it is used for the preliminary study for having a general idea of the system.

On the other hand thermocouples are very capable and easy to use. They can be used for both measuring air temperature and the body temperatures. Because of they are cheap, 20 or more of them can be used by a data logger at the same time so rather than scanning, locating the thermocouples on a specially design pattern can also give a temperature distribution of any system.

Thermocouples used in different steps of this study. They were especially useful for validating the newly developed method Mesh Infrared Thermography (MIT).

2.3.2 Planer Laser Induced Fluorescence (PLIF)

Planar laser-induced fluorescence (planar-LIF) is an optical measuring technique used to measure instant whole-field concentration or temperature maps in liquid flows. From looking that aspect it is a tool that can measure temperature distribution as PIV measures the velocity field.

Applications can be found in process engineering (e.g. mixing in stirring vessels, heating and cooling systems), biomedical engineering (e.g. transport of drugs in biological flows such as in model veins) and fluid dynamics research (e.g. turbulent mixing and heat-transfer modelling, indoor climate etc.)

A typical PLIF setup consists a source of light (usually a laser), an arrangement of lenses to form a sheet, fluorescent medium, collection optics and a detector. The light

from the source, illuminates the medium, which then fluoresces. This signal is captured by the detector and can be related to the various properties of the medium.

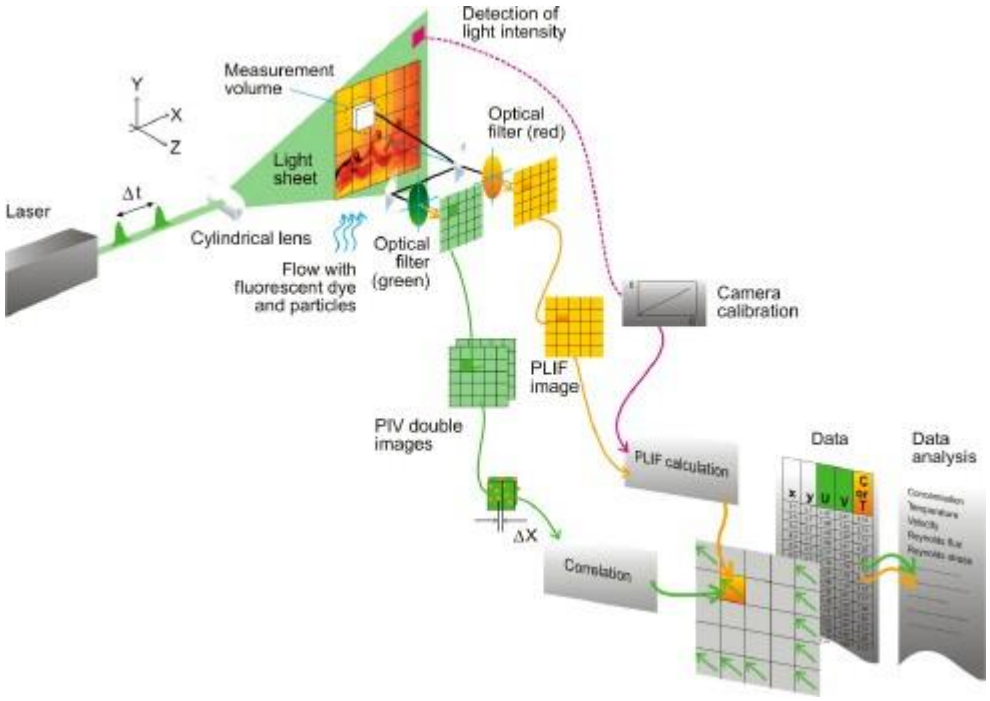

Figure 2.43 Schematic of the PLIF system (http://www.dantecdynamics.com)

The typical lasers used as light sources are pulsed, which provide a higher peak power than the continuous-wave lasers. Also the short pulse time is useful for good temporal resolution. Some of the widely used laser sources are Nd:YAG laser, dye lasers, excimer lasers, and ion lasers. The light from the laser (usually a beam) is passed through a set of lenses and/or mirrors to form a sheet, which is then used to illuminate the medium. This medium is either made up of fluorescent material or can be seeded with a fluorescent substance. The signal is usually captured by a CCD or CMOS camera (sometimes intensified cameras are also used). Timing electronics is often used to synchronize pulsed light sources with intensified cameras. In Figure 2.43 the schematic of the system can be seen.

2.3.2.1 Final Evaluation of PLIF

There can be no discussion that PLIF is a state of art method which can measure temperature distribution and the velocity field at the same time. However the seeding is very critical in this application. Some calibration experiment must be made before the main experiment for defining the seeding particles behavior at the experiment temperature scale.

Another point that must be taken care of is the seeding which is a fluorescent substance, generally a chemical that can harm human health so other than the experimental setup a specially designed test room is needed which is equipped with special air cleaning system. This situation makes the expensive experiment method PLIF, more expensive.

This experimental method could be used for this study however the price of this system exceeds the project budget therefore an alternative method measured.

2.3.3 Infrared Thermography Methods

Infrared thermography, thermal imaging, and thermal video are examples of infrared imaging science. Thermal imaging cameras detect radiation in the infrared range of the electromagnetic spectrum (roughly 9000–14,000 nanometers or 9–14 μm) and produce images of that radiation, called thermograms. Since infrared radiation is emitted by all objects above absolute zero according to the black body radiation law, thermography makes it possible to see one's environment with or without visible illumination. The amount of radiation emitted by an object increases with temperature; therefore, thermography allows one to see variations in temperature. When viewed through a thermal imaging camera, warm objects stand out well against cooler backgrounds; humans and other warm-blooded animals become easily visible against the environment, day or night. As a result,

thermography is particularly useful to military and other users of surveillance cameras.

Thermography has a long history, although its use has increased dramatically with the commercial and industrial applications of the past fifty years. Government and airport personnel used thermography to detect suspected swine flu cases during the 2009 pandemic. Firefighters use thermography to see through smoke, to find persons, and to localize the base of a fire. Maintenance technicians use thermography to locate overheating joints and sections of power lines, which are a tell-tale sign of impending failure. Building construction technicians can see thermal signatures that indicate heat leaks in faulty thermal insulation and can use the results to improve the efficiency of heating and air-conditioning units. Some physiological changes in human beings and other warm-blooded animals can also be monitored with thermal imaging during clinical diagnostics.

The appearance and operation of a modern thermographic camera is often similar to a camcorder. Often the live thermogram reveals temperature variations so clearly that a photograph is not necessary for analysis. A recording module is therefore not always built-in.

The CCD and CMOS sensors used for visible light cameras are sensitive only to the nonthermal part of the infrared spectrum called near-infrared (NIR). Thermal imaging cameras use specialized focal plane arrays (FPAs) that respond to longer wavelengths (mid- and long-wavelength infrared). The most common types are InSb, InGaAs, HgCdTe and QWIP FPA. The newest technologies use low-cost, uncooled microbolometers as FPA sensors. Their resolution is considerably lower than that of optical cameras, mostly 160x120 or 320x240 pixels, up to 640x512 for the most expensive models. Thermal imaging cameras are much more expensive than their visible-spectrum counterparts, and higher-end models are often export-restricted due to the military uses for this technology. Older bolometers or more sensitive models such as InSb require cryogenic cooling, usually by a miniature Stirling cycle refrigerator or liquid nitrogen.

2.3.3.1 Emissivity

Emissivity is a term representing a material's ability to emit thermal radiation. Each material has a different emissivity, and it can be quite a task to determine the appropriate emissivity for a subject. A material's emissivity can range from a theoretical 0.00 (completely not-emitting) to an equally-theoretical 1.00 (completely emitting); the emissivity often varies with temperature. An example of a substance with low emissivity would be silver, with an emissivity coefficient of .02. An example of a substance with high emissivity would be asphalt, with an emissivity coefficient of .98.

A black body is a theoretical object which will radiate infrared radiation at its contact temperature. If a thermocouple on a black body radiator reads 50 °C, the radiation the black body will give up will also be 50 °C. Therefore a true black body will have an emissivity of 1.

Since there is no such thing as a perfect black body, the infrared radiation of normal objects will appear to be less than the contact temperature. The rate (percentage) of emission of infrared radiation will thus be a fraction of the true contact temperature. This fraction is called emissivity.

Some objects have different emissivities in long wave as compared to mid wave emissions. Emissivities may also change as a function of temperature in some materials.

To make a temperature measurement of an object, the thermographer will refer to the emissivity table to choose the emissivity value of the object, which is then entered into the camera. The camera's algorithm will correct the temperature by using the emissivity to calculate a temperature that more closely matches the actual contact temperature of the object.

If possible, the thermographer would try to test the emissivity of the object in question. This would be more accurate than attempting to determine the emissivity of the object via a table. The usual method of testing the emissivity is to place a material of known high emissivity in contact with the surface of the object. The material of known emissivity can be as complex as industrial emissivity spray which is produced specifically for this purpose, or it can be as simple as standard black insulation tape, emissivity 0.97. A temperature reading can then be taken of the object with the emissivity level on the imager set to the value of the test material. This will give an accurate value of the temperature of the object. The temperature can then be read on a part of the object not covered with the test material. If the temperature reading is different, the emissivity level on the imager can be adjusted until the object reads the same temperature. This will give the thermographer a much more accurate emissivity reading. There are times, however, when an emissivity test is not possible due to dangerous or inaccessible conditions. In these situations the thermographer must rely on tables.

2.3.3.2 Final Evaluation of Infrared Thermography

The infrared thermography method is widely used in thermal engineering applications. As long as the emissivity of the measured body is known, precise measurement can be made by this method.

Therefore at first, infrared thermography method is used in this study for measuring the temperature of the outside body of the split air conditioner and the heat exchangers. Figure 2.44 show a “picture in picture” image of SAC from the front and Figure 2.45 show a “picture in picture” image of the heat exchanger of the SAC.

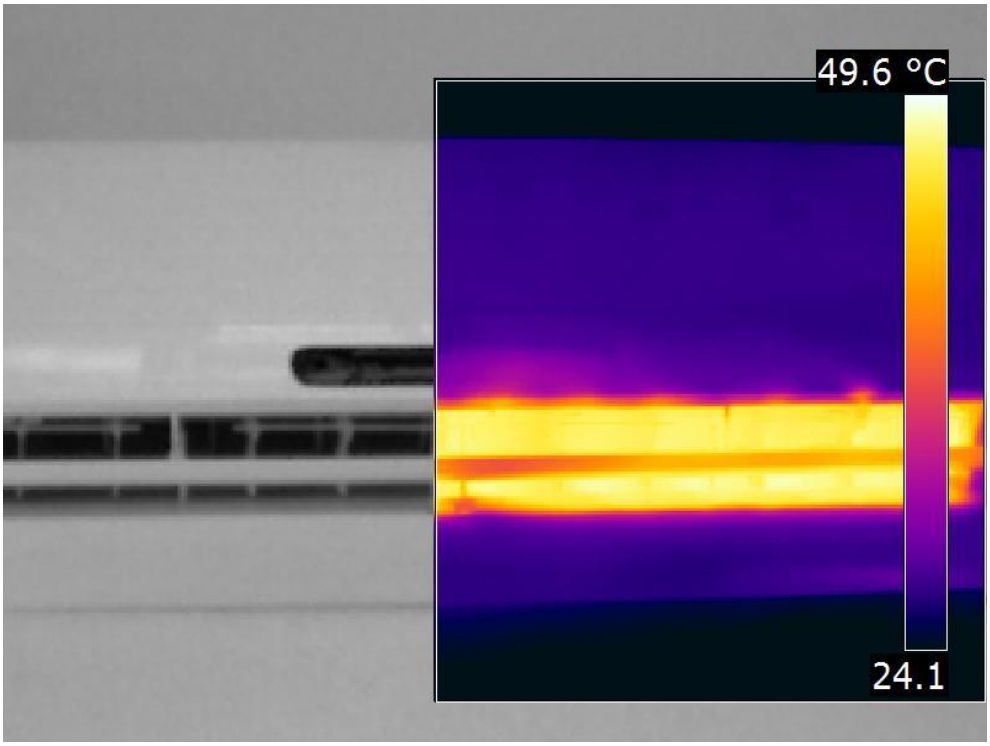

Figure 2.44 “Picture in picture” image of SAC from the front.

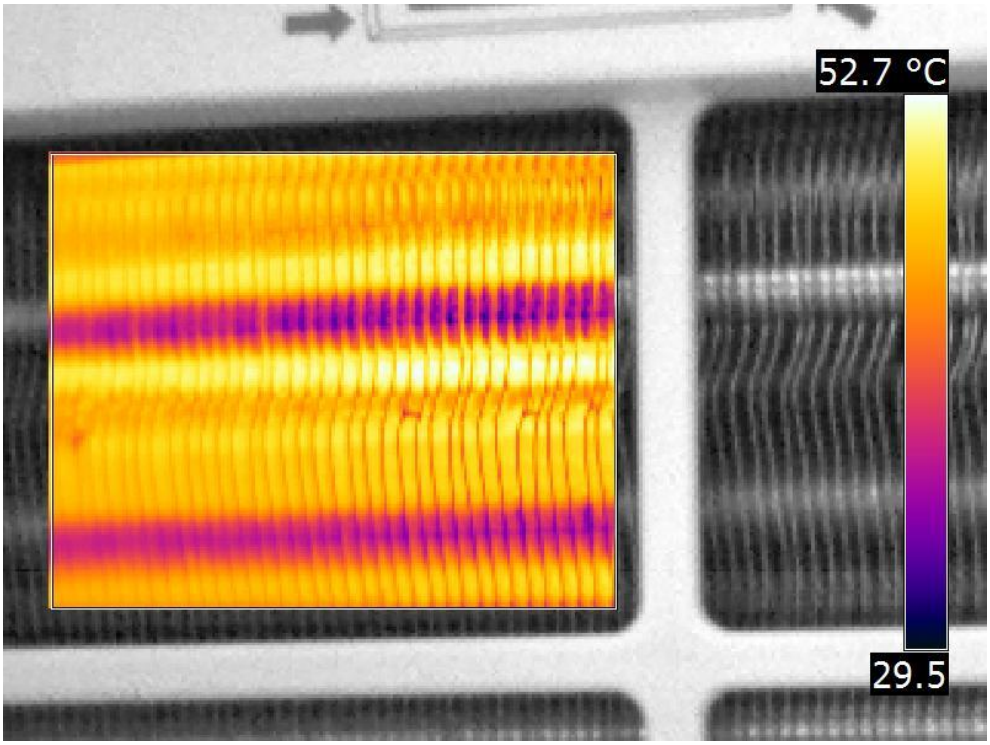

Figure 2.45 “Picture in picture” image of the heat exchanger of the SAC.

The “picture in picture” is an ability that infrared camera that is used in this study has. The camera posses an extra small digital camera which can see the measurement area and takes a normal image as the infrared image is taken. The normal and the infrared images are merged for user to understand which position the image has been taken.

The results of these measurements are investigated in details for controlling the design. Figure 2.46 is a different scaled version of Figure 2.44. It is clearly seen that the downwards of the SAC there is an overheat area. After finding out that area, it is investigated to for finding out if there is a design error creating that situation.

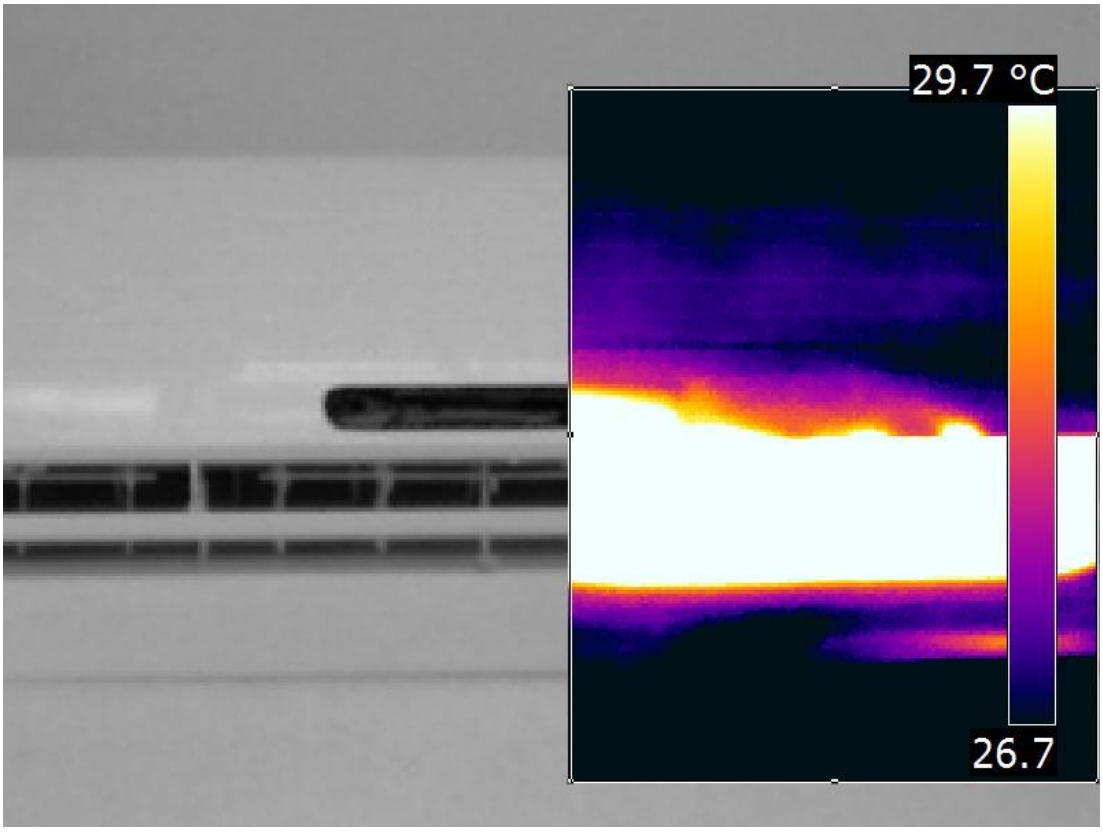

Figure 2.46 Infrared image that captured an overheat area.

This also shows the advantage of infrared thermography because detecting such situation with other methods is related with chance and generally not possible.

The data that gathered from these images also shared with the parallel studying CFD group. The data was given the group as inputs by averaging the measurement results or directly converting the experimental result to boundary conditions which is a more realistic input. The data also used for validating the CFD results.

The results gathered from this method for measuring the body temperature was so useful that, the ways of using this tool for measuring the air temperature was considered. The infrared camera hasn't the ability to measure the air temperature. At this point PIV has given the inspiration for searching an indirect measurement method which is called Meshed Infrared Thermography (MIT).

2.4 Meshed Infrared Thermography (MIT)

MIT method was founded by Ziya Haktan Karadeniz, Dilek Kumlutaş and Özgün Özer; as it is mention before in the previous part in the search for the ways of using infrared thermography for measuring the air temperature and this thesis also a part of its development.

2.4.1 The Methodology of MIT

MIT method is based on the measurement screen technique but luckily in the first literature search the research group run across with the measurement screen technique which has given the opportunity for a more free design.

In MIT method, the measurement screen is replaced with a measurement mesh which is formed by dull black painted metal spheres positioned periodically on pieces of ropes that are tightly fixed on a metal frame. Dimensions of the frame used were 200x200 mm and the horizontal and vertical distance between the spheres was both 25 mm forming a 7x7 nodes measurement mesh. The schematic of the measurement mesh is shown in Figure 2.47.

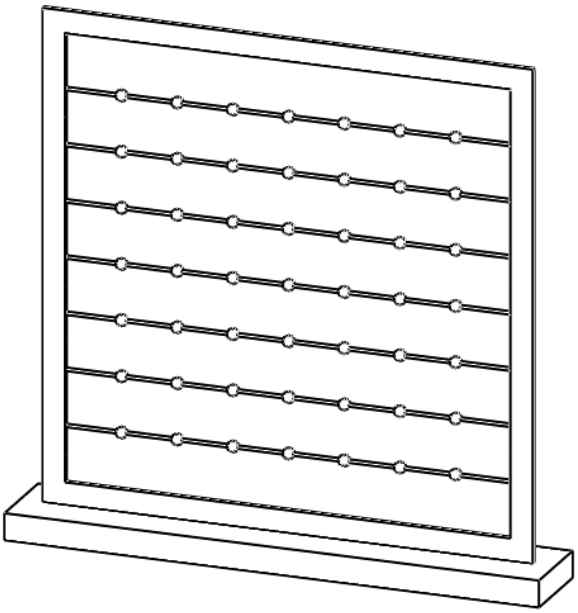

Figure 2.47 Measurement Mesh.

Measurement mesh is placed in the flow where the temperature distribution is wanted to be known and infrared camera is placed perpendicular to the measurement mesh to capture the infrared images. An infrared camera (FLIR T400) with 320x240 pixels of resolution, sensitive to infrared radiation between 7-13 μm wavelengths and having an accuracy of ±50mK at 30 C was used to capture infrared images of the measurement mesh. Figure 2.48 shows the image of a test experiment.

Temperatures of the spheres are assumed to be the air temperature at that point, therefore temperature distribution on the investigated plane is found. Although the frame, ropes and spheres may have some local effects on the flow, as long as the rope and frame are thin and spheres are small both in dimension and number, their effects on the flow is negligible.

Obtained infrared images are processed by a developed computer program in which the spheres are distinguished, their positions are found and temperatures of them are determined. Matlab used for coding.

Figure 2.48 A test experiment of MIT method.

In general the program uses a threshold algorithm for separating the metal spheres from back ground. Figure 2.49 shows an infrared image and its threshold.

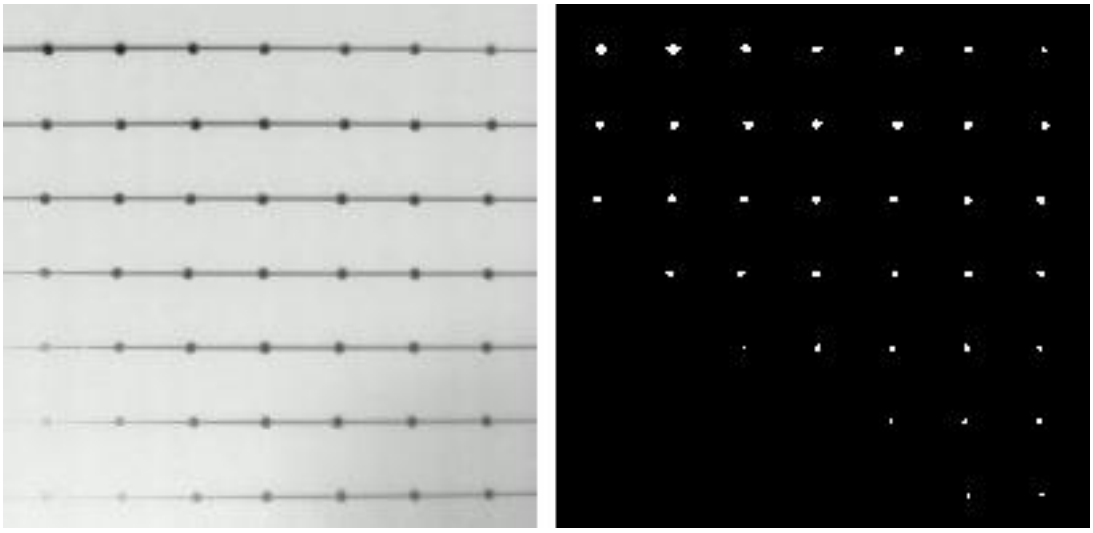

Figure 2.49 Infrared image and its threshold.

Then the threshold image also can be called an image mask. This mask's black areas are zero and the white areas are 1, so when we multiply the mask with the temperature data matrix, the back ground will be data will be eliminated. Then the image meshed and the program detects the maximum value on each mesh element. The maximums are use because the measurement spheres face that directly looking to the camera gives the right temperature measurement which is also the maximum.

As it can be seen in Figure 2.49 in automated detection some spheres dissolve to the background because of their temperature is very near to it. So when the image is meshed in some areas there is no sphere. In this position algorithm calculates the average of the background of this mesh and use this value in temperature mapping.

This phenomenon seems to be solved by using a different emissivity background that seems in different temperature for separating all spheres from it. But it is noted that this time there can be bigger problem that the spheres which have different temperature than background can be disappear. So this is not suggested.

Another solution to this situation is using manual masking. In this process user locate the spheres and creates the mask from the image. If the data set is imaged from the same point and if the measurement mesh does not move, then the mask for one of these images will work for all of them. In Figure 2.50 shows different manuel made masks. At up right infrared image, up left masked infrared image with 5 elements, down right masked infrared image with 13 elements, down left masked infrared image with 21 elements are showed.

The mask with 13 and 21 elements give better results because even the images taken by a camera that is fixed to a tripod, the image can be slightly tilt or shifted. The bigger masks can tolerate these mistakes more capably.

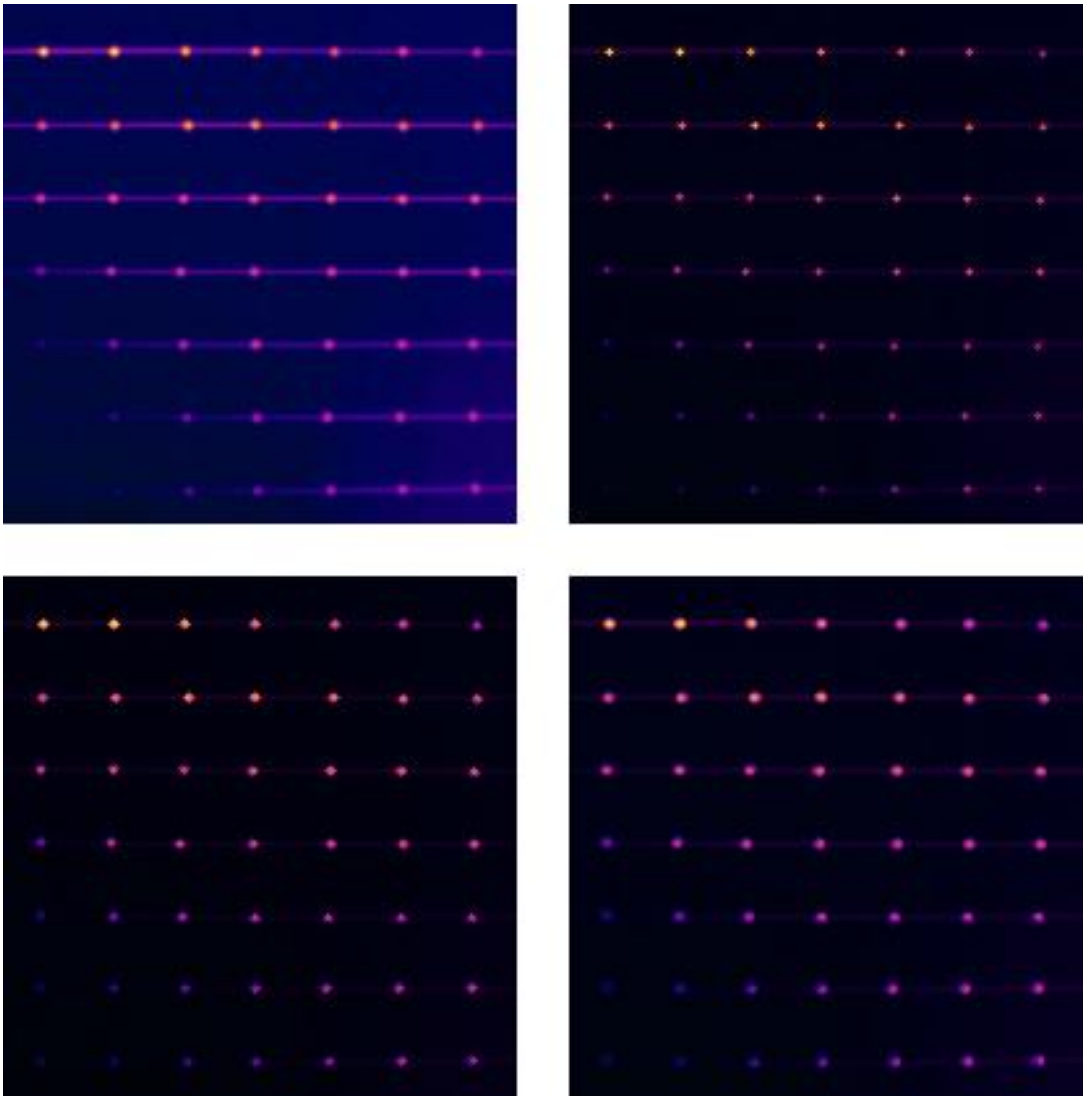

Figure 2.50 Up right infrared image, up left masked infrared image with 5 elements, down right masked infrared image with 13 elements, down left masked infrared image with 21 elements.

As the final result the instantaneous temperature distribution given as Figure 2.51. An average temperature distribution can be also obtained by calculating the average of the data set.

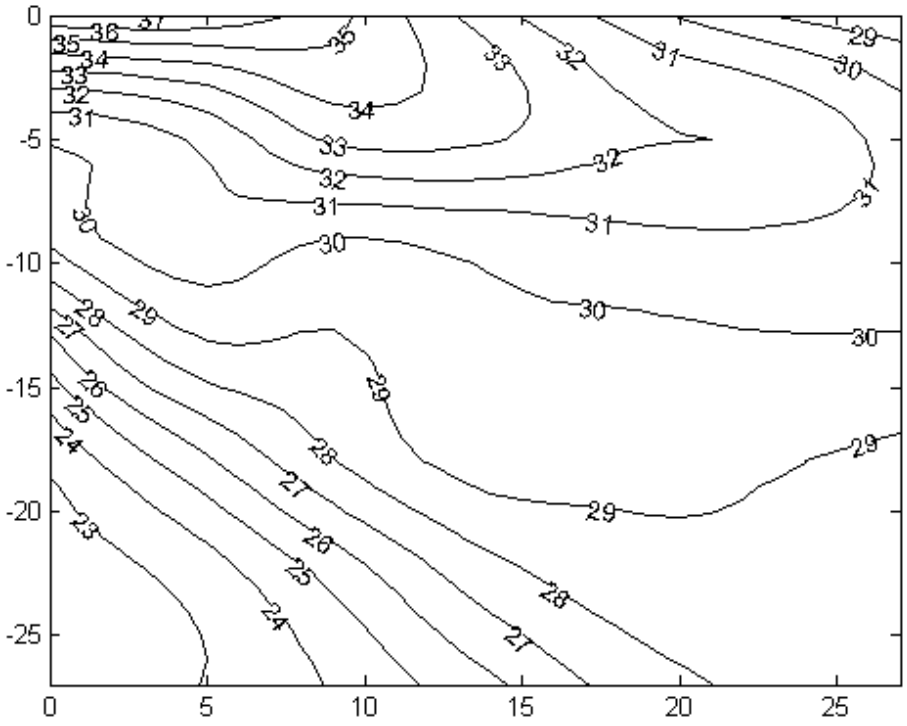

Figure 2.51 A sample temperature distribution.

2.4.2 Validation Experiment

A blower which produces an air jet at 50 C with 5m/s velocity at its outlet was used for validation of the method. Measurement mesh was placed into the flow parallel to the axis of the jet having the jet flow through its diagonal and with a distance of 40 mm from the top left corner of the measurement mesh to the outlet of the blower. Figure 2.52 show the schematic of the validation experiment and Figure 2.53 is the image of the validation experiment.

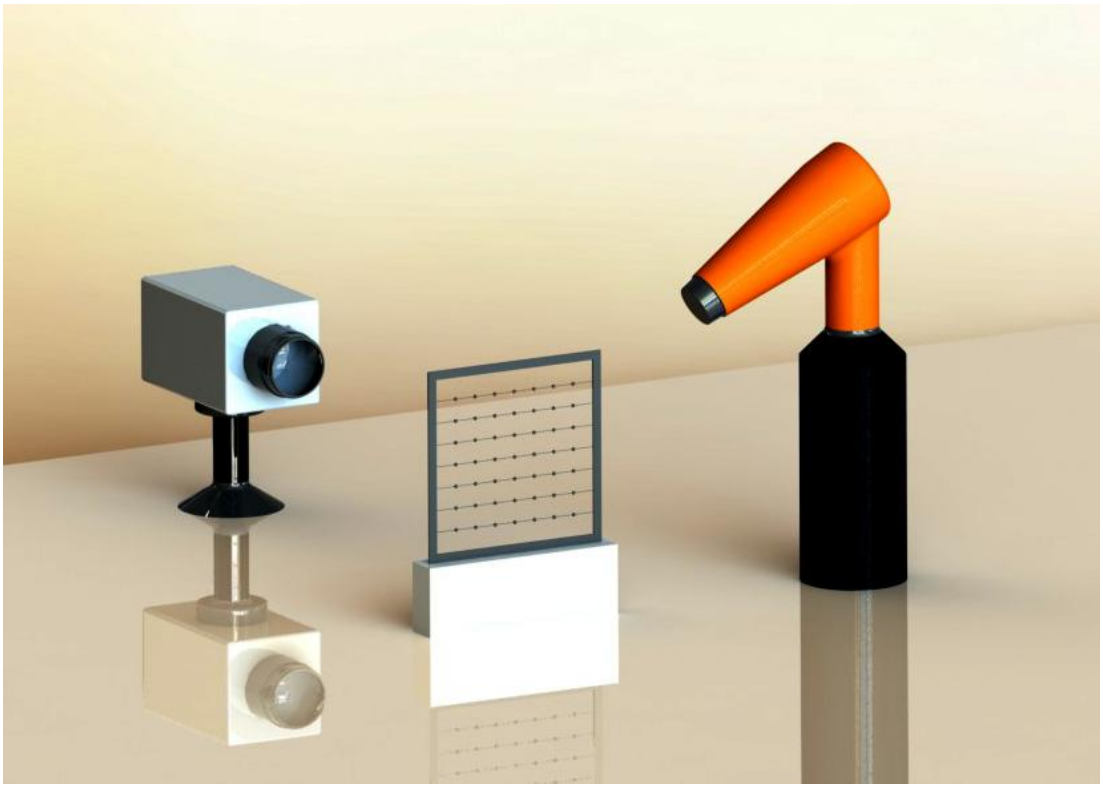

Figure 2.52 The schematic of the validation experiments.

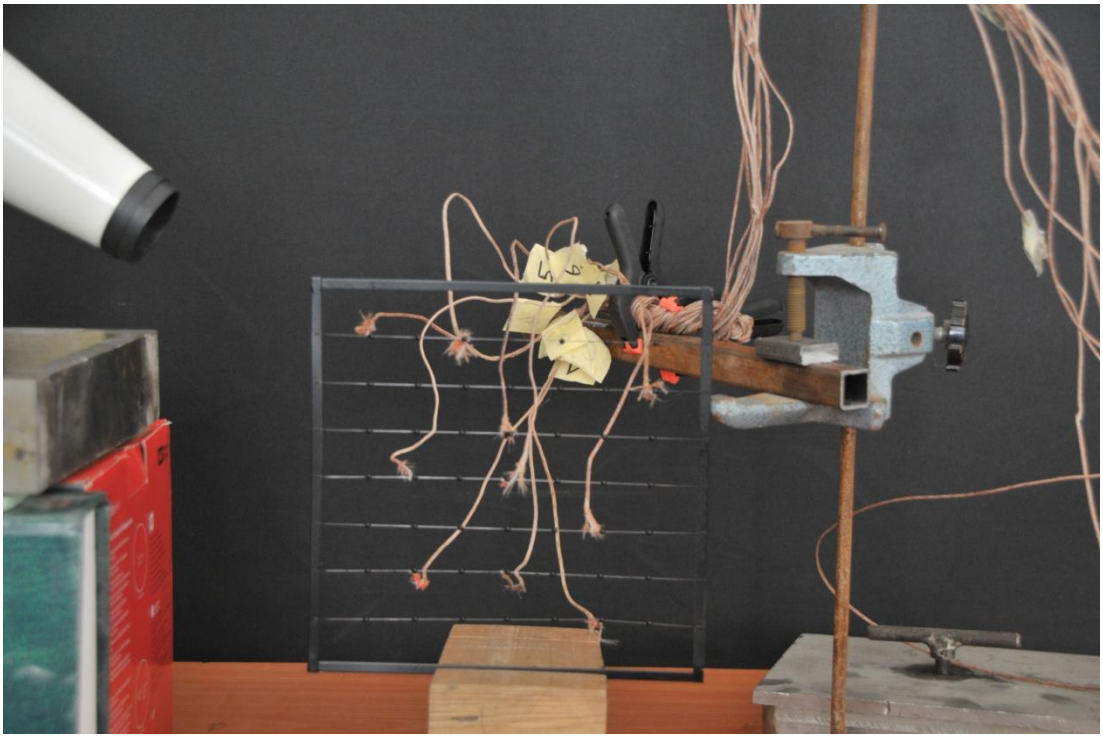

Figure 2.53 The image of the validation experiments.

Thermocouples were used for validating the results.10 K-type thermocouples were placed to the neighborhoods of the 10 randomly selected spheres for comparison and their positions are given in Figure 2.53 and Figure 2.54. Thermocouples were tested inside a water-bath at constant temperature (50 C) before the validation study and it is seen that absolute difference from the bath temperature is between 0.1 C and 0.5 C while standard deviation of the measured temperatures from different thermocouples is 0.15 C.

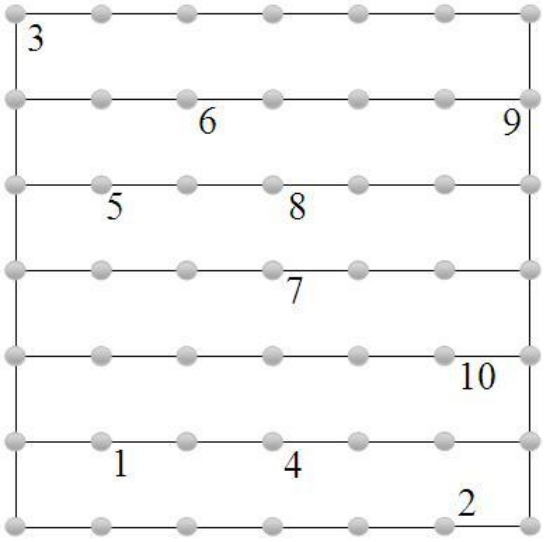

Figure 2.54 Thermocouple positions.

Steady state thermal behavior of the system was analyzed for determining the difference between the results of the MIT measurements and thermocouples. Steady state temperature measurements by MIT (indicated by IR) and thermocouples (indicated by TC) at points 1, 3, 6 and 10 on the measurement mesh and ambient temperature (Ta) are given in Figure 2.55. 32 infrared images were taken and they are processed to obtain instantaneous temperatures on comparison points. The absolute difference between the averages of these instantaneous temperature values on individual points and averages of the corresponding thermocouple data is between 0.15 and 2.7 C and standard deviation of the absolute differences for all points is 0.68 C. Therefore, MIT is adequate for visualizing the temperature distribution inside different flow sections.

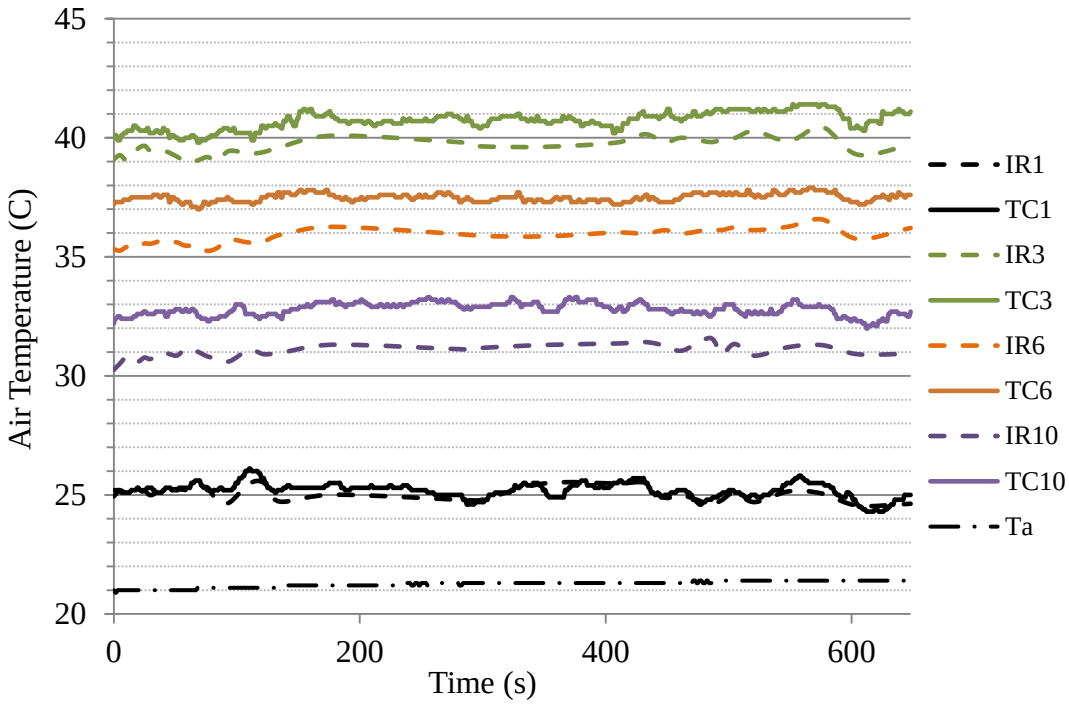

Figure 2.55 Steady state temperature measurements by PIIT (IR) and thermocouples (TC) at different points on the measurement mesh.

By this experiment the MIT method was validated and after the validation of the method, measurement mesh is placed in front of the SAC indoor unit at aforementioned sections which also used in PIV experiments.

CHAPTER THREE
RESULTS

In this chapter the experimental result will be shared.

3.1 Preliminary Experimental Studies

3.1.1 Velocity and Temperature Measurement Using Probe

As a preliminary study, a velocity and temperature measurement probe (Figure 3.1) is used for obtaining an average velocity and an average temperature. The probe includes a casing that covers the thin wire which is used for measurement. An opening is placed for the air to pass by while it measured, therefore the opening must be face to the flow direction (Figure 3.2). A plate was designed for stabilizing the flow.

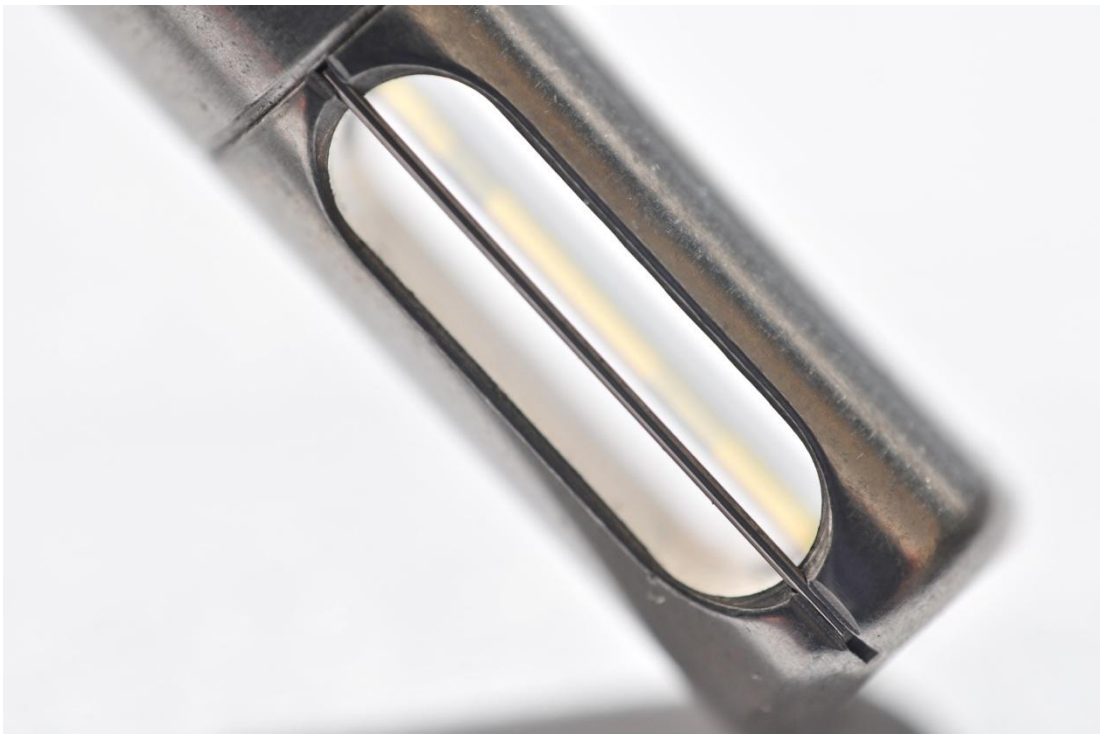

Figure 3.1 a velocity and temperature measurement probe.

Figure 3.2 Data acquiring with probe from exit of the SAC

Different experiments were made by moving the probe by hand along the exit of the SAC while measuring the temperature and the velocity (Figure 3.2). The results of the two of these experiments are shared in Table 3.1, Figure 3.3 and Figure 3.4. The two experiments have taken different period of time therefore there are different numbers of acquired data.

It can be seen in Figure 3.4 in one of the experiments there is an instant and huge drop in the velocity which can also be seen in Figure 3.3 as a minor drop in the temperature. This effect did not caused by the SAC but it is caused by the researcher movements. As the velocity is a vector quantity and the temperature is a scalar quantity, it is normal to the velocity measurement is more effected than the temperature because of such mistake.

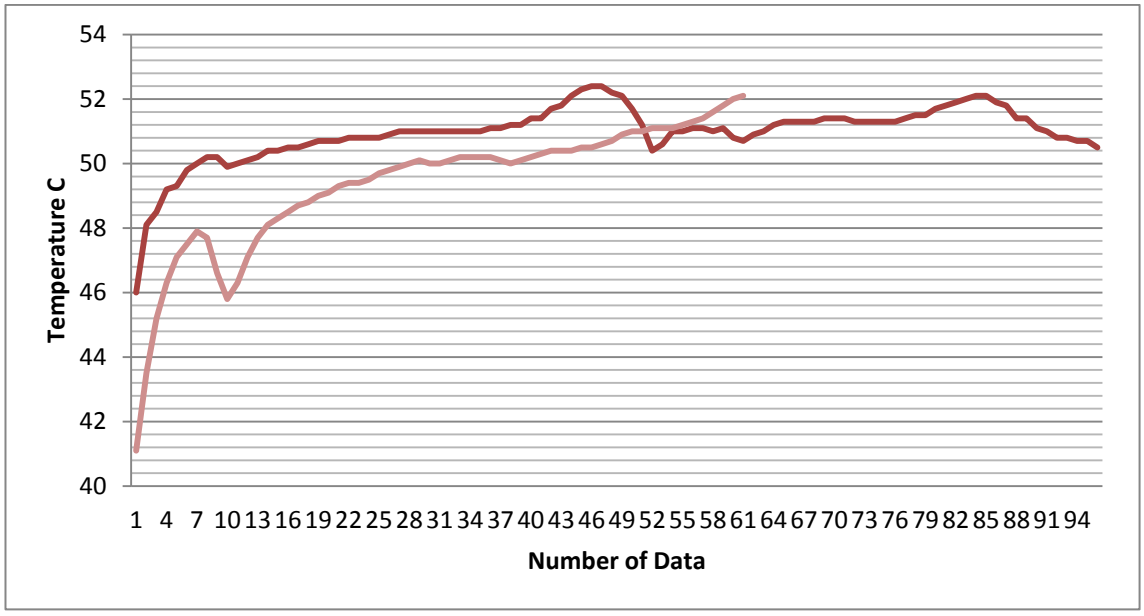

Figure 3.3 The temperatures data acquired from two different experiments.

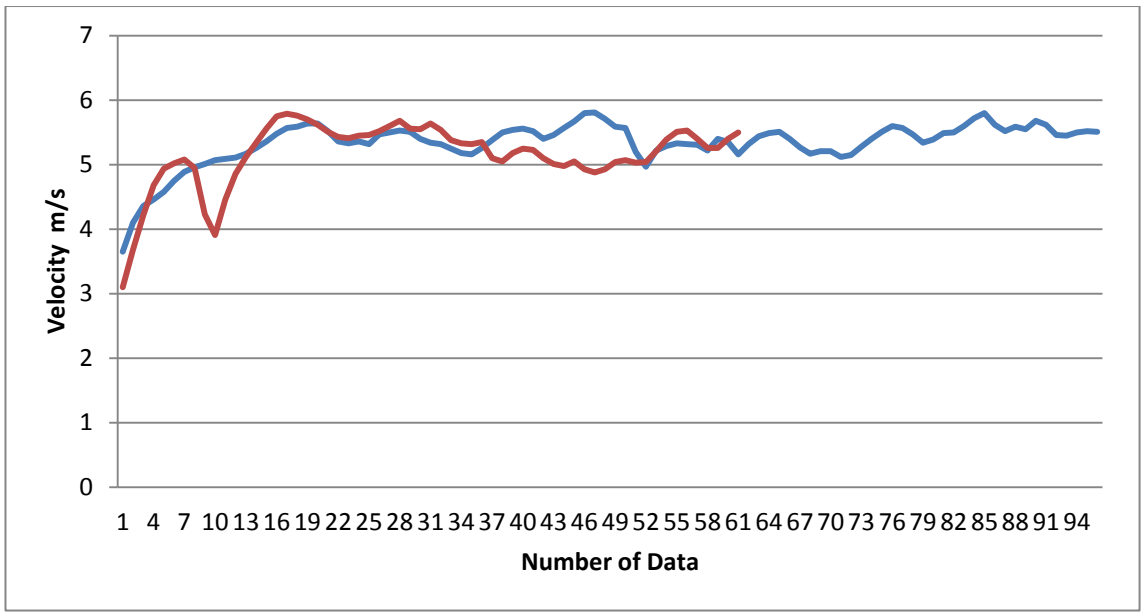

Figure 3.4 The velocity data acquired from two different experiments.

This shows the probe that is used by hand has not got the reliability the researchers any wrong move will modify the results and will cause errors. A better experiment could be made by using a traverse system but as it mentioned at the previous chapter, the system is nearly as expensive as a small PIV system which is more advanced system and has more capability then the probe used system.

Table 3.1 The average, maximum and minimum temperature and velocity data acquired with the probe.

	Experiment 1	Experiment 2
Average Temperature (C)	49.346	50.961
Maximum Temperature (C)	52.100	52.400
Minimum Temperateru (C)	41.100	46.000
Avarage Velocity (m/s)	5.161	5.337
Maximum Velocity (m/s)	5.790	5.810
Minimum Velocity (m/s)	3.100	3.650
Number of Data	61	96

So, because these movement errors, the minimum results that are shared in Table 3.1 cannot be used and also the average data contains some amount of error.

However, although the average results include some errors, these data gave a general overlook on the system. The velocity data gathered from these experiments were useful for PIV by giving a general idea and values for calculating the time between pulses before the experiments so more accurate data have been acquired.

It also gave general information about the exit temperature data which used in MIT experiment setup design and used for comparison of the preliminary experiments. These data also shared with the CFD group that parallel studying on the system for them to use as input and validation of their preliminary analyses.

3.2 The PIV Experiment Results

In this part of this study the results of the PIV experiments on a mid-design prototype will be presented. These studies separated into two groups. The out flow investigation and internal flow investigation.

In the outflow investigation part the SAC indoor unit was scanned by investigation planes and after that the averages of these measurements combined to obtain the whole flow profile of the SAC indoor unit.

In internal flow investigation a cut off model used and because of the optical access problems a determined plane that represents the general geometry of the SAC was investigated.

3.2.1 Outflow Investigation of the SAC

For obtaining the whole flow profile of the SAC indoor units, the SAC indoor units were scanned by investigation planes and after that the averages of these measurements combined. Figure 3.5 shows these investigation planes' positions on the SAC.

Figure 3.5 Positions of the investigation planes on SAC.

These experiments are critical for improving the SAC design because any problems in design that harms the flow structure can be detected in the outside of the SAC. This profile is also can be used for understanding the general flow that SAC creates in a room.

There are three types of results that is shared in this part of the study. The average three dimensional velocity distributions were obtained by SPIV experiment and 400 images were used for every map which means the maps are average on 100 measurement. A whole set of instantaneous measurement on an investigation plane seven is shared on part 3.2.1.3 for comparing the averages with the real flow structure. The vectors on these figures represent the flow in the measurement plane and the background black and white areas represent the out of plane flows. White areas shows +z which is towards the reader and the blacks are the opposite.

The second type of results is voticity maps. These data is shared for determining the main flow. As the color changes red to blue the intensity vorticity grows. These images used for qualitative purposes so they were not scaled.

The third type of the results is stream lines. Purpose of these figures is to show the flow direction more clearly because different flow directions on different sections of the SAC can create instantaneous moment forces which would cause vibration and noise.

3.2.1.1 Outflow Investigation of The SAC with a Skewed CFF

The skewed CFF was the main CFF of this proto type because it makes less noise and vibration. The general explanation of that is, it gives a lower velocity flow than the straight CFF.

The PIV results of the skewed CFF used SAC’s outflow on the investigation planes (that are defined in Figure 3.5) are presented at the flowing figures between the Figure 3.6 and Figure 3.41.

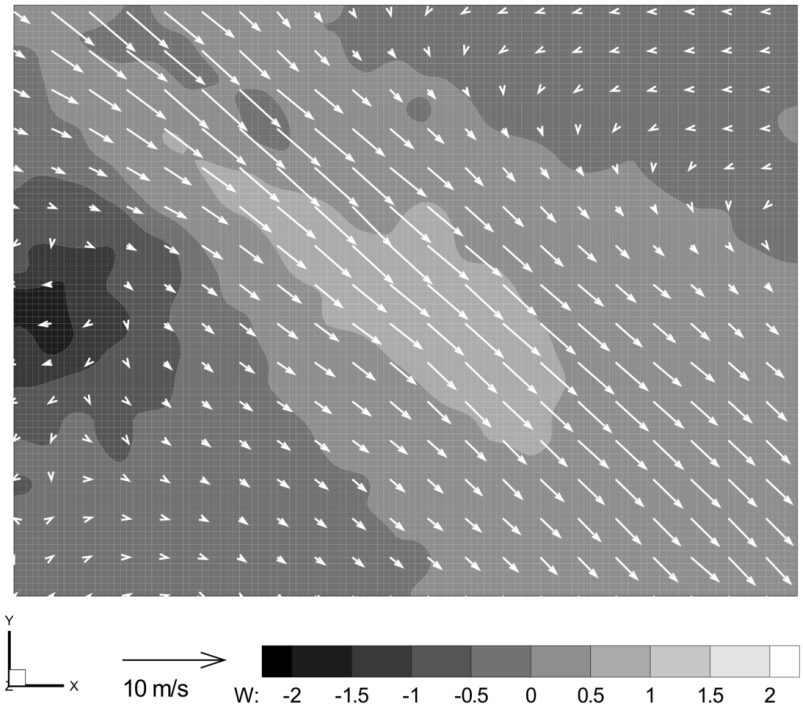

Figure 3.6 Average three dimensional velocity distribution of the skewed CFF used SAC on investigation plane 1.

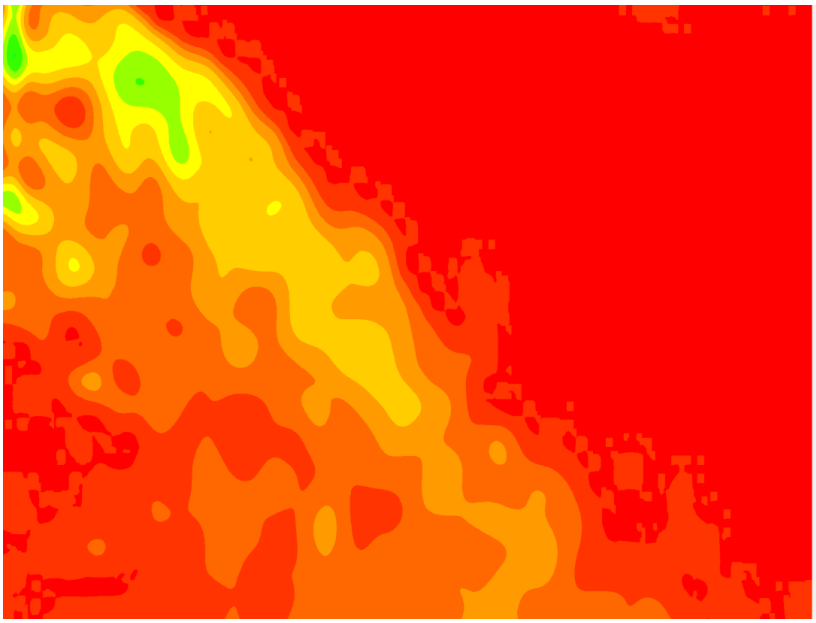

Figure 3.7 Average vorticity map of the skewed CFF used SAC on investigation plane 1.

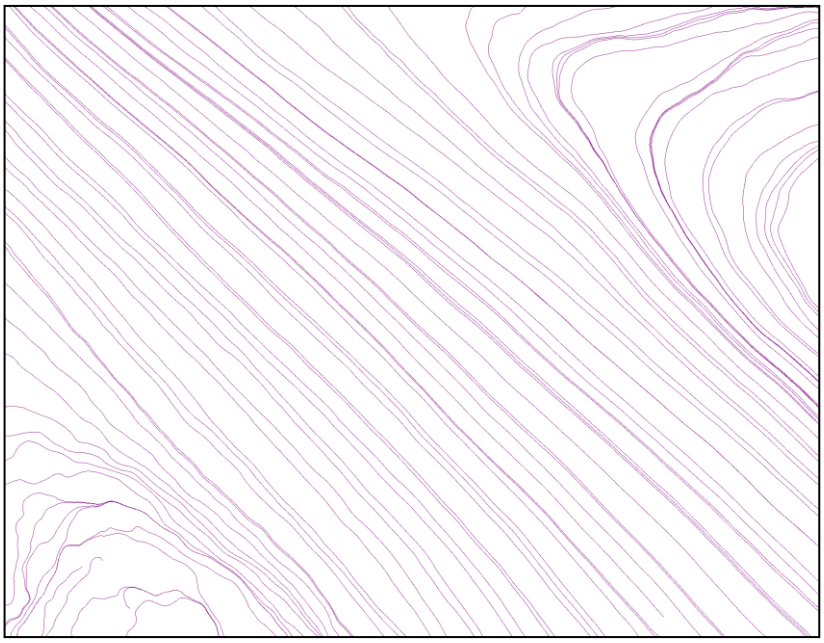

Figure 3.8 Average stream Lines of the skewed CFF used SAC on investigation plane 1.

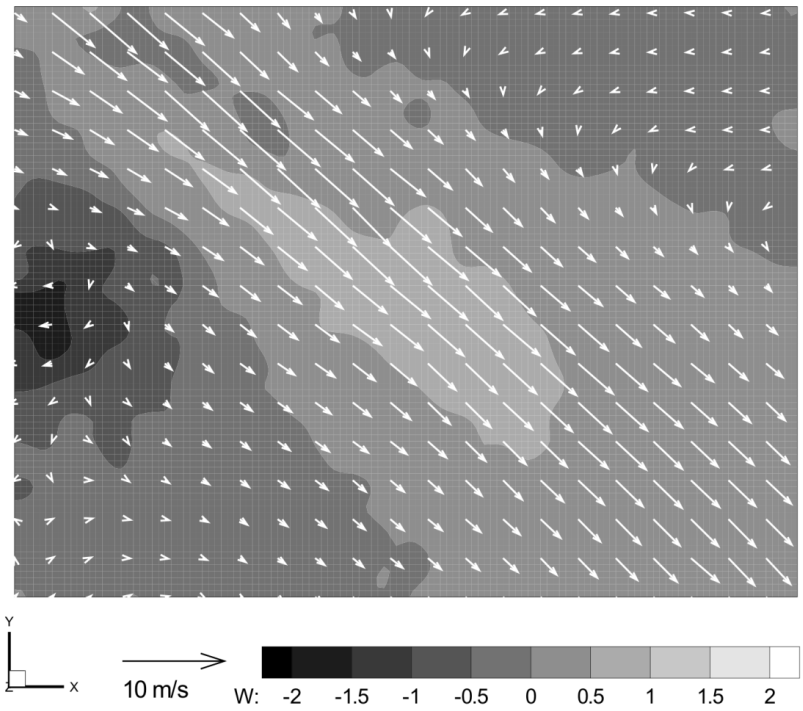

Figure 3.9 Average three dimensional velocity distribution of the skewed CFF used SAC on investigation plane 2.

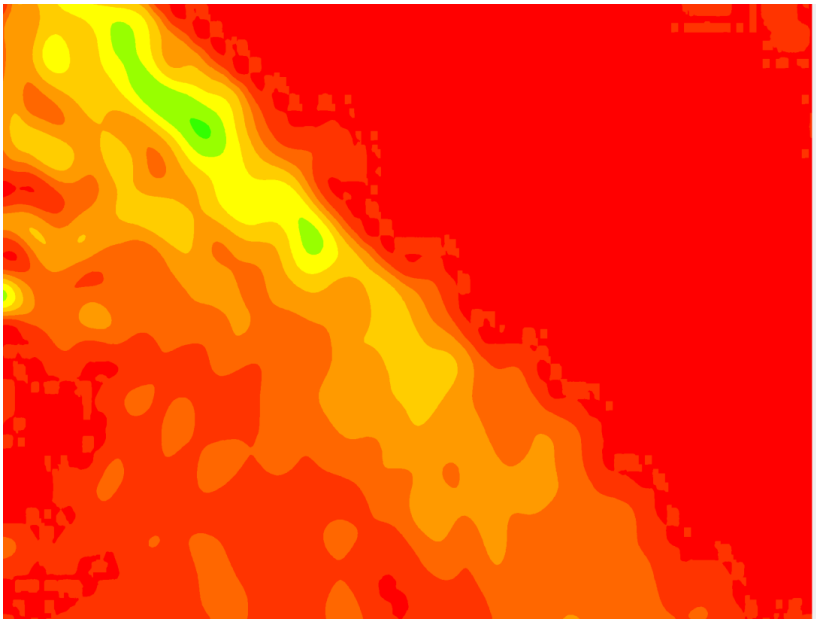

Figure 3.10 Average vorticity map of the skewed CFF used SAC on investigation plane 2.

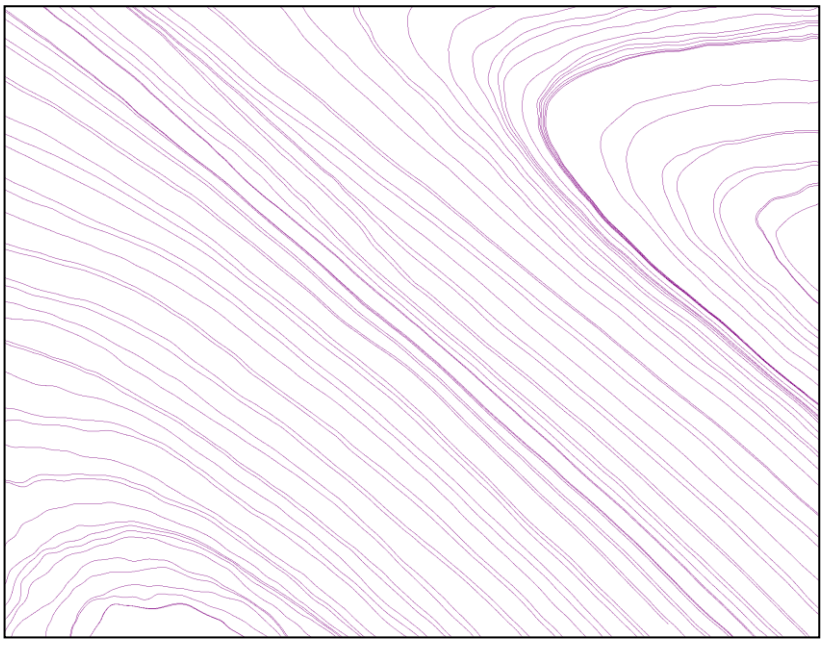

Figure 3.11 Average stream Lines of the skewed CFF used SAC on investigation plane 2.

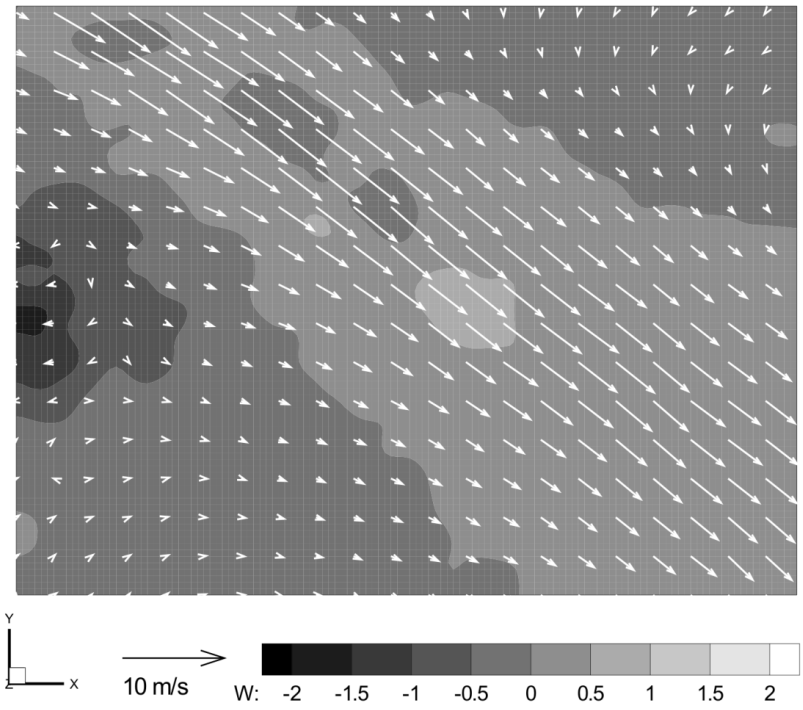

Figure 3.12 Average three dimensional velocity distribution of the skewed CFF used SAC on investigation plane 3.

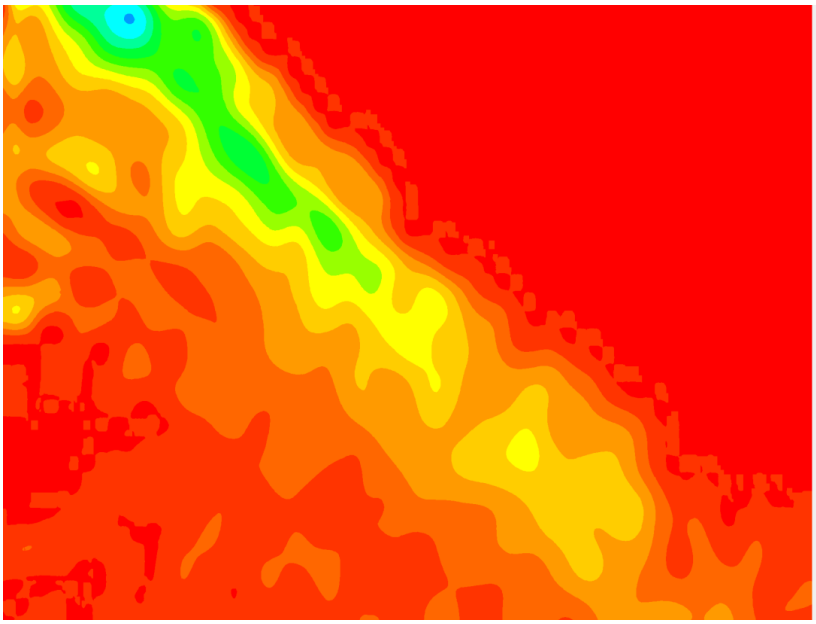

Figure 3.13 Average vorticity map of the skewed CFF used SAC on investigation plane 3.

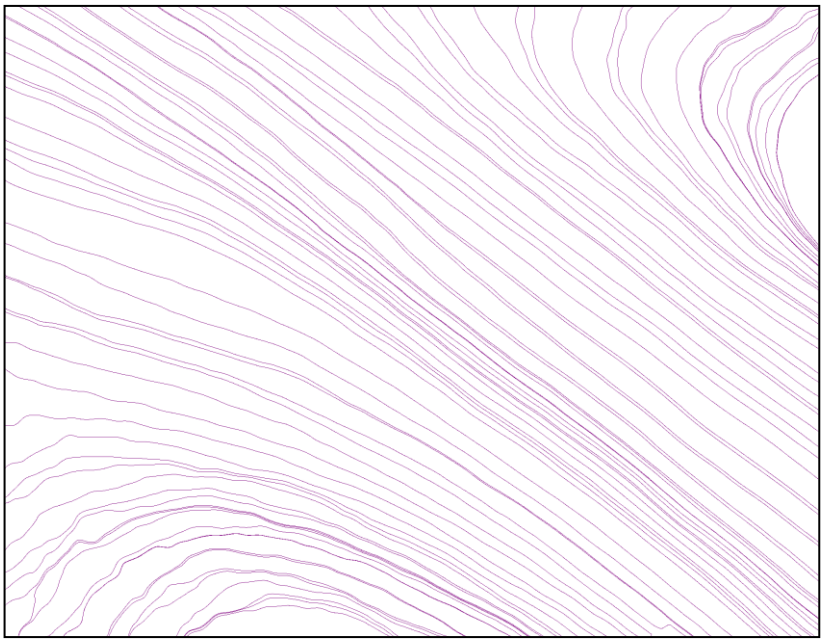

Figure 3.14 Average stream Lines of the skewed CFF used SAC on investigation plane 3

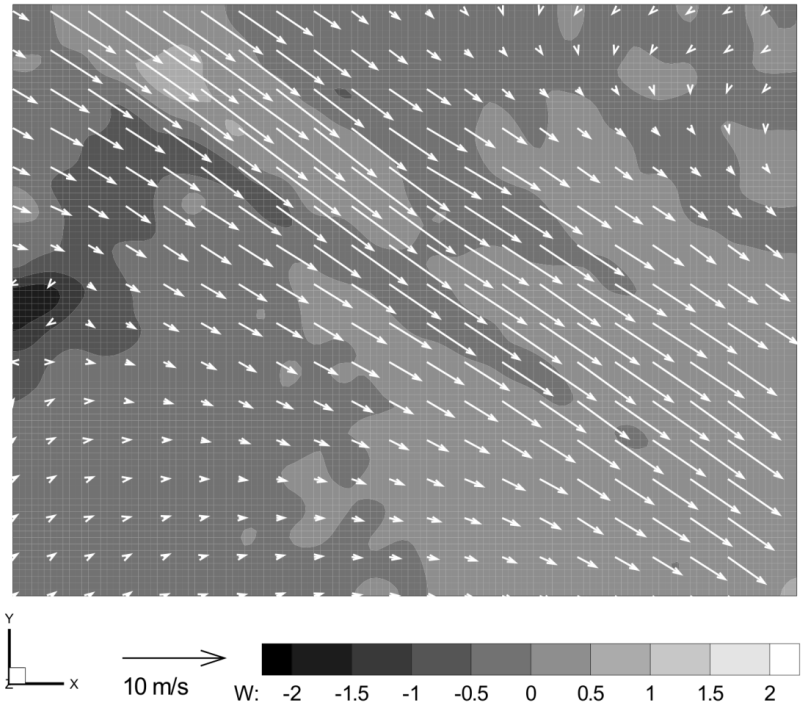

Figure 3.15 Average three dimensional velocity distribution of the skewed CFF used SAC on investigation plane 4.

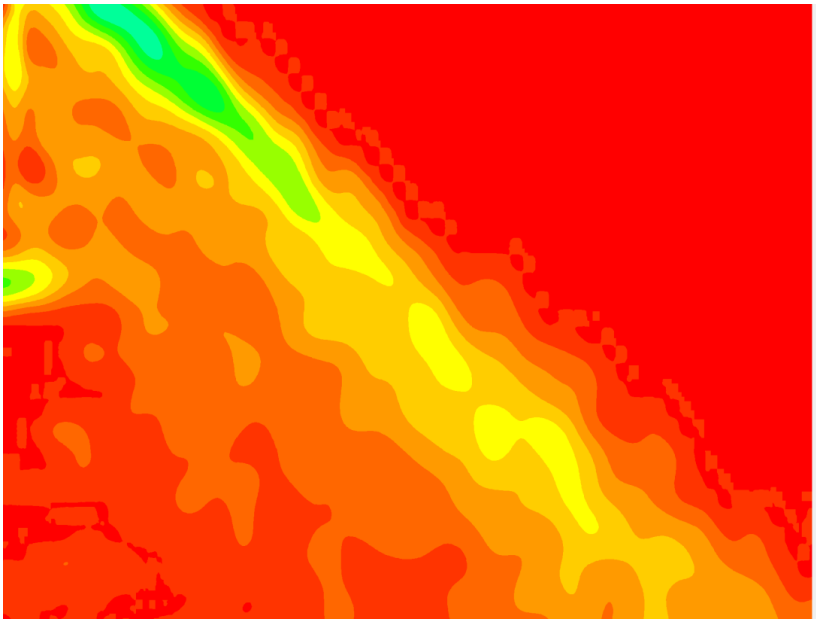

Figure 3.16 Average vorticity map of the skewed CFF used SAC on investigation plane 4.

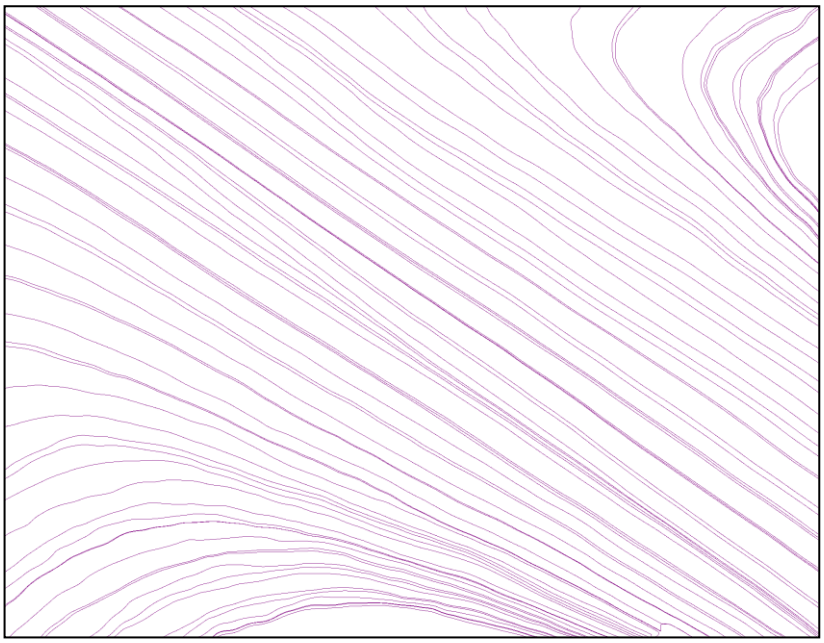

Figure 3.17 Average stream Lines of the skewed CFF used SAC on investigation plane 4.

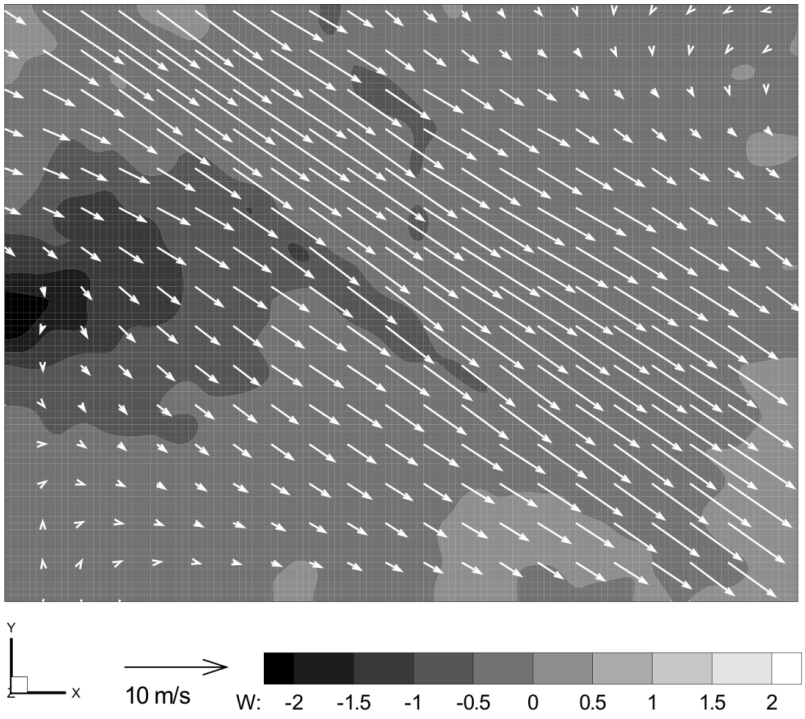

Figure 3.18 Average three dimensional velocity distribution of the skewed CFF used SAC on investigation plane 5.

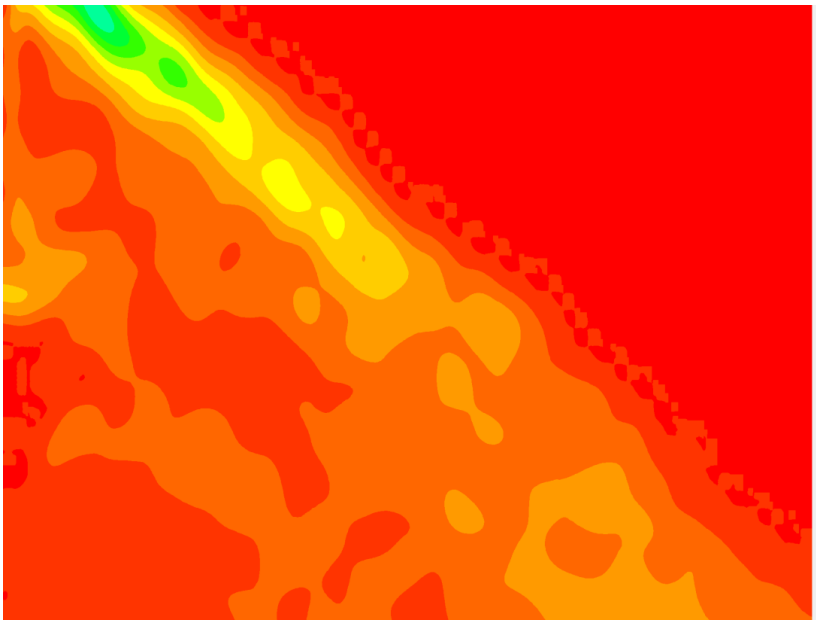

Figure 3.19 Average vorticity map of the skewed CFF used SAC on investigation plane 5.

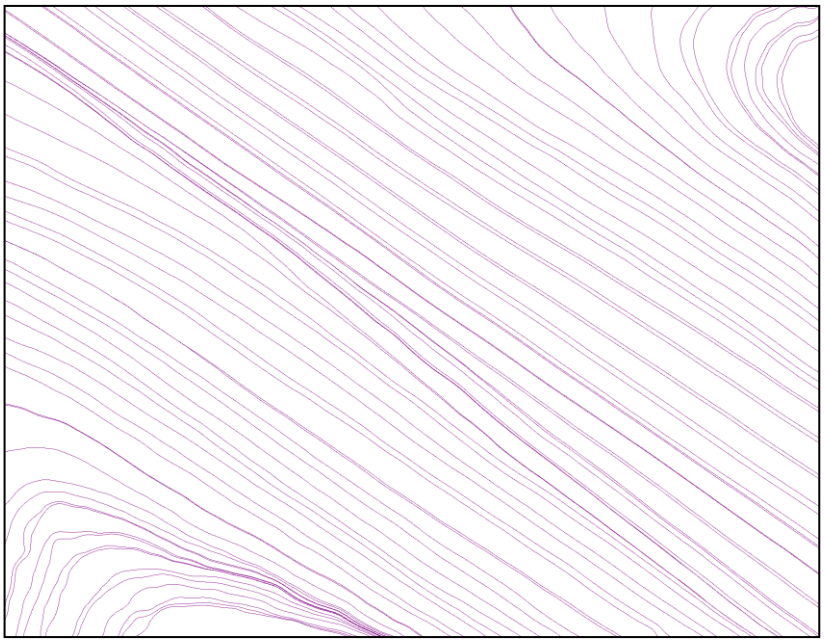

Figure 3.20 Average stream Lines of the skewed CFF used SAC on investigation plane 5.

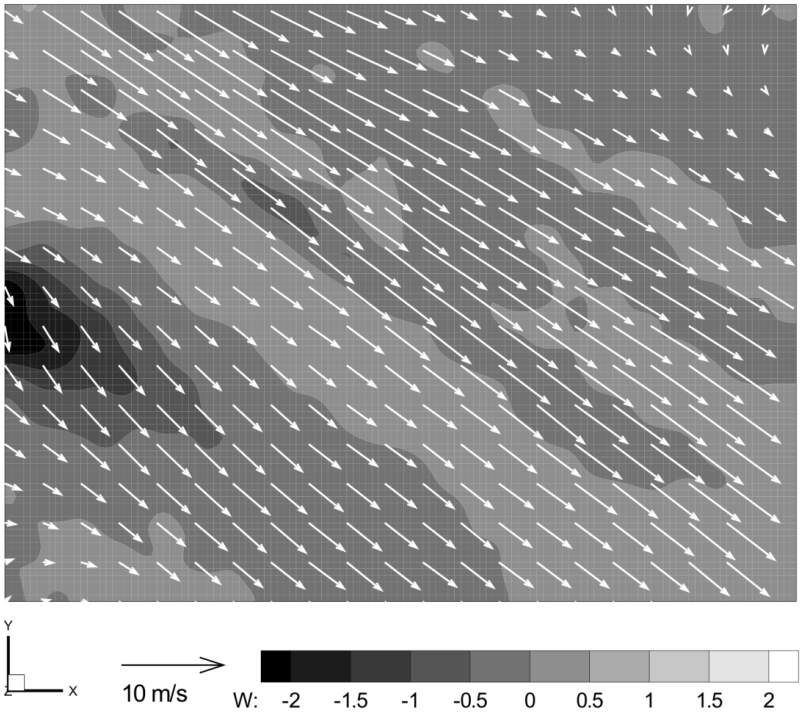

Figure 3.21 Average three dimensional velocity distribution of the skewed CFF used SAC on investigation plane 6.

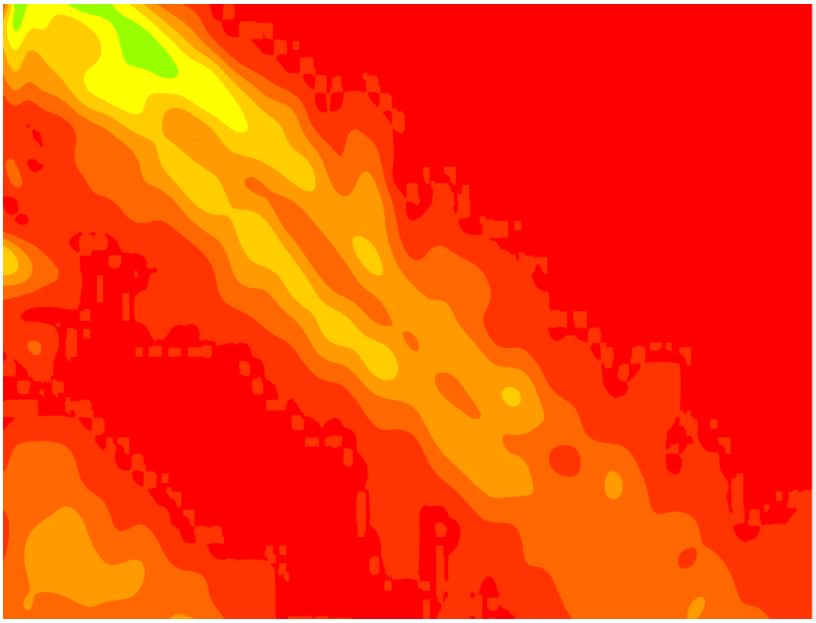

Figure 3.22 Average vorticity map of the skewed CFF used SAC on investigation plane 6.

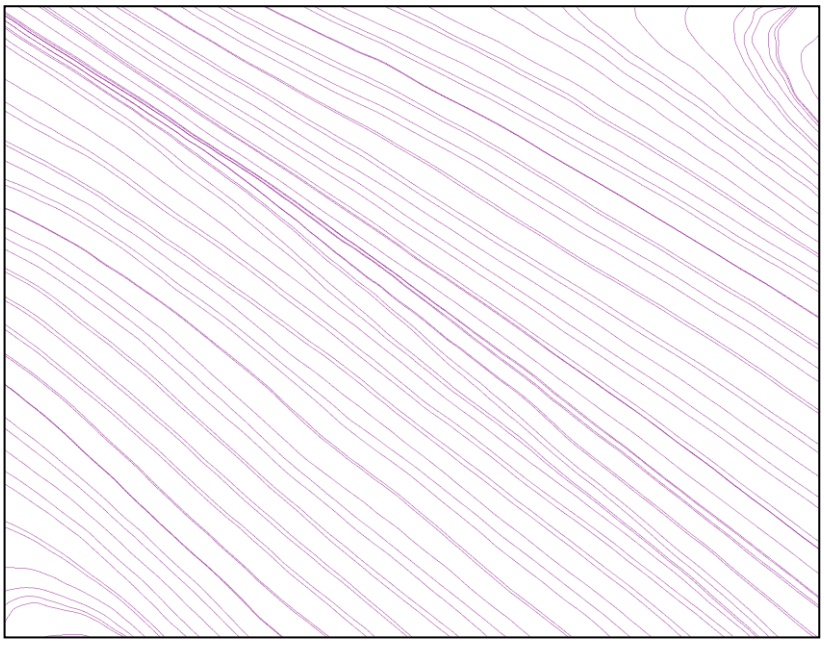

Figure 3.23 Average stream Lines of the skewed CFF used SAC on investigation plane 6.

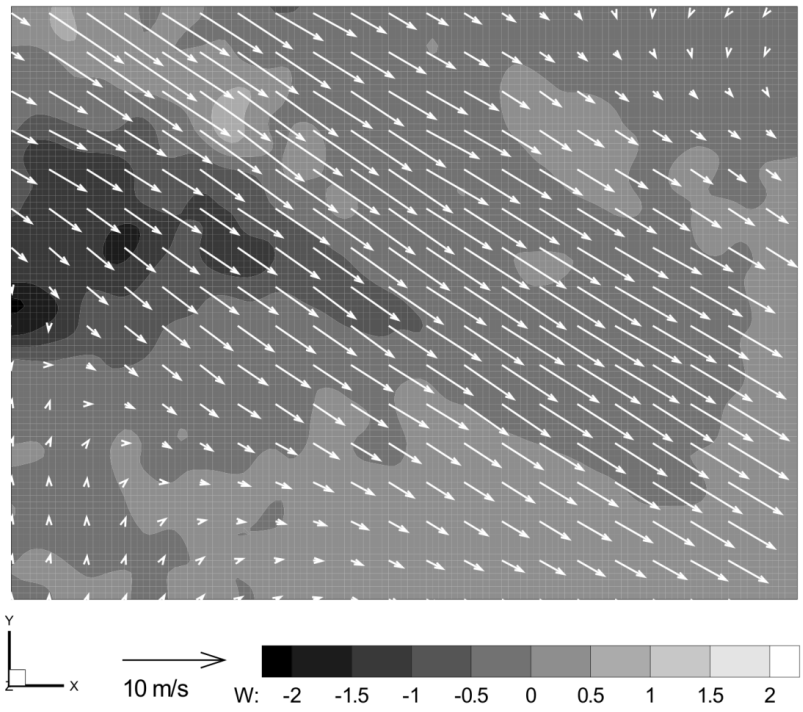

Figure 3.24 Average three dimensional velocity distribution of the skewed CFF used SAC on investigation plane 7.

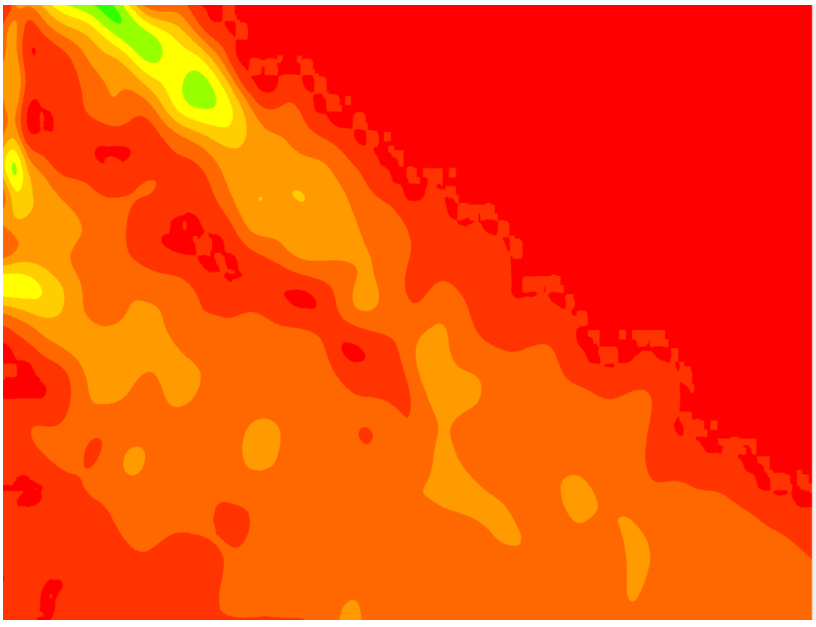

Figure 3.25 Average vorticity map of the skewed CFF used SAC on investigation plane 7.

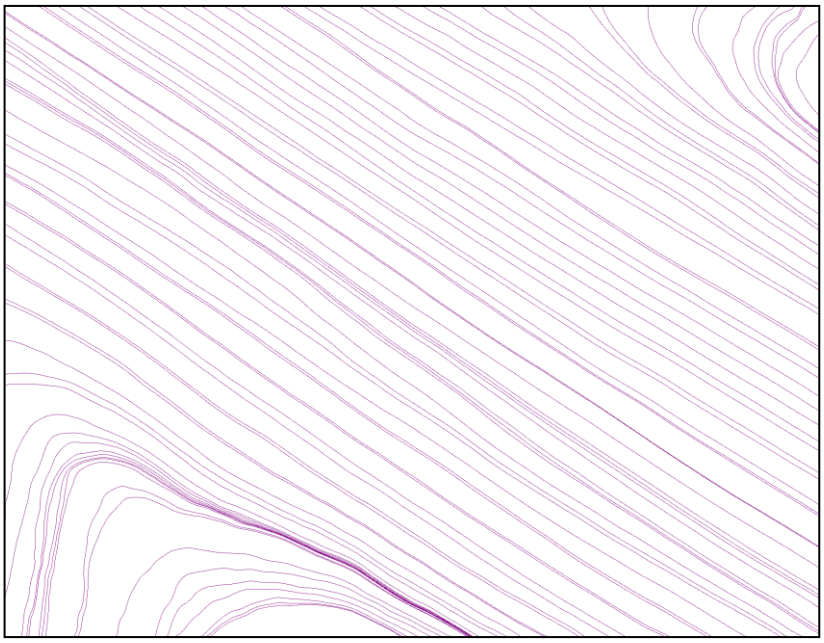

Figure 3.26 Average stream Lines of the skewed CFF used SAC on investigation plane 7.

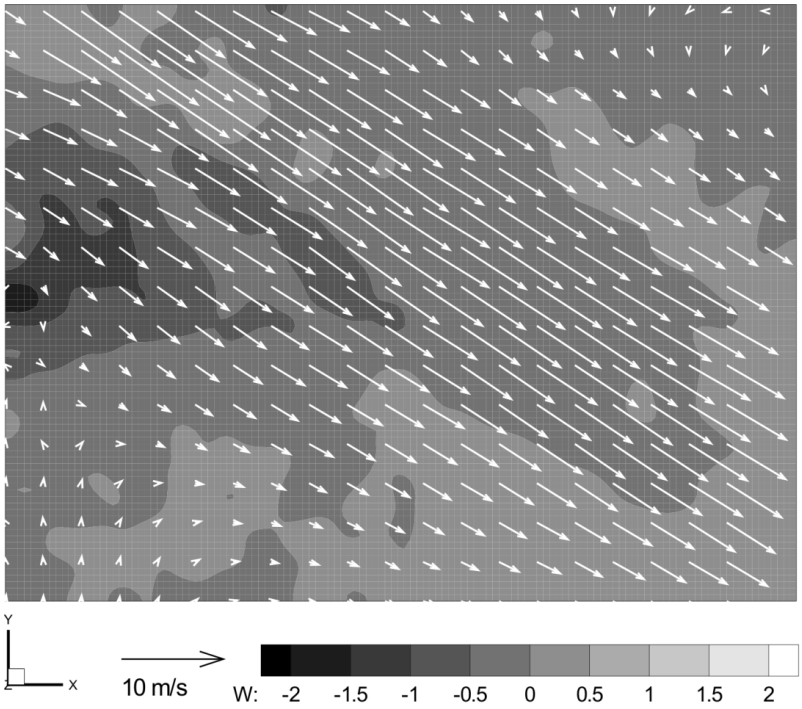

Figure 3.27 Average three dimensional velocity distribution of the skewed CFF used SAC on investigation plane 8.

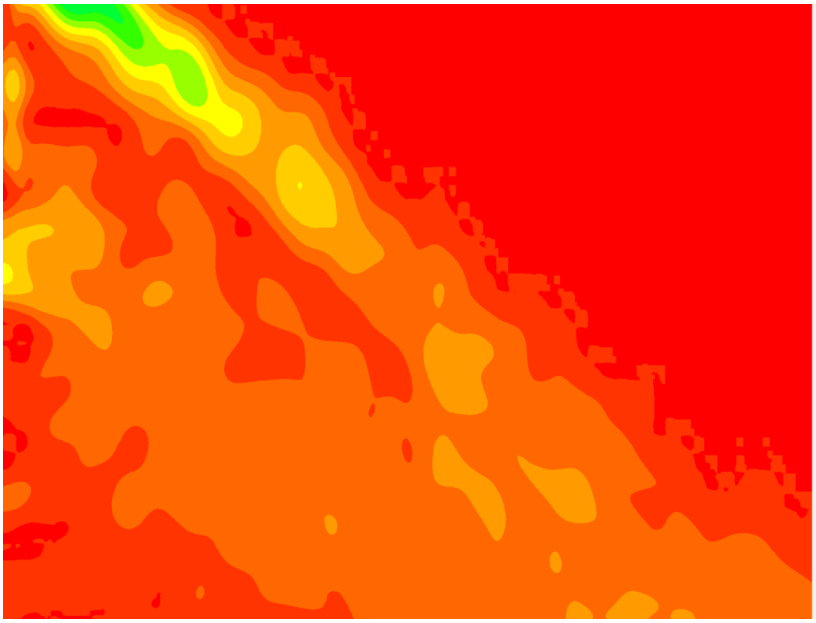

Figure 3.28 Average vorticity map of the skewed CFF used SAC on investigation plane 8.

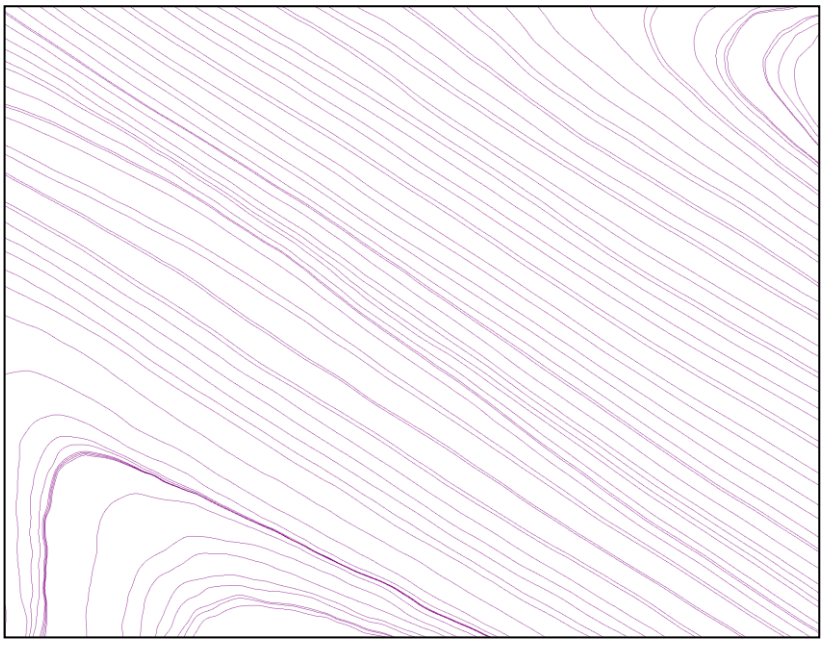

Figure 3.29 Average stream Lines of the skewed CFF used SAC on investigation plane 8.

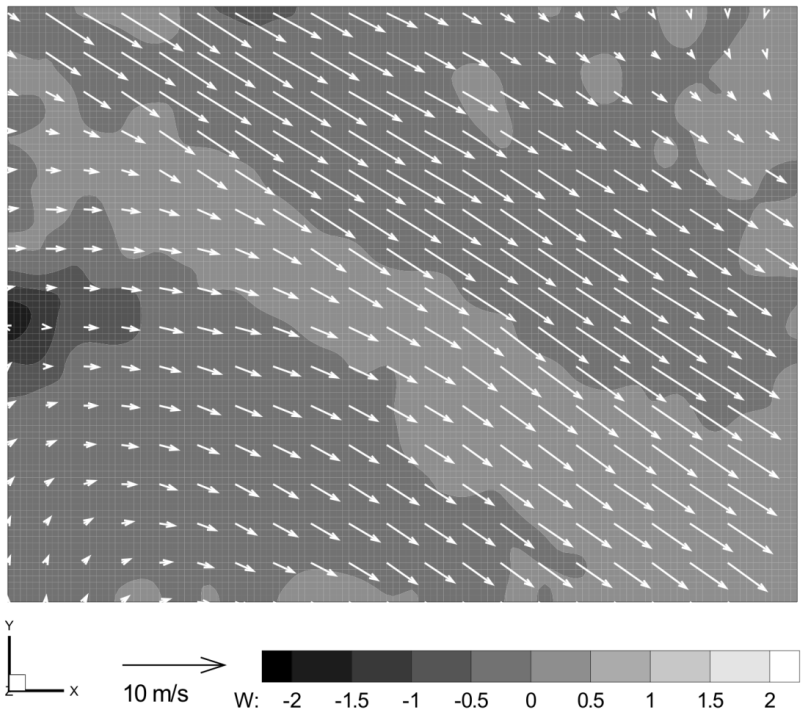

Figure 3.30 Average three dimensional velocity distribution of the skewed CFF used SAC on investigation plane 9.

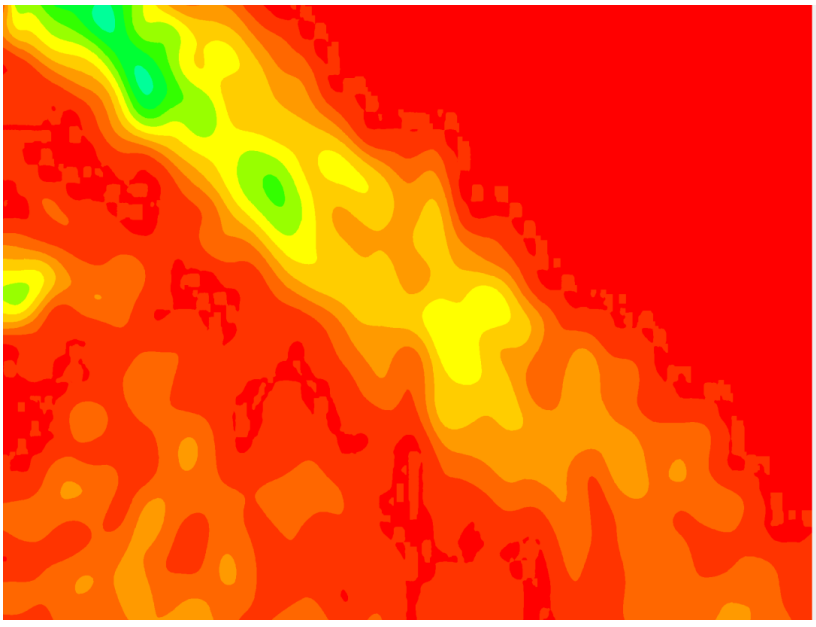

Figure 3.31 Average vorticity map of the skewed CFF used SAC on investigation plane 9.

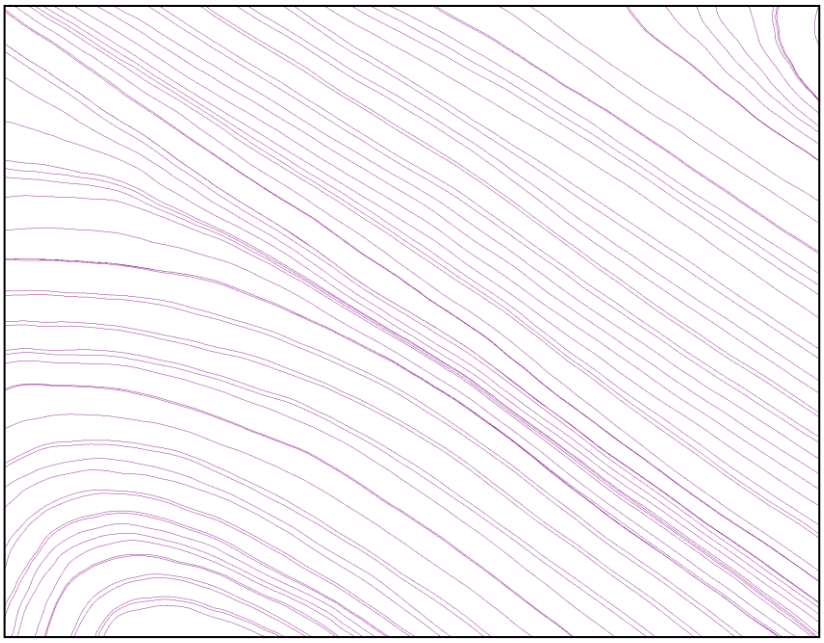

Figure 3.32 Average stream Lines of the skewed CFF used SAC on investigation plane 9.

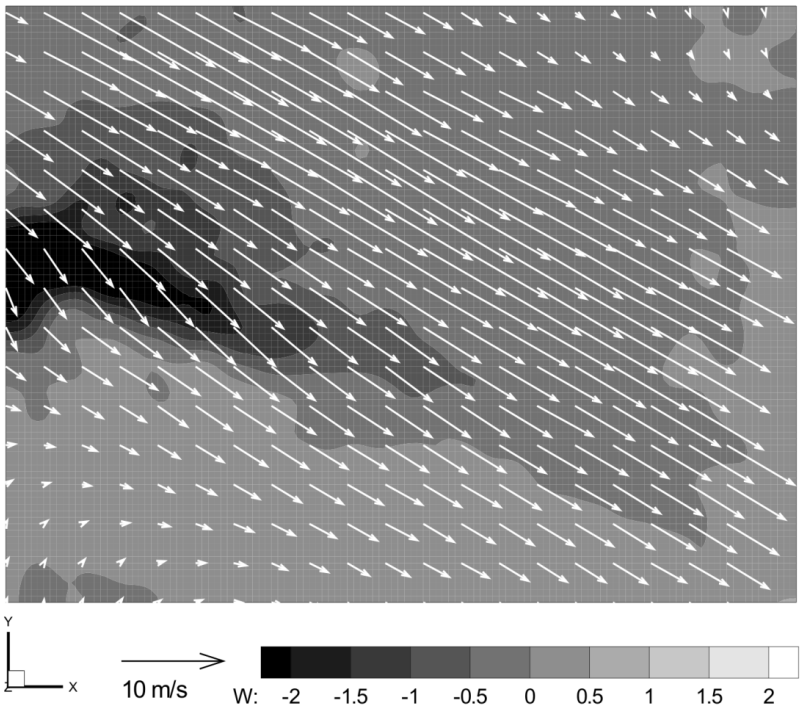

Figure 3.33 Average three dimensional velocity distribution of the skewed CFF used SAC on investigation plane 10.

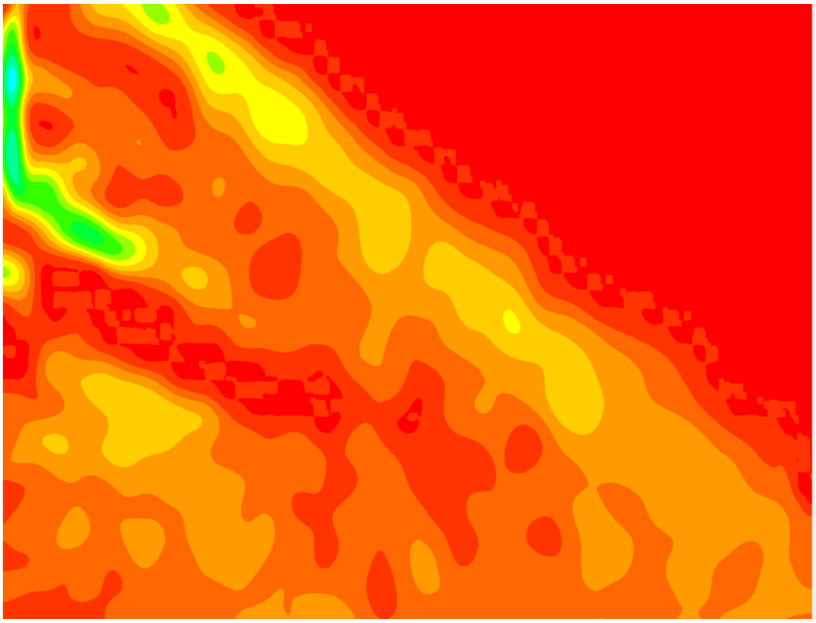

Figure 3.34 Average vorticity map of the skewed CFF used SAC on investigation plane 10.

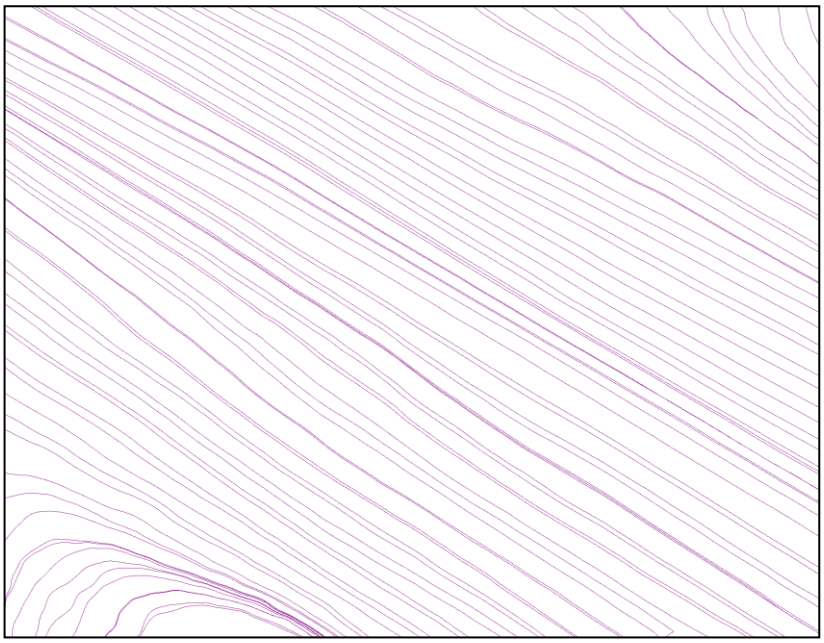

Figure 3.35 Average stream Lines of the skewed CFF used SAC on investigation plane 10.

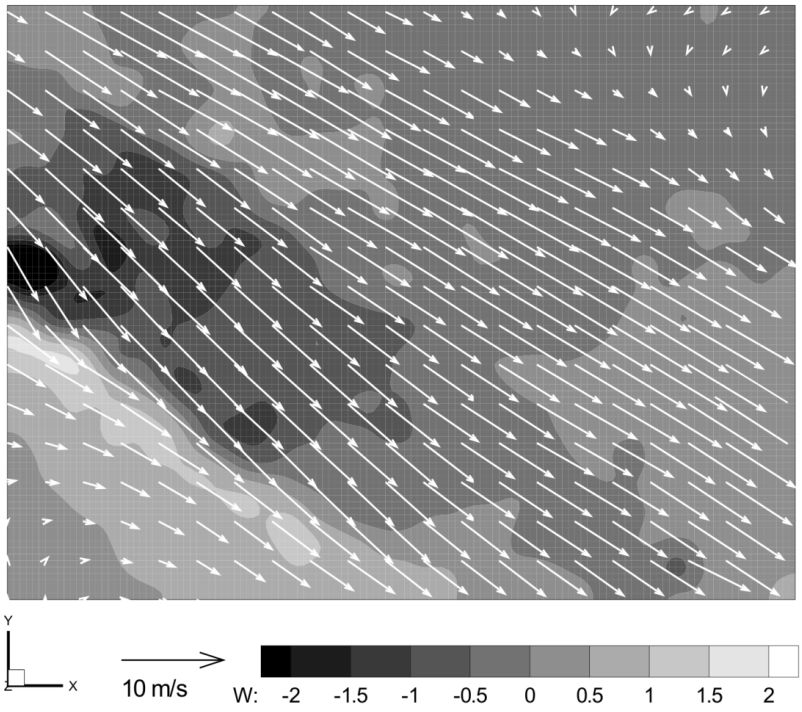

Figure 3.36 Average three dimensional velocity distribution of the skewed CFF used SAC on investigation plane 11.

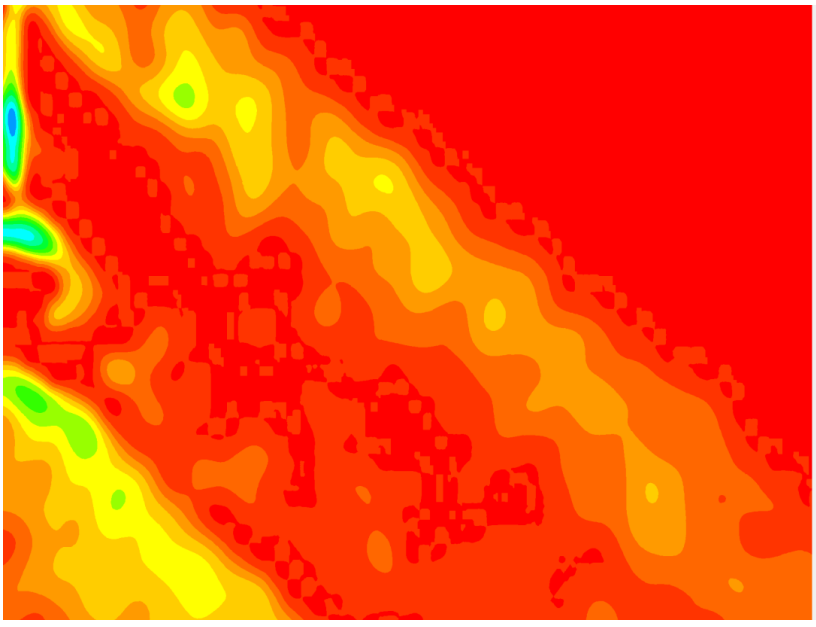

Figure 3.37 Average vorticity map of the skewed CFF used SAC on investigation plane 11.

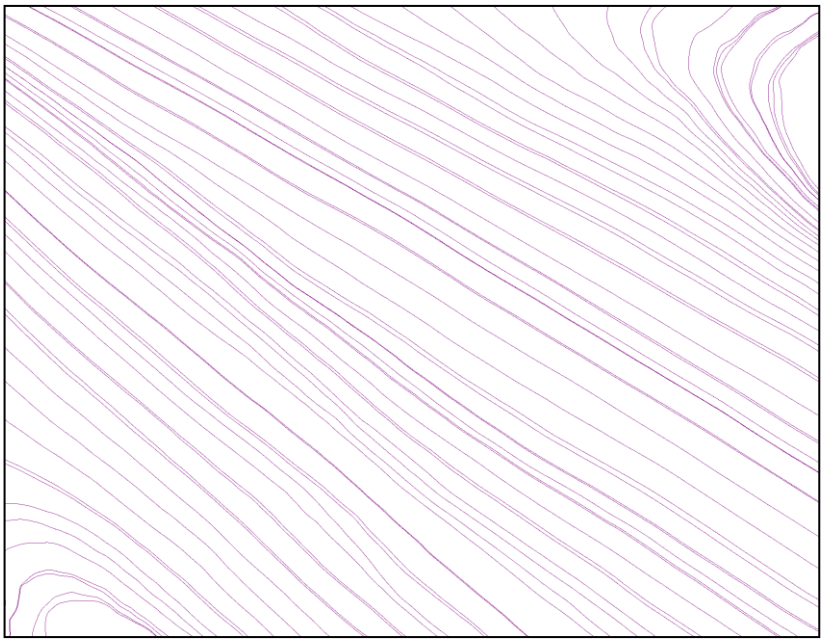

Figure 3.38 Average stream Lines of the skewed CFF used SAC on investigation plane 11.

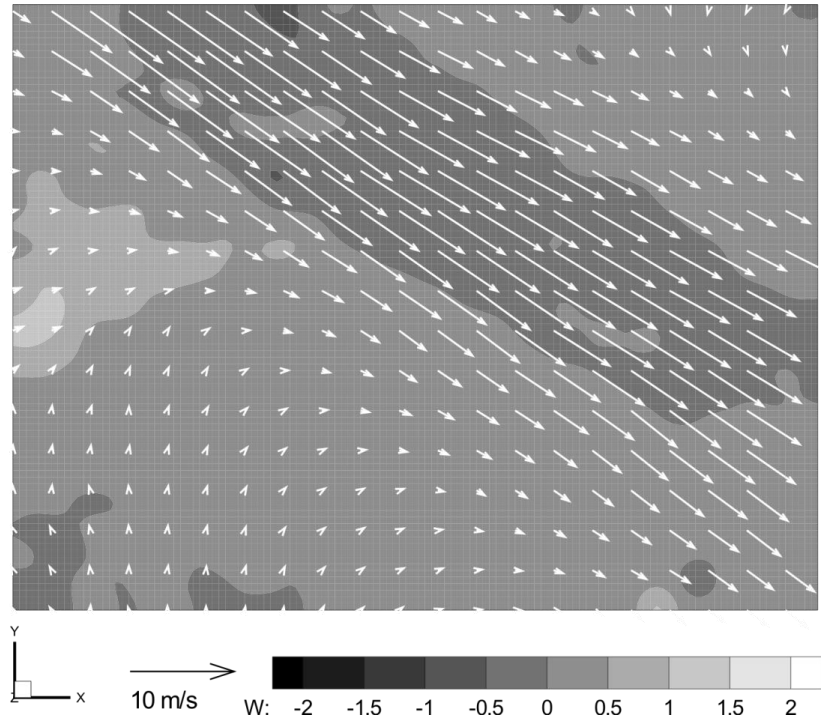

Figure 3.39 Average three dimensional velocity distribution of the skewed CFF used SAC on investigation plane 12.

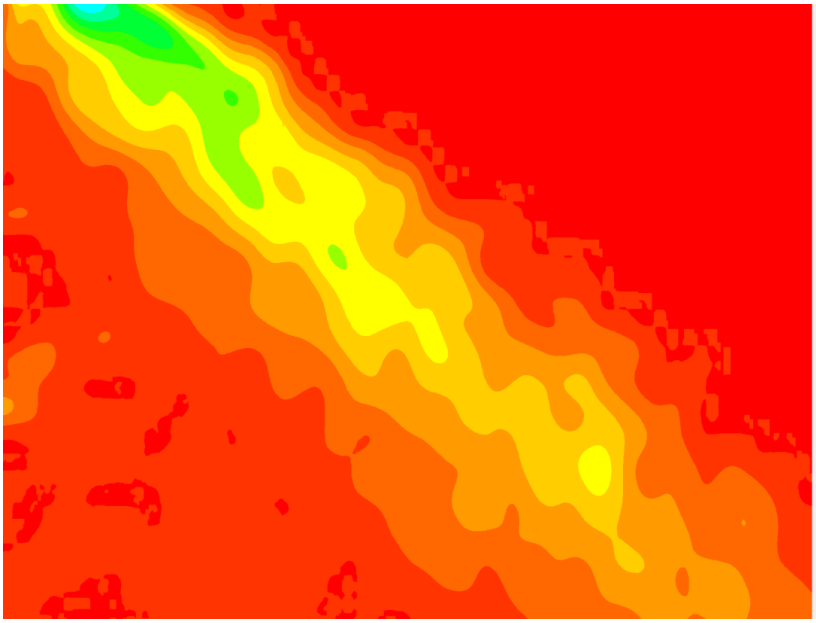

Figure 3.40 Average vorticity map of the skewed CFF used SAC on investigation plane 12.

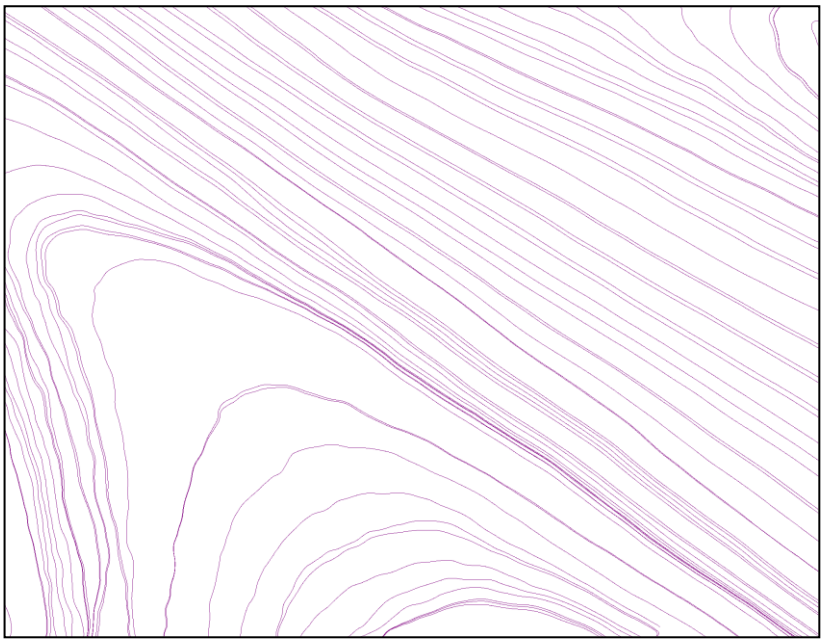

Figure 3.41 Average stream Lines of the skewed CFF used SAC on investigation plane 12.

As the velocity distributions investigated, it is seen that the velocity increases through the –z direction. This is natural because the CFF is skewed to that direction.

In investigation plane 1 and 2; the average velocity (Figure 3.6, Figure 3.9) is slower to the middle areas this is also natural to have this effect. In Figure 3.8 and 3.10 the stream lines of investigation plane 1 and 2 can be seen they are lightly downward. Then the flow balanced. In investigation planes 3, 4,5 and 6 the flow is widely developed on the diagonal (Figure 3.14, 3.17, 3.20 & 3.23) and the core of the flow also in this direction and position (Figure 3.13, 3.16, 3.19 & 3.22).

In investigation plane 7 there is a instant change of the flow profile (Figure 3.24, 3.25 & 3.26) the velocities decreases a bit and the flow pattern climbs upward. But this effect disappears in investigation plane 8 then the main stream widely develops on the diagonal again and the average velocities also increase at these investigation planes 8,9,10 and 11. In these areas the flow is strong and smooth which seams ideal for a SAC's outflow (Figures 3.27 - 3.38).

In investigation point 12 the flow climbs to upward again and the velocity decreases (Figure 3.39, 3.40 & 3.41). The behavior on this area seams slightly similar to the investigation area 7 which may mean that this situation has a relation between the length of the CFF.

In figure 3.42 the 3D reconstruction of these average velocity data can be seen. The values on areas between the investigation planes are iterated. The bold green areas are the iso-surfaces that has the velocity of 4.5 m/s. The light green areas are the iso-surfaces that has the velocity of 3.5 m/ and the cyan areas are the iso-surfaces that has the velocity of 2 m/s. It can be also detect from here that the flow faster in the right side of the SAC (which was natural because of the skewed CFF) and at the investigation plane 7 the flow pattern differs greatly.

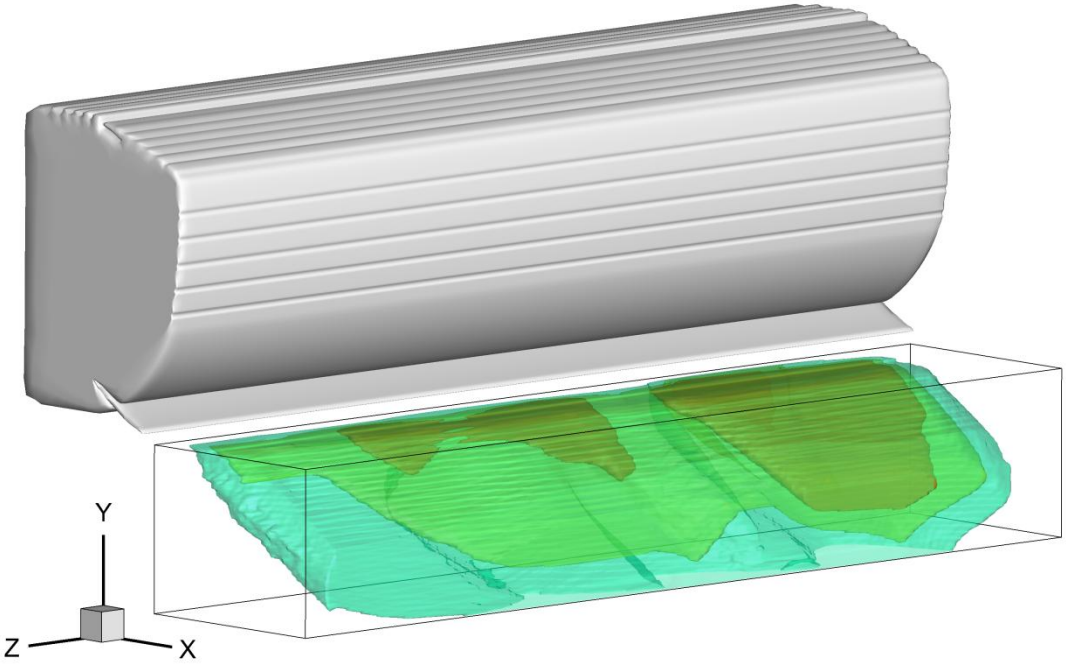

Figure 3.42 The average velocity iso-surface of the all 12 investigation planes on skewed CFF used SAC.

3.2.1.2 Outflow Investigation of the SAC with a Straight CFF

The straight CFFs blow stronger compared with the skewed CFFs. This enables having the same average flow speed with fewer motor cycles which means energy saving and also decreases the noise level that generated by the motor and its bearings.

However in this prototype this was causing vibration and noise problems. The system tested in the silent room and the noise source is founded on the left side of the air conditioner near investigation planes 1 or 2. But the reason of this noise could not detected by the probe measurements.

Therefore the system investigated with SPIV for both comparing with the skewed CFF and also for searching the reason of the noise.

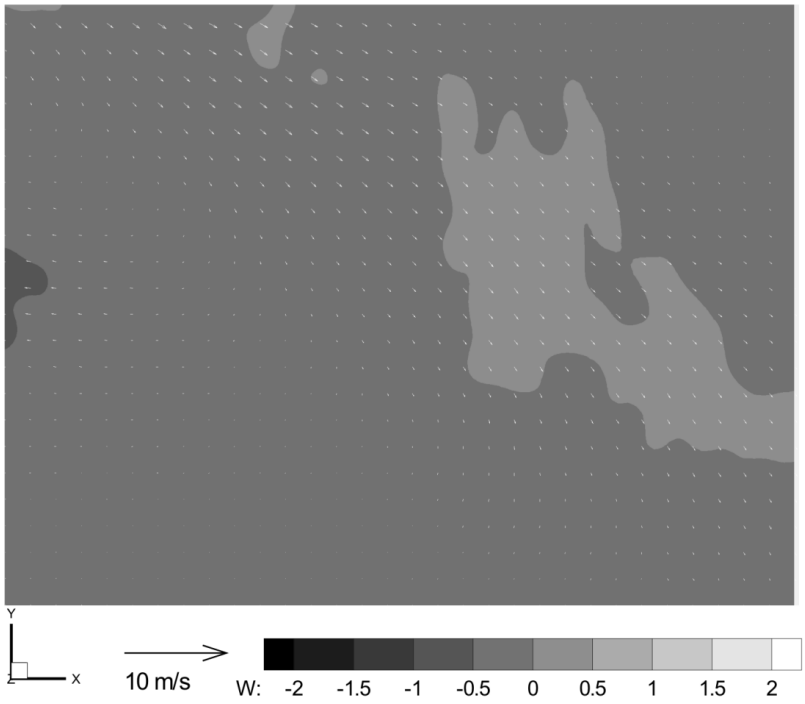

Figure 3.43 Average three dimensional velocity distribution of the straight CFF used SAC on investigation plane 1.

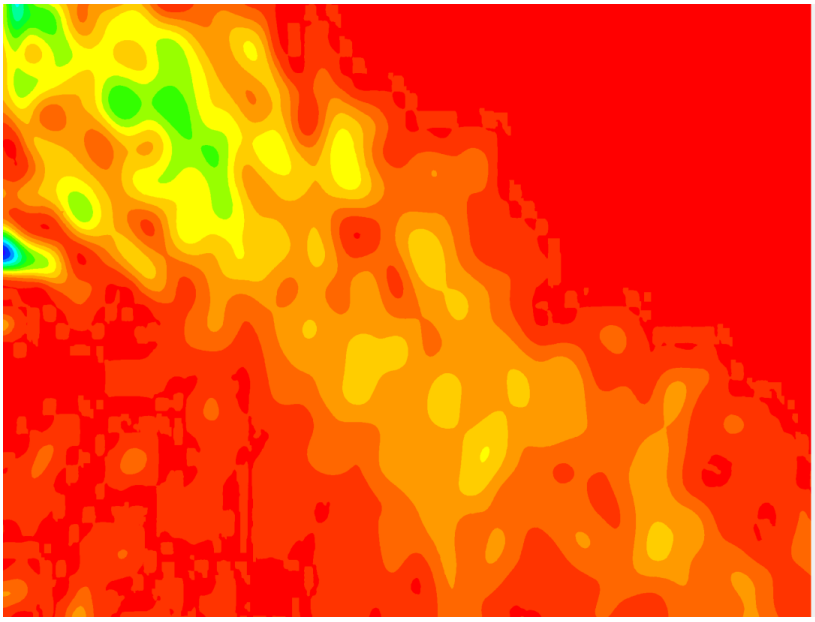

Figure 3.44 Average vorticity map of the straight CFF used SAC on investigation plane 1.

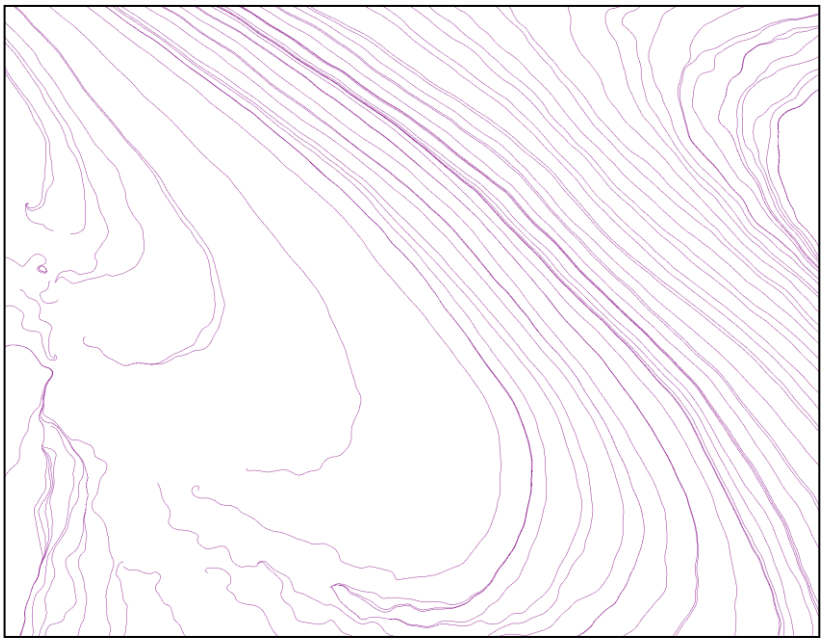

Figure 3.45 Average stream Lines of the straight CFF used SAC on investigation plane 1.

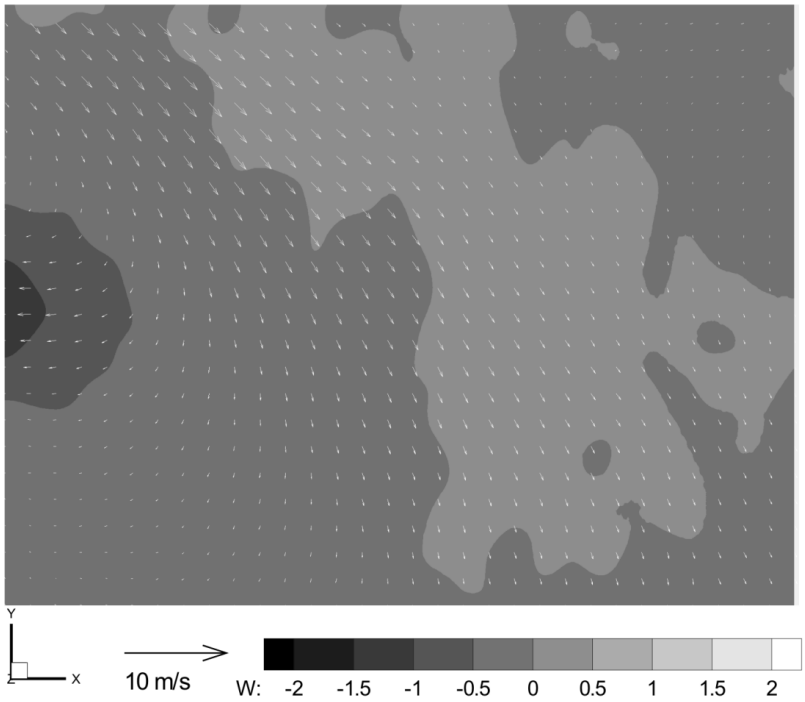

Figure 3.46 Average three dimensional velocity distribution of the straight CFF used SAC on investigation plane 2.

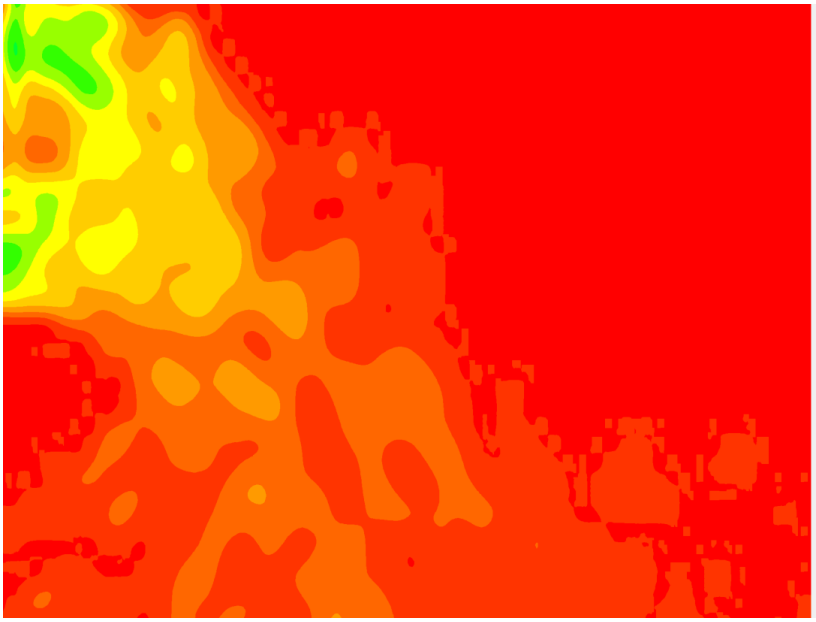

Figure 3.47 Average vorticity map of the straight CFF used SAC on investigation plane 2.

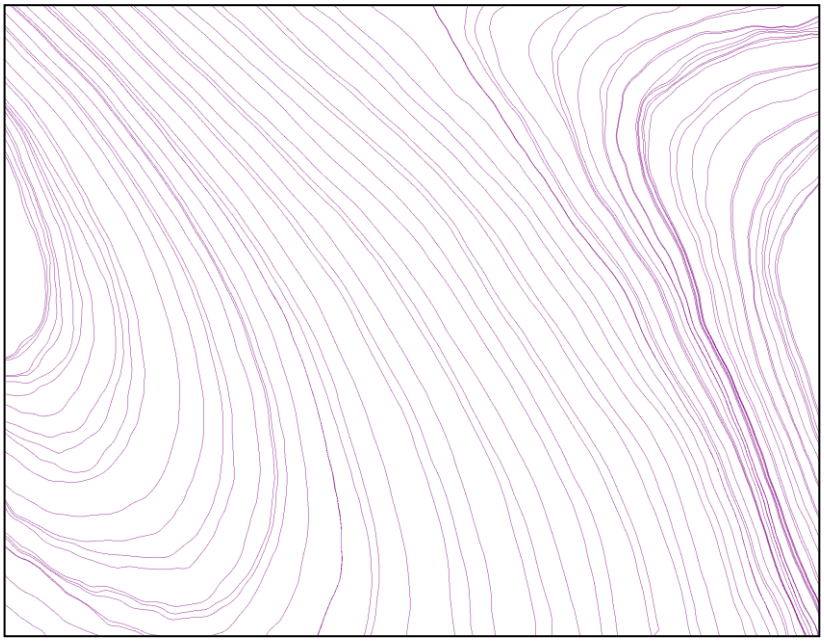

Figure 3.48 Average stream Lines of the straight CFF used SAC on investigation plane 2.

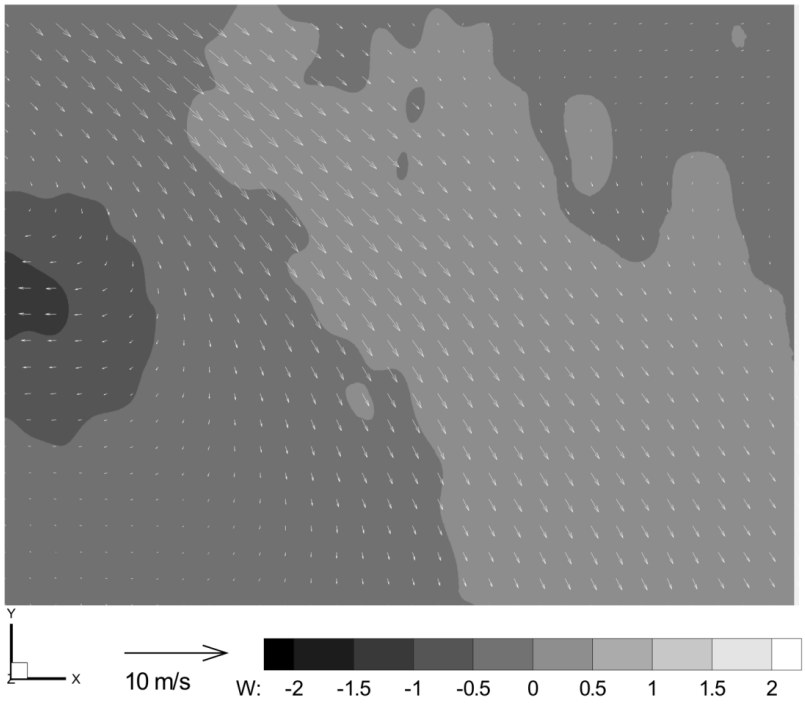

Figure 3.49 Average three dimensional velocity distribution of the straight CFF used SAC on investigation plane 3.

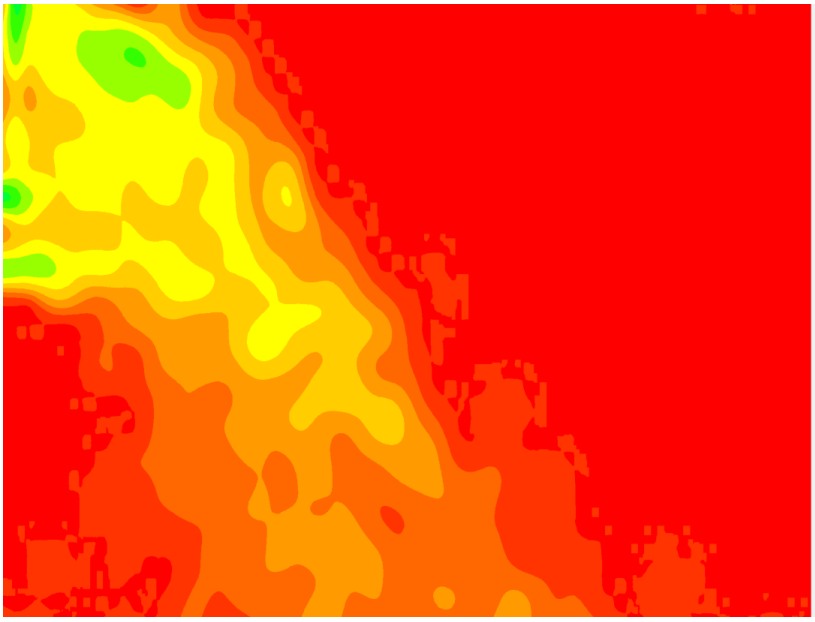

Figure 3.50 Average vorticity map of the straight CFF used SAC on investigation plane 3.

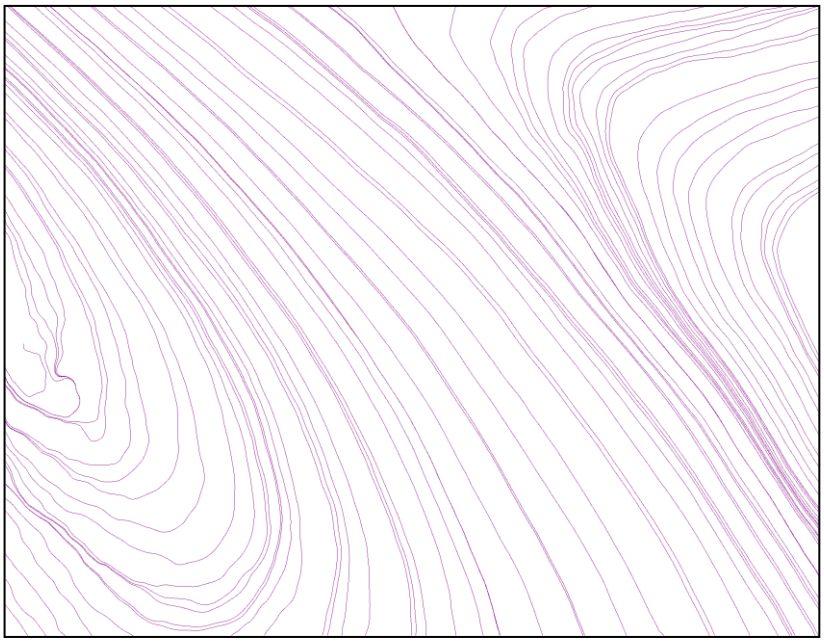

Figure 3.51 Average stream Lines of the straight CFF used SAC on investigation plane 3.

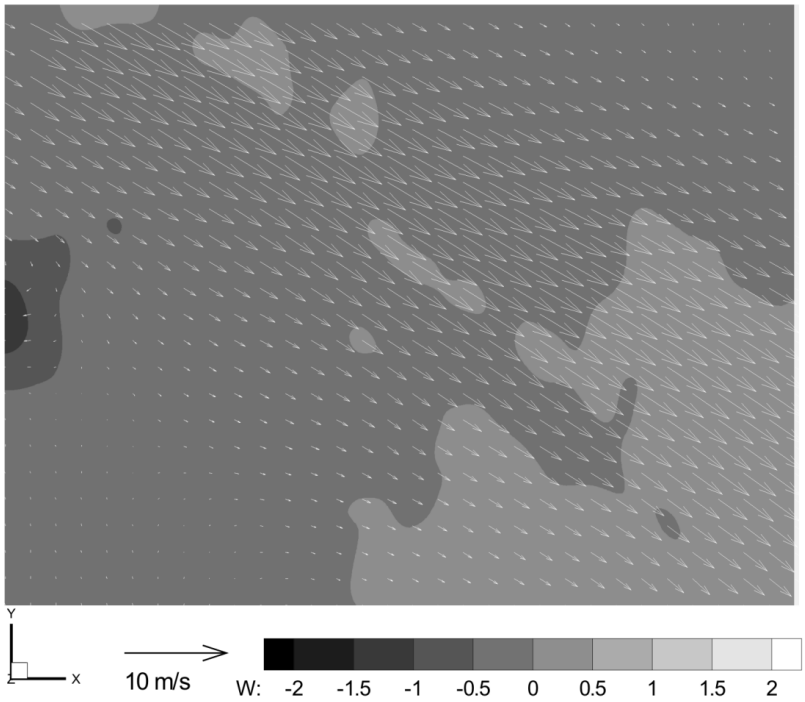

Figure 3.52 Average three dimensional velocity distribution of the straight CFF used SAC on investigation plane 4.

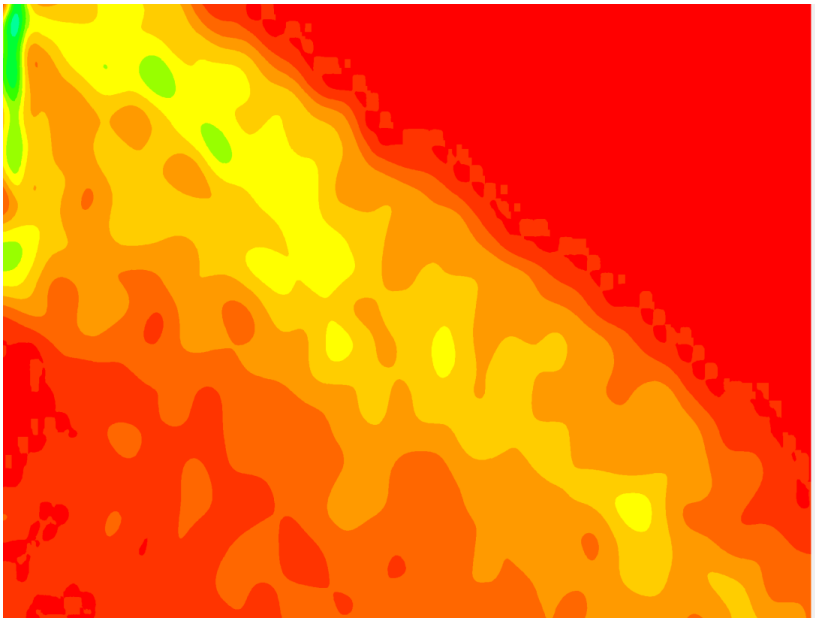

Figure 3.53 Average vorticity map of the straight CFF used SAC on investigation plane 4.

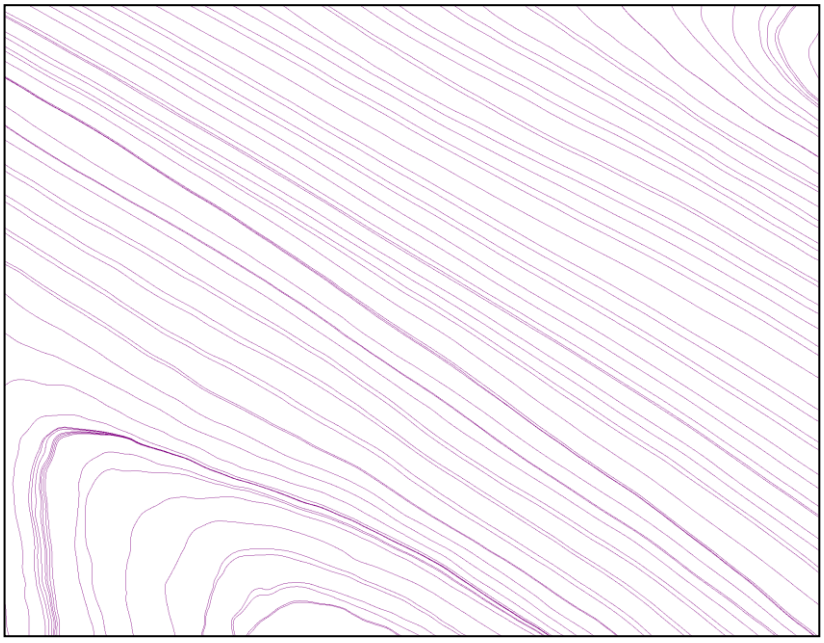

Figure 3.54 Average stream Lines of the straight CFF used SAC on investigation plane 4.

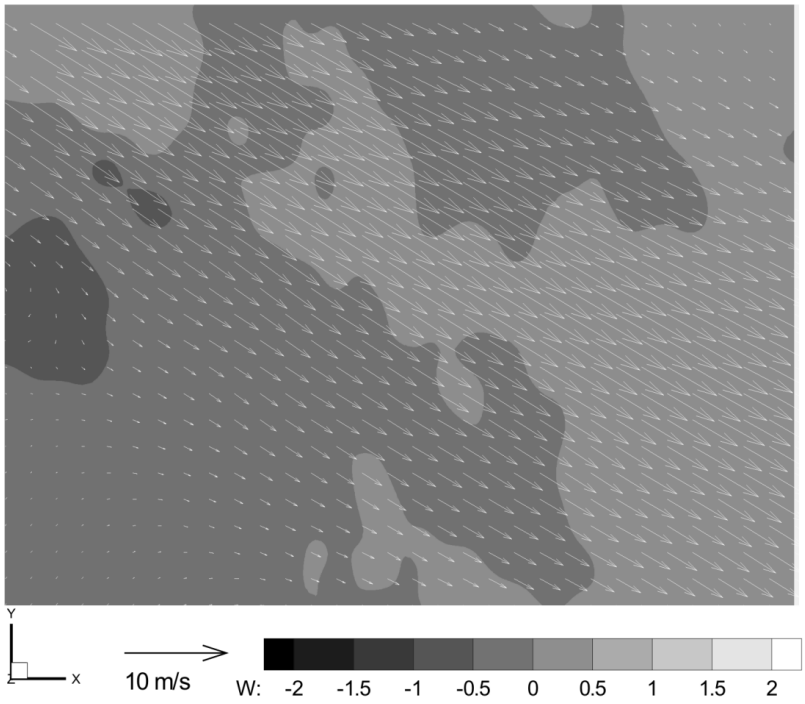

Figure 3.55 Average three dimensional velocity distribution of the straight CFF used SAC on investigation plane 5.

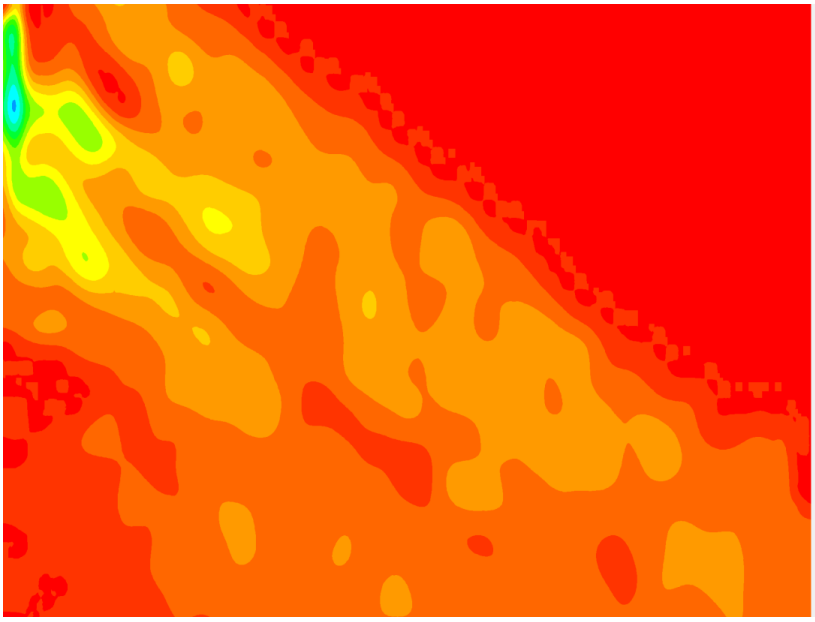

Figure 3.56 Average vorticity map of the straight CFF used SAC on investigation plane 5.

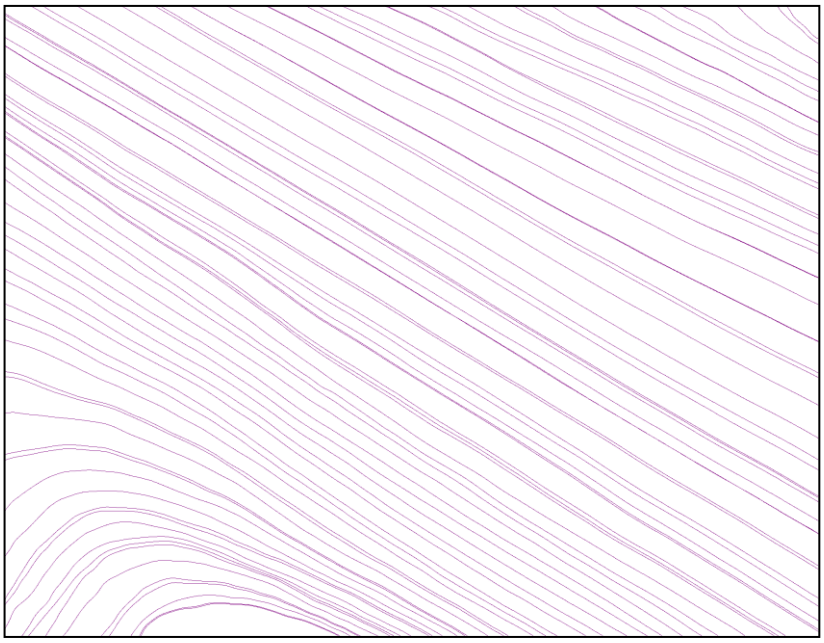

Figure 3.57 Average stream Lines of the straight CFF used SAC on investigation plane 5.

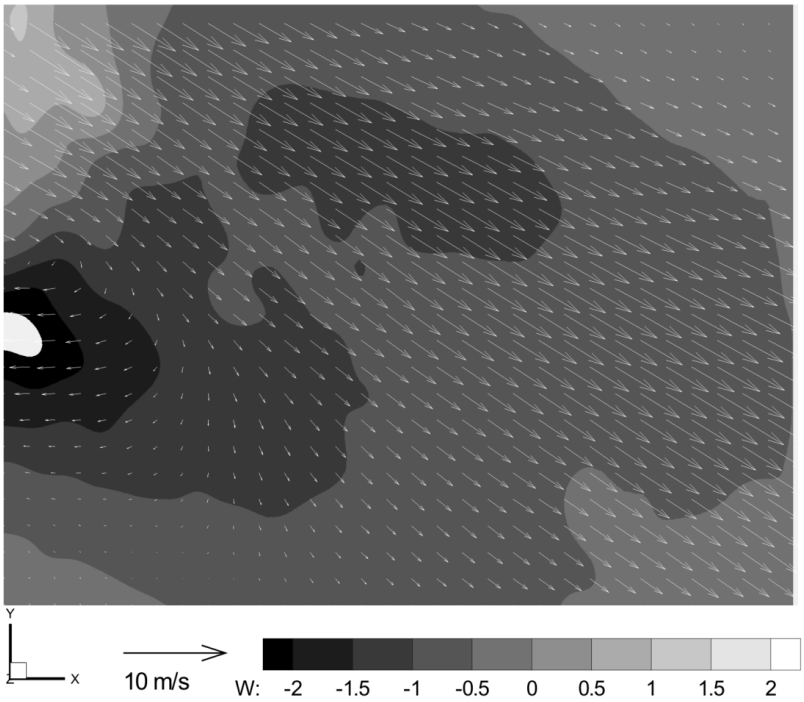

Figure 3.58 Average three dimensional velocity distribution of the straight CFF used SAC on investigation plane 6.

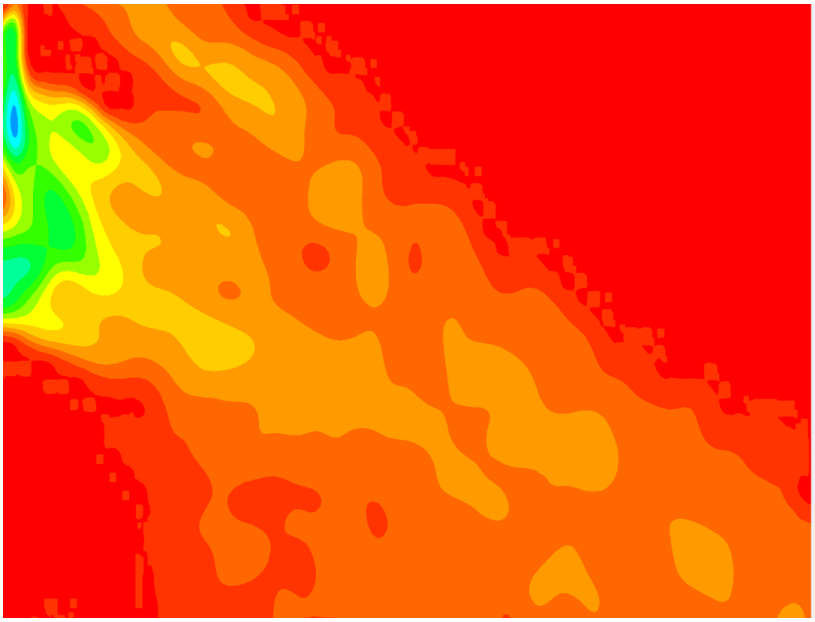

Figure 3.59 Average vorticity map of the straight CFF used SAC on investigation plane 6.

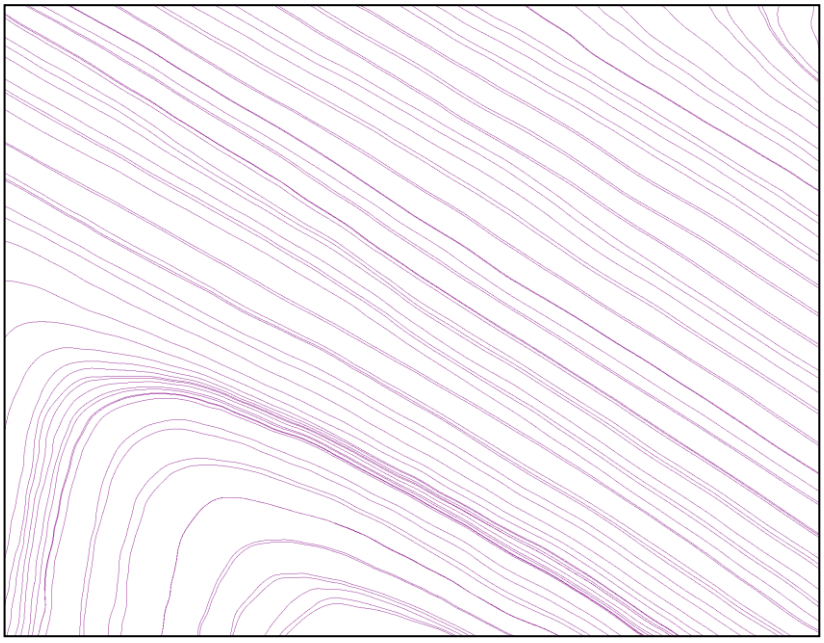

Figure 3.60 Average stream Lines of the straight CFF used SAC on investigation plane 6.

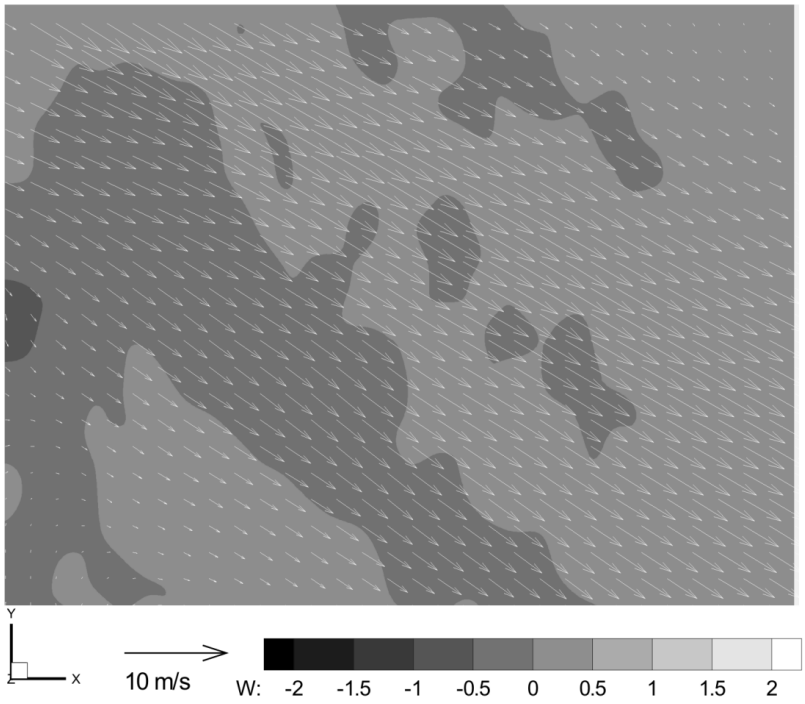

Figure 3.61 Average three dimensional velocity distribution of the straight CFF used SAC on investigation plane 7.

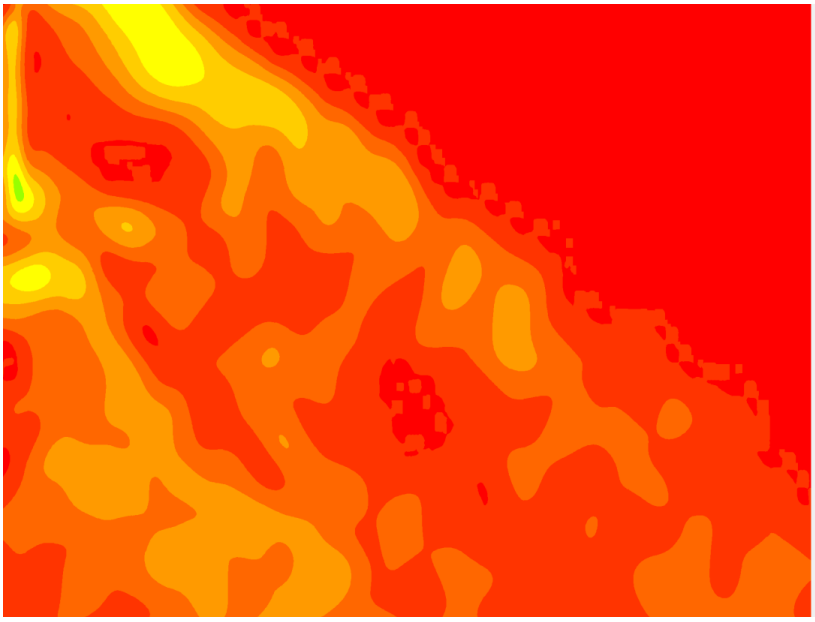

Figure 3.62 Average vorticity map of the straight CFF used SAC on investigation plane 7.

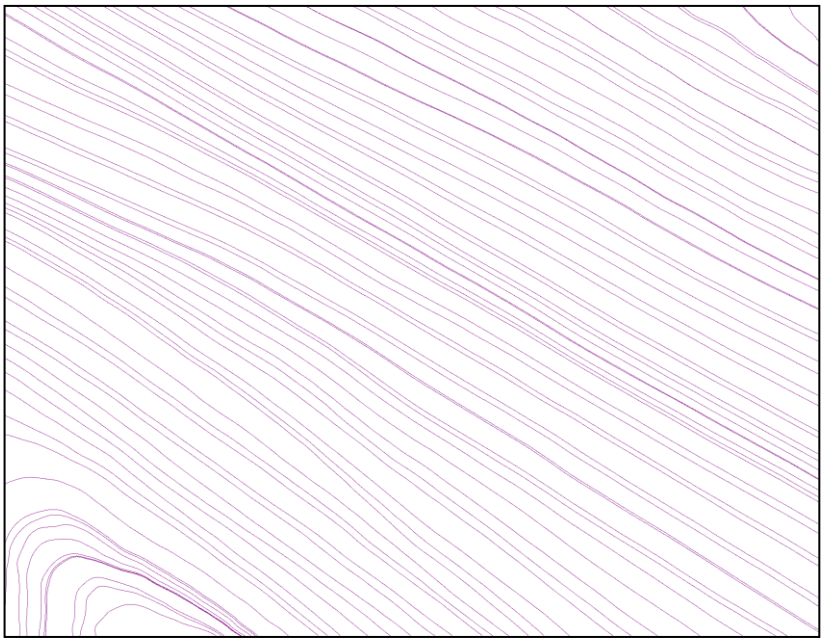

Figure 3.63 Average stream Lines of the straight CFF used SAC on investigation plane 7.

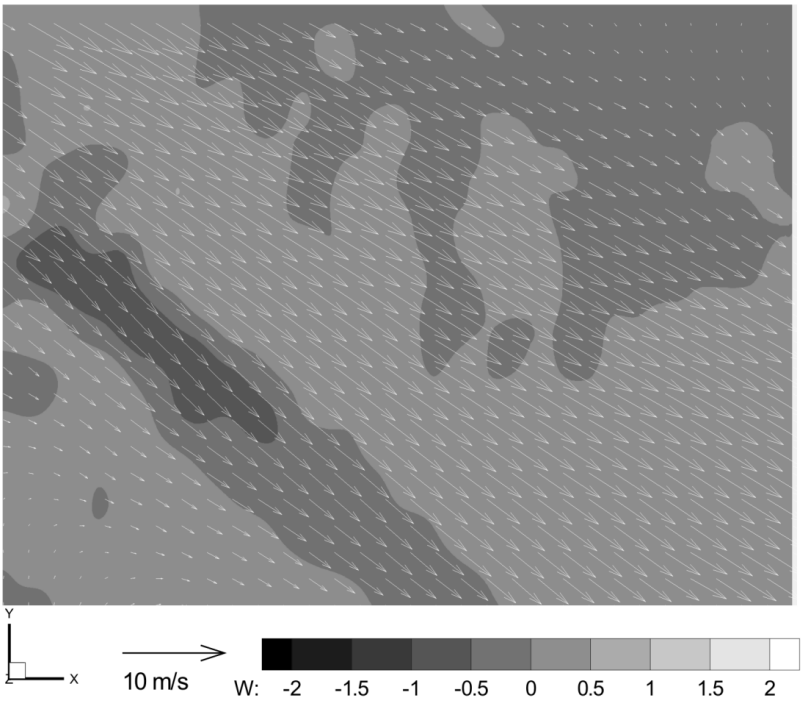

Figure 3.64 Average three dimensional velocity distribution of the straight CFF used SAC on investigation plane 8.

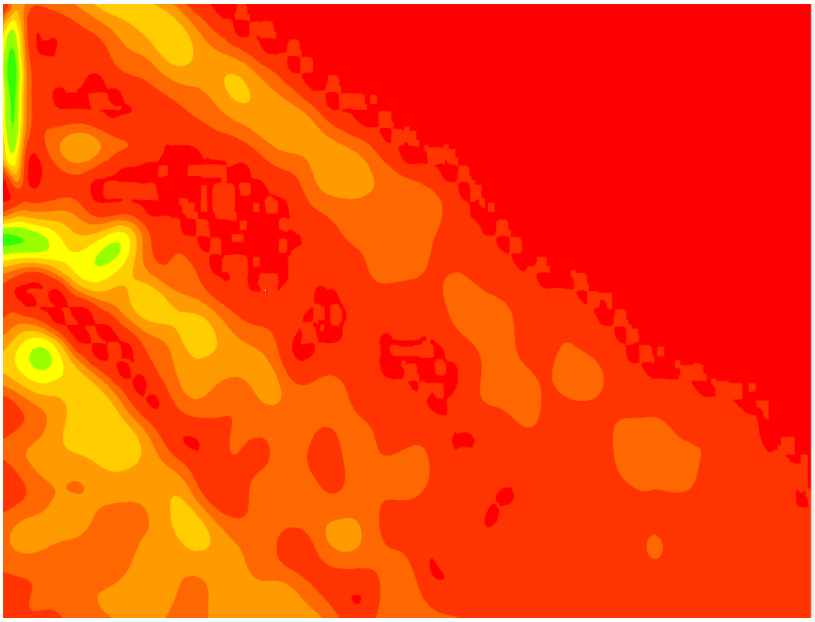

Figure 3.65 Average vorticity map of the straight CFF used SAC on investigation plane 8.

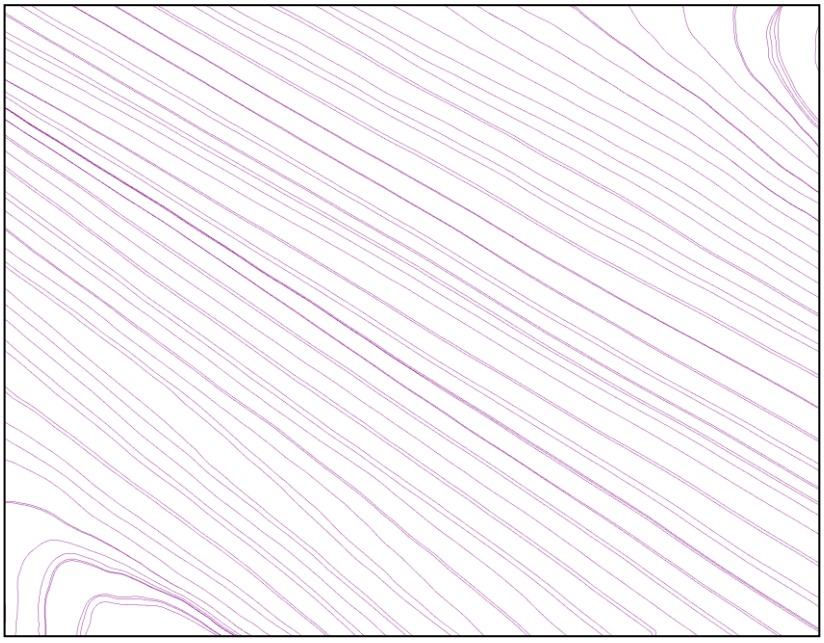

Figure 3.66 Average stream Lines of the straight CFF used SAC on investigation plane 8.

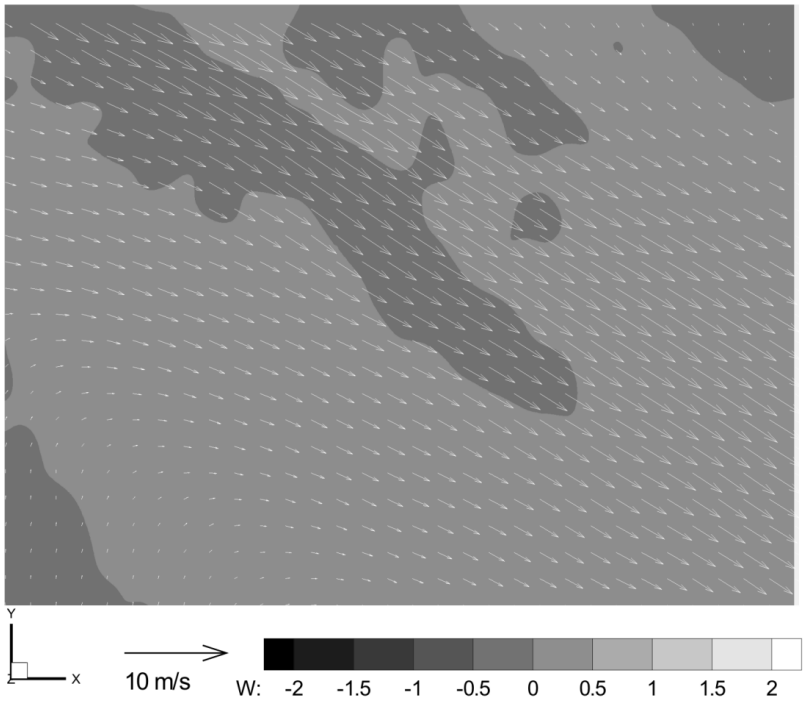

Figure 3.67 Average three dimensional velocity distribution of the straight CFF used SAC on investigation plane 9.

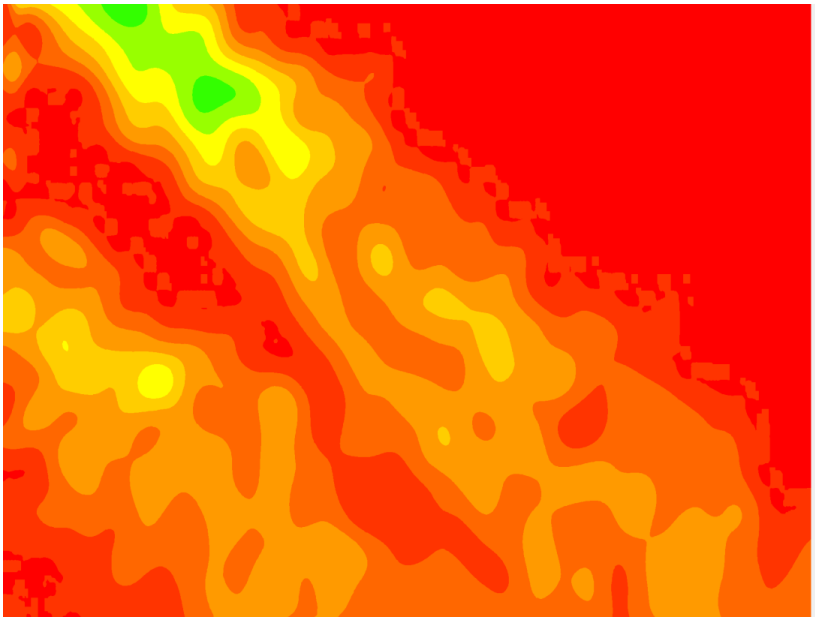

Figure 3.68 Average vorticity map of the straight CFF used SAC on investigation plane 9.

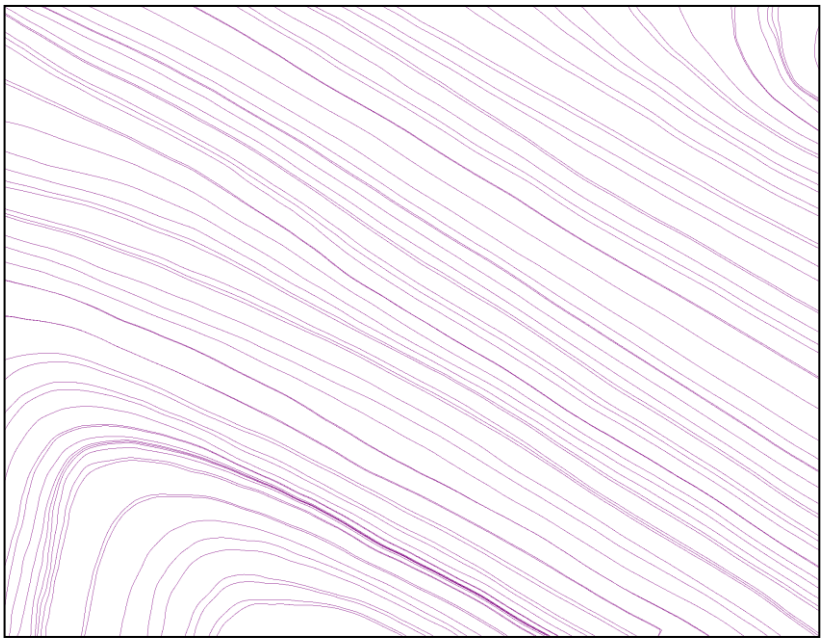

Figure 3.69 Average stream Lines of the straight CFF used SAC on investigation plane 9.

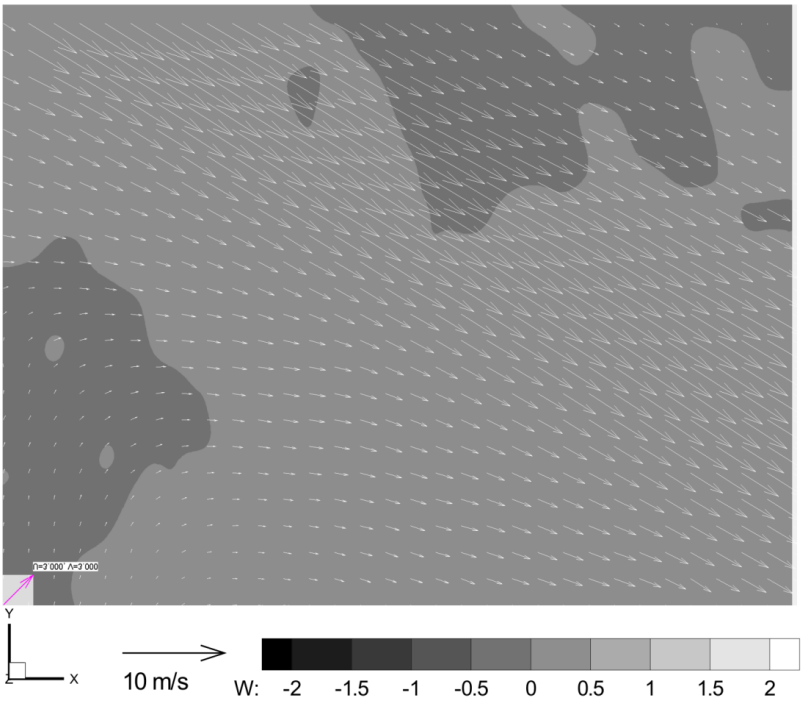

Figure 3.70 Average three dimensional velocity distribution of the straight CFF used SAC on investigation plane 10.

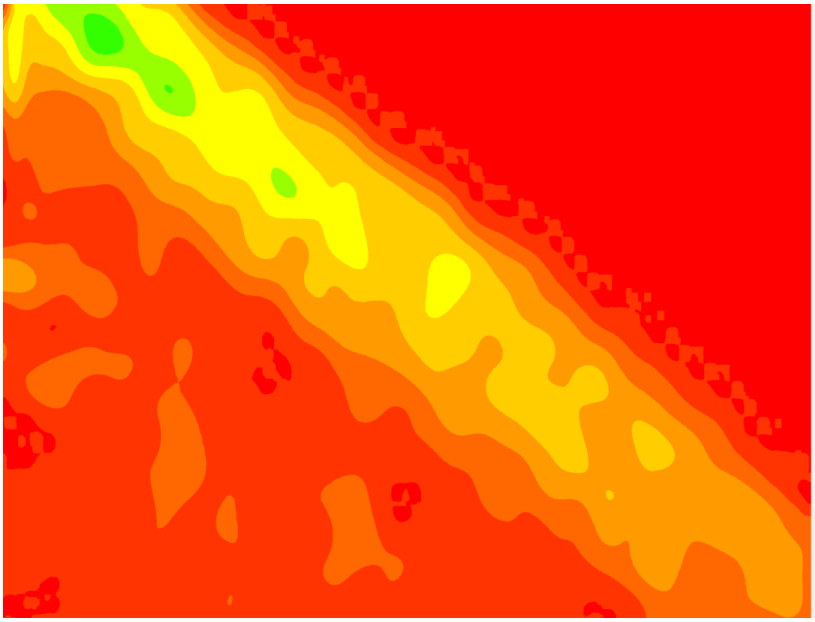

Figure 3.71 Average vorticity map of the straight CFF used SAC on investigation plane 10.

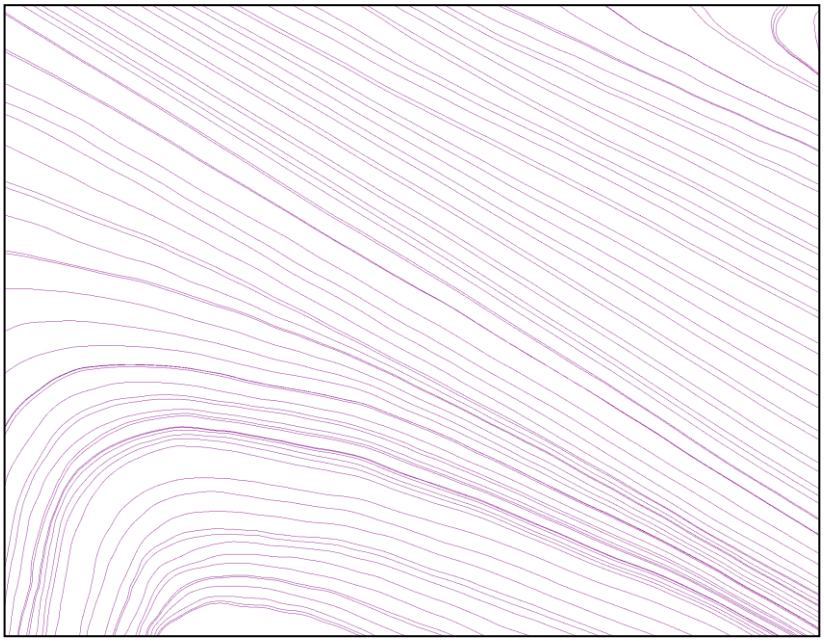

Figure 3.72 Average stream Lines of the straight CFF used SAC on investigation plane 10.

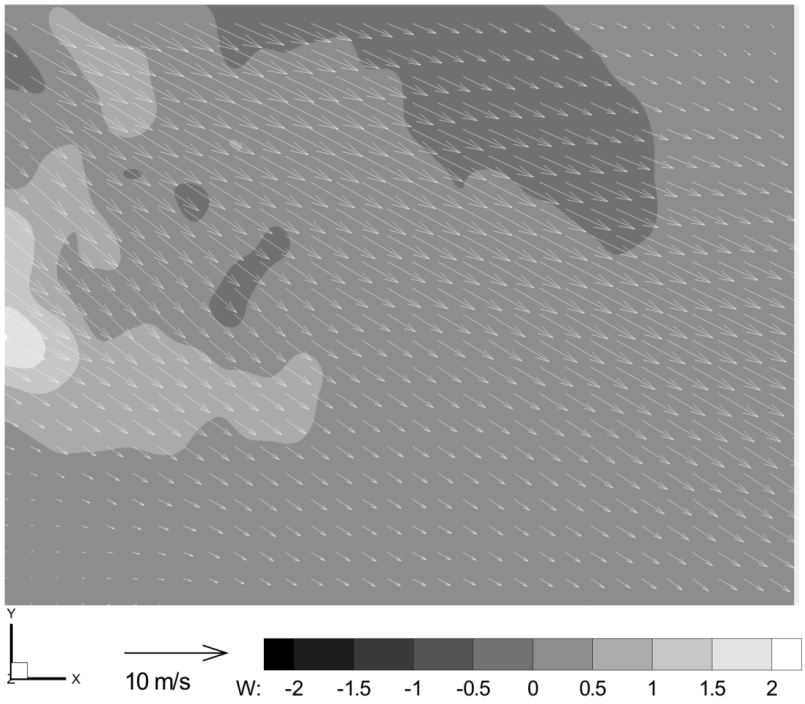

Figure 3.73 Average three dimensional velocity distribution of the straight CFF used SAC on investigation plane 11.

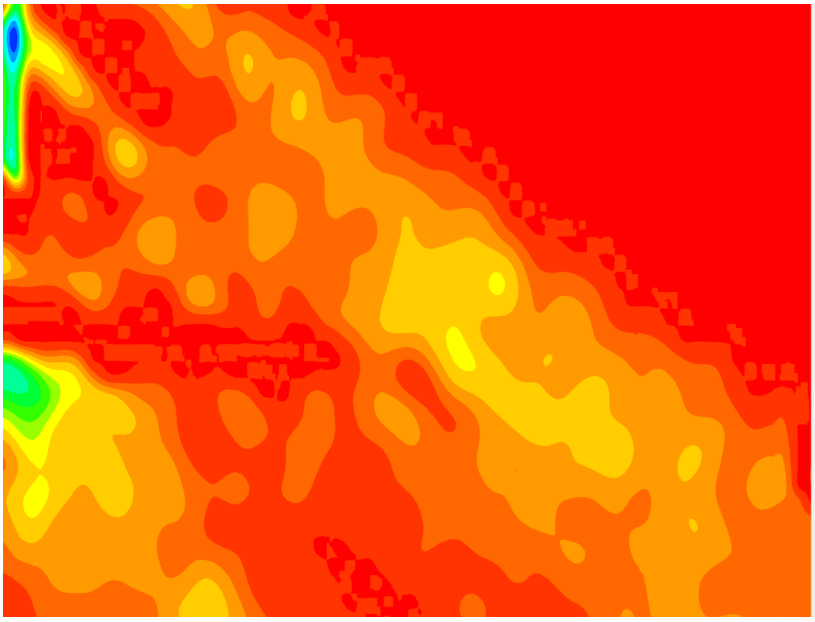

Figure 3.74 Average vorticity map of the straight CFF used SAC on investigation plane 11.

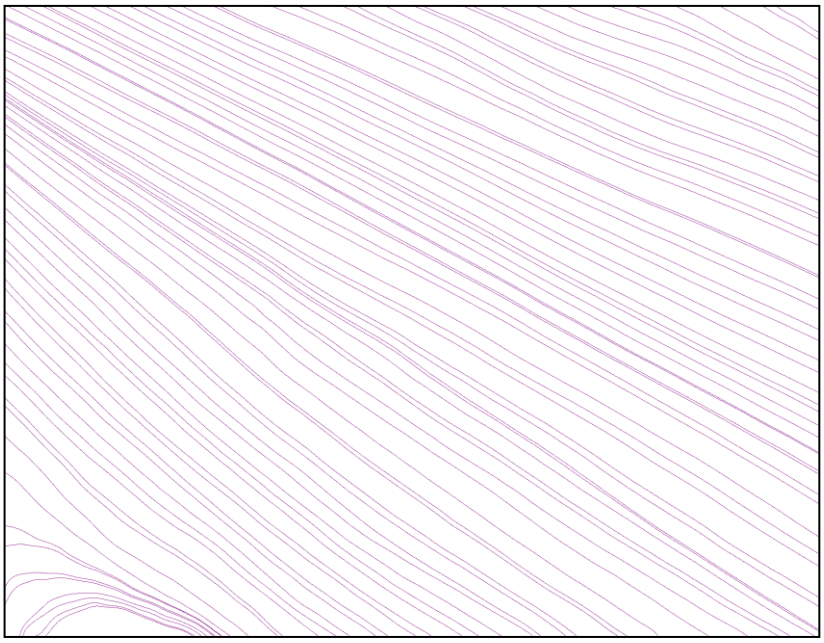

Figure 3.75 Average stream Lines of the straight CFF used SAC on investigation plane 11.

It can be clearly seen in Figure 3.45, 3.48 and 3.51 that the flow was bended like a s and the direction of the flow was nearly directly downward which is the possible explanation for the noise and the vibration on the left of the SAC where investigation plane 1, 2 and 3 positioned. Although the velocities on these areas slow when it is compared to the further investigation planes (Figure 3.43, 3.46 & 3.49), the voticity maps of these locations in Figure 3.44, 3.47 and 3.50 also show there were strong fluctuations behind the directing airfoil. Therefore investigating the effect of the directing airfoil on the flow is need for understanding the main flow structure of the SACs which was also investigated by endoscopic PIV and it is presented in the flowing parts of this chapter.

As the Figures from 3.52 to 3.75 investigated they show the straight CFF gives a better developed flow. Only around the investigation plane 6, a sudden air velocity drop occurred which looks like the air velocity drop at investigation plane 7 on the skewed CFF experiment. Although the position of this event lightly differs, it is the same phenomenon because the flow was shifted towards to right side. Thus the situation is not related with the type of the CFF. Its cause may the length of the CFF or it may the geometry of the SAC’s body.

As the results considered carefully it can be notice that in straight CFF experiment there is no data at the investigation plane 12. The reason of this is also the difference between the flow patterns of the CFFs. The straight CFF does not skew the flow therefore there is no flow area at investigation plane 12 unlike the skewed CFF.

The Figure 3.76 shows 3D reconstruction of these average velocity data can be seen. As it is mentioned the values on areas between the investigation planes are iterated. The bold green areas are the iso-surfaces that have the velocity of 4.5 m/s. The light green areas are the iso-surfaces that have the velocity of 3.5 m/ and the cyan areas are the iso-surfaces that have the velocity of 2 m/s. This figure also shows that the straight CFF has a better flow pattern then the skewed one.

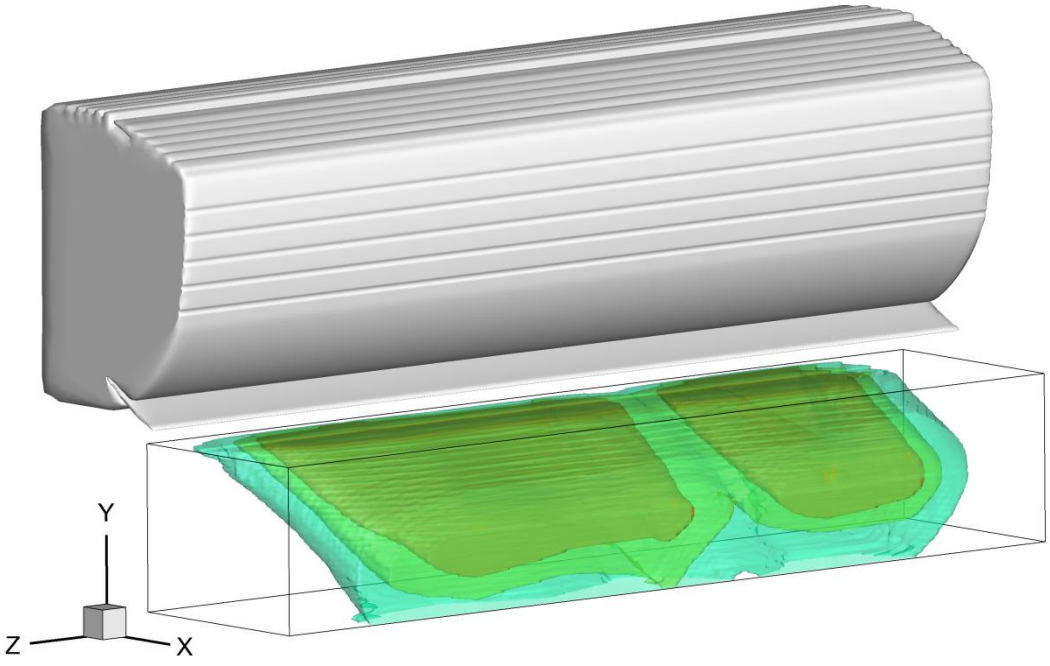

Figure 3.76 The average velocity iso-surface of the all 12 investigation planes on straight CFF used SAC.

3.2.1.3 Instantaneous Results of the Outflow of the SAC on Investigation Plane 7

The instantaneous results of the outflow of the skewed CFF used SAC at investigation plane 7 are given in Figures 3.77 to Figure 3.83 for showing the difference between the momentarily results and the average results. These Figures includes 100 vector maps which are a whole set of an experiment's results.

As it is mentioned before in CFF the flow is driven by the eccentric vortex. Therefore the flow structure of the CFF is directly a transient phenomenon. If the instantaneous experiment results are examined the flow fluctuating upwards and downwards can be seen while some small vortices climbs up along the main flow area.

Although the results give the feeling that there is some kind of periodicity, it cannot be said for sure because between two measurements 0.135 second passes and this much time is enough for the CFF to make nearly 3 cycles. Therefore the temporal resolution of the current PIV system may not be enough for investigating the transient behavior of the CFF.

The solution for this may be rearranging the experimental data by the position of the CFF. This can be made by assuming at the time that the first map was measured, the CFF was in the reference position. After that whole the other maps reordered according to the position on the CFF. However this only may work if the CFF is totally symmetrical and does not have a production error which is not possible in the current situation.

Thus only by tagging the position of the CFF while the experiments taking place is the only real suitable solution for investigating this phenomenon other than using higher speed cameras and lasers.

Although the cyclic phenomenon of CFF could not be analyzed, the instantaneous velocity maps give the idea of the real flow and still a useful tool for investigating the flow stability and vorticies.

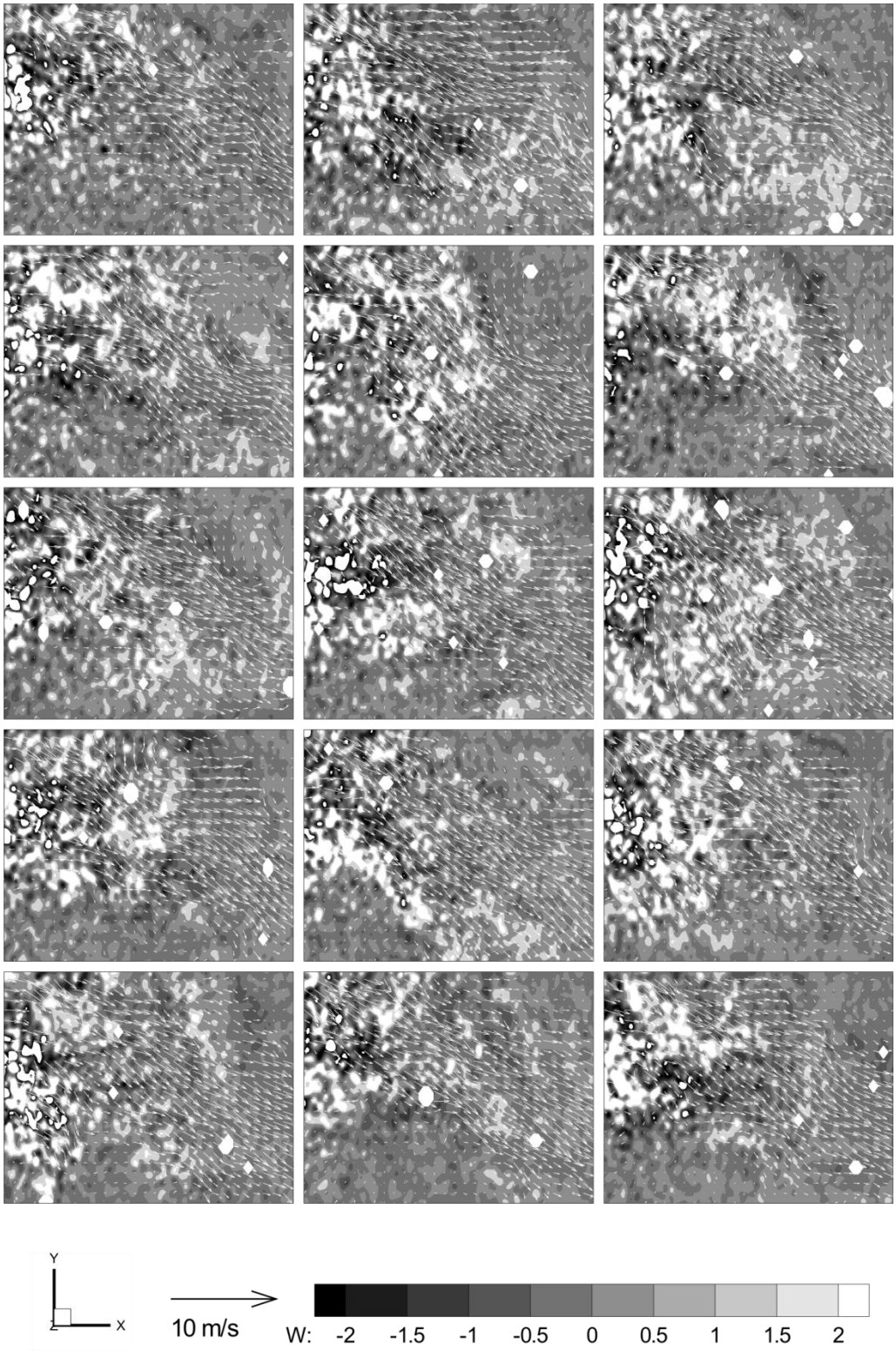

Figure 3.77 The instantaneous SPIV results at investigation plane 7 of a skewed CFF used SAC.

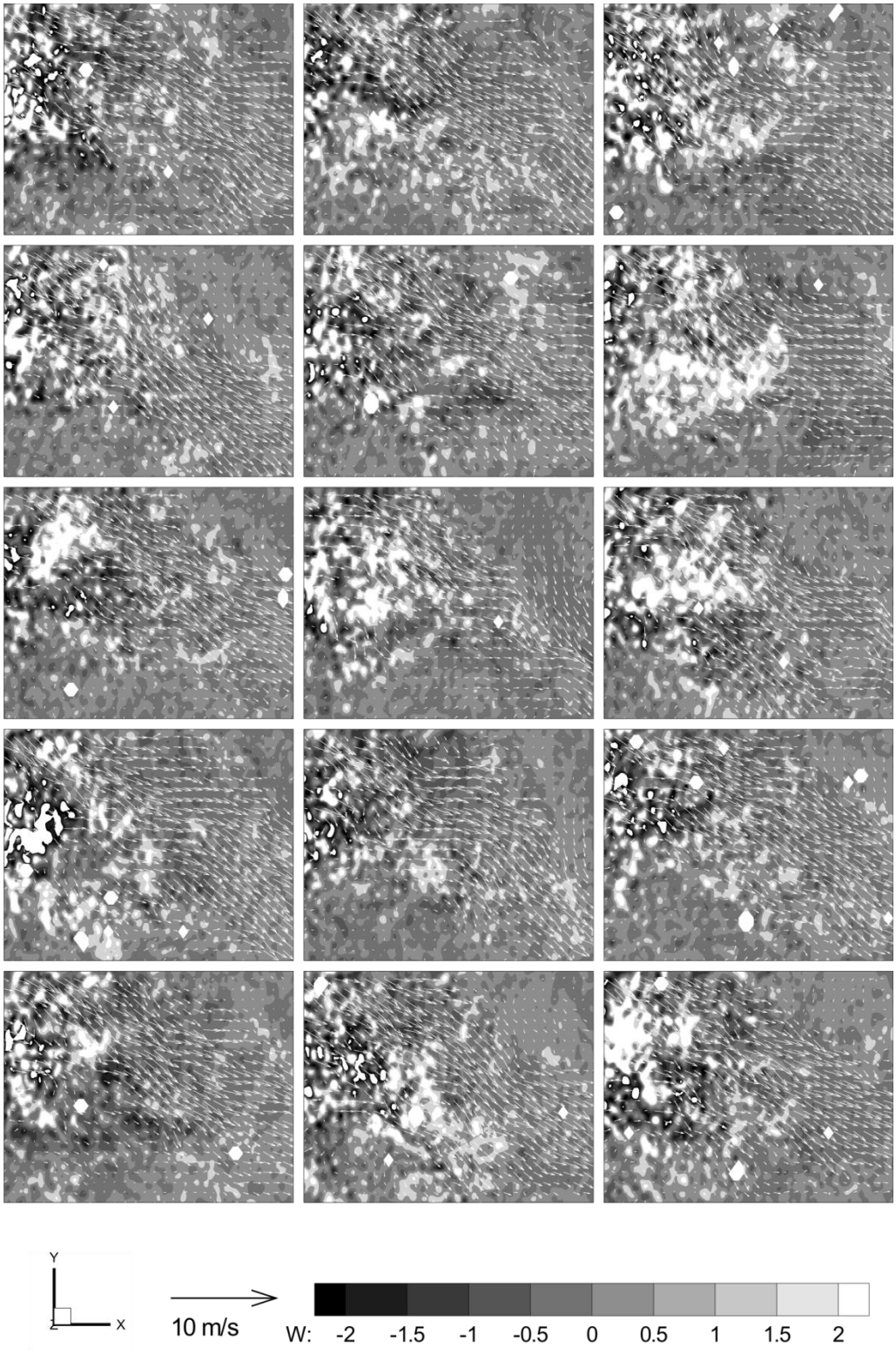

Figure 3.78 The instantaneous SPIV results at investigation plane 7 of a skewed CFF used SAC.

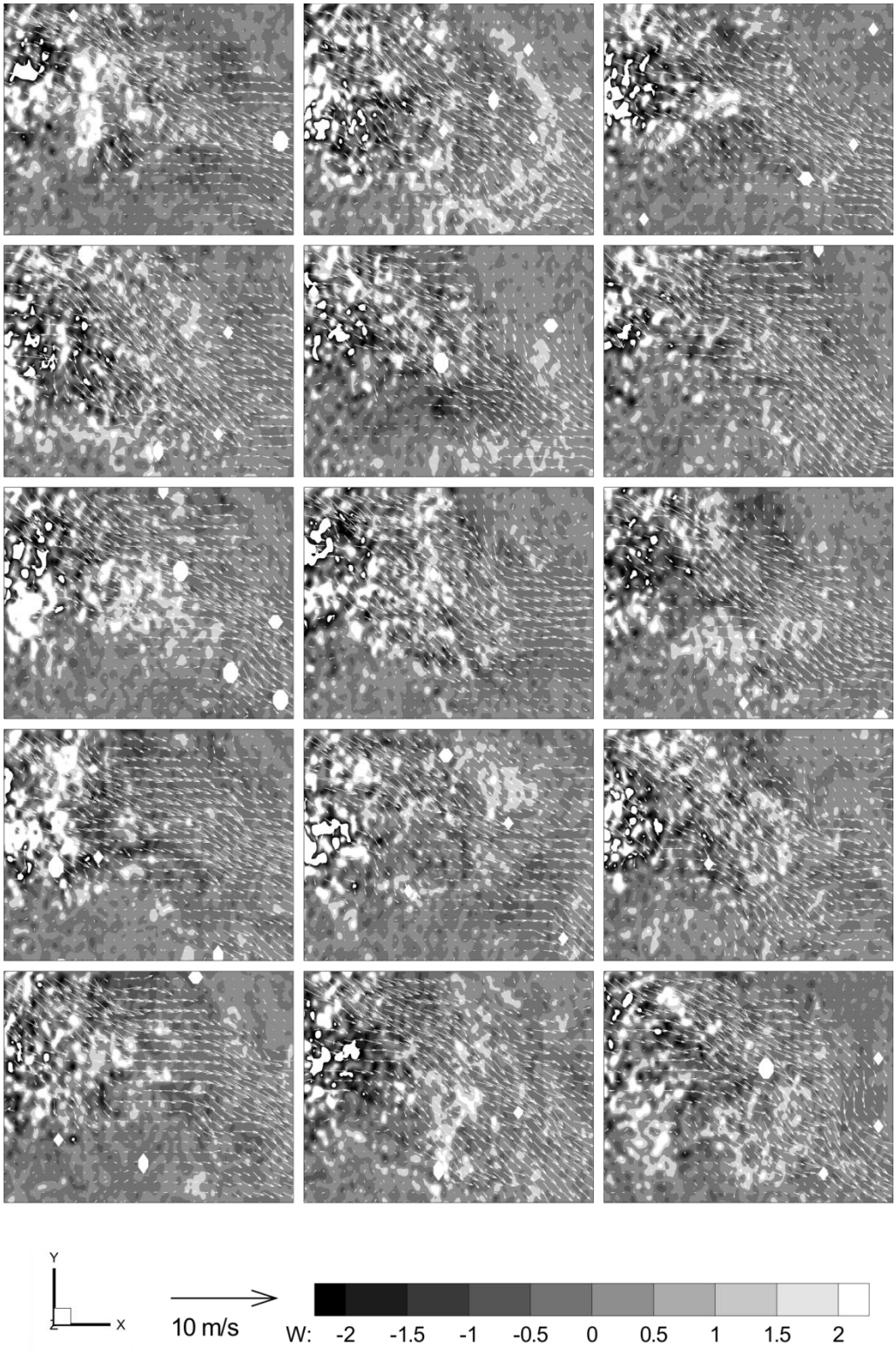

Figure 3.79 The instantaneous SPIV results at investigation plane 7 of a skewed CFF used SAC.

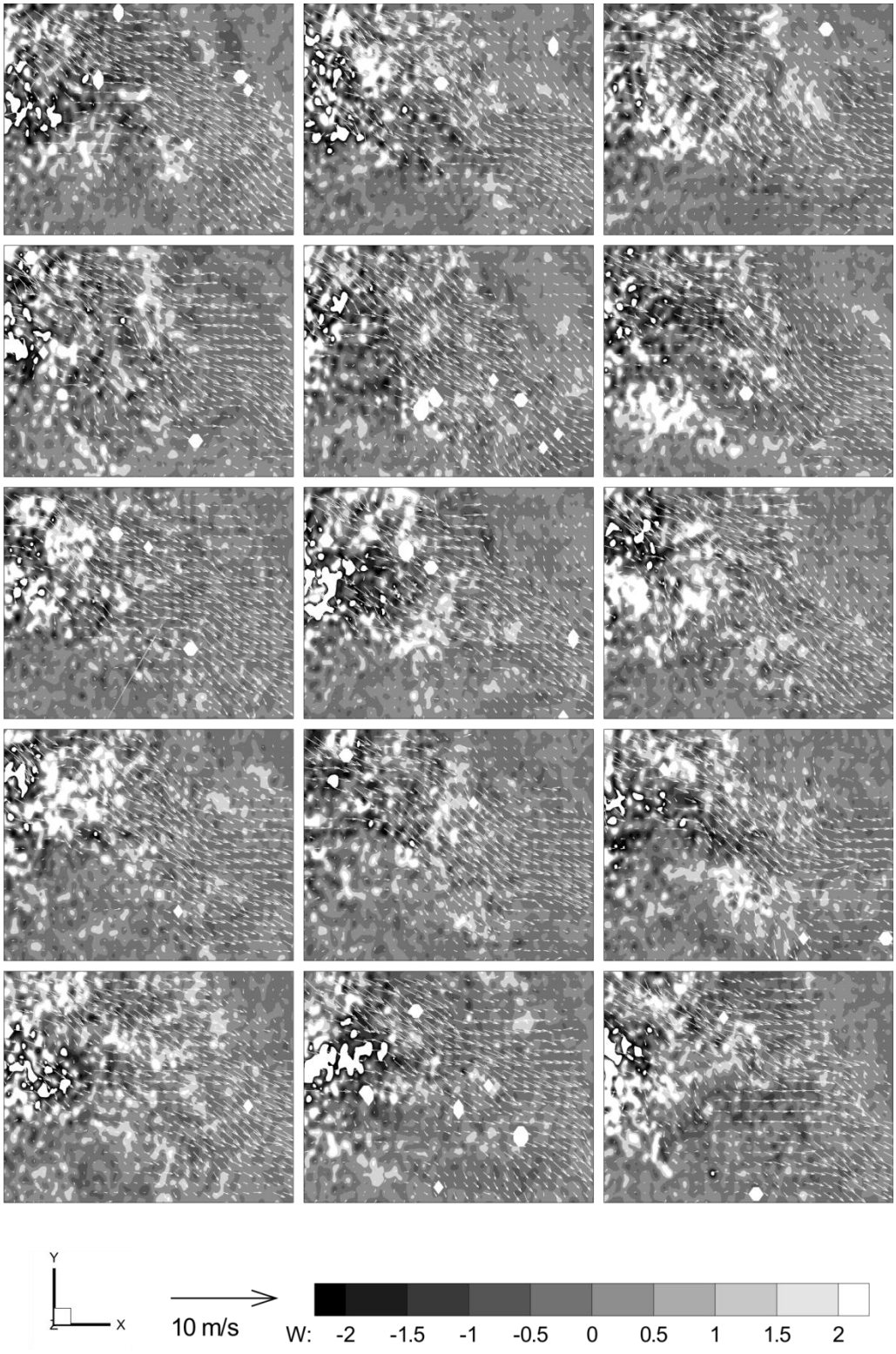

Figure 3.80 The instantaneous SPIV results at investigation plane 7 of a skewed CFF used SAC.

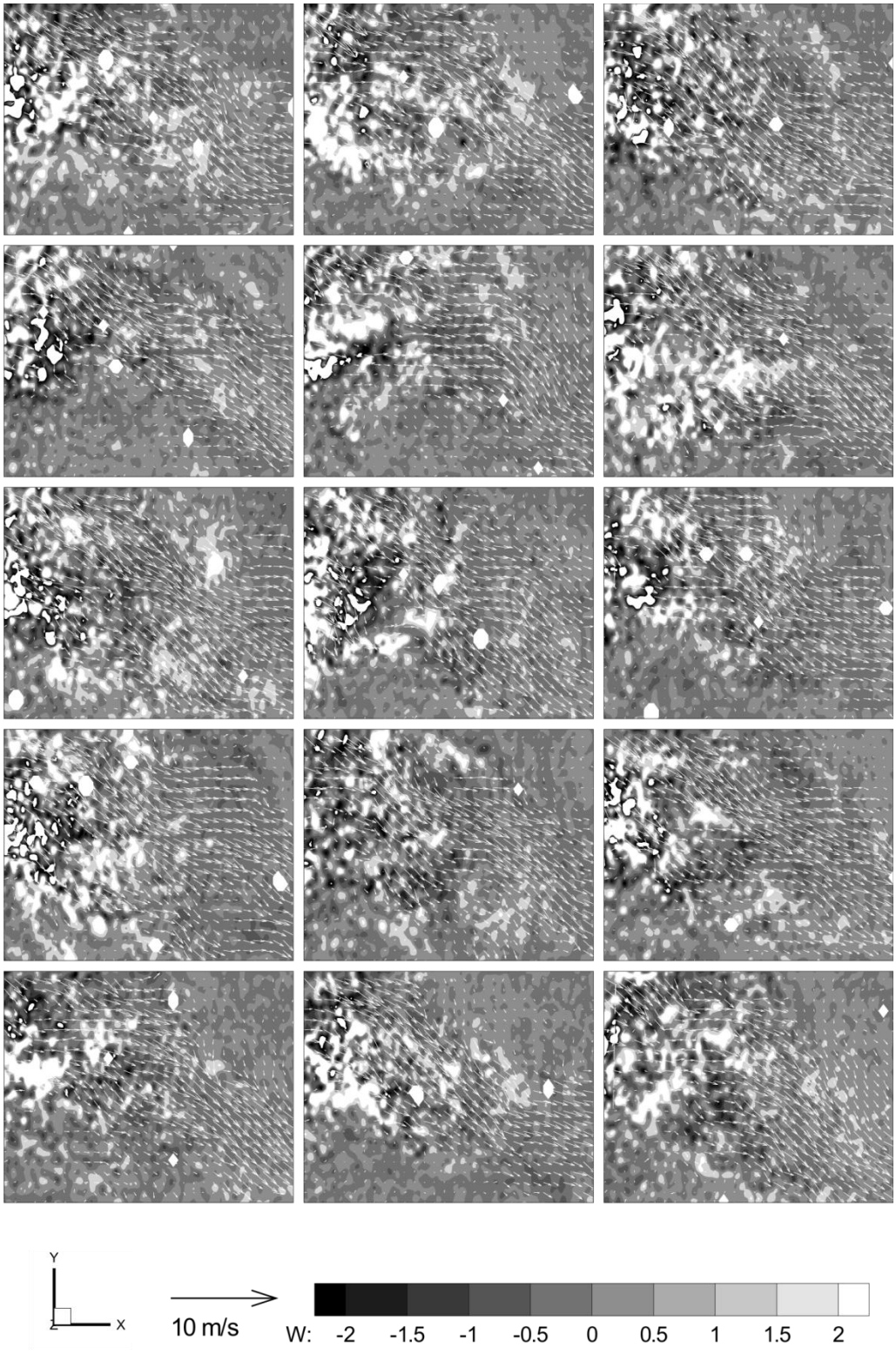

Figure 3.81 The instantaneous SPIV results at investigation plane 7 of a skewed CFF used SAC.

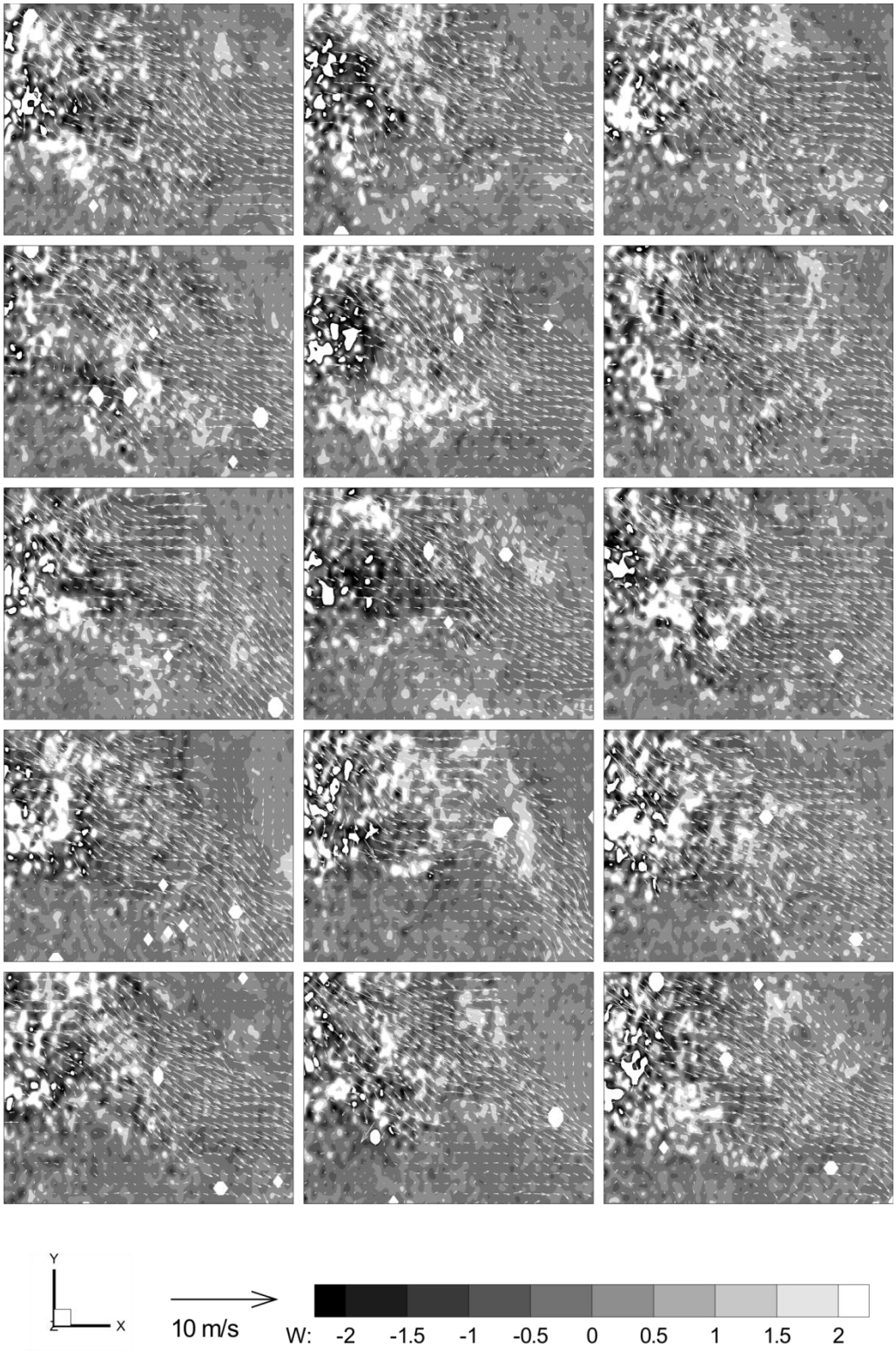

Figure 3.82 The instantaneous SPIV results at investigation plane 7 of a skewed CFF used SAC.

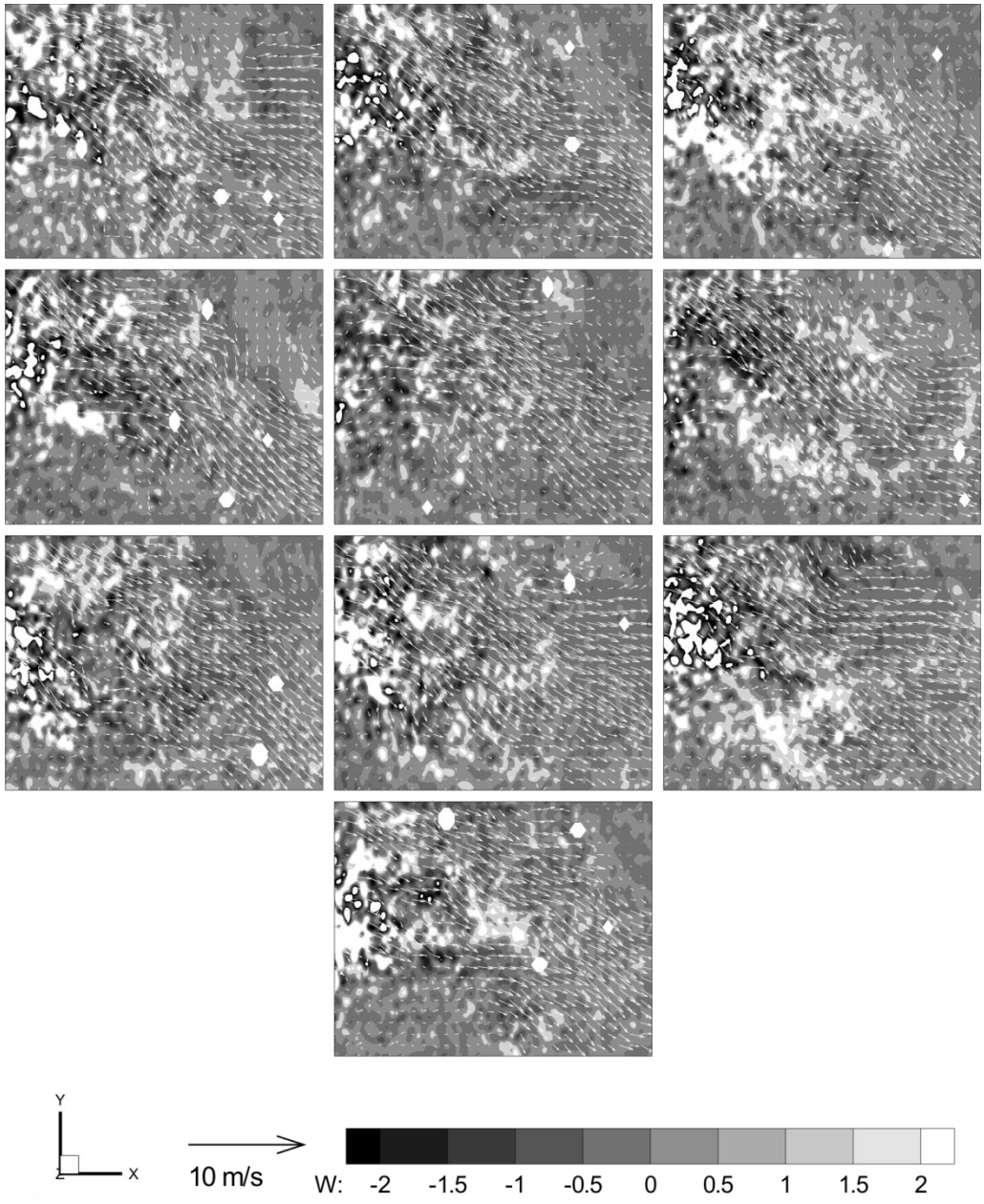

Figure 3.83 The instantaneous SPIV results at investigation plane 7 of a skewed CFF used SAC.

3.2.2 Internal Flow Investigation of the SAC

A cut off model was prepared to grant the optical access need for investigating the air flow inside of the SAC indoor unit. For investigating the different parts of the system, indoor unit was attached to the traverse in different orientations. The Figure 3.84 and 3.85 are the photographs of the cut off model and the traverse.

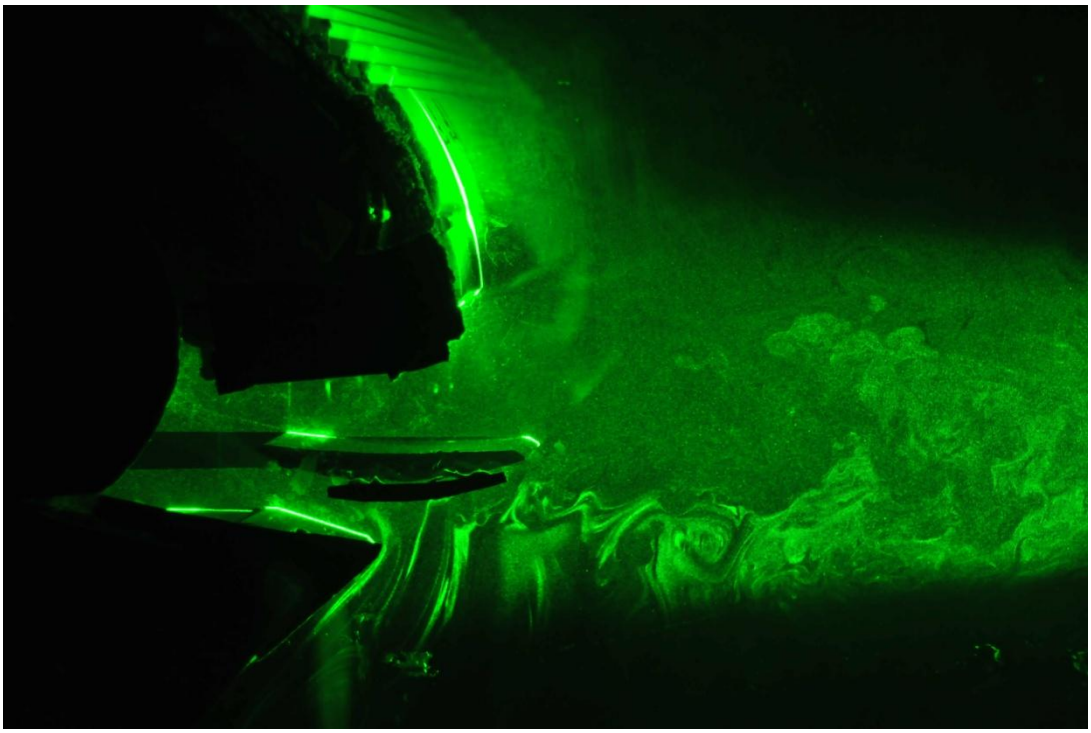

Figure 3.84 Cut off SAC model blowing seeded air and illuminated with the laser.

3.2.2.1 Effect of the Directing Airfoil on the SAC Outflow

The air flow is driven by the CFF in SAC should be controlled carefully for ensuring thermal and acoustic comfort for indoor applications of the SACs. Besides, to reduced energy demands for air conditioning it is important to control the flow of CFFs for improving their performance. The form and characteristics of this flow depend on the CFF parameters, the outlet section geometry and the directing airfoil's geometric parameters which also mentioned at chapter one. These parameters should

be well designed to control the outflow of the SACs, however except the outlet section geometry of the body, they depend on the different demands of the end user.

Angular position of the airfoil may change automatically for different operating conditions of the device (heating and cooling) or be adjusted by the users for their personal demands. In addition, new SAC models have some complex algorithms to control the airflow inside the room for which the angular position of the directing airfoil continuously changes.

Flow around an airfoil is a well known phenomenon because of the airfoils' large usage for aviation industry and there are numerous experimental and numerical studies on this subject. However, in most cases investigations are made under certain boundary conditions such as wind tunnel experiments. Distinctively in this case, flow formed by the CFF meets the airfoil and their interaction plays an important role on the outflow of the SACs. Although the producers might have been interested on this interaction to optimize the outflow, there are almost no studies on this subject in the literature. However, there are some numerical studies dealing with the outflow of SACs which are focused on noise problems and CFF performance. Cho & Moon's study in 2003 is an example of these studies.

Both the numerical and the experimental studies mentioned at the introduction part have some results on the outlet section of the CFF, but none of them modeled or included the directing airfoil. As in the case of SACs, directing airfoil may be in a close position to the CFF and the orientation of it may affect the CFF flow, resulting to a change in the performance. Therefore in this study, effect of the angular position of the flow directing airfoil of a SAC on the outflow characteristics was investigated by PIV.

SAC device is cut to two pieces for the optical access inside, and a new support was made for the free part of the CFF to ensure the operation of CFF is proper. This model was sealed at the outer edges and positioned between two plexiglas plates with 2 cm thickness. The plates and the device between the plates were hold by a traverse

system, also provided the movement of the device so without new calibrations different planes can be measured. Figure 3.85 shows the traverse and the cut off SAC indoor unit.

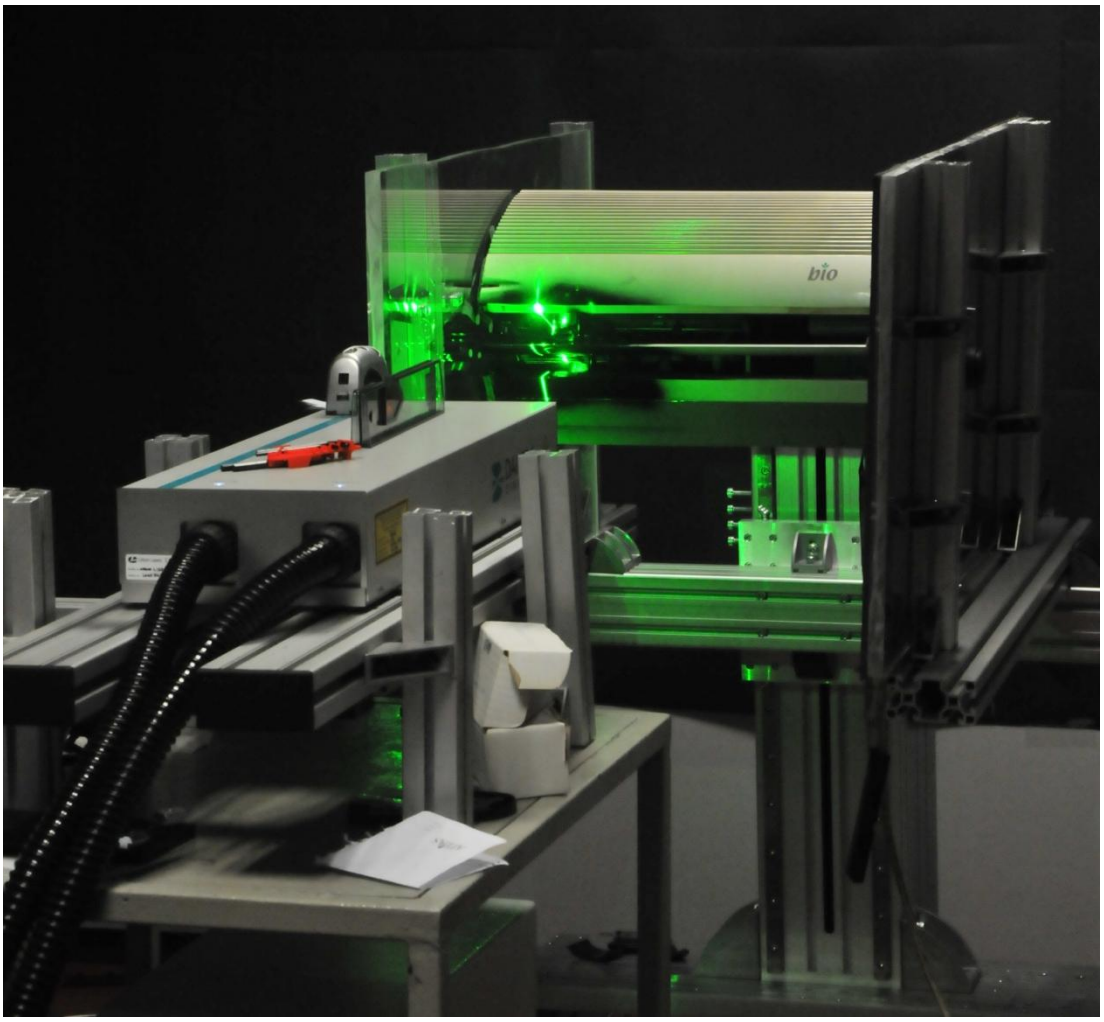

Figure 3.85 Image of the cut off SAC model, the traverse and the laser.

For all the measurements 200 image pairs from both cameras were taken for investigation. The raw data was processed for obtaining the instantaneous vector fields, and the results are given for the average of these 200 instantaneous velocity distributions.

The planar jet flow which is created by the large velocity difference between the conditioned and the ambient air and characterized by a shear layer which is

continuously growing through downstream, occurs where the air stream mixes with the surrounding air at the outlet section of the device.

To verify the results of the endoscopic PIV, a second camera placed parallel to the first one and also their field of view intersecting partially. This setup is called panoramic PIV.

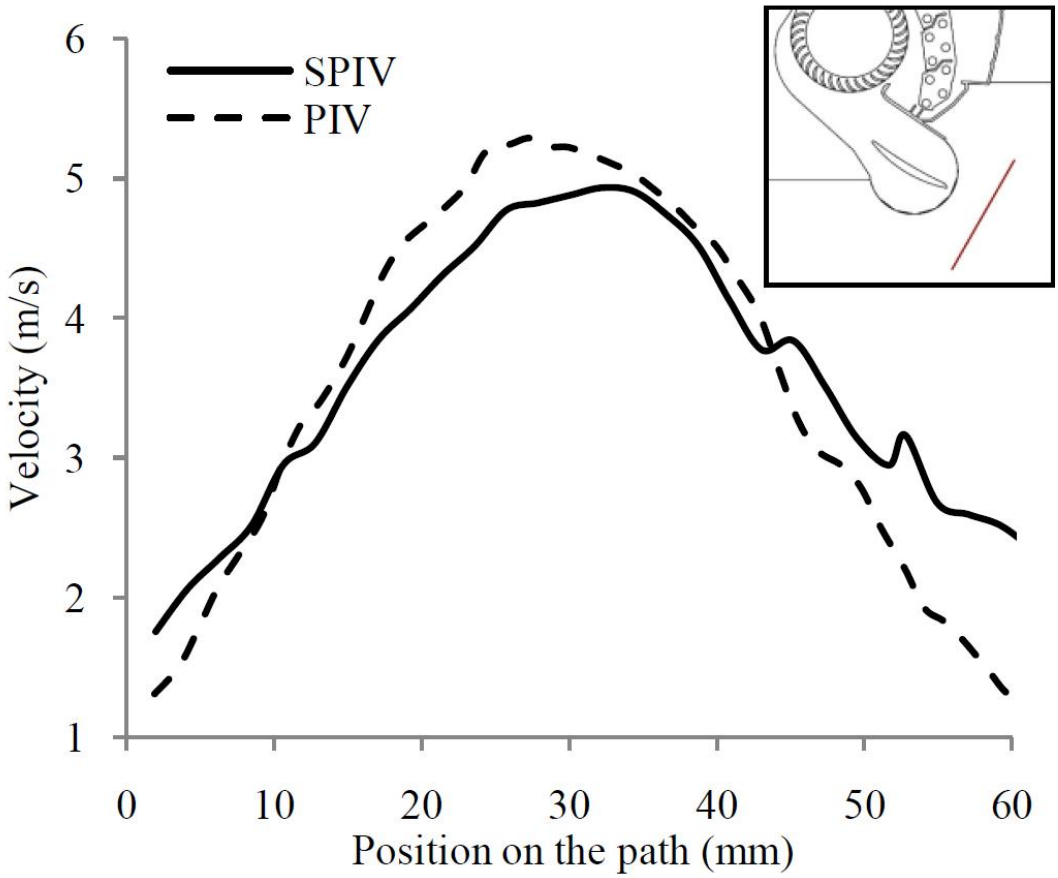

Figure 3.86 Validation of EPIV by using panoramic PIV comparing SPIV.

A path was defined at the outlet section of the device and the velocity profiles of the SPIV and panoramic PIV on the defined path were compared. As seen in Figure 3.86, the position and shape of the jet flow at the outlet of the device is similar on both measurements. The peak value and the position of the velocity is concordant, however there is a slight change on the right side of the velocity profile. The average velocity through the path is found as 3.56 m/s and 3.51 m/s for the SPIV and PIV measurements, respectively.

The angular position of the directing airfoil was defined by the angle between the chord and horizontal (β), and changed between 15 to 60 degrees with 15 degree increments. Higher values for β correspond to higher angles of attack for the airfoil considering the form of the CFF flow without any obstacles.

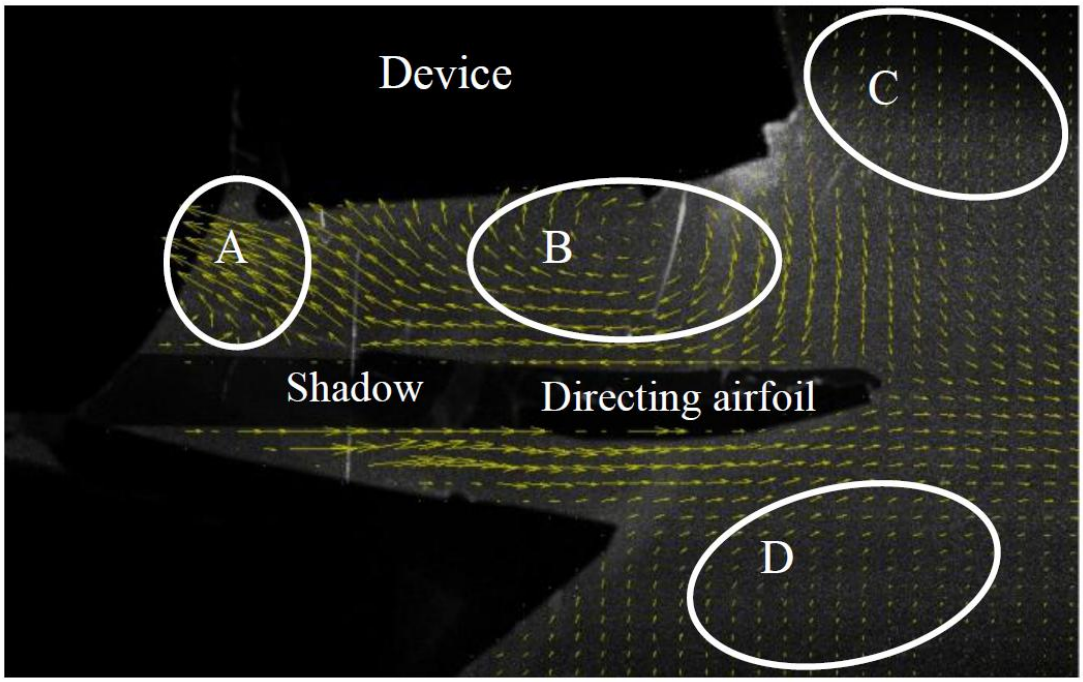

Figure 3.87 Vector field at the outflow section.

A close look to the flow at the outlet section of the device for β=60° is given, and the body of the device, directing airfoil and its shadow is shown in Figure 3.86. Velocity vectors are directed upwards towards the fan's rotating direction on the left side of the Figure 3.87 above the shadow (Region A). A part of the eccentric vortex which is the most important characteristic structure of a CFF flow is expected to be seen on this region. Eccentric vortex is the main source of the CFF flow because of the low pressure region on it, which provides the air suction from the upstream and behaves like a seal against the reversing flow of the air from the downstream. The vortex is situated above the airfoil (Region B) and Regions C and D in Figure 3.87 represent the movement of the steady air by the effect of the high velocity jet flow.

The effect of the angular position of the directing airfoil on the flow is given in Figures 3.88 and 3.89. For the β=15° (left side of Figure 3.88), the leading edge of the airfoil is nearly touching on the surface of the rear wall, therefore the air hits on the airfoil and cannot pass to the underside. As a result, the flow is redirected by the airfoil and the jet flow coming out of the device is clearly seen. Because of the difficulties in illuminating and visualizing, the eccentric vortex could not be seen on β=15° experiment result.

For the β=30° (right side of Figure 3.88), which is the predefined position, flow passes around the airfoil without facing any obstacles. Flow directed by the CFF is nearly parallel to the chord of the airfoil which corresponds to the 0° angle of attack. Only a small shift is seen on the flow while passing around the airfoil. Therefore velocity distribution on both sides of the airfoil is homogeneous and no separation is seen on the faces. The velocities of the jet flow at the outlet section is smaller than for the case of β=15°. In addition, a region (E) is seen on right of Figure 3.88 which might be a part of the eccentric vortex.

Flow is separated by the airfoil for the β=45° (left side of Figure 3.89). The lower part of the flow passes parallel to the lower side of the airfoil and get out of the device without facing any obstacles. A big vortex is observed on the upper concave face of the airfoil, which narrows the outflow section resulting to the lowest velocities at the outlet section for the investigated flow conditions. A reversed flow occurs on Region F that may be a part of the eccentric vortex and which means that the position of the eccentric vortex might be changing with the angular position of the airfoil.

For the β=60° (right side of Figure 3.89), results are similar to β=45° except the velocities at the lover side of the airfoil and at the outflow section are higher for this case.

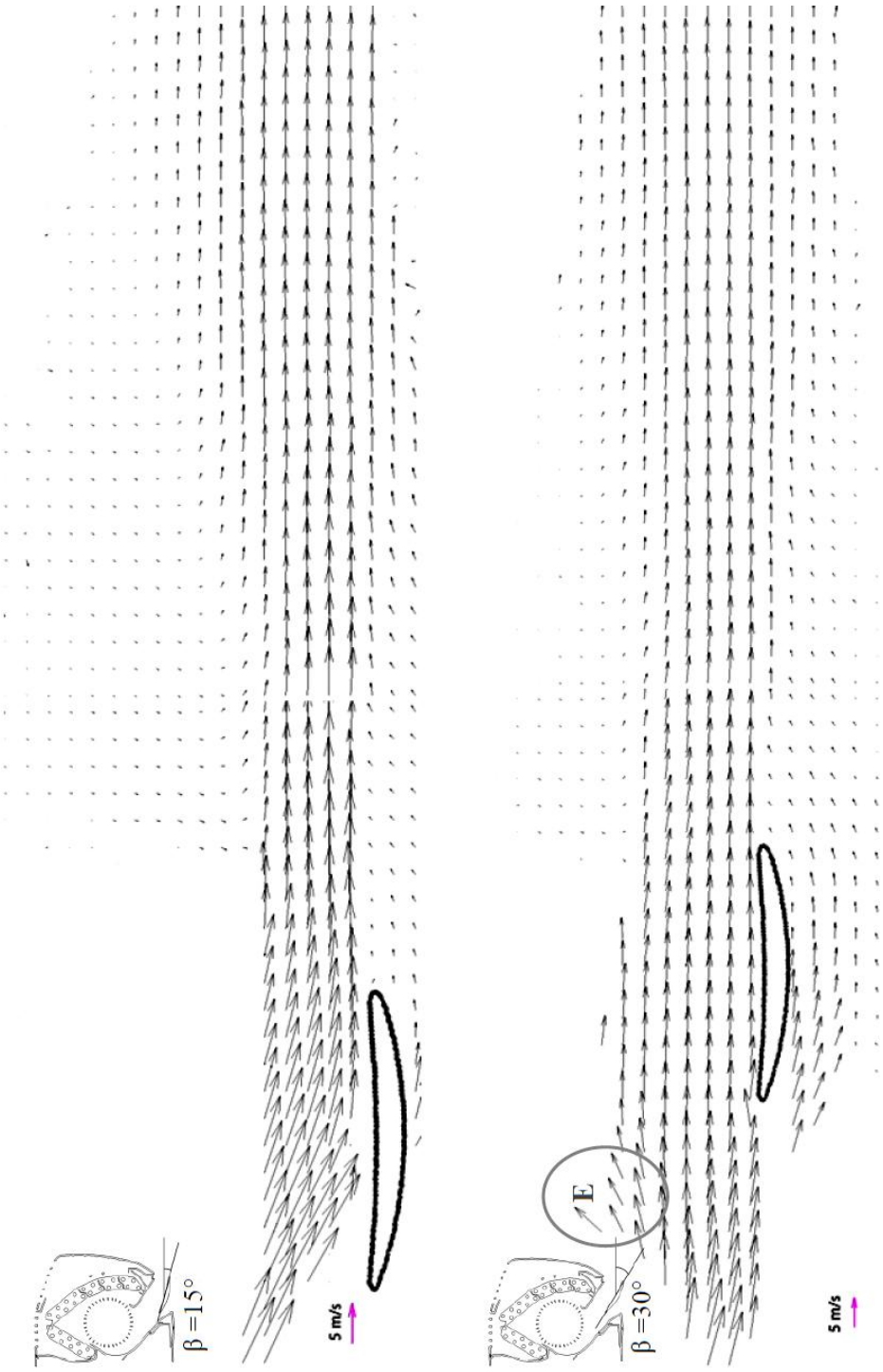

Figure 3.88 Velocity distribution at the outlet of the device for β =15° and β =30°.

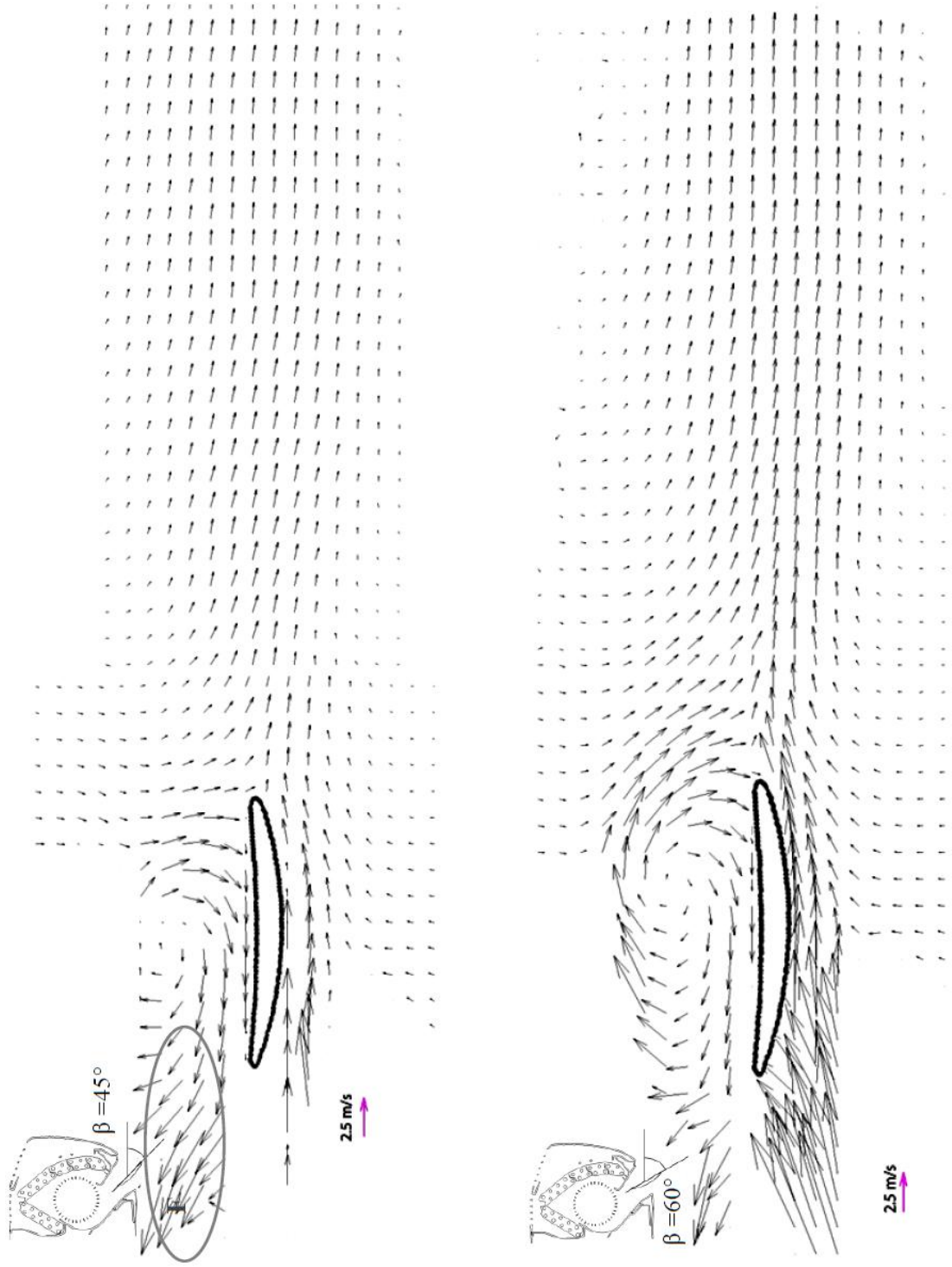

Figure 3.89 Velocity distribution at the outlet of the device for β =45° and β =60°.

Results of this part of the study show that flow is directed by the airfoil and a circulating region is observed above the airfoil for different angular positions. Flow

at the investigated section of the device includes a part of the eccentric vortex, which is the most important structure of a CFF flow, although a deeper investigation is needed for revealing this effect. The angular position of the airfoil affects the form and characteristics of the jet flow at the outlet section both on the shape and the velocity.

Panoramic PIV method was used for investigating the flow at the outlet section of a SAC for different angular positions of the directing airfoil. Results of the panoramic PIV measurements were compared with SPIV measurements to verify that there were not any defects on the flow because of the cutting and positioning processes of the device.

Critical angular position of the directing airfoil is between 30°-45° for which a transition from a smooth flow to a vortex above the airfoil occurs. For β=45° and 60°, the vortex above the airfoil behaves like a seal against the flow and forces the air to pass below the airfoil. Depending on the airfoil geometry, the distances between the leading edge of the airfoil, CFF and vortex wall may be the important parameters to control the flow.

3.2.2.2 EPIV Between the CFF and the Heat Exchanger

One of the most important flow areas of is the area that is between the heat exchanger and the CFF. For investigating this area a passage for laser beam was opened by drilling an 8 mm hole on the connection of the two coils. For creating the light sheet a cylindrical glass is placed vertically to the hole so the laser beam widen as it passes through the glass. The endoscope apparatus was not used because of its light sheet angle wasn’t covering the whole area of interest. Therefore EPIV applied by directly using the laser beam. Figure 3.90 show the schematic of this setup.

At that area the air that is sucked by the low pressure created by the eccentric vortex, came to this area after the heat transfer occurred on the heat exchanger. Thus

the low velocity flow at the suction of the SAC additionally regulated by the heat exchanger therefore a stable flow structure expected.

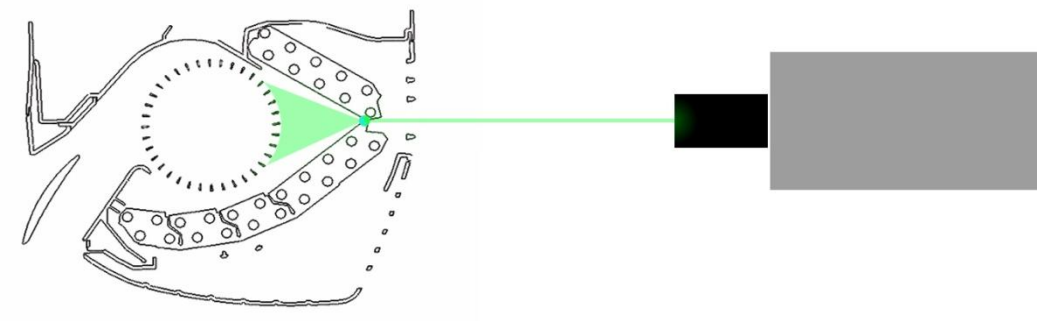

Figure 3.90 The schematic of the EPIV setup for investigating the area between the heat exchanger and the CFF.

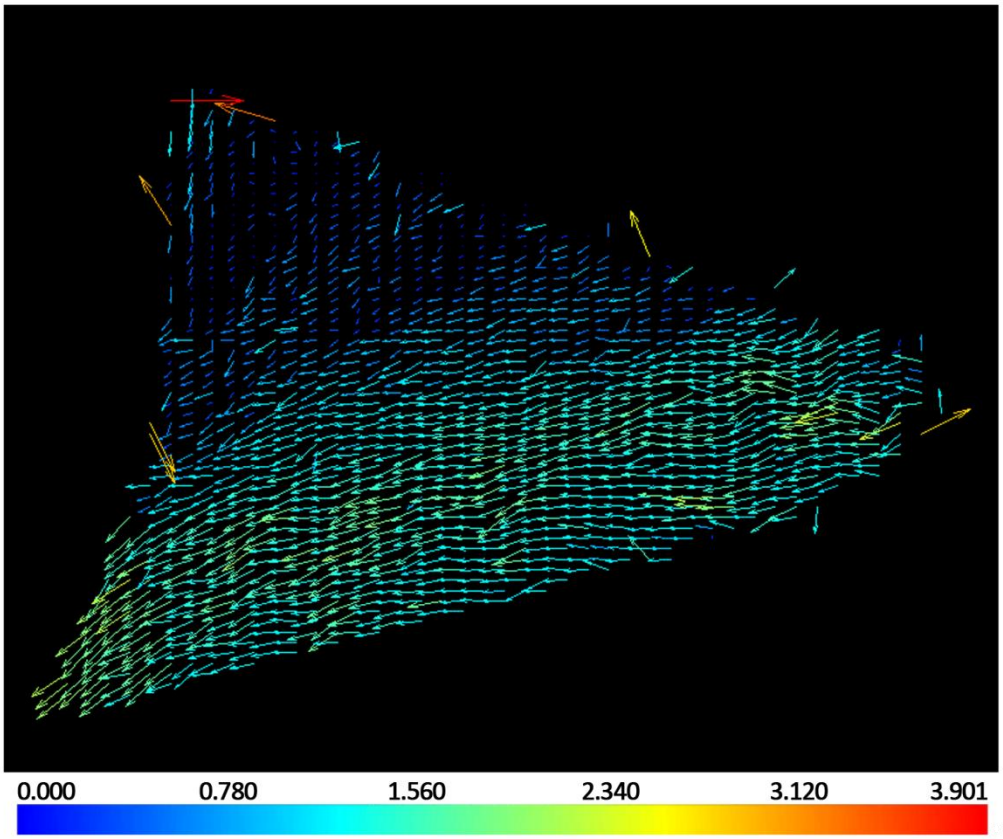

Figure 3.91 Instantaneous flow profile between the CFF and the heat exchanger.

The results of the experiments fulfill the expectation thus a slow and stable flow structure founded out. Figure 3.91 shows the instantaneous result however unlike the

outflow section of the SAC, in this area the average and the instantaneous results looks similar which also show that there were not strong vorticities or fluctuations.

Another result of the Figure 3.91 is that the main flow was moving at the down side of the area which may mean the coil near to the rear wall did not work properly because it received less flow. For the final conclusion about the subject another experiment was made at the other side of the coil.

3.2.2.3 EPIV Behind the Heat Exchanger

This experiment was made for investigating the air profile that recieved by the coil which is near the rear wall. The endoscope is used for this experiment because the angle of the light sheet was enough unlike the previous experiment. Thus using endoscope was more preferable because it creates a better quality light sheet. And addition to that there was no suitable place for fixing the cylindrical glass. The schematic of the experimental setup can be seen in Figure 3.92.

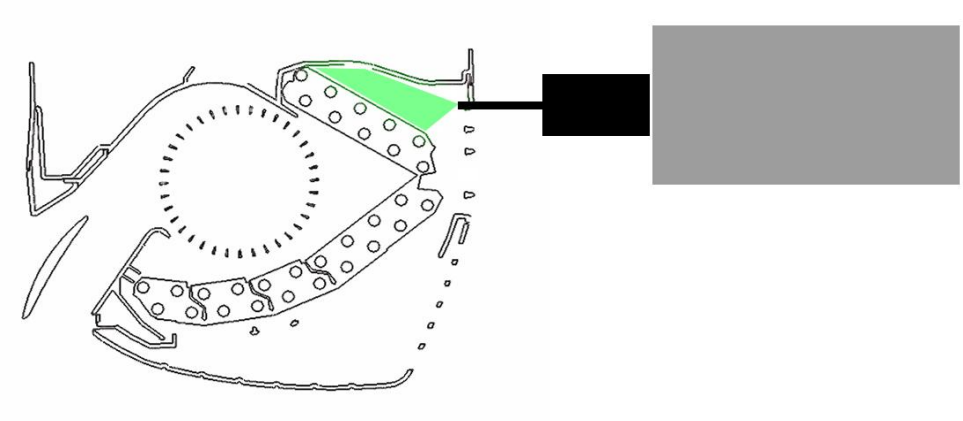

Figure 3.92 The schematic of EPIV setup for investigating the area between the rear wall and the heat exchanger.

The Figure 3.93 shows the results of this experiments which also the supports the previosus one. As the velocity map examined, it can be determined that the air passes the heat exchanger with a velocity around 1 m/s. So it can be said that the flow passes through the coil that is near to the rear wall has a low heat transfer coefficent caused by lack of velocity.

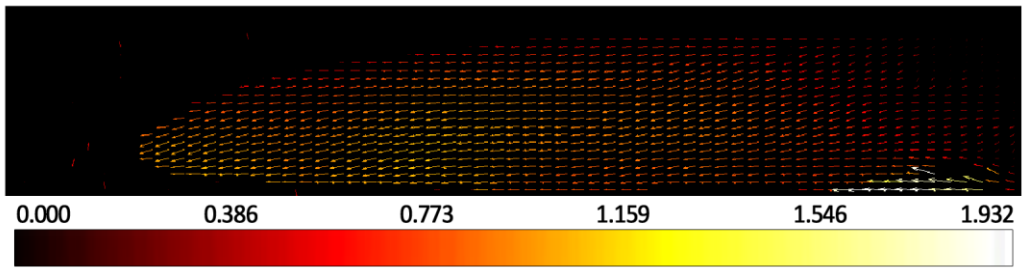

Figure 3.93 The avarage flow profile of the between the rear wall and the heat exchanger.

Figure 3.94 A SAC on the test room of the company.

This result was checked by measuring the difference between the entry temperature and the exit temperature of the refrigirent that enters the coil. These experimenst was made in the companies test labs. The results of the test showed that the temperature difference is nearly 1 C. As its mentioned at the introduction chapter in ideal refrigiration cycle, the temperature doesn't changes in the heat exchanger but

the refrigerent only phases. But in realty some sensible heat transfer also occures, thus the difference at other coils are near 3C. Therefore this 1 C temperature difference between the entry and exit of the refrigerent shows that there was so little heat transfer that even the phases change did not started.

As a final result the heat exchanger near the rear wall was not reciving the main part of the flow that is driven by the CFF. Thus Chaning the flow pattern or position of the heat exchanger will be a solution to this problem.

3.3 MIT Measurement Results

The validation of the MIT method was perused by the measurement of the temperature distribution at the outflow section of the SAC. The measurement mesh is placed parallel to the flow and the thermal camera placed perpendicular to the measurement mesh. Figure 3.95 show the experiment's setup. The same measurement planes that were used in PIV experiments also used in these experiments (Figure 3.5).

The experiment was done in the heating mode. The measurements stared after the SAC switch on and developed a steady flow. The thermostat temperature set to maximum (or minimum if the experiments done in cooling mode) to prevent the system stop during the experiment.

Twenty infrared image taken in every investigation plane and these images post processed as it was presented at the previous chapter. Then the average temperature distributions obtained on every investigation plane. Figures 3.96 to 3.107 shows these temperature distributions.

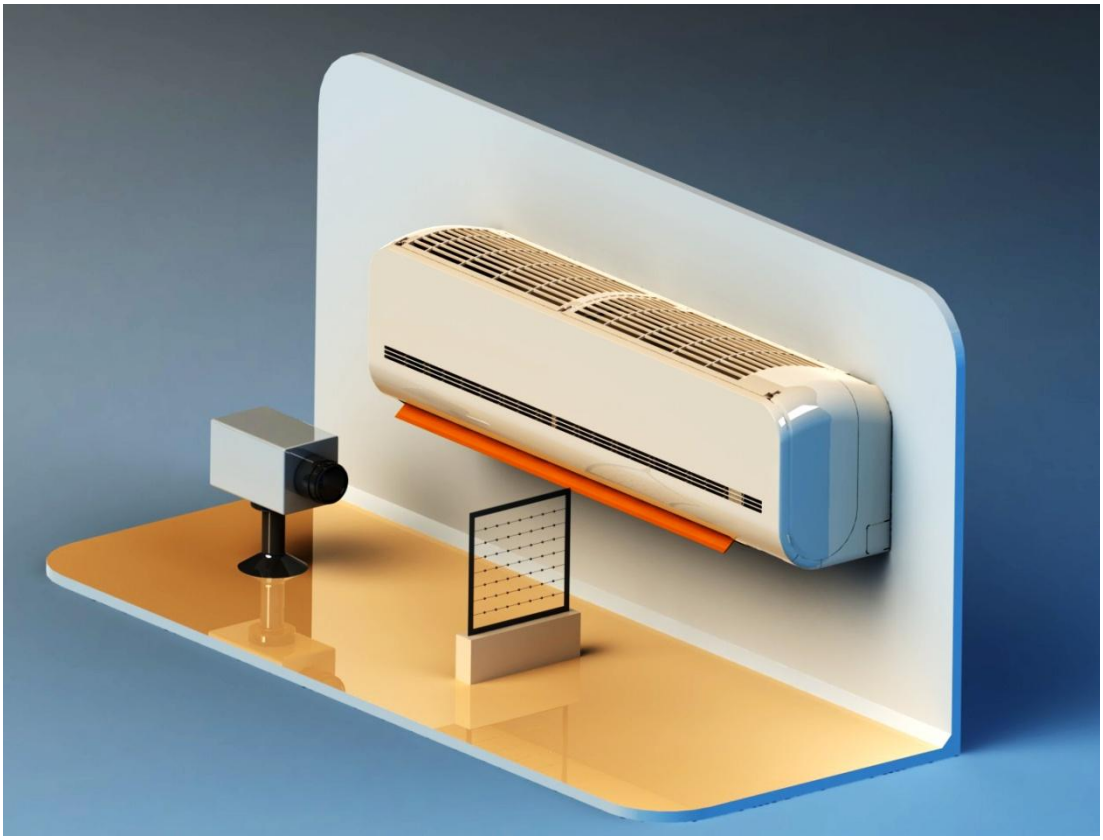

Figure 3.95 the 3d model of MIT measurement at the outflow section of a SAC.

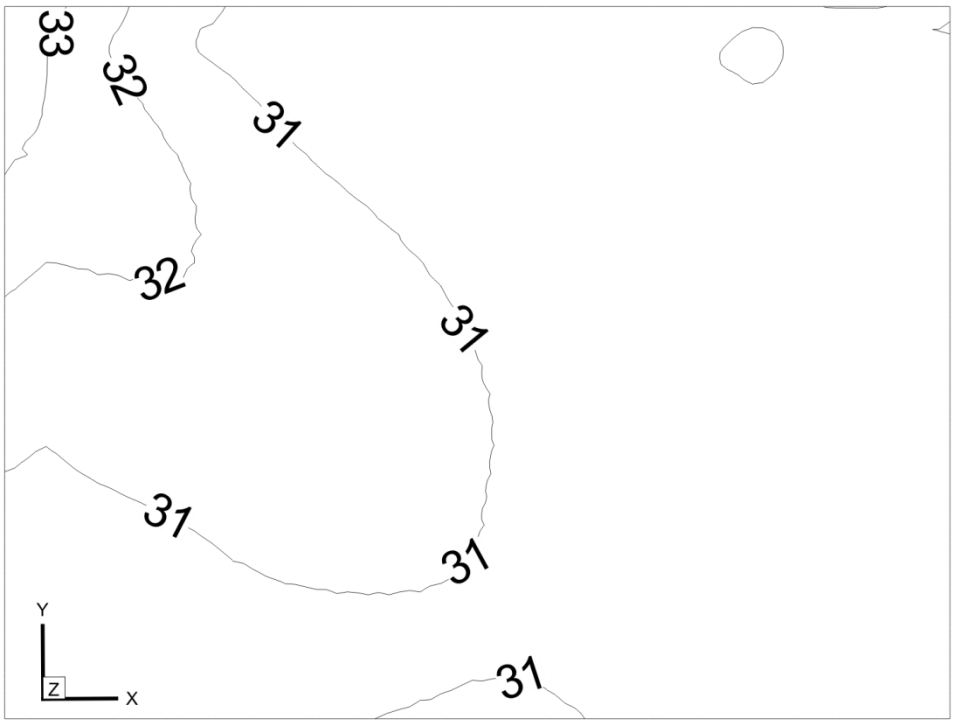

Figure 3.96 Temperature distribution on investigation plane 1.

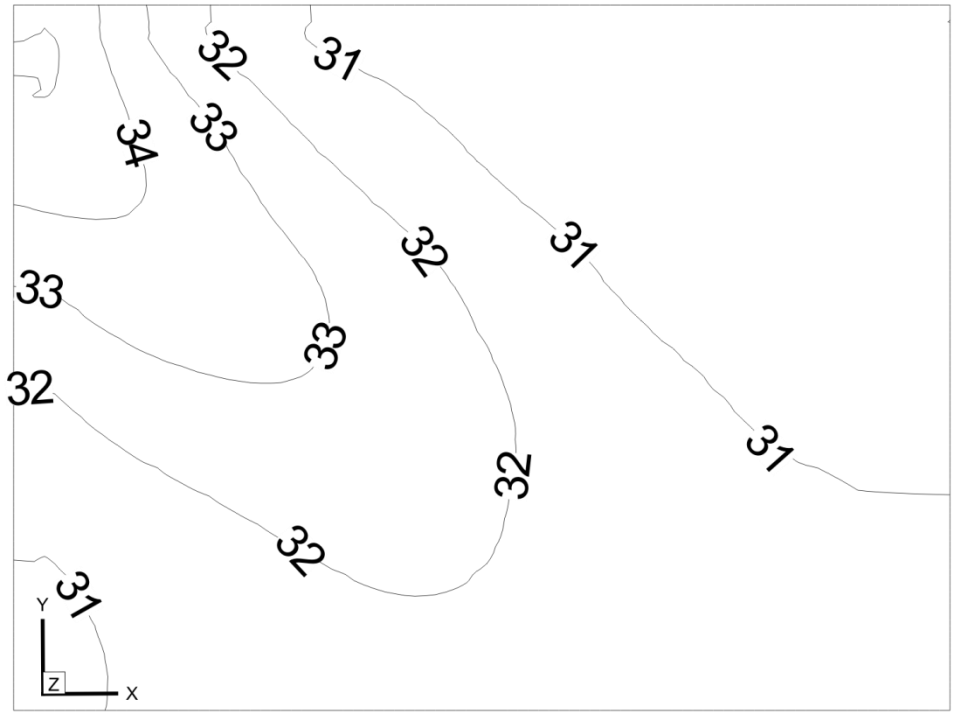

Figure 3.97 Temperature distribution on investigation plane 2.

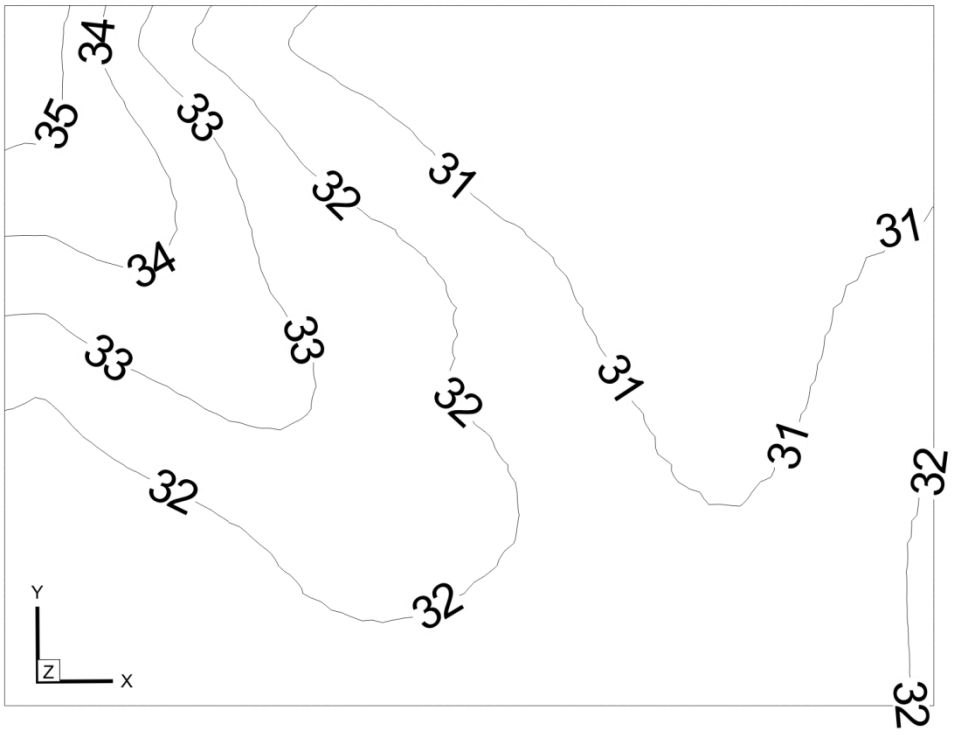

Figure 3.98 Temperature distribution on investigation plane 3.

Figure 3.99 Temperature distribution on investigation plane 4.

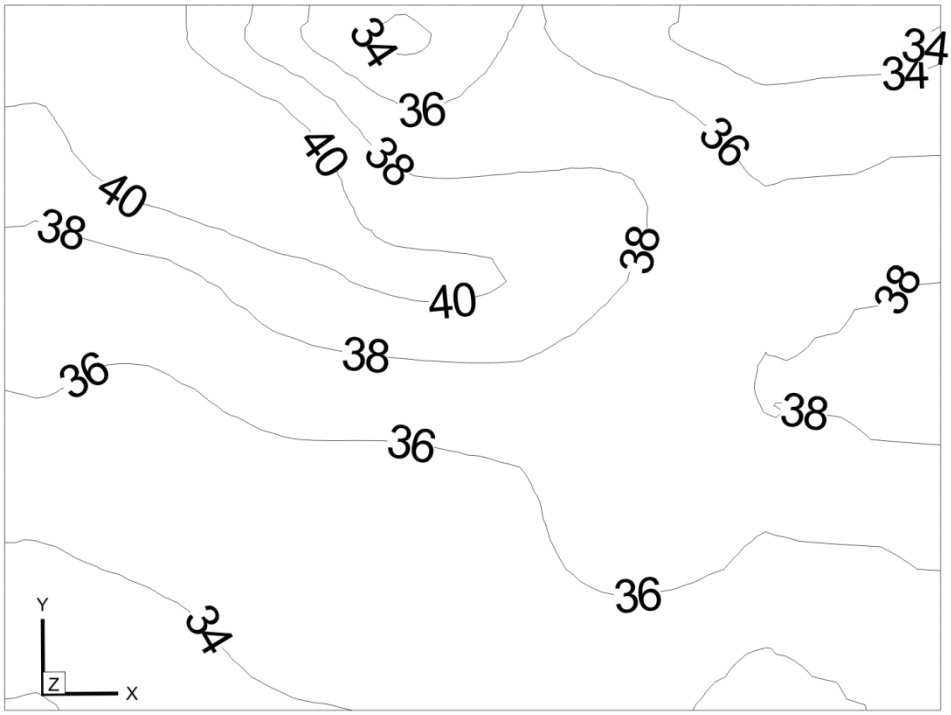

Figure 3.100 Temperature distribution on investigation plane 5.

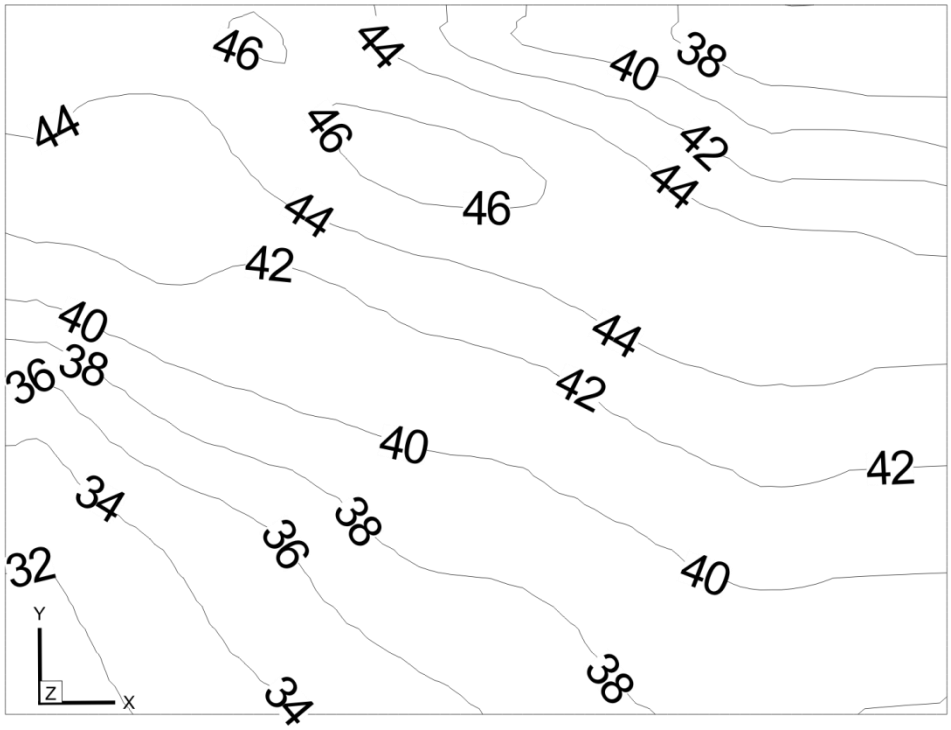

Figure 3.101 Temperature distribution on investigation plane 6.

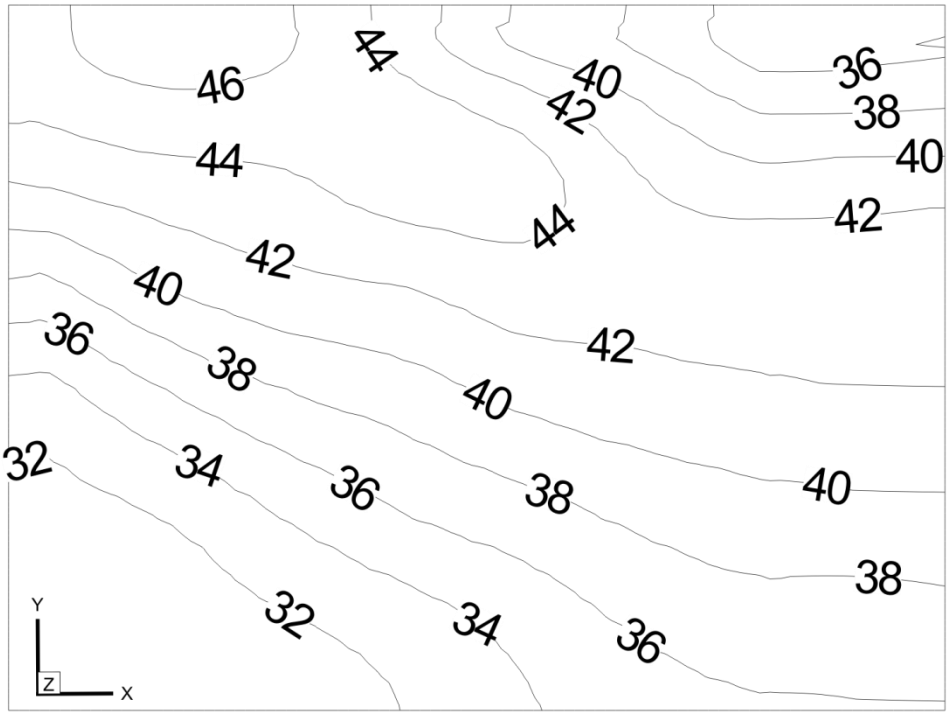

Figure 3.102 Temperature distribution on investigation plane 7.

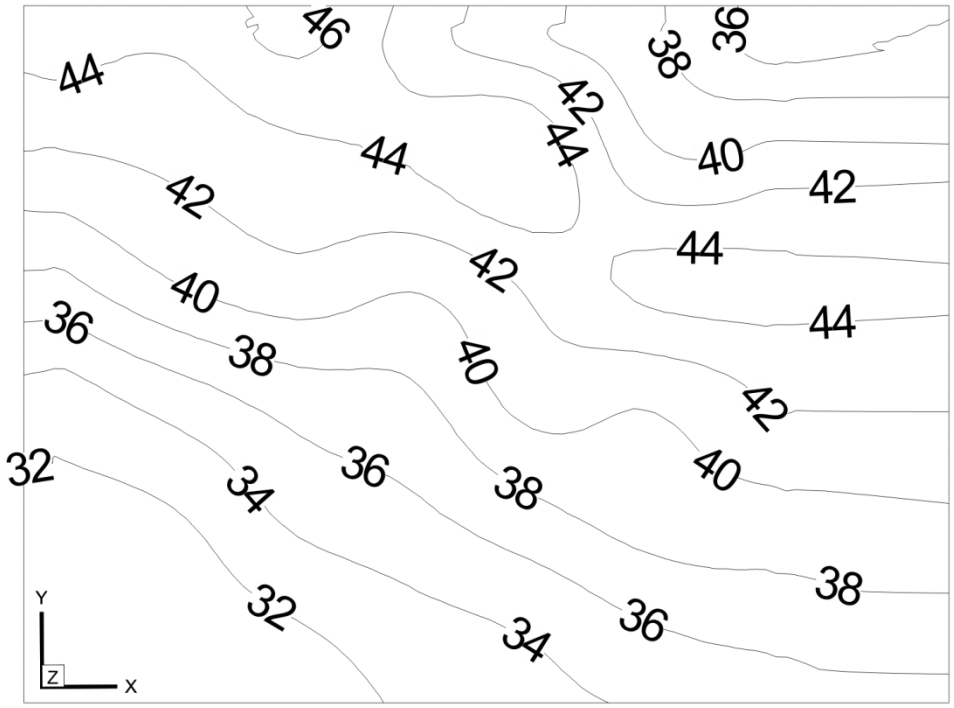

Figure 3.103 Temperature distribution on investigation plane 8.

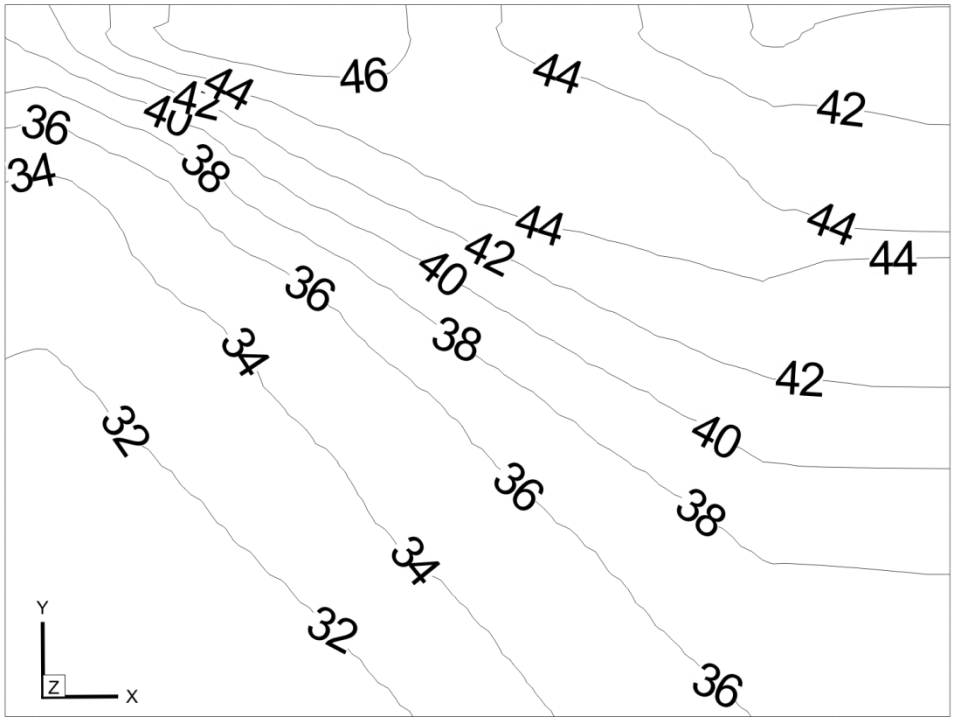

Figure 3.104 Temperature distribution on investigation plane 9.

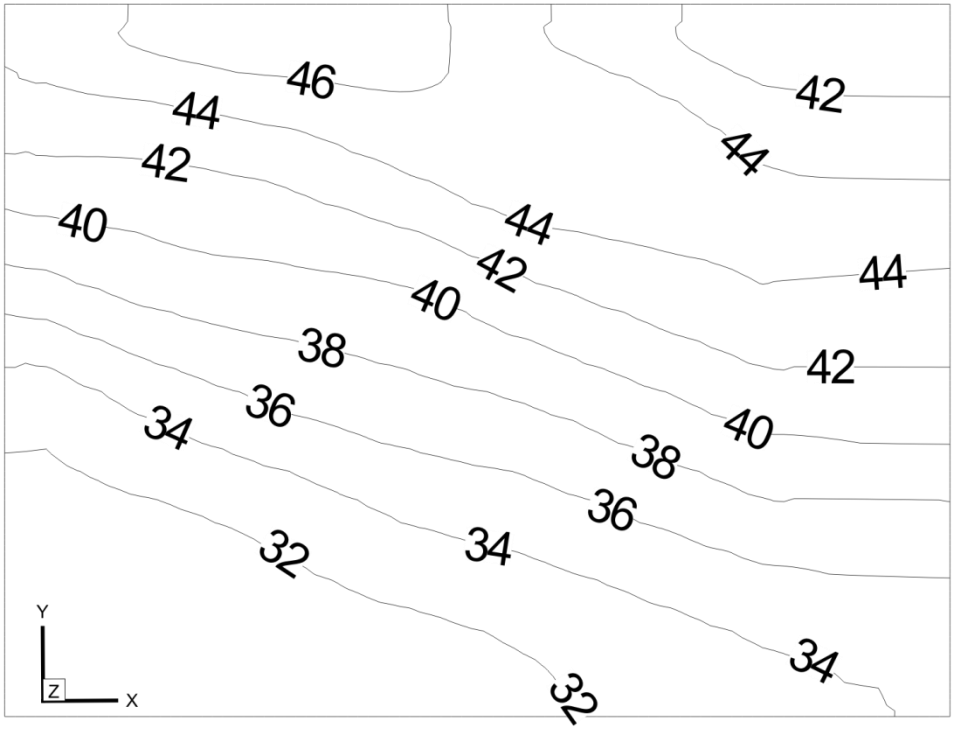

Figure 3.105 Temperature distribution on investigation plane 10.

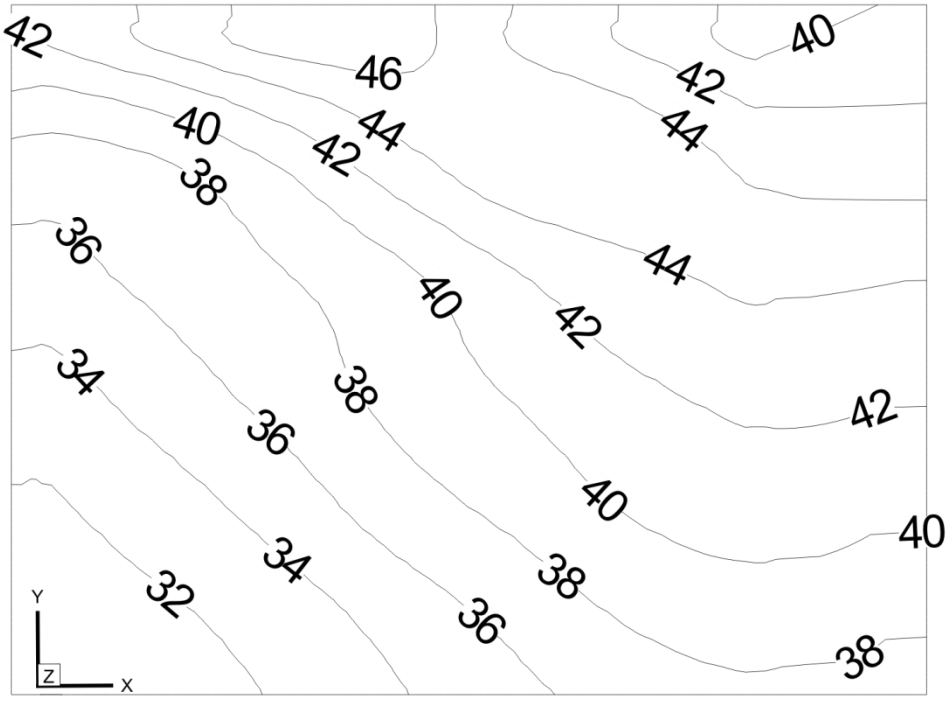

Figure 3.106 Temperature distribution on investigation plane 11.

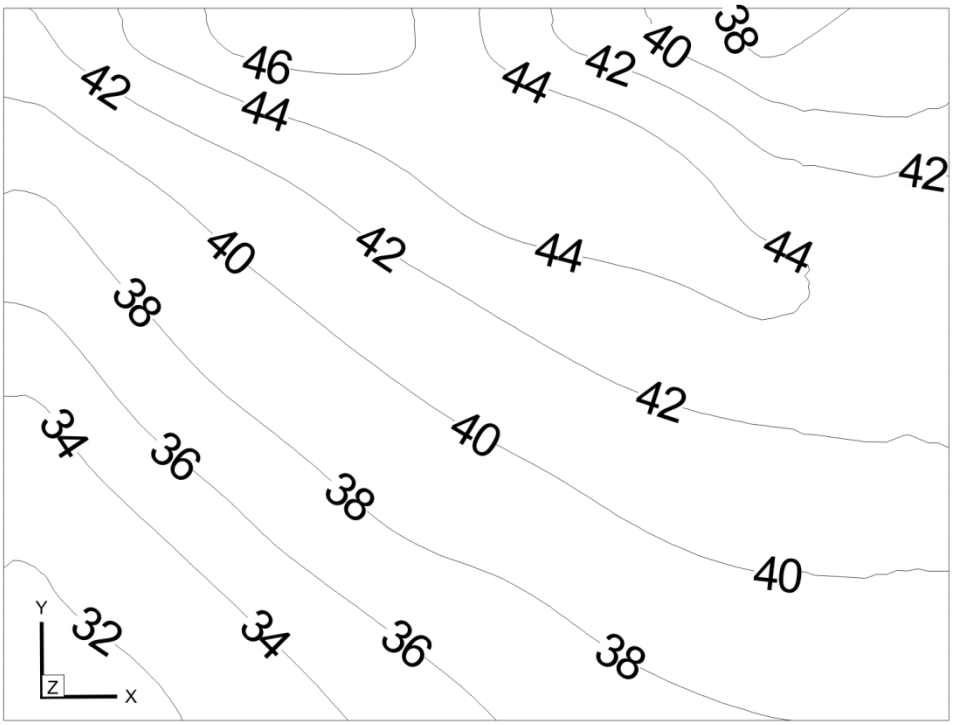

Figure 3.107 Temperature distribution on investigation plane 12.

As the SAC that was measured includes a skewed CFF, the investigation plane 1 has some cooler areas because of the skewed flow of the SAC. It is also noted that this effect continues in plane 2, 3, 4 and even in plane 5 (Figures 3.97 to 3.100). In velocity measurement this effect was not seen in investigation planes 4 and 5 (Figure 3.16 and 3.19).

After the investigation plane 5 the core temperature of the flow comes up to 46 C and continued the same way till the plane 12.

Figure 3.108 is the 3D reconstruction of these average temperature data. The values on areas between the investigation planes are iterated. The scale of the temperatures for the iso-surfaces is given in the bottom of the figure.

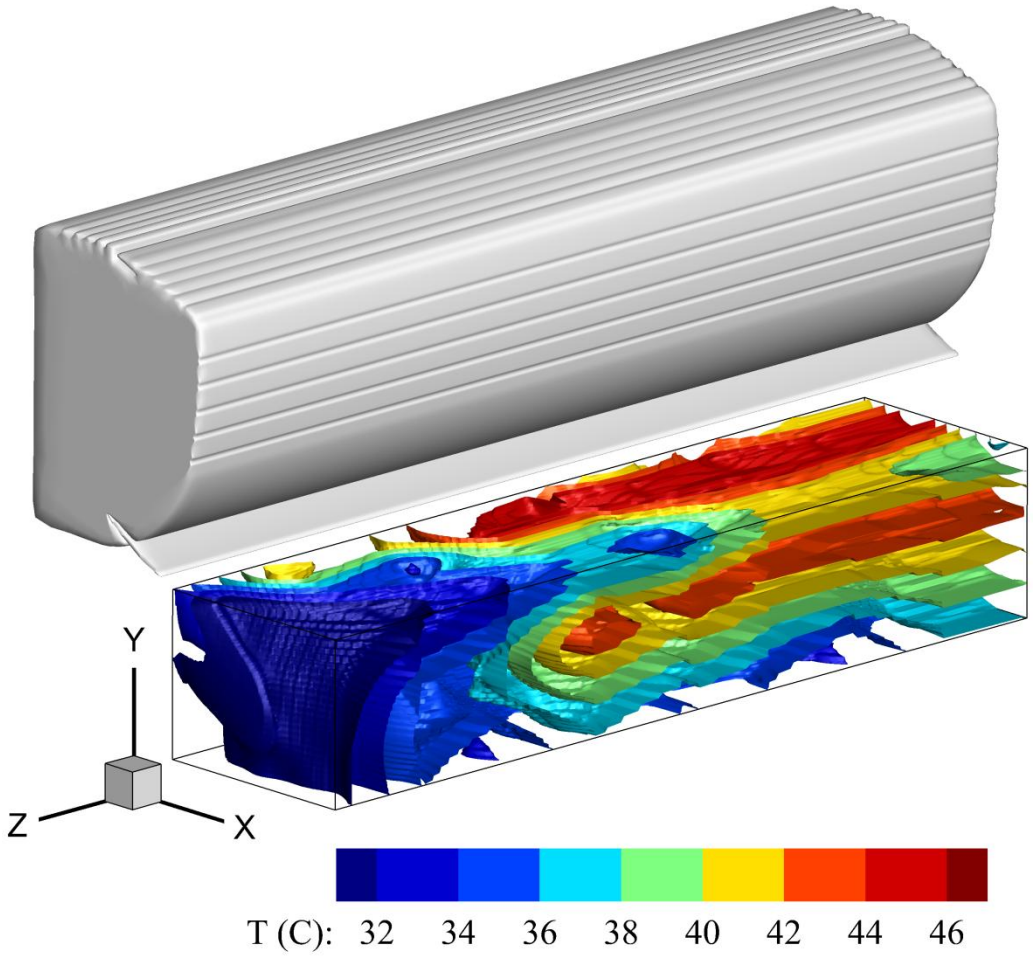

Figure 3.108 The average temperature iso-surface of the all 12 investigation planes on skewed CFF used SAC.

3.4 Merging Temperature Distribution with Velocity Distribution

After the velocity distributions and temperature distribution were obtained, as a final study, these data merged together. For achieving that the investigated areas on the same investigation planes gathered at the same media. Putting two data on each other wouldn't be enough because of slight differences of their positions. Thus the data is repositioned according to the global coordinates then the non-intersecting data was cropped.

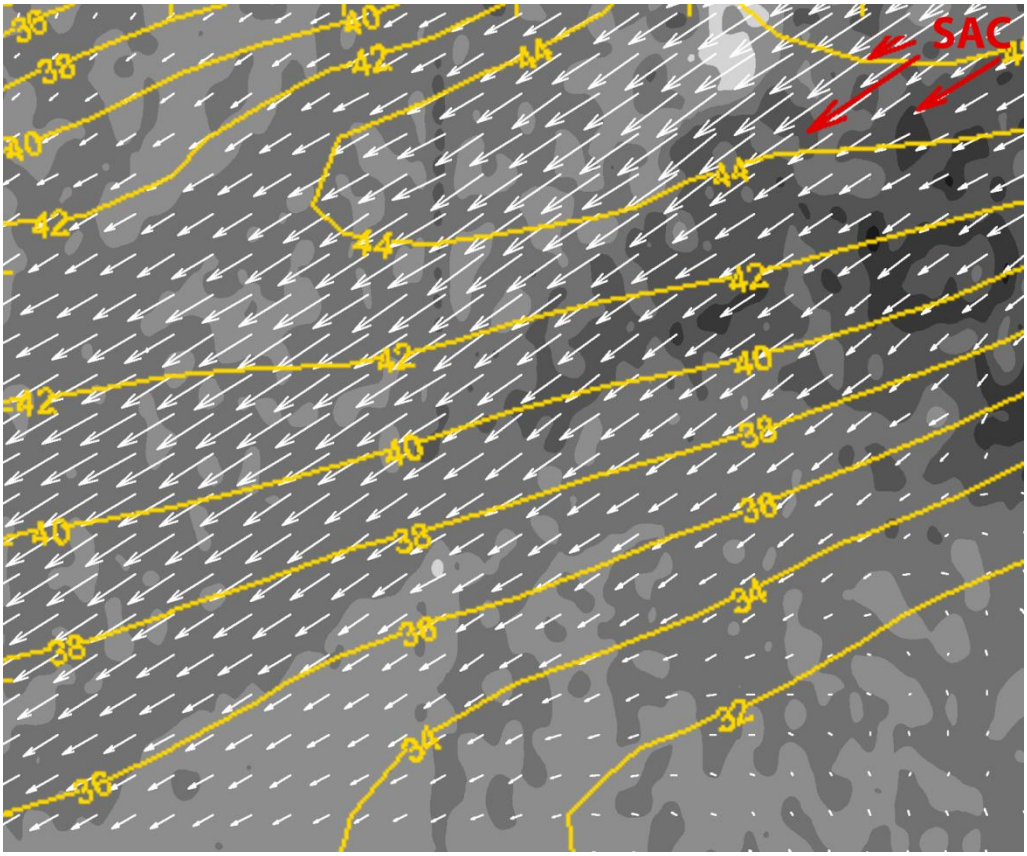

Figure 3.109 Temperature distribution merged with a three dimensional velocity distribution.

The Figure 3.109 is the temperature distribution merged with the three dimensional velocity distribution of the same investigation plane. The yellow lines indicates the temperature distribution, the SAC's position is tagged by red.

Both distributions seem to fit in good agreement thus it can be assumed as another validation of the measurements. Also investigating temperature with velocity together gives a better chance to understand a system. In addition to that these data set also very suitable for using in CFD as inputs.

CHAPTER FOUR
CONCLUSION

In the scope of this thesis, the velocity and the temperature measurement methods examined for suitability to measurement inside of a SAC indoor unit.

PIV method has been chosen as the most suitable method for the velocity measurement. Thus a PIV setup that can investigate the flow structure of the SAC is designed and composed. For revealing the flow structure inside the SAC indoor unit, some PIV experiment has been made on the outflow section of the SAC and the flow profile of the SAC indoor unit was obtained by the combining together the investigation planes data. These data also used for validating the cut off model for investigating the inside of the SAC indoor unit.

Endoscopic PIV and panoramic PIV were used together to successfully investigating the inside flow structure. In panoramic PIV applications while one camera acquisitioning data from the cut model's inside, second camera captured the data that can be combined with the first one which later can be used for comparing the with the SPIV results that is gathered from the outflow section of the SAC. As the result of these experiments the data of the camera which was looking through the cut off model, was validated with SPIV results so the air velocity distribution inside of the SAC was gathered successfully. The other areas that the light sheet cannot be created directly were investigated by Endoscopic PIV. Therefore whole SAC units flow structure data acquired.

For temperature measurement infrared thermography was used for solid body measurements and the novel method MIT was developed for investigating the air temperature. After the validated of the method, it was used for measuring the temperature distribution at the exit section of the SAC indoor unit.

In this study also the method for converting the experimental data to inputs for the CFD or other finite methods using programs are investigated and found. Thus the

experimental data can be used directly in these programs for more realistic analysis which may used for investigating the whole systems together more detailed or a non-optically accessible part of it.

As a final result of this thesis, PIV and its side methods are very useful tools for investigating any flow structure that can be optically accessed. The infrared thermography is already a well known technique for measuring temperature distribution on a solid which can be also used in SAC indoor unit. Besides that with MIT method, infrared thermography also can be used for the air temperature distribution measurements. Therefore it can be said that by using these methods, the velocity and the temperature distribution inside a split air conditioners indoor unit experimentally investigation accomplished.

REFERENCES

ASHRAE Inc., (2004). *The Systems and Equipment volume of the ASHRAE Handbook*, Atlanta:GA.

Adrean, R. J. (2005). Twenty years of particle image velocimetry, *Experiments in Fluids*. 39, 159–169.

Çengel, Y. A. & Boles M. A. (1989).*Thermodynamics an engineering approach (1st ed.)*. New York: McGraw-Hill.

Çengel, Y. A. & Boles M. A. (2006).*Thermodynamics an engineering approach (5th ed)*. New York: McGraw-Hill.

Cho, Y., & Moon, Y. J. (2003) Discrete noise prediction of variable pitch cross-flow fans by unsteady navier-stokes predictions. *Journal of Fluids Engineering*, 125, 534-550.

Dantec Dynamics (n.d.). Retrieved 10 October 2011 from http://www.dantecdynamics.com/default.aspx?ID=1169

Eck, B. (1973). *Design and operation of centrifugal axial flow and cross flow fans*. Oxford: Pergamon Press.

Gabi, M., & Klemm, T. (2004). Numerical and experimental investigations of cross-flow fans. *Journal of Computational and Applied Mechanics*. 5(2), 251-261

Gad-el-Hak M. (2000). *Flow control: passive, active and reactive flow management*. Cambridge: Cambridge Univercity Press.

Gharib, M., Kremers, D., Koochesfahani, M.M. & Kemp, M., (2002). Leonardo's vision of flow visualization. *Experiments in Fluids*. 33, 219–223

Gemici, Z., Eğrican, A. N., & Koca, A. (2010). Theoretical and experimental examination of air conditioner heat exchangers. *Internatiol Communications in Heat And Mass Transfer*.

İSKİD, (İklimlendirme-Soğutma-Klima İmalatçıları Derneği) (2011) *Sale Istatistics Report.*

Jacob, R.E., Ray, S. F., Attridge G. G. & Axford N. R., (2000) *Manual of Photography, (9th ed.)* Oxford: Focal Press

Karadeniz, Z.H., Kumlutaş, D. & Özer, Ö. (2011). Effect of the angular position of the directing airfoil on the room air conditioner outflow characteristics. *9th international symposium on particle image velocimetry – piv'11*, 21-23.

Murata, S. & Nishihara, K. (1976a). An experimental study of cross flow fan (1st report, effects of housing geometry on the fan performance). *Bulletin of the JSME*, 19(129), 314-321.

Murata, S. & Nishihara, K. (1976b). An experimental study of cross flow fan (2nd report, movement of eccentric vortex inside impeller). *Bulletin of the JSME*, 19(129), 322-329.

Murata, S., Ogawa, T., Shimizu, I., Nishihara, K., & Kinoshita K. (1978). A study of cross flow fan with inner guide aparatus. *Bulletin of the JSME,* 21(154), 681-688.

Omega Engineering (n.d.). Retrieved 10 October 2011 from http://www.omega.com

Prasad, A. K. (2000). Stereoscopic particle image velocimetry. *Experiments in Fluids*, 29, 103-116.

Raffel M., Willert C., Wereley S. & Kompenhans J., (2007), *Particle image velocimetry a practical guide (2nd ed.).* New York: Springer.

Shih, Y. C., Hou, H. C., & Chiang, H. (2008). On smilitude of the cross flow fan in a split-type air-conditioner. *Applied Thermal Engineering* (28), 1853-1864.

Tanaka, S., & Murata, S., (1994). Scale effects of cross-flow fans (Effects of fan dimensions on performance curves). *JSME International Journal Series B*, 37(4), 844-852.

Tuztas, M., & Egrican, A. N. (2002). Mathematical model of finned tube heat exchangers for thermal simulation software of air conditioner. *International Commitee Of Heat And Mass Transfer , 29* (4), 547-556.

Uskaner, Y. A., & Göksel, Ö. T. (1999a). Effects of rear casing on cross flow fan performance. *Proceedings of MMO Denizli Division Science Meeting (in Turkish)* (pp. 44-50). Denizli: MMO.

Uskaner, Y. A., & Göksel, Ö. T. (1999b). Effects of rotor parameters on cross flow fan performance. *IV. Proceedings of National HVAC and Sanitary Convention and Exhibition (in Turkish)*. 2, pp. 579-597. İzmir: MMO.

White, F. M., (1999). *Fluid Mechanics* (4th ed.). New York: McGraw-Hill.

Wikipedia (n.d.). Retrieved 10 October 2011 from http://en.wikipedia.org/wiki /Air_conditioner.

Wikipedia (n.d.). Retrieved 10 October 2011 from http://en.wikipedia.org/ wiki/Doppler_effect.

Yamafuji, K. (1975a). Studies on the flow of cross-flow impellers (1st report, experimental study). *Bulletin of JSME,* 18(123), 1018-1025.

Yamafuji, K.(1975b). Studies on the cross-flow impellers (2nd report, analytical study). *Bullerin of the JSME,* 18(126), 1425-1431.

Yan, W., & Sheen, P. (2000). Heat transfer and friction characteristics of fin-and-tube heat exchangers. *International Journal Of Heat And Mass Transfer* (43), 1651-1659.